Temporal analysis of parkin-dependent mitophagy using mass spectrometry-based proteomics

Dissertation

der Mathematisch-Naturwissenschaftlichen Fakultät

der Eberhard Karls Universität Tübingen

zur Erlangung des Grades eines Doktors der Naturwissenschaften

(Dr. rer. nat.)

vorgelegt von

Katharina Isabell Zittlau

aus Heidelberg

Tübingen

2022

Gedruckt mit Genehmigung der Mathematisch-Naturwissenschaftlichen Fakultät der Eberhard Karls Universität Tübingen

Tag der mündlichen Qualifikation: 19.12.2022

Dekan:	Prof. Dr. Thilo Stehle
1. Berichterstatter:	Prof. Boris Maček
2. Berichterstatter:	Prof. Michal Sharon

Erklärung

Ich erkläre hiermit, dass ich die zur Promotion eingereichte Arbeit:

“Temporal analysis of parkin-dependent mitophagy using mass spectrometry-based proteomics”,

nur die angegebenen Quellen und Hilfsmittel benutzt und wörtlich oder inhaltlich übernommene Stellen als solche gekennzeichnet habe. Ich erkläre, dass die Richtlinien zur Sicherung guter wissenschaftlicher Praxis der Universität Tübingen (Beschluss des Senats vom 25.5.2000) beachtet wurden. Ich versichere an Eides statt, dass diese Angaben wahr sind und dass ich nichts verschwiegen habe. Mir ist bekannt, dass die falsche Abgabe einer Versicherung an Eides statt mit Freiheitsstrafe bis zu drei Jahren oder mit Geldstrafe bestraft wird.

Declaration

I hereby declare, that I have produced the work:

“Temporal analysis of parkin-dependent mitophagy using mass spectrometry-based proteomics”,

Submitted for the award of a doctorate, on my own (without external help), have used only the sources and aids indicated and have marked passages included from other works, whether verbatim or in content, as such. I swear upon oath that these statements are true and that I have not concealed anything. I am aware that making a false declaration under oath is punishable by a term of imprisonment of up to three years or by a fine.

Tübingen, den 31.10.2022 _____

Table of Contents

Summary

Mitochondria fulfill several key functions in cellular energy metabolism and signaling, such as the generation of ATP by oxidative phosphorylation and life-death decisions. Dysfunctional mitochondria pose a threat to cellular homeostasis and have to be quickly removed by the cell. PINK1/Parkin-dependent mitophagy is an important pathway for the mitochondrial quality control (MQC) mechanism to protect cells against pathogenic accumulation of dysfunctional mitochondria. During the initiation of this multistep process post-translational modifications (PTMs), such as phosphorylation by the PINK1 kinase and ubiquitylation by the E3-ubiquitin ligase parkin, function together on ubiquitin, the ubiquitin like (UBL) domain of parkin and outer mitochondrial membrane (OMM) proteins. Quantitative proteomics has already been used to investigate the crosstalk between PTMs during early stages of this process. However, late stages of mitophagy that ultimately lead to the degradation of mitochondria remain understudied.

To obtain a deeper insight into parkin-mediated mitochondrial degradation, I initially established a subcellular fractionation workflow to analyze mitochondrial proteins as well as their ubiquitylation and phosphorylation dynamics by quantitative proteomics after induction of mitophagy in HeLa cells. To this end, I combined cytoplasmic, membrane-bound and soluble nuclear protein fractions, which enabled analysis of exclusive mitophagy-relevant fractions and met the requirements of high quantity input material for subsequent phosphoproteome and ubiquitylome analyses. I then applied different chemical labeling strategies, such as dimethyl labeling and tandem mass tags in combination with high-resolution orbitrap mass spectrometry to study the regulation of protein degradation, ubiquitylation and phosphorylation during early (2-6 h post induction) and late stages (12-18 h post induction) of mitophagy in parkin wild-type and ligase-dead HeLa cells, which were generated and treated with the protonophore Carbonyl cyanide m-chlorophenyl hydrazone (CCCP) in the group of Philipp Kahle. Integration and extensive bioinformatic analysis of all three proteomic datasets revealed that mitochondrial degradation proceeds stepwise and protein ubiquitylation precedes protein degradation. Unexpectedly, protein phosphorylation revealed only a minor effect during this process. In the presence of functional parkin, mitochondrial proteins are ubiquitylated followed by degradation in an outside-in fashion on the mitochondrion. This begins on the OMM and proceeds inwards to the inner

mitochondrial membrane (IMM) and finally the mitochondrial matrix. Several OMM proteins displayed a similar pattern of modification by ubiquitylation, with an overall minor cross-talk between phosphorylation and ubiquitin-dependent protein degradation.

Further analysis of the mechanisms underlying the stepwise degradation of mitochondrial subcompartments revealed its strong dependency on lysosomal, as well as on proteasomal activity. By application of quantitative proteomics techniques, I could validate the biochemical experiments from the Kahle group that pointed to a general dependency of mitochondrial protein degradation on proteasomal activity. In a temporal study involving inhibition of the proteasome at various timepoints upon induction of mitophagy and subsequent proteome measurements, I could confirm that especially OMM proteins like TOM70 fail to be degraded.

In summary, this thesis provides new insights on the mechanisms involved in parkin-dependent mitophagy and will serve as a resource for future work on this essential cellular process.

Zusammenfassung

Mitochondrien spielen eine wichtige Rolle für die Aufrechterhaltung der zellulären Homöostase, zum Beispiel durch die Generierung von ATP innerhalb der Atmungskette oder deren Beteiligung an dem programmierten Zelltot. Funktionsgestörte Mitochondrien stellen ein Sicherheitsrisiko für die Zellhomöostase dar, und müssen darum schnellstmöglich entfernt werden. Ein wichtiger mitochondrialer Qualitätskontrollmechanismus ist der PINK1/Parkin-Signalweg, der die Zelle vor einer Akkumulierung potentiell pathogener Mitochondrien schützt. Besonders zu Beginn dieses Prozesses spielen posttranslationale Modifikationen eine wichtige Rolle. Diese werden durch die mitochondriale Proteinkinase PINK1 und die cytosolische E3-Ligase Parkin katalysiert. Hier wird Ubiquitin und Parkin während der Initiationsphase der Mitophagie von PINK1 phosphoryliert. Diese Phosphorylierungen aktivieren Parkin, das daraufhin mehrere Proteine der mitochondrialen äußeren Membran ubiquityliert. Gerade in der Initiationsphase von Mitophagie haben sich quantitative Proteomstudien als höchst effizient gezeigt um den Einfluss von PINK1 und parkin zu untersuchen. Allerdings existieren nur wenige Studien, die sich mit den späteren Prozessesn der Mitophagie beschäftigen. Diese sind jedoch besonders für den Abbau der geschädigten Mitochondrien relevant.

Um hier ein detaillierteres Bild zu erhalten habe ich zuerst ein Protokoll zur quantitativen Untersuchung entwickelt und optimiert. Dieses kombiniert die subzelluläre Fraktionierung und die Untersuchung von mitochondrialen Proteinen und deren Ubiquitinierungs- und Phosphorylierungsdynamiken. Um ausschließlich für die Mitophagy bedeutsamen zelluläre Fraktionen zu untersuchen, habe ich die mit zytoplasmatischen, membrangebundenen und löslichen, nuklearen Proteinen angereichten relevanten Fraktionen kombiniert und weiter untersucht. Dieses Protokoll erlaubte außerdem die anschließende Analyse des Phosphoproteomes und Ubiquitylomes, die beide ein hohes Maß an Proteineinsatz erfordern. Desweiteren habe ich verschiedene chemische Peptidemarkierungsstrategien Dimethyl- oder mit „tandem mass tagging“ (TMT) angewendet. Hochauflösende Massenspektrometrie schließlich erlaubte die Anaylse von Dynamiken in Proteinabbau, Ubiquitinierung, und Phosphorylierung während frühen (2-6 h post- Mitophagieinduktion) und späten Phasen (12-18h post- Mitophagieinduktion) von Mitophagie in HeLa Zellen zu untersuchen, die entweder Parkin Wildtyp oder eine Ligase-inaktive Version von

Parkin exprimieren. Die Generierung dieser Zellen, sowie deren Behandlung mit dem Protonophor Carbonylcyanid-m-chlorphenylhydrazon (CCCP) wurden in der Gruppe von Philipp Kahle durchgeführt.

Durch die Integration und weitreichende bioinformatische Analysen der verschiedenen Datensätze zeigte sich, dass Mitophagie anders als bisher angenommen als stufenweiser Prozess stattfindet, bei dem die Ubiquitinierung der Protein ihrem Abbau vorrausgeht. Überraschenderweise spielt die Phosphorylierung der Proteine und das Zusammenwirken von Phosphorylierund und Ubiquitinierung nur eine untergeordnete Rolle in diesem Prozess. Nur in Gegenwart von funktionsfähigen Parkins findet das Zusammenspiel zwischen Protein Ubiquitinierung und Abbau statt und zwar in einem Prozess von Außen nach Innen, bei dem zuerst Proteine der äußeren mitochondrialen Membran, dann an der inneren Membran und schließlich in der mitochondriellen Matrix abgebaut werden.

In einer Folgestudie wurden die Mechanismen untersucht, die zu diesem stufenweisen Abbau von mitochondrialen Unterstrukturen führt. Überraschenderweise offenbarte sich hierbei nicht nur die bereits bekannte Abhängigkeit an lysosomaler, sondern auch von proteasomaler Aktivität. Mithilfe von Massenspektrometrie, konnte ich hier die Befunde der biochemischen Experimente der Kahle Gruppe validieren. Grundsätzlich findet Mitophagie nur in Abhängigkeit von funktionsfähigem Proteasom statt. Eine zeitabhängige Studie, die der in Kombination mit der Induzierung von Mitophagie nach verschiedenen Zeitpunkten das Proteaosm inhibiert wurde ergab, dass besonders äußere Membranproteine wie zum Beispiel TOM70 über den proteasomalen Signalweg abgebaut werden.

Zusammengefasst eröffnet diese Arbeit neue Erkenntnisse über die Mechanismen die der Parkin-abhängigen Mitophagie unterliegen und für weitere Studien an diesem wichtigen zellulären Prozess hilfreich sein werden.

1. Introduction

1.1. Mitochondrial biology

Mitochondria are considered as essential subcellular organelles[1]. They are vital for maintaining cellular homeostasis and viability by fulfilling many functions that exceed their long believed exclusive role as energy producer[2]. However, their multiple functions like aerobic respiration, biogenesis of iron-sulfur clusters or regulation of cellular processes such as cell survival, evolved and were tuned throughout evolution by re-modeling the traits of the mitochondrial progenitor. The evolution of present-day mitochondria, resembling an epicenter of cellular signaling and energy metabolism was only possible with a massive turnover of the original proto-mitochondrial proteome[3].

1.1.1. Origin of mitochondria

A common feature of all eukaryotic cells is either the presence, secondary loss or reductive modification of mitochondria (mitosomes/ hydrogenosomes)[4]. Understanding the origin of mitochondria is an important basis in explaining functionality and specializations of present-day mitochondria, as their biology is directly linked to their function[5]. Furthermore, a deep understanding of the mitochondrial proteome helps in explaining mitochondria-related diseases and development of therapies[6].

The origin of mitochondria goes back to the last eukaryotic common ancestor (LECA), which existed one to two billion years ago[7–9]. A common theory on how the contemporary mitochondria developed is the endosymbiont theory. Here, mitochondria are considered as remnants of an internalized, formally free-living bacterium into a host cell[10]. Many opposing hypotheses have been discussed on the identity of the endosymbiont, the host cell and the internalization process of the endosymbiont itself[11].

Although there is a general agreement that the emergence of eukaryotic cells (eukaryogenesis) is among the most important events that shaped life on earth, there is much disagreement about the involvement of mitochondria in the evolution of this domain of life[12,13]. One hypothesis describes the internalization into an a-mitochondrial proto-eukaryotic host that was similar to modern eukaryotic cells equipped with e.g. the endomembrane system[14]. However, phylogenomic findings support the hypothesis that the mitochondrial progenitor first underwent symbiosis with a member of the

simple organized asgard archaea group and only then developed into eukaryotic cells as we know them today[8,15–18].

Phylogenetic analysis of the mitochondrial DNA (mtDNA) clearly traced back the mitochondrial origin to the gram-negative alphaproteobacterium class[19,20]. Remnants of the bacterial ancestry in contemporary mitochondria are, for example, the bacteria-typical circular DNA, absence of DNA methylation as found in the eukaryotic nuclear genome, and the bacterial derived lipid and protein composition of the outer mitochondrial membrane (OMM) and inner mitochondrial membrane (IMM)[21–24]. However, the precise identity of the alphaproteobacterial lineage giving rise to mitochondria is still not clear. Competing evidence of a mitochondrial origin from an obligate intracellular bacterial parasite lineage like Rickettsiales or the free living Rhodospirillales are still in disagreement[25–27]. Clarification of the mitochondrial progenitor's lifestyle will explain characteristics of the internalization process and the resulting symbiotic lifestyle that gave rise to the present-day mitochondria-eukaryote relationship.

Initially it was proposed that phagocytosis, the intake of organic material by invagination of the host's plasma membrane, was the underlying mechanism of mitochondrial internalization[28,29]. However, the ability of phagocytosis was only acquired after the endosymbiotic event took place[28–30]. Predatory interaction represents an alternative model, in which a protobacterial predator internalized into the host cell and developed from an attenuated bacterial parasite to the mitochondrial organelle[31–33]. Apart from solving the question on how, the question why an alphaproteobacterium got internalized into the archaeal host remains challenging to answer and is lively discussed[34]. The evolvement of a syntrophic relationship, in which the viability of both partners depend on another was hypothesized to be forced by increased oxygen (O_2) levels on earth that made adaptations of the anaerobe archaeal cell living in marine sediment inevitable[17,35]. Teaming up with the proto-mitochondria would have allowed the host protection against toxic oxygen and supplied the endosymbiont with a proton acceptor in the last step of oxidative phosphorylation (OXPHOS) of the energy metabolism process[36,37]. However, metabolic reconstruction points towards a reverse flow model, in which syntrophic H_2 exchange from the archaeal host to the bacterial symbiont was the driving force behind the evolving relationship[38,39].

Although many mysteries on the evolvement of present-day mitochondria persist, it ultimately led to the transformation from an independent bacterium to a fully integrated and semi-autonomous organelle[40].

1.1.2. Role of mitochondria in eukaryogenesis

Throughout evolution, functional specialization of the mitochondrial progenitor was prompted by adaptations in their compartmentalization[41]. Mitochondria consist of two membranes, the OMM and the IMM that are separated by the aqueous intermembrane space (IMS), and the innermost matrix. Each of these highly specialized subcompartments needed fine-tuned adaptations when the endosymbiont evolved into a fully integrated organelle[42].

Only by symbiosis with the alphaproteobacterium did the first eukaryotic cell gain an energy source sufficient to push forward the developments that enabled the present-day features of eukaryotic cells. In fact, this enabled a ~ 5,000-fold increase in energy consumption for protein biosynthesis in contrast to prokaryotic cells alone[43,44]. This in turn allowed for experimentation with new protein families, as it was declared that 1,421 novel proteins emerged relatively early during eukaryogenesis[45]. These newly acquired proteins are related to intracellular trafficking, signal transduction, ubiquitin-based protein degradation, but also to cytoskeletal and RNA-processing, facilitating novel competences like phagocytosis[44,45].

Endosymbiotic gene transfer (EGT), the transfer of originally mitochondrial genes to the eukaryotic nucleus sealed the symbiotic relationship between endosymbiont and host: neither can the mitochondrion act without nuclear encoded genes, nor can nuclear genes be expressed without the mitochondrial power[46]. In contrast, redundant bacterial genes e.g. for lipopolysaccharide (LPS) biosynthesis were lost throughout evolution[47]. Although highly dependent on the eukaryotic organism, a small number of genes remain in the mitochondrial matrix, ranging from three genes in *Plasmodium falciparum* to 100 in *Jakobidis Andalucia*[48–50]. Human mtDNA encodes for thirteen genes that are members of the mitochondrial protein translation machinery and energy metabolic respiratory chain[51,52]. In contrast, 99% of mitochondrial proteins involved in all kinds of mitochondrial function e.g. mitochondrial energy metabolism, protein import or amino acid synthesis are now encoded by nDNA[53]. This transfer did not only make the coordination with the nuclear gene transcription and the cytosolic translation machinery necessary, but also the transport of mitochondrial proteins across the

mitochondrial double membrane system and the sorting into the four main mitochondrial subcompartments[47].

1.1.3. Import and sorting system of mitochondria

As most of the mitochondrial proteins are encoded by nuclear genes, the maintenance of mitochondrial viability requires a dedicated import machinery of mitochondrial proteins[2]. A complex network of import complexes, assembly machineries and chaperons navigate the unfolded mitochondrial precursor proteins from their cytosolic site of translation to their respective target localizations within mitochondria and mediate their insertion and proper folding to gain functionality[54]. Thereby, the import route is defined by targeting sequences that direct proteins to the respective submitochondrial localization[2]. So far, five major import pathways have been described: 1) A cleavable presequence that targets proteins to their final or at least transient localization at the matrix. In contrast, non-cleavable internal target signals are 2) Cys-rich sequences targeting proteins to the IMS; 3) a β-barrel motif that target proteins to the OMM; 4) internal hydrophobic targeting signals that localize carrier proteins to the IMM or IMS; and 5) α-Helical carrying proteins that are targeted for OMM localization[54] (**Figure 1**).

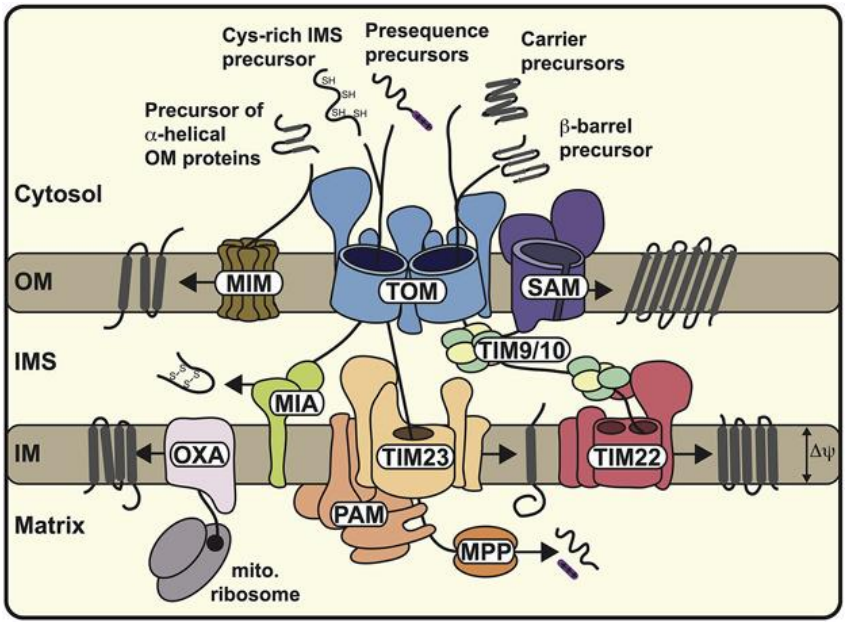

Figure 1: Main routes of the mitochondrial import system. Defined by their submitochondrial targeting sequence proteins are delivered to the OMM, IMS; IMM, and matrix. Adapted from Becker at al 2018[860]

Most of the mitochondrial proteins (~60%) are directed to the matrix, but also IMS and IMM localized proteins are imported via the presequence pathway[55]. The presequence

is located at the protein amino-terminus and consists of an amphipathic helix carrying a positively charged and a hydrophobic surface. The presequence is recognized by cytoplasmic protein chaperons (e.g. Hsp70, Hsp90) that preserve mitochondrial precursor proteins in their import-competent state by protecting them from aggregation and degradation[56,57]. Although rather poorly conserved in their sequence, presequences are highly preserved in length (10-60 amino acids) and charge (+3 to +6)[58].

Next, the mitochondrial matrix targeted proteins are recognized by the main entry gate, which for most mitochondrial proteins is the translocase of the outer membrane (TOM) complex[59]. The complex consists of ten membrane protein subunits: two TOM40 that form a β-barrel twin pore across the membrane, three receptors (TOM70, TOM22, TOM20) that face into the cytoplasm (cis-binding site) and are involved in precursor recognition and three small α helical subunits that surround the pore to stabilize it (TOM5, TOM6, TOM7)[60,61]. Although all three, TOM70 TOM22 and TOM20 partially overlap in their preprotein recognition specificity, TOM70 prefers binding of hydrophobic domains of internal targeting signals, while TOM20 preferentially interacts with N-terminal presequences[57,62–65]. TOM22 stabilizes the whole TOM complex and supports the precursor binding[57,61]. After precursors are recognized, the unfolded or at least semi-folded proteins are threaded through the TOM40 pore[66]. Thereby, the TOM40 channel interior acts as intramitochondrial sorting unit that interacts differently with targeting sequences, and therefore guides them towards different exits of the pore that face to the IMS (trans-binding site). Presequence-carrying proteins leave the pore at the trans presequence-binding site, formed by TOM22, TOM7 and TOM40 that hands over the preprotein to the translocase of the inner mitochondrial membrane (TIM) complex[67]. Proteins without this presequence exit the channel in proximity to TOM5 and the N-extension of TOM40 that ensures further navigation[67]. Proteins with presequence and destined for final, or at least transient, mitochondrial matrix location are further navigated to the TIM23 translocase complex[68]. The TIM23 complex can be divided into three functional domains: (i) receptor domain, (ii) channel and (iii) import motor domain[68]. First, the presequence of the precursor proteins are recognized by TIM50[69]. Mediated by the proton gradient across the IMM, protein precursor carrying the positively charged presequence are transported through the activated Tim23 channel into the negatively charged matrix[54,70]. The ATP-dependent matrix facing presequence translocase-associated motor (PAM) complex is composed of the

mtHSP70 and five additional co-chaperones[68]. This complex pulls the precursor protein into the matrix[71]. Once the precursor protein entered the matrix, the pre-sequence is cleaved off by matrix peptidases like the mitochondrial-processing peptidase (MPP)[72]. It then allows the matrix targeted proteins to fold into their functional three-dimensional structure. Proteins targeted to the IMM can be laterally sorted by the TIM23 complex gatekeeper MRG2 into the IMM (stop transfer) before reaching the matrix[58,73,74]. In addition, IMM localized proteins, such as mtDNA encode members of the ETC (electron transport chain) complexes, use the sorting oxidase assembly (OXA) translocase machinery to be sorted into the IMM[75].

IMS proteins, such as TIM chaperons carry a characteristic cysteine motif[76]. After transportation via the TOM complex into the IMS, the mitochondrial intermembrane space assembly (MIA) oxidoreductase stabilizes the protein conformation by the formation of disulfide bonds[77,78].

β-barrel proteins like the voltage-dependent anion-selective channel (VDAC) are integral membrane proteins of the OMM that are characterized by several transmembrane β-strands an a β-hairpin targeting signal[79]. After their cytosolic synthesis, they are imported into the IMS by the TOM-complex and inserted into the membrane by the OMM localized sorting and assembly machinery (SAM)[80].

Hydrophobic mitochondrial metabolite carriers of the IMM do not possess a cleavable presequence, but several internal targeting sequences[54]. The precursors of the IMM carriers are transported through the TOM complex and interact on the IMS side with TIM chaperons that present them to the carrier insertase TIM22[2].

α-helical OMM proteins are classified according to their integration into the OMM as tail-anchored or polytopic (multispanning) proteins[54]. Although a targeting signal for polytropic OMM proteins is so far unknown, tail-anchored proteins carry an amino- or carboxy-terminal α-helical transmembrane domain that are flanked by positively charged amino acids[2]. Polytopic OMM proteins are first recognized by TOM70, before they are inserted into the OMM by the mitochondrial import (MIM) complex localized at the OMM, while signal-anchored proteins are directly inserted by the MIM complex[81]. In contrast, tail-anchored OMM proteins are import into the OMM simply by integration into the lipid composition of the membrane[82].

The specialization of prokaryotic originating (SAM, OXA) or newly evolved (TOM, TIM23-PAM) mitochondrial import machinery compartments during organellogenesis allows mitochondria to preserve integrity even though the majority of the gene

replication and expression system had been outsourced to the nucleus and cytoplasm[47,83–85].

1.1.4. Cross talk between mitochondria and cell

When the endosymbiont evolved into a fully integrated organelle, bacterial processes like energy metabolism, signal transduction, and biogenesis had to become integrated into the hosts infrastructure[47]. For example, mitochondria cannot be assembled *de novo*, but only increase their number by growth and division of already existing mitochondria (mitochondria biogenesis)[87]. The integration results in certain benefits for the endosymbiont, for example energy conservation by genome simplification[47]. However, since most mitochondrial proteins are encoded by the nucleus and synthesized outside the organelle, a high level of organization between mitochondria and their environment is needed to guarantee proper adaptation, for example in energy metabolism, size and number according to cellular energy demands[47].

1.1.4.1. Biogenesis of mitochondria

Mitochondrial biogenesis is under control of the nuclear encoded peroxisome proliferator-activated receptor gamma coactivator (PGC)-1α transcription factor[88]. PGC-1α first activates nuclear-encoded transcription factors such as the nuclear respirator factor (NRF-1/2)[89]. Next, transcription factors for mitochondrial genes such as transcription factor A (TFAM) and estrogen related receptor alpha (ESRRA) are activated[90,91]. Apart from induction by stress (e.g. cold) PGC-1α is activated at a reduced cellular energy level, that is monitored by high levels of AMP[89,90]. Under conditions of glucose deprivation, starvation or exercise AMP-activated protein kinase (AMPK) regulates PGC-1α activity, thereby promoting mitochondrial biogenesis and ATP production[92–95]. Therefore, PGC-1α is considered to be the master regulator for mitochondrial biosynthesis that coordinates adaptation to long- or short-term cell demands and can even navigate tissue-specific energy demands[92].

1.1.4.2. Communication between mitochondria and other organelles

The communication between host cell and mitochondria is not only unidirectional from the nucleus to the mitochondria in an anterograde way (anterograde cross-talk)[96,97]. In addition, mitochondria can signal via a retrograde mitochondria-to-nucleus signaling

path to impact nuclear gene expression by mitochondrial dynamics (fission and fusion) or cell proliferation by mitochondrial fitness signaling[98–101].

To uphold functionality and to expand the number and size of mitochondria, the lipid content of the OMM and IMM have to be maintained. Lipids of the OMM and IMM are synthesized by the mitochondria themselves or are derived by modified lipids of the endoplasmic reticulum (ER)[47,102]. The ER and mitochondria are physically linked by the ER–mitochondria encounter structure (ERMES) complex, which plays an important role in e.g. phospholipid biosynthesis[103,104]. Phosphatidylcholine (PC) and phosphatidylethanolamine (PE) make up most of the lipid bilayer content of both the OMM (~83%) and IMM (75%)[105]. One way of PC synthesis involves the ER, in which the precursor phosphatidylserine (PS) is first synthesized before proteins of the IMM transforms PS into PE, which is then re-shuttled to the ER to generate PC[106]. In addition, the mitochondria-ER contact is important for calcium homeostasis, mtDNA replication and mitochondrial fusion and fission[107].

Furthermore, mitochondria are hooked up to the cytoskeleton network[47]. Notably, actin filaments are involved in mediating mitochondrial dynamics (fusion and fission), mitochondrial biogenesis and metabolism, distribution into daughter cells during mitosis as well as trafficking[108]. Especially in elongated cells (e.g. neuronal cells), local energy demands need to be covered by mitochondria trafficking[109]. Thereby, mitochondria connect to motor proteins (actin-based myosins, or microtubule-based kinesin1 and dyneins) via OMM-localized Miro and adaptor proteins TRAKs (trafficking kinesin-binding proteins) for mitochondrial repositioning[110].

1.1.4.3. Fitness signaling of mitochondria

Apart from direct physical contact with their environment, mitochondria can communicate their fitness by the release of signaling molecules (**Figure 2**). These strategies impact the gene expression, catabolic adaptation, response to inflammation, cell fate, functional remodeling and cell death[96].

The tricarboxylic acid (TCA) cycle is connected to the ETC and also generates many metabolic intermediates that act in both anabolic and metabolic reactions. Therefore, metabolite levels of the TCA cycle can serve as a readout for overall mitochondrial viability and cellular energy levels[96]. Among others, TCA cycle intermediates e.g. α-ketoglutarate or fumarate, acetyl-CoA represents the bona-fide example on how intermediates of the TCA cycle modulate cell fate[96]. Acetyl-CoA is the starting point of

the TCA cycle and thus vital to keep this metabolic hub running. It can be generated from different sources like mitochondrial-localized oxidation of pyruvate, β-oxidation of fatty acids or by the degradation of amino acids (leucine, isoleucine, tryptophan)[96]. Conversely, acetyl-CoA can be used as precursor to synthesize fatty acids, steroids, or amino acids (glutamic acid, proline, arginine)[111]. Therefore, acetyl-CoA levels mirror the availability of precursors and occupancy of the TCA cycle. At the nucleus, acetyl-CoA can regulate gene expression by serving as substrate for histone acetylation[112]. Mitochondrial dysfunction can lead to a decrease in acetyl-CoA levels and low levels of histone acetylation that ultimately results in the disregulation in gene expression[113]. On the other side, high levels of acetyl-CoA reflect a state of high energy that lead to hyperacetylation of histones and the expression of genes involved in cell growth and proliferation[96].

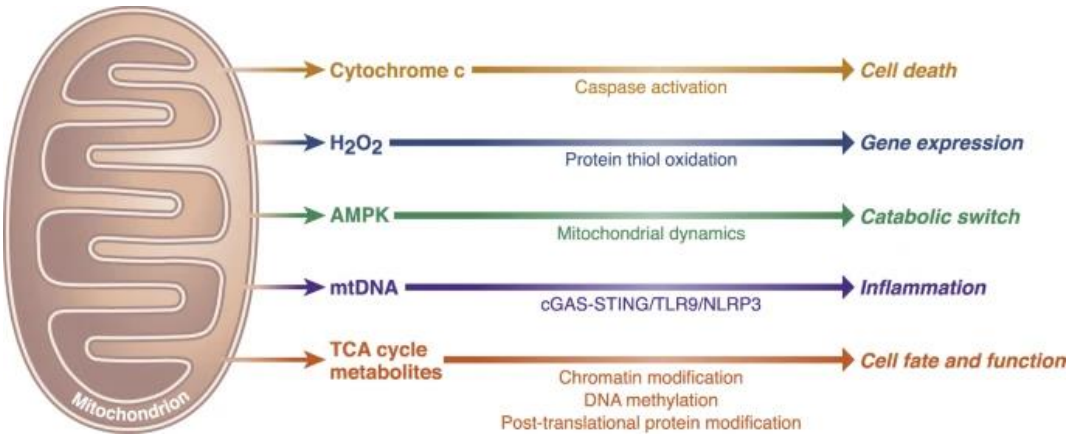

Figure 2: Communication of mitochondrial fitness signaling. The mitochondrion informs the cellular and extracellular environment on their functionality by the release of e.g. metabolic intermediates. Thereby mitochondria can keep cellular homeostasis, activate repair mechanisms and even trigger cell death. Adapter from Martínez-Reyes, and Chandel, 2020[96]

Reduction in the cellular ATP- and an increase in AMP-levels reflect an impairment of the mitochondrial energy metabolism. High levels of AMP activate the cytosolic AMPK, resulting in the phosphorylation of the OMM protein mitochondrial fission factor (MFF), mediated by the mitochondrial fission initiator dynamin related protein 1 (DRP1)[114]. Therefore, AMPK was shown to reprogram cellular energy metabolism by induction of mitochondrial fission and degradation of dysfunctional mitochondria under conditions of low cellular energy levels[94,115].

The term reactive oxygen species (ROS) describes unstable molecules such as hydrogen peroxide (H_2O_2), hydroxyl radical (OH^-), singlet oxygen ($^1O_2$) and superoxide (O_2^-) that are byproducts of the OXPHOS energy synthesis system. They have a

damaging effect on proteins, lipids or nucleic acids that can generate more ROS, and also execute signaling activity[116]. ROS are mostly produced by mitochondria and can therefore serve as a mitochondrial health status report for the cell[117]. For example, the ROS H_2O_2 transmits signals by oxidizing thiol groups of proteins that alter nuclear gene expression of e.g. heat shock proteins[101,118].

Apart from its role as electron carrier during OXPHOS and antioxidant that protects against damaging ROS, the release of cytochrome c from the IMS into the cytoplasm is part of the intrinsic apoptosis pathway[119]. Apoptosis takes place in multicellular organisms and is either activated by death receptor signaling (extrinsic pathway) or mediated by mitochondrial signaling (intrinsic pathway). By unbalancing the sensitive antagonistic interplay between pro- and anti-apoptotic members of the B-cell lymphoma 2 (BCL-2) family, mitochondrial outer membrane permeabilization (MOMP) becomes activated[120]. Once released into the cytosol, cytochrome c binds to the apoptotic protease activating factor-1 (APAF-1), that further oligomerizes into the apoptosome. This activates the initiator caspase-9 that further triggers a caspase signaling cascade leading to global protein cleavages and nucleus condensation[119]. Upon losing the mitochondrial membrane potential, mitochondria themselves become aberrant in their dynamics and fragment[120].

Mitochondria are also involved in the response to inflammation because of the immunostimulatory activity of mtDNA. During bacterial or viral infection or apoptosis, mtDNA is released into the cytosol where it activates the cyclic GMP-AMP synthase-stimulator of interferon genes (cGAS-STING) signaling. Since the mtDNA still carries some bacterial features derived from their ancestor, cytosolic localized mtDNA is recognized as “foreign” and triggers response mechanisms against pathogenic invasion e.g. interferon beta (IFN-β)[121,122]. Furthermore, released mtDNA can be transferred to neighboring cells, as a stimulus to activate cellular inflammation[121].

1.2. Functions of mitochondria

Mitochondrial activity is highly complex since this organelle impacts almost all cell processes ranging from traditional energy metabolism- a remnant of the original endosymbiont- to cell fate decisions that has been acquired throughout evolution when mitochondria became a fully integrated organelle. Other mitochondrial functions were re-targeted, for example β-oxidation of long-chain fatty acids that can be performed by both, mitochondria and peroxisomes[123]. Since 13-18% of the peroxisomal proteins

show an alphaproteobacterial origin it was suggested that peroxisomes represent a simplified mitochondrion, specialized for the β-oxidation pathway[124].

1.2.1. Architecture and dynamics define mitochondrial function

Mitochondria consist of four subcompartments (OMM, IMS, IMM, Matrix) that allow for compositional and functional specialization (**Figure 3A**). For example, compartmentalization can benefit the metabolic efficiency due to an increased concentration of metabolites, a reduced diffusional distance of substances and an optimized milieu that supports chemical reactions within the compartment. In addition, it offers protection from damaging intermediates (e.g. ROS) that are contained within the compartment[33]. Furthermore, mitochondrial functionality is maintained by forming a highly dynamic network that constantly undergoes fission and fusion events (**Figure 2B**).

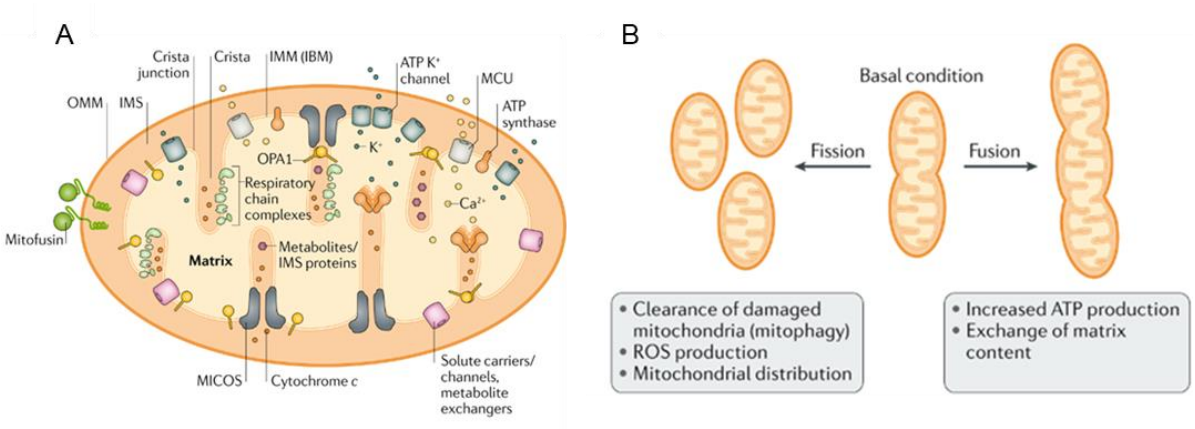

Figure 3: Mitochondria architecture defines functionality. A) Mitochondria are subdivided in the four compartments, outer mitochondrial membrane (OMM), inter membrane space (IMS), inner membrane (IMM) and matrix. Cristea increase the IMM surface to extend the oxidative respiration capacity. B) Mitochondria undergo constant fusion and fission. Thereby mitochondrial dynamic helps to determine the health status of individual organelles and allow adaptation to changing environmental conditions (e.g. mow energy levels) and stress (ROS production). Adapted from Giacomello et al. 2020[125]

1.2.1.1. Outer mitochondrial membrane (OMM)

The OMM serves not only as diffusion barrier for cytosolic or IMS molecules bigger than 5 kDA, but also functions as organellar signaling hub that is involved in a multitude of signaling pathways[125]. The bona fide example for OMM-mediated signaling is the programmed cell death (apoptosis). Here, a multitude of signaling events at the OMM such as the interplay between Bcl-2 family members, lipid composition or membrane dynamics precede MOMP. The OMM additionally participates in organelle-organelle communication by membrane contact sites (MCSs). These sites of close proximity

(~30 nm) are best described by the mitochondria-ER contact e.g. to allow exchange of phospholipids[106]. Furthermore, MCSs with the plasma membrane or peroxisomes can modulate cell fate, Ca^{2+} homeostasis, or allow for metabolic exchange[125]. The OMM contains few channels with a broad spectrum to transport ions and small hydrophilic metabolites. VDACs and the relatively newly discovered acyl-dihydroxyacetone phosphate reductase (AYR1), and the two additional anion-selective channels (OMC7 and OMC8) with so far undefined substrates mediate the selective transport across the OMM[126]. In addition, several β-barrel (TOM40, SAM50, MDM10) and one α-helical (MIM1) protein transporter reside within the OMM, responsible for the translocation and sorting of most mitochondrial proteins into their respective subcompartments[127].

1.2.1.2. Inner mitochondrial membrane (IMM)

The second mitochondrial membrane (IMM) became highly specialized for energy production throughout evolution by increasing the membrane surface and therefore capacity for oxidative phosphorylation through invaginations (cristae)[102,128]. Negative curvatures of the IMM are induced by the non-bilayer forming properties of the phospholipid PE and Cardiolipin (CL), the latter exclusively found in the IMM[105,129,130]. Furthermore, cristae form different functional micro subcompartments: segments of the inner boundary membrane (IBM) that are parallel to the OMM carry members of the IMM import machinery. Cristae membranes which harbor members of the ETC system, are separated by cristae junctions that prevent diffusion of ions and membrane proteins[131]. Here, members of the mitochondrial contact site and cristae organizing system (MICOS) complex are enriched playing important roles in mitochondria architecture, phospholipid metabolism and protein import[132]. Furthermore, the MICOS complex connects the IMM with the OMM, by interacting with various members of the OMM proteome (e.g. TOM complex). Since the ERMES complex was often found in proximity to the MICOS complex, the mitochondria-ER contact might regulate mitochondrial dynamics[131,133,134].

1.2.1.3. Inter membrane space (IMS)

Although being the smallest of the two mitochondrial aqueous subcompartments, the IMS has important functions as an exchange platform of metabolites, lipids or proteins[135]. Segregation by cristae of the IMM is mirrored in the IMS, that segregates in the OMM/IMM enclosed part and the lumen within cristae (intercristae space). Local

concentration of IMS proteins was suggested to aid protein import and to counteract the oxidizing environment generated by the OXPHOS system[78,135]. This includes chaperons (TIM9/TIM10), proteins with a dual protease/chaperon function (YME1) and proteins involved in the retro-translocation of IMS proteins to the cytosol for protein degradation[135–137].

1.2.1.4. Mitochondrial matrix

Several vital carbon metabolism and protein biosynthesis reactions take place in the mitochondrial matrix. Among these are the TCA cycle or β-oxidation of fatty acids. Maintaining some parts of the mtDNA also preserves the DNA processing and protein translation machinery. As a remnant of the bacterial origin, mtDNA together with proteins involved in replication and transcription (e.g. mtDNA polymerase, transcription factors) are organized in nucleoids that are tethered to the IMM[138]. The micro-organization of the nucleoid separates the central core with mtDNA and the DNA replication system from the periphery with proteins that are part of the transcription and translation machinery[139].

1.2.1.5. Mitochondrial dynamic

In contrast to well-known textbook schematics of mitochondria, depicting them as steady bean-like structures, mitochondria are highly plastic and form a dynamic network that constantly undergoes fusion and fission (**Figure 3B**)[140]. To maintain mitochondrial homeostasis and integrity, both processes are well balanced[141]. During mitochondrial fission initiation the cytosolic GTPase DRP1 is activated and recruited to the OMM localized MFF, or mitochondrial fission protein 1 (FIS1)[140]. Next, DRP1 wraps around a pre-defined constriction side of the OMM in an oligomeric ring-like form[142,143]. Thereby, the constriction site selection is driven by ER-mediated actin filament polymerization and bending of the membrane[144] A complete division of the mitochondria is achieved by the action of dynamin-2 (DYN2)[145]. In case of high energy demands, mitochondria tend to undergo fission events, as it was hypothesized that this increases membrane surface area and therefore enhances OXPHOS activity[146]. While mitochondrial fission results in small and round shaped mitochondria, mitochondrial fusion generates a tubular and branched mitochondrial network with mixed matrix content. During mitochondrial fusion, OMM- anchored GTPase mitofusin (MFN1/2) and IMM localized optic atrophy protein 1 (OPA1), mediate the fusion of OMM and IMM

respectively[147,148]. Both events can be spatially coordinated at ER-mitochondria contact sites that allow fast adaptations in stress situations[140]. Mitochondrial fusion helps in restoring mitochondrial function while the reverse process of mitochondrial fission initiates the removal of damaged mitochondria that are beyond repair[149].

1.2.2. Mitochondrial energy production

Mitochondria represent an important signaling organelle involved in all major cellular pathways[150]. However, their major function lies in the production of ATP for cell homeostasis[40]. During highly complex biochemical reactions, pyruvate becomes oxidized to CO_2 by oxidative phosphorylation (OXPHOS) that is coupled to ATP production Thereby, mitochondrial respiration covers 95% of the cellular ATP generation flagging this organelle as the “powerhouse of the cell”[78]. Mitochondrial energy production involves 1) the mitochondrial matrix localized fatty acid oxidation that feeds its products into 2) the TCA cycle. The reduced cofactors generated during the TCA cycle fuel the 3) IMM localized ETC to utilize the chemiosmotic power of protons to generate ATP[151]. Membrane localized ADP/ATP carriers ultimately export the generated ATP into the cytosol where it is further transported to sites of local energy demands (**Figure 4**)[152].

During catabolic fatty acid β-oxidation, the beta carbon of the fatty acid is oxidized to a carbonyl group, thereby breaking apart two carbon-long acetyl-CoA molecules and generating NADH and $FADH_2$[153]. Acetyl-CoA serves as primary substrate in the TCA cycle for enzymatic oxidation, while the co-factors NADH and $FADH_2$ feed their electrons directly into the ECT[111]. Depending on the fatty acid length the β-oxidation pathways is a series of four (for short and medium long fatty acids) or two for (long fatty acids) enzymatic reaction that cleaves off acetyl-CoA from fatty acids[154]. The enzymatic generation of acetyl-CoA from very long fatty acids is localized at the IMM and is mediated by the very long chain acyl-CoA dehydrogenase (VLCAD) and the single trifunctional protein (TFP). In contrast, matrix localized 2-enoyl-CoA hydratase (ECH), 3-hydroxyl-CoA dehydrogenase (HAD), and 3-ketothiolase (KT) together with the acyl-CoA dehydrogenase (ACAD) catabolize short and medium long fatty acid chains[154].

The TCA cycle is an eight enzymatic reaction loop, which is considered to be one of the most important metabolic hubs[96]. Although present in the cytoplasm of the archaea host, only mitochondria possess the TCA cycle in present-day eukaryotes[33]. One

important hallmark of the TCA cycle is that it accepts multiple substrates at any point of the circle to be replenished (anaplerosis)[96,155]. In one round of the TCA cycle, one acetyl-CoA is oxidized in two molecules of CO_2 thereby generating one ATP and three NADH and one $FADH_2$ that are fed into the ETC complex I and complex II, respectively[96].

All five members of the ETC, Complex I (NADH:ubiquinone oxidoreductase), Complex II (succinate dehydrogenase), Complex III (coenzyme Q:cytochrome c reductase), Complex IV (cytochrome c oxidase), and Complex V (ATP synthase) are integrated into the IMM -although complex II does not span the membrane. All complexes consist of multiple subunits that are encoded by both, mtDNA and nDNA (complex I: 44mtDNA/ 7 nDNA, Complex II: 4 mtDNA, Complex III: 11 mtDNA/ 1 nDNA, complex IV: 20 mtDNA/ 4 nDNA and complex V: 19 mtDNA/ 2 nDNA)[156]. It was hypothesized, that mitochondria exclusively kept the DNA to encode for these complexes, to be flexible in local energy demands[157]. TCA and OXPHOS are inseparably coupled, as oxidized NADH donates its electron pair to complex I and FADH2 donate electrons to Complex II[158]. From complex I and II, electrons are transferred to ubiquinol (Q). The now reduced ubiquinol (QH_2) gives its electrons to Complex III that re-targets them to cytochrome c. Finally, cytochrome c gives the electrons to Complex IV that transfers in total eight electrons and four protons from the IMS pool to molecular oxygen that becomes reduced to two molecules of H_2O. The transfer of electrons results in pumping of four protons each of Complex I and III. A total of eight protons minus two that are used for the reduction of oxygen are pumped by Complex IV. This imbalance by the electrochemical proton gradient results in the mitochondrial membrane potential ($\Delta\Psi$). Finally, the protonmotive force, established by the potential gradient (~150-160 mV) and proton concentration (~0.5 pH units) is used to fuel one phosphate to ADP by Complex V. The $\Delta\Psi$ plays an additional important role in e.g. mediation of membrane trafficking or initiation of mitophagy[159]. While proton pumps line the flat areas of cristae, the complex V dimers (ATP synthase) settle at the edges to allow protons to “sink” deeper towards the cristae edges and therefore increase ATP synthesis[160]. Of note, high-resolution imaging present different membrane potentials in the mitochondrial cristae population, hinting at a safeguard level (if the membrane potential of one break down, this does not ultimately affect total mitochondrial energy production) and/ or assigning different functions to cristae (e.g. energy metabolism vs. ROS signaling)[161].

ADP/ATP shuttling is one of the first and last steps during OXPHOS. Monomeric ADP/ATP carrier (AAC1/2/3/4) transport the discharged ADP back to the site of OXPHOS and export recharged ATP into the cytosol[152].

ROS are generated as byproduct of the ETC through electron leakage (0.15 – 5%) mainly from complex I and III[162]. Electrons of complex III escape into the IMS and the matrix, while electrons of complex I exclusively leak into the mitochondrial matrix[163]. The toxicity of ROS is contained by the protective ROS-scavenging system[164]. Reaction of leaking electrons to O_2 generates superoxide anions (O_2^-) that can further dismutate by the mitochondrial matrix localized manganese superoxide dismutase (MnSOD) or IMS localized Cu/Zn SOD to hydrogen peroxide (H_2O_2)[156,165]. These can either diffuse through the OMM into the cytosol to act as second messenger in cell signaling (e.g. muscle cell differentiation) or become neutralized by e.g. glutathione (GSH) peroxidase to water[163,166]. However, enzymatic anti-oxidation by ROS quenching is not perfect. Therefore, ROS-induced damage can result in base substitutions, missense mutations, and deletions within the mitochondrial genome[167].

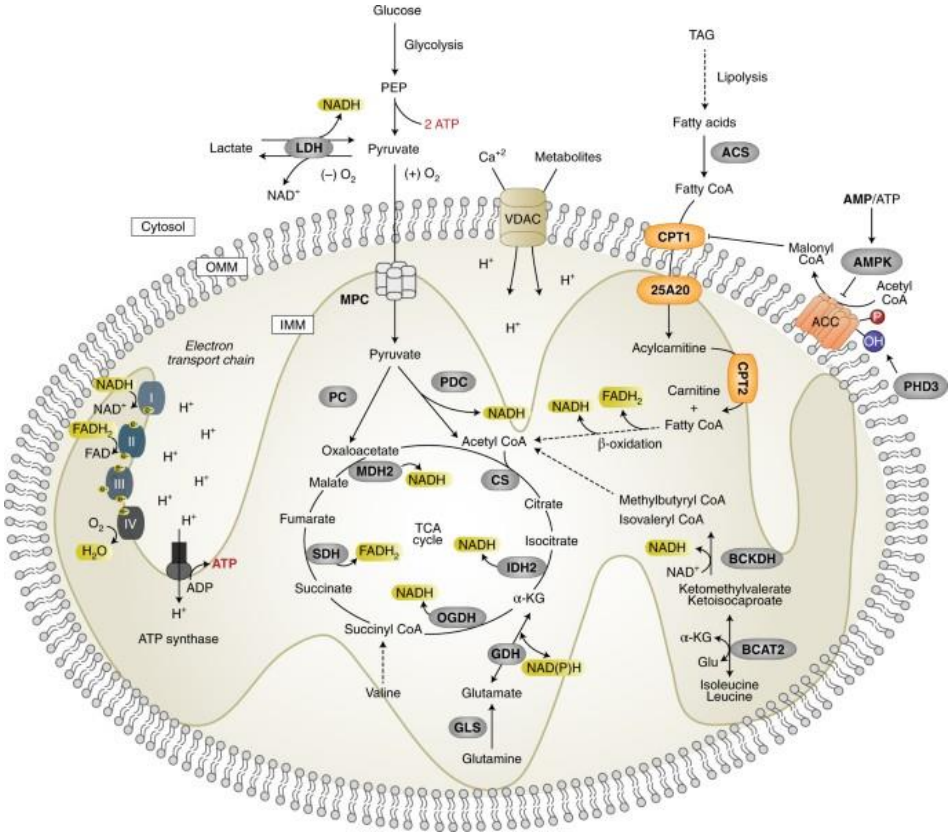

Figure 4: Mitochondrial contributions to cellular metabolism. Mitochondria are the main producer of cellular ATP that is generated by the cooperating actions of the β-oxidation of fatty acids, the tricarboxylic acid (TCA) cycle and the electron transport chain. The TCA cycle generates reduced co-factors that are needed to generate a proton gradient across the IMM. Intermediates from different metabolic processes (e.g. Glycolysis, β-oxidation of fatty acids), can be fueled into the TCA cycle. Adapted from Spinelli et al 2018[168]

1.2.3. Biosynthesis pathways localized in mitochondria

Mitochondria are involved in a multitude of cellular processes like calcium homeostasis, amino acid and nucleotide metabolism, fatty-acid catabolism, as well as lipid, quinone and steroid biosynthesis- most of which are interlinked with each other[2]. Mainly localized to the cytoplasm, mitochondria participate in the fatty acid synthesis (mtFAS) involving the key-mediator acyl-carrier protein (ACP)[169]. Apart from its function in the reverse β-oxidation of fatty acids, ACP was found to play a vital role in e.g. Fe/S cluster biogenesis and assembly of the ECT[170].

In addition, mitochondria are the site of iron-sulfur (Fe-S) cluster assembly, an inherited process from the bacterial progenitor. These cofactors are essential for electron transport proteins of the ETC (complex I, II and III), enzymatic activity (e.g. mitochondrial aconitase of the TCA cycle) or adaptation to oxidative stress (superoxide response [SoxR] protein)[171]. The mitochondrial Fe-S cluster assembly machinery consists of 14 subunits that operate at the mitochondria matrix and provides precursors for cytosolic/nuclear Fe-S cluster assembly. First, the cysteine desulfurase (NFS1) generates persulfide ions that form together with iron ions a 2Fe-2S cluster at the scaffold iron-sulfur protein (ISC). Next, the glutaredoxin chaperon mediates the transfer to target proteins[172]. Alternatively, two 2Fe-2S cluster can be delivered to the matrix-localized iron-sulfur assembly protein (ISA) complex to generate 4Fe-4S clusters, an important cofactor for polymerase stability[173].

Apart from the ER, mitochondria have the highest cellular Ca^{2+} storage capacity[174]. This buffering capacity (50-500 nM) protects the cell from Ca^{2+} overload[175]. Ca^{2+} is transported across the OMM and IMM via VDACs or by mitochondrial calcium uniporter (MCU) into the matrix[174]. Furthermore, many mitochondrial functions such as metabolism, dynamics, apoptosis signaling are regulated by Ca^{2+} levels and were found to be disturbed in diseases like cancer[176].

1.3. Mitochondrial quality control (MQC)

The constant exposure to various stresses, like ROS, or impaired mitochondrial import makes mitochondria especially vulnerable for dysfunctionality[177,178]. To preserve mitochondrial functionality, they are monitored by stringent quality control mechanisms. This involves several lines of damage recognition, repair mechanisms like separation of damaged mitochondria by fission or content exchange by mitochondria fusion, selective removal of damaged mitochondria (mitophagy) and the

biogenesis of healthy new mitochondria[146]. Failure of the MQC system is often connected to the development of severe diseases[6].

1.3.1. High copy number of mtDNA

In contrast to nDNA, mtDNA does not exist in only two but roughly 1000 copies per cell, with 1-10 copies within a single nucleoid that undergoes cell-cycle independent continuous replication with a half-life of seven to ten days[138,179] . The high transcription rate of mtDNA is reflected by a high level of mRNA produced. For example, in the human heart ~30% of total mRNA is generated by mitochondria[180]. As all of the thirteen mtDNA encoded proteins give rise to members of the ETC or are involved in the synthesis of these it is not surprising, that defects related to mtDNA replication and gene expression can have severe outcomes[181]. In contrast to nDNA, mtDNA is not protected by histones, making it especially vulnerable to point mutations, small- and large-scale deletions or duplications[182]. Therefore, the proximity to the frequently generated ROS increases the likelihood of mutations in mtDNA to 10-20-fold that of better protected nDNA[87]. An additional source of mutations in mtDNA is introduced by e.g. replication errors[183]. These mutations generate a pool of wild-type and mutated mtDNA variants within a single cell (heteroplasmy)[179]. Depending on the severity of the introduced mutation, mitochondrial function can endure threshold levels of about 60-90% of aberrant mtDNA as long as some wild-type mtDNA remains to provide functionally active proteins[179,184,185]. The selection of wild-type over mutated specific mtDNA has been shown during early oogenesis in e.g. fly or mouse model[83,186,187]. The success of this selection process is especially important, since mitochondria and therefore mtDNA is subjected exclusively to maternal inheritance in most species[188,189]. In a bottleneck effect, only fittest mitochondria and consequently the healthiest mtDNA are selected for transmission to the next generation, while less efficiently ATP producing mitochondria (with putative highly mutated mtDNA) are removed via mitophagy[186].

1.3.2. Dynamics of MQC

Early studies on mitochondrial fusion and fission events, showed that the knockout of either fusion-mediating MFN1/2 and OPA1 or fission-organizing DRP1 have severe or even fatal impact[190–192]. Mitochondrial fusion events can buffer the negative effects of damaged mtDNA by dilution with wild-type DNA between different organelles to

preserve a minimal mitochondrial activity[193]. Mitochondrial Stomatin-like protein 2 (SLP2)-dependent hyperfusion following cytosolic protein translation stress was found to increase mitochondrial ATP generation as a pro-survival adaptation[194]. Furthermore, mitochondrial recycling by refreshing the pool with “healthy” mtDNA has been suggested. For example, neuronal damaged mitochondria are transported from axons to the cell body for repair as an alternative mechanism for mitochondrial degradation[195].

Mitochondrial fission, lead to a high number of fragmented mitochondria. Thereby, the membrane potentials of the fragmented mitochondria reflect their OXPHOS activity levels that serves as a readout of mitochondrial health status[196]. Consequently, a low membrane potential results in low OXPHOS efficiency and therefore flags putative mutation prone mitochondria that are henceforth excluded from the mitochondrial network and are degraded[146]. The decision between either mitochondrial biogenesis or mitophagy is reached by the DRP1 fission site. While fission at the mitochondrial center promotes mitochondrial proliferation, fission towards the periphery segregates damaged mitochondria for degradation[197]. The type and severity of the stress decides between mitochondria fusion and fission to counteract mitochondrial damage and to preserve cellular homeostasis[196]. Mitochondrial fission mediating DRP1 and fusion mediating MFN1/2 even cooperate to mediate transient fusion events, e.g. to refurnish stationary neuronal mitochondria at distinct cellular locations with fresh mtDNA from motile mitochondria to maintain a pool of “healthy” mtDNA[198].

1.3.3. Selective clearance of damaged mitochondria

Several layers of defense exist, to protect against the accumulation of defective mitochondrial proteins and disrupted mitochondrial functionality. A complex network of cytoplasmic control mechanisms involving chaperons and the ubiquitin-proteasome system (UPS) detects and removes misfolded proteins that fail proper mitochondrial import[177,199]. In addition, each mitochondrial subcompartment harbors chaperons (e.g. mtHsp60, mtHSP70) and proteases (e.g. ATPase associated with various cellular activities proteases [AAA proteases]) that aid proper folding and removal of superfluous, mislocalized or damaged proteins[200].

During severe and irreversible damage of mitochondria, more extreme measures such as the clearance of damaged mitochondria are used to protect overall cell homeostasis (**Figure 5**). Further damage by dysfunctional mitochondria is prohibited for example by

clearing damaged mtDNA from the heterogeneity pool of all mtDNA that would otherwise distribute between healthy and damaged mitochondria[87]. Although being the most extensively studied pathway, several other pathways exist for the selective clearance of damaged mitochondria independent of PINK1/Parkin activity[201]. For example, the receptor- or mTOR/AMPK-mediated pathway[202,203]. Both the serine/threonine kinase PINK1 (phosphatase and tensin homologue-induced kinase 1) and the E3 ligase Parkin are categorized as Autosomal Recessive Parkinson´s Disease (ARPD) genes as they are frequently mutated in early onset PD[178,204,205]. Although impairment in PINK1/Parkin-mediated mitophagy is mostly connected to Parkinson´s disease it also plays roles in cardiovascular or prion disease, and cancer[206–210].

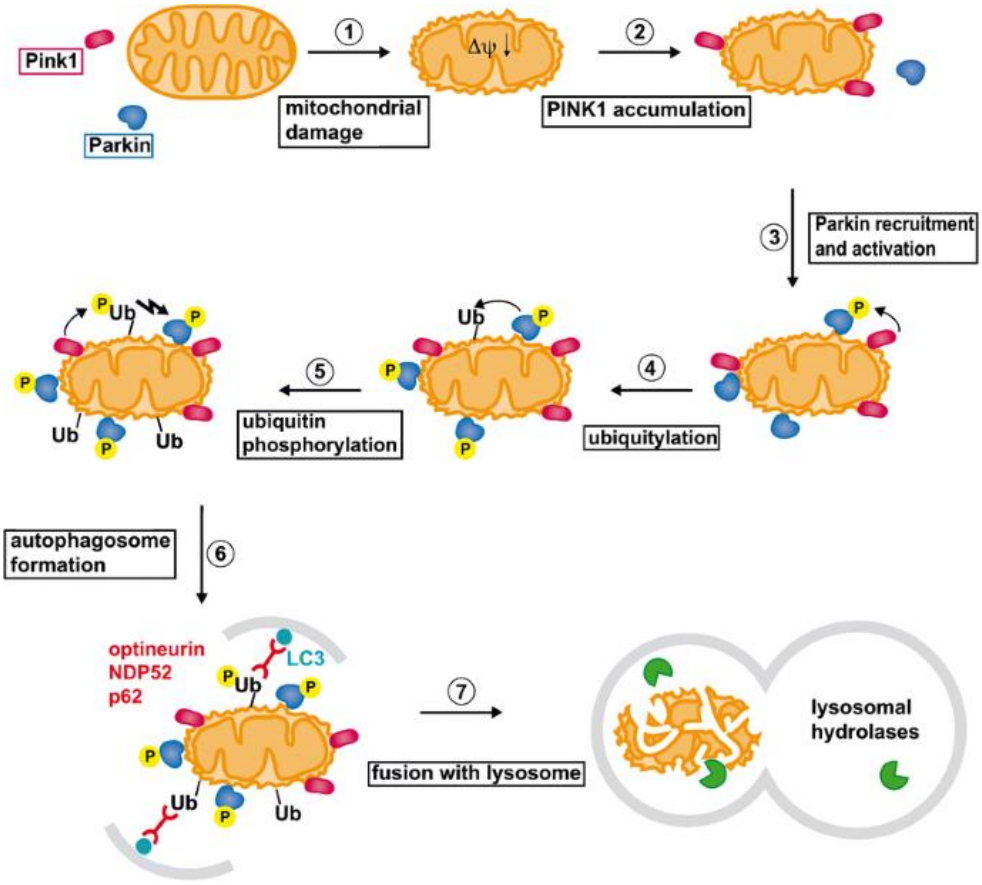

Figure 5 Selective clearance of mitochondria by PINK1/parkin-dependent mitophagy. 1) Mitochondrial damage is reflected by decreased functionality (low activity of the ETC) resulting in low membrane potential (Δψ). 2) The Δψ-driven import and degradation of PINK1 is impaired in damaged mitochondria, leading to the accumulation of PINK1 at the OMM. 3) PINK1 phosphorylates ubiquitin (not shown) and Parkin (within its UBL domain) on S65 fully. This recruits the fully activated parkin to the mitochondria. 4-5) Here, parkin generates a carpet of short polyubiquitin chains with distal PINK1-mediated phosphorylation events. 6) These multi-ubiquitylation pattern attracts e.g. p62/SQSTM1 that further induces autophagosome formation. 7) Damaged mitochondria are fully degraded upon fusion of the autophagosome with lysosomes. Adapted from Rüb et al. 2017[240]

One of the most upstream events in PINK1/Parkin-dependent mitophagy is the activation of PINK1[211]. Like most mitochondrial proteins, PINK1 is encoded by the nucleus and needs to be imported into mitochondria after synthesis. An N-terminal mitochondrial targeting sequence of PINK1 is recognized mainly by TOM70 of the TOM-complex[212]. Driven by the mitochondrial membrane potential, PINK1 is transported to the mitochondrial matrix. Here, the mitochondrial targeting signal is cleaved by the MPP[213]. The truncated PINK1 is further inserted into the matrix where it is subsequently cleaved within its transmembrane domain by the PINK1/PGAM5-associated rhomboid-like (PARL) protease[214]. Finally, PINK1 becomes retro-transported to the cytosol for proteasomal degradation according to the N-end rule[215]. Under stress conditions that disrupt the electrochemical potential across the membrane or accumulation of protein aggregates within the matrix, PINK1 import is arrested[216]. This leads to an accumulation of PINK1 at the OMM in dependency of the TOM complex (TOM7-mediated OMM-tethering) or even within the TOM40 channel[212,217]. Thereby, a negatively charged motif close to the transmembrane domain strengthens PINK1 OMM localization[217]. Autophosphorylation on Ser228/S402 fully activates PINK1, now capable of phosphorylating ubiquitin, polyubiquitin and Parkin[204,218–221].

PINK1 phosphorylates ubiquitin on serine 65 (phosphoUb) and to a minor extend threonine 66[222]. PhosphoUb leads to both, gain-of and loss-of functions: only in the phosphorylated state can ubiquitin function as allosteric activator of parkin[219,223,224]. In contrast, phosphoUb inhibits the ubiquitin system, since many E2/E3 ligases (e.g. Parkin) cannot utilize this modified version for poly-ubiquitin chain assembly and most deubiquitinates (DUBs) fail to hydrolyze phosphoUb-chains[221].

Parkin is a cytosolic E3 ligase that once activated transfers ubiquitin molecules from an E2-conjungating enzyme like the ubiquitin-conjugating human enzyme 8 (UbcH8) to a substrate localized to the OMM[225]. Apart from the ligase-mediating RING domains, Parkin possesses an N-terminal ubiquitin-like domain (UBL) that regulates further Parkin-activity[226]. Same as for ubiquitin, catalyzes PINK1 phosphorylation of Parkin at S65 within its UBL domain, that convert parkin from its autoinhibitory to the fully activate form[227]. After these two activating phosphorylation steps, Parkin is stabilized in its open, activated form and together with phosphoUb and VDAC assembles in a 500 kDa complex at the OMM[228,229]. Once activated, Parkin generates a carpet of short ubiquitin chains on OMM, such as VDAC1, without recognition of a defined sequence

motif on these target proteins[230,231]. To prevent a refusion with healthy mitochondria, MFNs are among early substrates of Parkin-mediated ubiquitylation[232]. Parkin generates mostly mono and short K63, K48, K11, K27 and K6 linked polyubiquitin chains[233–235]. Approximately 20% of ubiquitin attached to mitochondrial proteins are phosphorylated by PINK1, mostly on mono-Ub or the distal Ub of polyubiquitin chains[234,236]. The ubiquitylation of MOM proteins recruits the autophagosome assembly machinery that further delivers the damaged mitochondria for lysosomal degradation. First p62/SQSTM1 (sequestosome-1) is recruited to damage mitochondria by recognition of polyubiquitin chains[231,237]. p62/SQSTRM1 further aggregates at the OMM, thereby attracting the microtubule-associated protein 1 light chain 3 (LC3) of autophagosomes[238]. Alternatively, are the OMM proteins BNIP3, FUNDC1, PHB2 recognized LC3[239]. The double membrane autophagosomes engulf the mitochondria and ultimately fuse with lysosomes for final destruction of the damaged mitochondria. However, not all mitochondrial proteins are degraded via the lysosome. Instead, OMM proteins such as MFN 1/2 or Miro1 are extracted from the membrane and degraded via the AAA ATPase VCP/p97 that facilitates subsequent proteasomal degradation[233].

1.3.4. Diseases related to mitochondria

Due to their important roles in metabolism, bioenergetics and involvement in many different cellular pathways, it is not surprising that disturbances in mitochondrial functions can result in a variety of different pathogenic phenotypes[6]. Mitochondrial genes with human disease-related observation are mostly assigned to mitochondrial metabolism (27%) and OXPHOS (21%), and mostly linked to diseases of the central nervous system and metabolism diseases[241]. Damaged mitochondria are characterized by high levels of ROS, low ATP:ADP ratios, decreased levels of oxidized cofactors (e.g. NAD^+), impaired mitochondrial biogenesis, dynamics and MQC, and alteration in signaling such as correct life or death decisions[242]. Especially organs with high energy demand (e.g. heart, neurons, skeletal muscles) are prone to mitochondria-related diseases[243]. Mitochondrial diseases are classified into primary- mutation in nDNA or mtDNA that lead to impaired mitochondrial function, and secondary diseases-mitochondrial dysfunction, a down-stream effect that arises from mutations outside mitochondrial action[242]. Therefore, mitochondria are an important target for the development of novel therapeutic approaches. By now, more than 150 mitochondrial-

related diseases have been described, most related to defects in the respiratory chain[244]. Therefore, tremendous efforts are put into development of therapies against mitochondrial diseases, as of 2020 there are 49 registered clinical trials targeting notably the reduction of ROS or CL[245].

1.3.4.1. Mitochondrial DNA diseases

Although very small in comparison to the nuclear encoded DNA, more than 300 deleterious mutations (point mutations, deletions or duplications) have been associated to the 16 k base pairs mtDNA[244]. Two kind of mutations of mtDNA had been described as source for mitochondrial disease: i) single-base changes and ii) large-scale partial deletions[179]. A prominent example for a single-base exchange is the A3243G or A8344G mutation in the gene of the mitochondrially encoded tRNA leucine 1 (MT-TL1)[246]. Under healthy conditions, it functions as tRNA and transfers the amino acid leucine to the newly synthesized polypeptide strand. Given that mitochondrial expressed genes play key roles in vital pathway, this tRNA abnormality has serious impact on cell viability and can ultimately result in the severe mitochondrial Myopathy, Encephalopathy, Lactic Acidosis and Stroke-like episodes (MELAS) syndrome, Maternally-Inherited Diabetes and Deafness (MIDD) or Myoclonic Epilepsy and Ragged-Red Fiber disease (MERRF)[247,248].

Large-scale partial deletions of mtDNA can affect notably tRNA or COX activity, as observed for the Chronic Progressive External Opthalmoplagia (CPEO) disorder and Kearns Sayre Syndrome (KSS)[249–252]. Furthermore, mutations in the mitochondrial replication system e.g. in the nuclear encoded polymerase γ can lead to a severe loss in mtDNA, associated with tumorgenesis[253,254].

1.3.4.2. Mitochondria disease accumulation during aging

Mitochondria related diseases accumulate throughout aging, caused by an increase of dysfunctional mitochondria that are marked by e.g. a high content of mutated mtDNA or reduced efficiency of the MQC system[242,255]. Therefore, it was proposed that by slowing down mitochondrial biogenesis (e.g. by blocking mitochondrial import mechanisms) and the subsequent rewiring of mitochondrial pathways, can prolong an organisms lifespan[255]. Mitochondrial biogenesis is an important target for therapies not only in context of aging, but also in promoting metastasis. For example, the transcription factor PGC-1α is abused by invasive breast cancer to increase

mitochondrial biogenesis and therefore ATP production to promote metastasis[256]. In addition, many neuronal diseases had been linked to an impaired mitochondrial transport. Defects in the anterograde mitochondria transport (site of mitochondrial biogenesis into axons), result into unanswered local energy demands. In contrast, during impaired retrograde transport in which damaged mitochondria are no longer transported back for degradation or repair[195]. There is a multitude of evidence, that both events are vital for mitochondrial integrity and connection to pathologies[257,258].

One bona fide example for mitochondrial disease during aging is the neurodegenerative disorder Parkinson's disease (PD)[259]. Dopaminergic neurons in the substantia nigra are very sensitive to dysfunctional mitochondria and this ultimately results in the PD-typical loss of these cells. Among other functions, PD is strongly connected to disturbances in mitophagy since mutations in the genes of mitophagy mediating PINK1 and PARK2 are well established marker proteins for Parkinson's disease[260].

1.4. Discovery proteomics

Proteomics provides tools to assess all proteins present at a distinct time and under defined conditions in a specific cell, tissue or organism[261]. Studying the proteome can be challenging, as in comparison to the parental DNA counterparts (~20-25,000 genes in human), the proteome is greatly increased in number of proteoforms (several million)[262,263]. Derived from a single gene, a protein is individualized by e.g. alternative splice forms, single amino acid polymorphisms, or PTMs (proteoform)[264–266] . Inherent challenges to investigate the proteome arise from the limited sample material, that cannot be amplified like DNA; the dynamic range of protein expression that can vary up to seven orders of magnitudes; and the enormous number of PTMs[261,267]. Mass spectrometry-based proteomics is an approach that takes up this challenge and moreover enables for the large-scale analysis of complex suits of proteins and sub-proteomes, such as the phosphoproteome or ubiquitylome[261,268]. Proteomics can be classified into discovery and targeted proteomics. While discovery proteomics aims to study the maximum number of peptides in a sample, targeted proteomics aims for the focused analysis of a defined subset of analytes[269].

To investigate the proteome, three basic strategies have been developed so far: i) top-down ii) middle-down and (iii) bottom up proteomics[270]. In top-down analysis, intact proteins or protein complexes can be analyzed by mass spectrometry. This allows

conclusions on e.g. genetic variations, alternative RNA splicing and post-translational modification on biological active molecules[271,272]. However, challenges in protein solubility, protein separation and ionization efficiency limit the broad application of this strategy[272]. In contrast, in bottom-up proteomics also described as shotgun proteomics, proteins are first digested into peptides by one or more proteases before measurement[270,273]. Here, higher order structures of extracted proteins are broken by high concentrations of denaturizing agents such as urea. Furthermore, disulfide-bonds between cysteine residues of the proteins are reduced and alkylated until the proteins remain in their primary structure with an optimal protease accessibility[274]. Most commonly, the endopeptidase trypsin is chosen for protein digestion, cleaving C-terminal of the amino acids arginine and lysine[275]. Combinatorial or alternative peptidases like Lys-C, Asp-N, Glu-C) are often applied[276]. The extra step in sample preparation and the resulting complexity in data processing is compensated by more profound data acquisition due to the smaller number of charges per peptide and increased sample homogeneity as in comparison to top-down approaches[277]. To compensate for the increased sample complexity that impacts ion suppression and data quality, different protein/peptide separation techniques are applied such as one- or two-dimensional gel electrophoresis, ion exchange or reversed phase chromatography[278,279].

1.4.1. Post-translational modification of proteins

More than 400 PTMs have been described, which append a new level of diversity and complexity to the regulation of protein activity, stability, localization, turnover, signaling, interaction and many more[280,281]. Protein modifications can occur during (co-translational) or after translation (post-translational) at specific amino acid residues[280]. PTMs are very beneficial for cells, since they can transmit internal and external signals very fast (milliseconds as in contrast to minutes and hours for protein expression), economize energy consumption (otherwise spent to generate new proteins), are reversible and allow for PTM-dependent multitasking of protein function[282–284]. PTMs are classified as irreversible and reversible modification. An example for irreversible PTM is the proteolytic cleavage during the maturation of insulin[285]. Reversible modifications are further classified according to the modification which can be (i) a chemical group (e.g. phosphorylation, acetylation, methylation), (ii) a complex molecule (glycosylation, AMPylation) or (iii) a polypeptide (e.g. ubiquitylation,

SUMOylation)[284]. In many cases, “writers” (e.g. ubiquitin ligase) add a PTM that is recognized and further evaluated by “readers” (e.g. ubiquitin binding domains) before removed by “erasers” (e.g. deubiquitinases)[286]. PTMs are concentrated to specific amino acids that can be targeted by several PTMs, with a maximum of 15 different modifications described for the amino acid lysin[287]. Although PTMs can occur in theory at any of the respective residues within the polypeptide chain, functionally active PTMs show a bias towards intrinsically disordered structures and exposed amino acids[288].

Interestingly, PTMs can be in cross-talk with each other on the same (intra-protein PTM crosstalk) or between multiple proteins (inter-protein PTM crosstalk)[289]. This cross-talk involves the competition for the same amino acid reside (e.g. ubiquitylation and acetylation on lysine), modification of a PTM (e.g. phosphorylation/acetylation of ubiquitin) and the cross-reaction of PTMs within proximal (PTM hot-spots) or distal modification sites[289,290].

Since PTMs are able to change a proteins function, it is not surprising that they are involved in many fundamental cellular processes (e.g. gene expression) and that dysregulation can have severe impacts, ultimately leading to diseases such as cancer, diabetes or neurodegenerative diseases[286,291].

1.4.1.1. Phosphorylation

Protein phosphorylation describes the reversible addition of a phosphoryl group (PO_3^{-2}) from e.g. the ubiquitous donor ATP to the functional hydroxyl group of serine, threonine, tyrosine, or hydroxyproline (*O*-phosphomonoester), a nitrogen of histidine, arginine or lysine (*N*-phosphoramidates), the thiol group of cysteine (S-phosphothioesters) or the carboxyl group of aspartic acid (phosphoanhydrides)[292–294].

In eukaryotes, the most prominent amino acids modified by phosphorylation are serine (86%), threonine (11.8%), and tyrosine (1.8%) with phosphorylated serine, being the most reported PTM type in general[280,283,295].

Phosphorylation adds a negative charge and thereby increases the hydrophilic character of the modified protein. This facilitates its interaction, spatial orientation within and between proteins, subcellular localization or the regulation of cellular processes like cell cycle, growth factor stimulation or apoptosis (**Figure 6**)[283,292,296–298].

Dynamic phosphorylation and dephosphorylation are catalyzed by protein kinases and phosphatases, respectively and phosphate groups can function as “on” or “off” switches for cellular processes[299]. This includes among others the cell cycle,

metabolism and gene expressin[300,301]. Here, the cellular significance of kinases is highlighted by the prominent representation in the human genome: 2% (530) of all human genes encode for kinases[302]. Due to their important roles in for example signaling cascades, kinases represent attractive targets for drug development with 71 approved drugs by the Food and Drug Administration- (FDA) in 2021[303]. Protein kinases are classified based on the residue they phosphorylate, such as bispecific like serine/threonine kinases or tyrosine kinases. Kinases typically recognize a sequence motive which consists of flanking amino acids surrounding the target phosphorylation site. These motives can be highly specific for different kinases[304,305]. In contrast, much fewer phosphatases (~40) counteract kinase activity in humans[306]. Given, that 70% of all human proteins become phosphorylated at any point of their life cycle, the overall complexity of kinase/-phosphatase substrate network is very high[307].

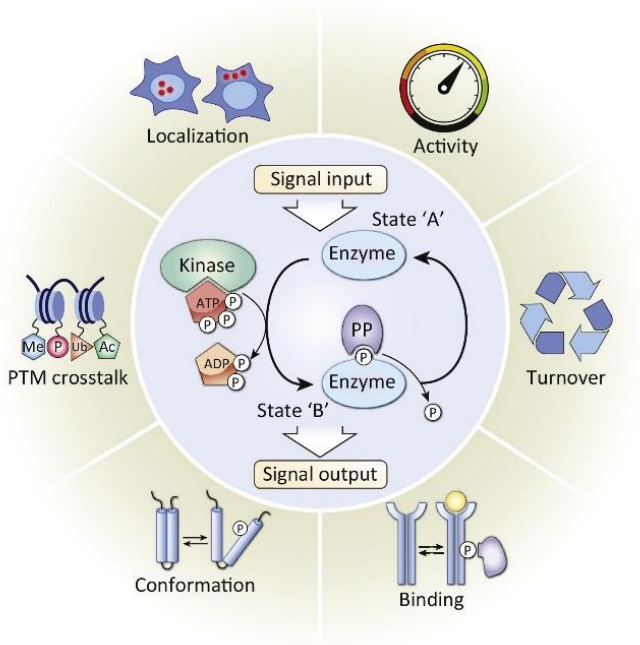

Figure 6 Protein phosphorylation as dynamic switch for the regulation of cellular functions. Phosphorylation and dephosphorylation are mediated by protein kinases and phosphatases (PP). The addition of the negatively charged phosphoryl group impacts protein fate by modulating e.g. its activity, localization or interaction. Adapted from Humphrey et al. 2015[299]

1.4.1.2. Ubiquitylation

The 76 amino-acid long ubiquitin represents the most prominent member of the ubiquitin family, only existing in eukaryotes[308]. In common with other members like NEDD8 and SUMO, they possess a signature ubiquitin fold and a C-terminal Glycine-Glycine (GG) residues that becomes attached to a target primary amino group, like ε-

amino group of lysine[308]. Due to the seven internal lysine residues (K6, K11, K27, K29, K33, K48, and K63) and the modifiable protein N-terminus of methionine of ubiquitin, proteins can not only be modified by a single ubiquitin (mono-), but also by branched chains of ubiquitin molecules (polyubiquitin) (**Figure 7**). The resulting polyubiquitin chains give rise to a tremendous level of variation by the different number of ubiquitin molecules, the linkage type (homo-/heteroubiquitin chain) and the option for a branched architecture[309]. Therefore, post-translational modification by ubiquitylation allows for more specific fine tuning of biological processes as compared to for example phosphorylation (switch “on”/”off”)[310].

The transfer of ubiquitin to a substrate is mediated by a three-step enzyme cascade (E1-E3)[308,311]. First, the C-terminal glycine of ubiquitin is activated in dependency of ATP by the E1 (activating enzyme) and transferred to a cysteine of the E2 (conjugating enzyme). The ubiquitin loaded E2 enzyme transfers ubiquitin to the complex of the E3 (ligase) and the substrate. The substrate specificity is thereby defined by the E3 protein, which is also reflected in the sheer number of different E3 ligases (> 600 in human) in comparison to E2 (35 in human) and E1 (two in human)[312–314]. The categorization of the E3 ligases into for example Homologous to E6AP Carboxy Terminus (HECT) proteins, UFD2 homology (U-box) proteins, and Really Interesting New Gene (RING) proteins distinguish the actual ubiquitin transfer mechanism[312]. During the last ligase step, the C-terminal glycine of ubiquitin is attached to the ε-amino group of lysine or the N-terminus[315]. For the formation of polyubiquitin chains, several mechanisms had been reported that describe the one-by one and the “en-bloc” addition of ubiquitin that is mediated by singly or multiple E2/E3 ligases[316]. Deubiquitinates (DUBs) function as erasers of the ubiquitinylation signal, that in turn are regulated via post-translational modifications[317]. They differ in their substrate and polyubiquitin chain linkage specificity, and the number of cleaved ubiquitin (like diubiquitin)[310]. For example, most members of the ubiquitin proteasome system (USP) system show a clear substrate but not ubiquitin linkage specificity[318].

The ubiquitin code on proteins determines the biological readout of this PTM[319]. Thus, protein ubiquitylation is virtually involved in any biological process like regulation of cell cycle, cell death and signaling[320–322]. Monoubiquitinylation on for example histones is mostly associated with DNA transcription and repair, that was often found to be misregulated in cancer[323]. Protein ubiquitylation can occur at any stage of the target proteins life time. However, the K48 and to a minor extend K63 polyubiquitin chain

linkage signal for proteasomal degradation and are therefore attached during the end of a proteins lifetime[324]. In addition, K63 polyubiquitin chain linkage was also found to play an important role in DNA damage repair[325]. Less abundant polyubiquitin chains fulfill additional vital biological roles, for example, K6-linked polyubiquitin chains are involved in DNA-damage repair and MTC[318,326].

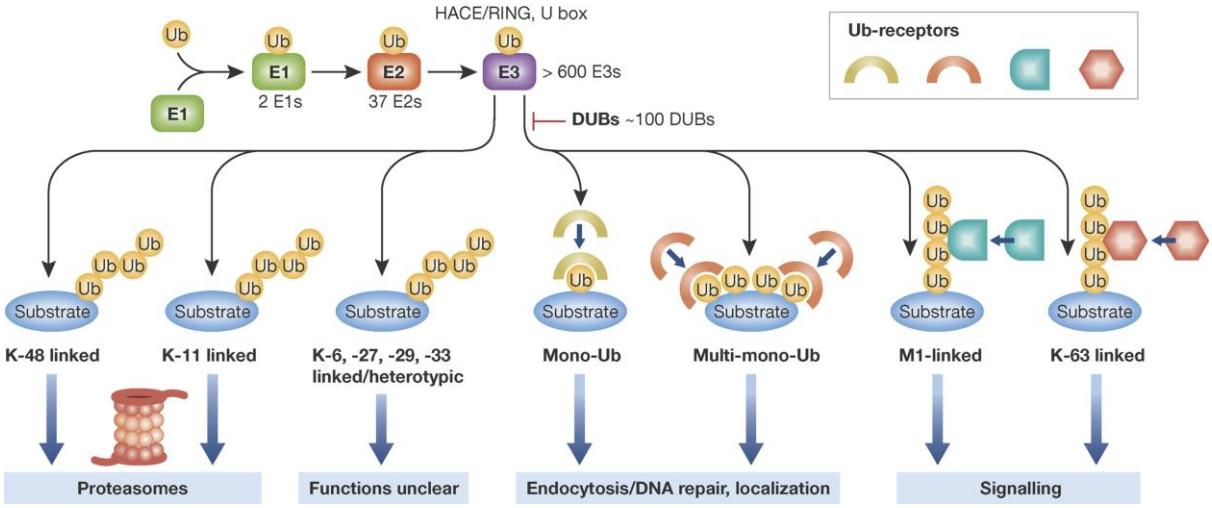

Figure 7 Ubiquitylation mediates cellular functions. In a three-step enzymatic cascade, ubiquitin is transferred to a target protein (Lysine or N-terminal amino group). Due to the seven internal lysine residues, polyubiquitin chains can be build up. Depending on the polyubiquitin chain linkage type and branching architecture (not shown) the biological readout differs from proteasomal degradation e.g. K48 poly ubiquitin chain linkage) to signaling (N-terminal methionine linear chain linkage). Deubiquitinateses (DUBs) serve as erase of the ubiquitin signaling. Adapted from Fulda et al. 2012[327]

1.4.2. Mitochondrial proteome

Due to its ancestry, the mitochondrial proteome is considered as a mosaic of different origins. It was suggested to categorize the mitochondrial proteome into α-proteobacterial, general prokaryotic, general eukaryotic and organism specific proteins[328]. Therefore, it is estimated that out of the ~1,500 mitochondrial annotated proteins only 116-138 (~10%) have an alphaproteobacterial origin[329].

MS has evolved to become one of the most powerful method in defining the complete set of the mitochondrial proteome. Using human placenta, initial studies assigned 46 proteins to mitochondria[330]. Almost 20 years after the initial report and with further developments of this technique, 1,158 proteins were annotated for mitochondrial localization using samples from 14 mouse tissues[331]. This study highlighted that the mitochondrial proteome gains in complexity when considering the diverse specifications of mitochondrial function in different tissues. Adapted to the organellar function, mitochondria overrepresent specific functions like fatty acid oxidation in

skeletal muscle[244,332]. Across 14 mouse tissues, only 63%–88% of the mitochondrial proteome are shared across different organels[74]. These studies evolved further into the MitoCarta3.0 compendium[331,333]. This freely available database contains 1,136 reviewed human mitochondrial genes with submitochondrial specification and categorization into the seven most prominent mitochondrial functions. In 2021, using human cell culture, 1,134 proteins were identified with high confidence as localized to the mitochondria, with 91 proteins newly assigned to this organelle[241]. This revealed that the mitochondria proteome accounts for up to ~10% of the total human proteome[138]. However, while initial studies put an emphasis on mining the mitochondrial proteome, there are still numerous mitochondrial proteins without clear function.

One way to predict a proteins function relay on the definition of its protein-protein interactions (PPIs). For example, biotin proximity labeling approaches assign protein functions by identifying proteins that are in close contact with putative known functions[334]. In 2020, a proximity-dependent biotinylation assay (BioID) assigned the interactome of 100 mitochondrial proteins[335]. Here, marker proteins of multiple submitochondrial localizations were used as baits to define their functional module for example as dual localized proteins, mapping of OMM contact site forming proteins, and defining cross-talk between different functional matrix assemblies[335]. Protein-protein interaction have also been analyzed by copurification (for example by affinity tag-purification) of individual target proteins, or by complexome analysis, in which complexes are purified by for example blue native followed by MS-based identification of the individual assembled proteins[241].

In 2022, 200 clustered regularly interspaced short palindromic repeats (CRISPR)-mediated knockout cell lines for orphan mitochondrial proteins that lack a clear functional annotation were profiled to study effects on their proteome, lipidome and metabolome[336]. This showed the great complexity of mitochondrial protein function to impact many omics-layers and helped explaining the diverse clinical phenotypes observed for mitochondrial gene dysfunction.

Interestingly, quantitative proteomics can even be applied to assign differences in mitochondrial protein import when mitochondrial membrane potential was disrupted. Import of proteins related to mitochondrial translation, TCA cycle and ETC are mostly affected by disrupted membrane potential, while others with no clear biological function show unchanged import[337].

One limitation of MS approaches to uncover the mitochondrial proteome is the precise localization of the proteins to the submitochondrial compartment, as experimentally separating the highly interconnected four mitochondrial compartments can be challenging and is affected by high background noise[338]. Therefore, *in silico* prediction tools have been applied. Initial strategies employed the presence of a mitochondrial targeting sequence to assig mitochondrial localization[339,340]. Further developments such as deep learning approaches can be applied to predict the submitochondrial localization like DeepMito, iDeppSubMito[341,342].

1.5. Mass spectromtry-based proteomics

Tandem mass spectrometry coupled with liquid chromatography (LC-MS/MS) represents a powerful tool to assess a variety of proteomic applications like protein identification/ quantification, large/small scale discovery/targeted approaches[343]. Various applications utilize this method, for example the detection of profiling of proteins and PTMs from a variety of different sources (from cell lines to tissues, and body fluids) in various fields (e.g. biomedicine)[343–345].

1.5.1. High performance liquid chromatography (HPLC)

High performance liquid chromatography (HPLC) has evolved a powerful peptide separation method, which in combination with MS (LC-MS) allows for the most complete coverage of the proteome across a broad dynamic range[346]. Most proteomic approaches apply reversed phase (RP) LC. Here, the stationary phase is nonpolar (for example C4-, C8-, or C18-alkyl chains) and the mobile phase consist of a polar solvent (water and water-organic solvent such as acetonitrile or methanol)[347]. The peptide mixture is separated based on the solubility in the first aqueous mobile phase along its transition into a stronger organic phase in a mostly linear gradient[348]. Based on the different strength of hydrophobic peptide stationary phase interactions, peptide retention on the column differs during elution until the non-polar elution solution matches the peptides hydrophobicity[349]. A high content of uncharged amino acids increases the hydrophobicity of a peptide, resulting in a delayed retention time and thereby later elution from RP columns. In addition, an acid like TFA or FA are added to the mobile phase as proton donor for subsequent peptide ionization[350]. Depending on the application, peptides are separated in a nano- (nl/min) or micro- (µl/min) flow rate. Nano-flow LC-MS (nLC-MS) allows peptides to elute in a more concentrated

fashion with sharper elution peaks, which supports an increased detection sensitivity[351]. However, in contrast to micro-flow (µLC-MS), the risk of sample overloading, which results in a poor peak shape and diminished data quality is much higher[352].

The retention time provides further information on the hydrophobic properties of a peptide and can therefore add an additional layer of confidence in peptide identification[278]. Based on the amino acid sequence of a peptide, dedicated models predict the retention time and can compensate retention time shifts in case of post-translationally modified peptides[353,354].

LC-MS can be performed in an offline or online mode[355]. During offline HPLC, peptide fractions are collected separately and injected one by one into the ion source of the MS[355]. In contrast during online LC, the chromatography interface is coupled to the MS. Once the analyte is released form the column, it is directly transferred to the mass spectrometer. To increase the depth of peptide identification by decreasing sample complexity, consecutive and orthogonal separation techniques are applied that separate molecules based on different molecular properties (multidimensional chromatography)[356,357]. Orthogonal to peptide separation at a low pH, separation techniques like high pH RP LC increases the depth of for example phosphopeptide identification[358].

1.5.2. The mass spectrometer

Mass spectrometry provides a technique to identify and quantify the mass of ionized molecules (e.g. peptide ions) by measuring their mass-to charge (*m/*z) ratio. A mass spectrometer consists of the three characteristic compartments: i) ion source, ii) the mass analyzer and iii) the detector[359]. Hybrid MS instruments additionally contain a fragmentation chamber, in which peptide fragment ions are generated for subsequent peptide sequencing. In standard proteomics measurements, all peptides co-eluting at a specific retention time are recorded in a MS1 spectrum. Next, only a subset of peptides (typically one peptide species) is isolated in the mass analyzer by its specific *m/z* ratio and fragmented before recording the fragment ions (MS/MS or MS2) (**Figure 8A**).

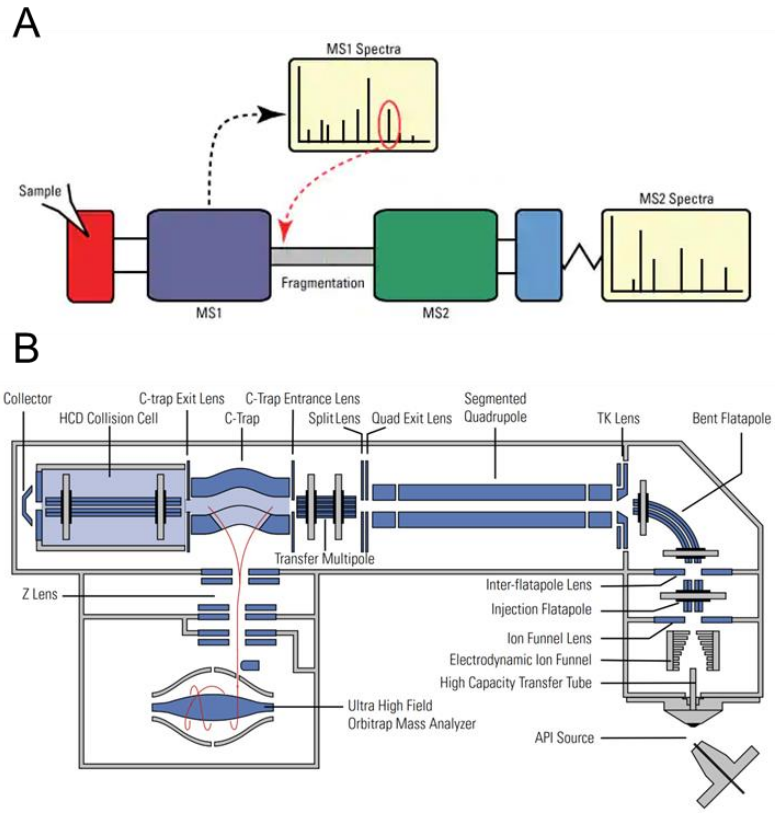

Figure 8 Principle of tandem mass spectrometry (MS1 and MS2/ MS/MS). A) An ionization source transfers the peptides into gas phase (red box). Next mass analyzers (purple, green boxes) separate ions based on their m/z ratios. Finally, a detector measures the ion signal intensities (blue box). Dependent on the instrument setting, additional compartments are added e.g. additional analyzer for tandem mass spectrometry and fragmentation chambers. Adapted from *Thermo Fisher Overview of Mass Spectrometry for Protein Analysis (https://www.thermofisher.com/de/de/home/life-science/protein-biology/protein-biology-learning-center/protein-biology-resource-library/pierce-protein-methods/overview-mass-spectrometry.html)* **B)** Schematic of the Q-Exactive HF-X mass spectrometer. The hybrid quadrupole-Orbitrap mass spectrometer possesses an ion-optics system the guides the ion to the segmented quadrupole, and a collision chamber (HCD collision cell) for peptide fragmentation. Adapted from Kelstrup et al. 2018[360]

1.5.2.1. Ionization of peptides

One major challenge is the transition from peptides in liquid or solid phase to the ionized gas phase without fragmentation of the fragile molecules. Therefore, different peptide ionization strategies have been developed that can be distinguished based on the ionization technique and properties: the site of ionization (*in vacuo*) in the MS vacuum chamber or API at atmospheric pressure, the ionization energy (soft/harsh ionization) or the matrix of the analyte (solid, liquid)[361–363].

Electrospray ionization (ESI) is the standard ionization technique for LC-MS proteomics, as it is a soft ionization method that transfers peptides from the liquid into the gas phase[363]. Peptides elute from the emitter tip of the analytical column form a Taylor cone at high voltages (2- kV) that segue in a jet dispersing in a plume of charged droplets[364,365]. These shrink further and the ionized peptides enter the gas phase. The droplet charge originates from the proton donor like H^+, Na^+ NH_4^+-ions in the acidic

HPLC solvent[366,367]. Usually, tryptic peptides carry a charge state of +2, due to the protonation of N-terminal ammonia and C-terminal basic residues (arginine, lysine) in an acidic buffer[274,368].

Another technique is matrix-assisted laser desorption and ionization (MALDI). This represents likewise a soft ionization technique *in vacuo* or atmospheric pressure (AM-MALDI), restricted to ionization of molecules embedded in a solid matrix[369]. Several hundred laser pulses are shot on the matrix embedded analyte, heating up the matrix and the acidified analytes, thus transferring the peptides into the gas phase as mostly singly charged ions[357].

1.5.2.2. Mass analyzer and detectors

The generated ions are then transferred from the ion source via a strong electromagnetic field (2-6 kV) into the mass analyzer. Afterwards the ions are separated according to their *m/z* ratio in the mass analyzer[370]. The mass analyzers differ in their resolution, accuracy, ion transmission, dynamic and mass range, and speed of data acquisition[357]. The ability to distinguish between two ion spectral peaks (resolution) can be described by the full width at half maximum (FWHM) (M/FWHM with M = *m/z*)[371]. A mass analyzers accuracy is a measure of the accurate measurement of *m/z.* Deviations between the actual and measured *m/z* values of molecule ions can be described in Da or in parts per million (ppm). Ions can be analyzed only within a mass analyzers specific mass range (*m/z*)[372]. The scan speed or scan rate, describes the time an analyzer requires to scan a defined m/z range. Commonly used mass analyzers are quadrupoles that separate ions according to their m/z stability, ion-trap, orbitrap, Fourier Transform Ion Cyclotron Resonance (FTICR) analyzers that utilize ion m/z resonance frequency for separation, or time-of-flight (TOF) analyzers that measure the ion flight time[357,373]. In the final step, ions reach a detector. Here, ion currents are recorded, and amplified to determine the abundance of the ions with a currency of 1.6×10^{-18} A, equal to 10 ions per second[355].

Quadrupole mass analyzer or quadrupole mass filter (QMF) consist of four, parallel rods that apply a radio frequency (RF) voltage between opposing rods[372]. Depending on the voltage applied, only ions with a specific *m/z* value are able to oscillate through the quadrupole[355]. In contrast, ions with non-matching *m/z* value follow an unstable trajectory and ultimately collide with the rods.

Orbitrap mass analyzers consist of three electrodes: two outer cup-shaped electrodes and a central, spindle like electrode. A radial electric field together with the canonical shape allows for an axial oscillating trajectory of the ions[374]. These oscillating patterns are recorded by the outer electrodes and are Fourier transformed into a *m/z* spectrum[374]. Orbitrap mass analyzers offer robust data acquisition with high resolution and mass accuracy. State-of-the-art mass spectrometers (Thermo Fisher Exploris480/ Orbitrap Ascend Tribrid Mass Spectrometer) offer resolutions up to 480,000 and mass error <3 ppm[375].

TOF analyzers utilize a high voltage to accelerate ions within a flight tube. Thereby, the flight time before the ion hits a detector is defined by the *m/z* value of the analyte[376]. The main advantage of the TOF analyzer in comparison to others is the basically unlimited m/z detection range[376].

In tandem MS, two or more mass analyzers are sequentially aligned (tandem in space or time)[361,377]. Possible combinations include multiple detectors of the same type, like triple quadrupole or combinations of different analyzers like linear ion trap (LTQ)-Orbitrap hybrid mass spectrometers (**Figure 8B**)[355,378]. A tandem mass spectrometer can utilize the first mass analyzer (e.g. quadrupole) as a mass filter, only allowing a specific type of ions with defined *m/z* to pass, become fragmented and the resulting fragment ions being further analyzed by a second mass analyzer (e.g. orbitrap)[360].

During peptide fragmentation the parental/precursor ion breaks into daughter/fragment ions that carry the information on the peptide sequence. Thereby, fragmentation takes place in dedicated compartment (fragmentation cells), in which energy is transferred to the selected ions, for example by collision with an inter gas like helium, nitrogen, or argon[377]. Depending on the breakage point within the amino acid sequence a-, b-, or c-ions with their respective counterpart ions x-, y-, z- are generated[274]. Most commonly, the amide bond between to amino acids breaks, giving rise to b-ions (charge is retained by the peptide N-terminus) and y-ions (charge is retained by the peptides C-terminus)[274]. Those fragment ions are recorded in a second MS scan (MS/MS or MS2).

1.5.2.3. Data acquisition modes

In discovery proteomics, proteins are analyzed by the identification and quantification of the corresponding peptides in a data dependent acquisition (DDA) or data independent acquisition (DIA). DDA is a semi-stochastic data acquisition method and often used in high throughput proteomics[379]. For example, in the most commonly used

top-N method only the N most intense ions are selected from full (MS1) scan for fragmentation[380]. To improve the sequencing of ions with low intensities, the repetitive acquisition of high intense ions can be prohibited by a dynamic exclusion or dedicated retention time alignment algorithms[381]. However, DDA suffers from the missing-value problem that arises from low reproducibility of selecting especially low abundant ions between runs[382].

In contrast, during DIA spectra acquisition a scan of the parental ions is omitted. Instead, MS/MS spectra of all co-eluting peptides within a pre-defined *m/z* isolation window, are co-analyzed independent of their intensity[383]. DIA acquisition requires a highly stable chromatographic system to avoid retention time shifts[384]. The gain in reproducibly recording a broader dynamic range comes at the cost of a drastically increased spectra complexity. Dedicated software tools (e.g.OpenSWATH, Spectronaut™, Skyline) help with the identification and quantification of protein, mostly by the aid of in-depth spectral libraries that have been recorded by previous DDA acquisition methods and which have high correlation to their peptide retention time[385– 387].

Peptide identity is determined by matching the acquired MS1/MS2 spectra against a target database[388]. This database is generated by the *in silico* digestion of all hypothetical proteins of the sample resource (e.g. mouse, human). Thereby the digestion mode equals the experimental procedure in terms of the enzyme used for proteolytic digestion, mass spectrometer settings such as ion fragmentation mode (e.g. HCD, ETD) and others. To match the *m/z* spectrum of a measured peptide, it is compared to all *in silico* generated peptide spectra. The accuracy of a peptide-spectrum match (PSM) is shown by the PSM score[389]. Several data analysis platforms for PSMs are available such as MaxQuant with the integrated search engine andromeda, Mascot or SEQUEST[390–392]. To estimate the false discovery rate of the peptide/protein identification, spectra are also searched against a decoy database[388].

1.5.3. Proteomics for PTM analysis

Bottom-up mass spectrometry proved to be a powerful tool in studying PTMs like phosphorylation or ubiquitylation. However, several challenges have to be overcome to ensure accurate detection and correct biological interpretation of PTMs[393]. In comparison to simple protein identification, which usually provides multiple peptides, investigation of PTMs require the measurement of modified peptides, which are often

present with low stoichiometry[394]. Usually, dedicated enrichment strategies are required to concentrate low abundant modified peptides. In addition, the stability of PTMs during sample preparation and data acquisition requires adjustments. Especially labile modifications are instable under certain experimental conditions such as, phospho-histidine that becomes hydrolyzed under acidic conditions[395]. Furthermore, labile modifications (e.g. phosphorylation, sulfonation) are prone to cleave during peptide fragmentation in a tandem MS/MS scan without generating a detailed peptide fragment spectrum, thereby limiting peptide sequencing and modification site localization[394].

The addition of a phosphoryl group to a protein (phosphorylation) changes its hydrophilic character that persists on the respective phosphorylated peptide[292,396]. Like for other PTMs phosphopeptides can be low abundant in a pool of unmodified peptides and a dedicated enrichment method needs to be applied to boost the number of ions ultimately used for data acquisition and localization to a specific amino acid[394]. Common techniques are for example metal oxide affinity chromatography (MOAC) or immobilized metal affinity chromatography (IMAC), as well as antibody-based affinity purification[282]. Most enrichment protocols consist of the three main steps binding, washing and elution. In IMAC and MOAC, the negative charge of the phosphate group binds to the positive charge of the metal ion (e.g. iron or titanium). The low pH of the enrichment buffer (2-3), ensures the deprotonation of the phosphate group and the protonation of negatively charged amino acids (e.g. glutamic and aspartic acid) that would otherwise bind to the metal ion, too[397]. Next, unmodified peptides are washed out. By changing the pH to basic conditions, the phosphate group becomes protonation, thereby dissociating from IMAC or MOAC matrices[397].

In bottom-up proteomics that applies trypsin digestion, the ubiquitin sequence itself is cleaved, leaving only the N-terminal GG-remnant of ubiquitin attached to lysine side chains (KGG). Dedicated antibodies recognize this remnant di-Gly motif and allow for the enrichment of respectively modified peptides[398]. A more unambiguous ubiquitin enrichment method, that is less prone for the enrichment of ubiquitin-like proteins applies for the UbiSite antibody, that recognizes thirteen C-terminal amino acids of ubiquitin[315]. Importantly, during sample preparation of GlyGly modified tryptic peptides, alkylation of reduced disulfide bonds has to be considered. The addition of two molecules of the standard alkylating agent iodacetamide (IAA), result in an identical mass shift as a GlyGly remnant on a peptide and should therefore be replaced by other

alkylating agents (e.g. chloracetamide)[399]. Furthermore, information on polyubiquitin chain architecture usually gets lost after tryptic digestion. However, specialized proteases (e.g. $Lb^{pro}*$) only partially digest ubiquitin within a poly-ubiquitin chain and leaves a truncated version, which still carries chain linkage information (UbClipping)[235]. To correctly assign a PTM (e.g. phosphorylation or GG) to a specific amino acid, proper peptide fragmentation and completeness of the resulting b- and y-ion spectrum are required[394]. During standard collision induced dissociation (CID) fragmentation, the most labile chemical bond such as the phosphoesterbond breaks first. Consequently MS/MS spectra of phosphopeptides can be dominated by the peptide backbone after neutral loss of the phosphate group[400]. To better identify modification sites, dedicated fragmentation methods like multi stage activation (MSA), in which hybrid MS-MS spectra derived from the original peptide fragmentation and the fragmentation of the neutral loss precursor can be applied[401]. Alternatively, electron transfer dissociation (ETD) that only fragments peptide backbones, generate complete b-any y-ion fragment ion series, which allow better site localization assignment[402]. MS/MS spectra of ubiquitin modified peptides can be more complex, since they contain not only b- and y ions of the peptide backbone, but also of the remnant amino acids after protein digestion (i.e. GG)[403].

1.5.4. Quantitative proteomics

Quantitative proteomics extends the field from the mere identification of proteins towards the accurate and reliable quantification of thousands of proteins within and between samples[404]. Therefore, conclusions can be drawn for example on the absolute or relative expression levels, the regulation of proteins or protein modifications between experimental conditions. Several labeling techniques have been developed that are tailored for distinctive biological questions and integrability to the sample preparation workflow (**Figure 9A**)[405].

Quantitative bottom-up proteomic approaches can be classified based on the absolute or relative information acquired. In absolute quantification (AQUA) isotopic-labeled synthetic peptides of known concentration are spiked into the sample to be analyzed[406]. A prior knowledge of, for example, m/z-ratio or charge states of the peptide of interest is indispensable to introduce a physiochemical identical reference peptide. Comparison of signal intensities between the peptide of interest and the reference peptide give information on the stoichiometry of protein complexes or the

concentration of a protein within a sample[407,408]. Major drawbacks of this method are the restricted number of peptides that can be quantified at once and the higher costs that are connected to the synthesis of labeled peptides.

Relative quantification methods are based on abundance ratios of peptides or proteins that are determined by label-free or label-based approaches. Although less accurate in comparison to for example AQUA, label-free quantification (LFQ) methods such as intensity based absolute quantification (iBAQ) overcome this limitation. iBAQ values can be calculated by dividing the summed intensity of measured peptides by the theoretical number of all peptides of this protein[409,410]. Unlike most labeling methods, LFQ allows for protein quantification of an unlimited number of samples without extending sample preparation by time and costs. However, because of the semi-stochastic nature of the mostly applied DDA, many LFQ data suffer from missing values for especially low abundant peptides between samples[411].

Labeled amino acids or labeled tags carrying stable heavy isotopes for example ^{13}C, ^{15}N, ^{18}O, or ^{2}H can be metabolically, chemically or enzymatically introduced into peptide sequences or proteins. Stabile isotope labeling by amino acids in cell culture (SILAC) established as a reliable and most common used metabolic labeling approach[412]. Here, essential, stabile isotope labeled amino acids such as arginine and lysine are introduced during the active metabolic phase of the organism[413]. Therefore, differently labeled samples can be combined at an early stage in the workflow, thereby greatly reducing variations during downstream sample preparation. Choosing trypsin for protein digestion ensures, that all peptides harbor a label and can be used for quantification (i.e. light- or heavy-labeled arginine or lysine). Stable isotopes of an element are, except for their mass, chemically indistinguishable and labeled peptides reveal an identical behavior during sample preparation and LC separation. Only during MS1 data acquisition, peaks of SILAC pairs can be identified by the specific mass shift. As for all MS1 based quantification techniques, SILAC is limited in the number of labeling channels that otherwise increases dramatically spectra complexity. Typically, three labeling channels are used for SILAC (Light, Medium, Heavy) although even five have been reported[295,414]. In addition, full labeling can only be guaranteed for organisms auxotrophic for the respective amino acids. Without the genetical manipulation or careful workflow adaptations, prototrophic organisms like bacteria or plants are mostly excluded from the application of SILAC[415,416]. Although it had been shown for fly and mouse, the application of SILAC for higher organisms is limited, due

to higher economical costs and long preparation times for fully labeled organisms[417,418]. The *in vivo* labeling flexibility of SILAC allows for further applications like the dynamic SILAC approach. Here, one label is substituted by another, leading to a shift in the incorporation of isotopic labels into newly synthesized proteins while the experiment is performed. Therefore, dynamic SILAC remains the method of choice for studying protein turnover[241,419].

Furthermore, a label can be introduced, on the protein or peptide level by enzymatical or chemical reactions[420,421]. Because the label is introduced only relatively late during sample preparation, this quantification strategy can be applied to basically all kind of samples (e.g. cell culture, tissues, biofluids). Same as for SILAC labeling, the addition of a label induces a pre-defined mass shift, that allows for relative quantification on the MS1 (e.g. dimethyl labeling) or the MS2 level (e.g. Tandem-mass tag [TMT]). During dimethyl labeling, primary amino groups (N-terminus and ε-amino group of lysine) are modified with light, medium or heavy isotopologues of formaldehyde and cyanoborohydride (**Figure 9B**)[422,423].

All isobaric labels consist of i) a peptide reactive group, ii) an isotopic reporter group and iii) a balancer group (**Figure 9C**)[424]. During labeling, the reactive group is attached to a specific site in the peptide sequence. Most isobaric labeling strategies (e.g. TMT, iTRAQ) follow a N-hydroxysuccinimide (NHS) chemistry reaction targeting primary amino groups (N-terminus, ε-group of lysine residues). The isotopic reporter group serves for the actual quantification and is unique for each labeling channel. Finally, a balancer group normalizes the respective isotopic reported group, to equalize the total mass of each labeling channel. Same as for dimethyl labeling, pH plays an important role during TMT peptide labeling. Preferred is a slight basic pH (8.0-8.5) to avoid the protonation of the amino group and complete hydrolyzation of the NHS ester[425]. Furthermore, the mass spectrometer needs to meet the requirements of an accurate quantification for example by increased resolution in the low m/z range[426]. Labeled peptides derived from different experimental conditions, have an identical mass that is not distinguishable in the MS1 scan. Only after isolation, fragmentation and for the MS2 or if applicable MS3 scan, the reporter groups break off and can be detected. The resulting fragment ion spectrum contains fragment ions that lead to the identification of the peptide sequence and the isotopic reporter ions in the lower *m/z* range that carry the quantitative information. State-of the art TMT-approaches allow for multiplexing of up to 18 labeling channels in one MS run[427].

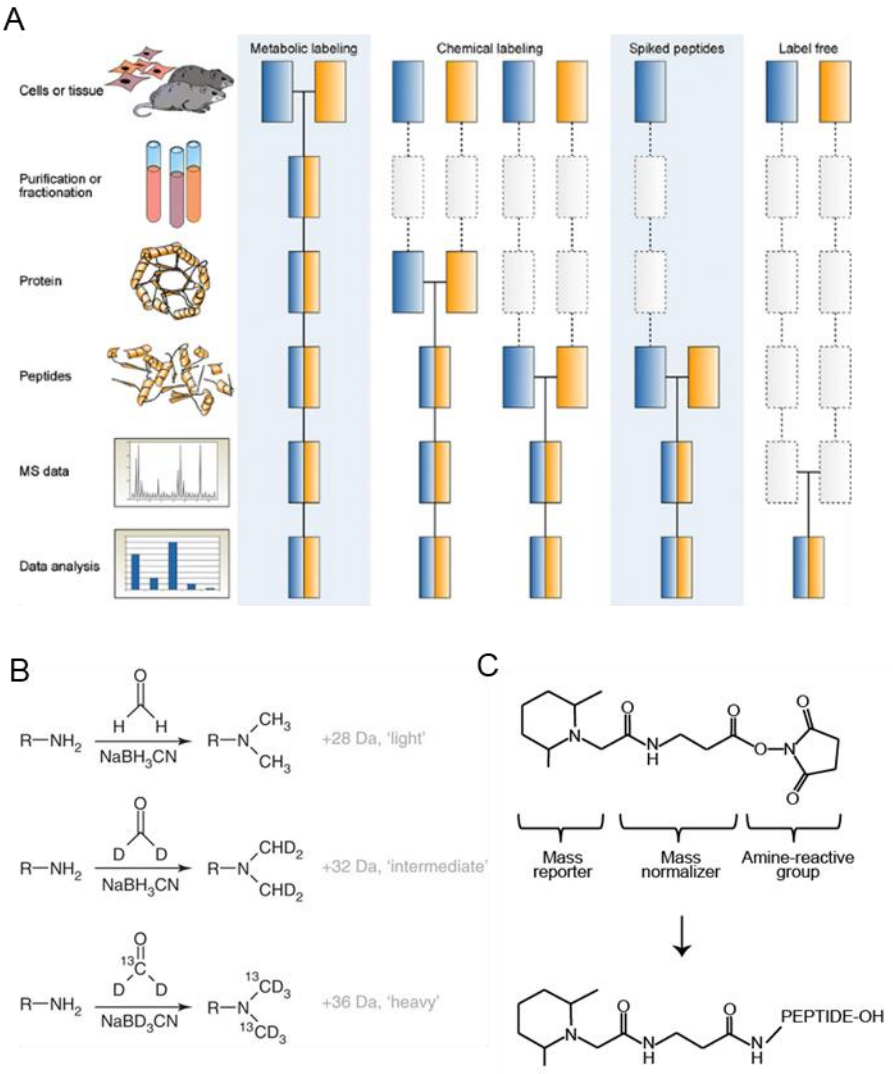

Figure 9: A) Comparison of quantitative proteomic workflow. Depending on the labeling strategy, samples can be combined early (metabolic labeling) or only during the last step in the experimental procedure (label free). Adapted from Bantscheff et al, 2012[405] B) Principle of the dimethyl labeling reaction on primary amines. The combination of (deuterated) formaldehyde and Cyanoborohydride/-deuteride generates a mass increases of 28, 32 or 36 Da. Adapted from Boersema et al, 2009[422] C) Principle of TMT labeling approach. TMT label reagents are composed of an amine-reactive group that interacts with the primary amino group of amino acids, a mass normalized and a mass reporter. Combination of heavy isotopes (^{13}C, ^{15}N) allow for duplex and 6-, 10- 11-, 16-, 18-multiplex. Adapted from Bachor et al; 2019[428].

2. Aims and Objectives

Mitophagy represents a fundamental mechanism for cells to dispose of dysfunctional and putative pathogenic mitochondria. The initiation of this process, involving the activity of PINK1 kinase and the E3-ligase parkin, has been studied in great detail. However, little is known on the involvement of ubiquitylation and phosphorylation on mitochondrial protein degradation during late stages of this process. Therefore, the overall aim of my thesis was to utilize the analytical power of quantitative proteomic tools to study the impact of post-translational modifications on protein dynamics during early and late stages of parkin-dependent mitophagy. An additional aim was the elucidation of pathways involved in mitochondria degradation during late stages of parkin-dependent mitophagy. This involved the establishment of dedicated protocols for sample preparation as well as the integration of the proteome, ubiquitylome and phosphoproteome results during data analysis. In detail, the aims and objectives were:

1.) Temporal analysis of protein ubiquitylation and phosphorylation during parkin-dependent mitophagy
    a. Exploring the best cell fractionation protocol for in-depth studies of the mitophagy-relevant proteome, ubiquitylome and phosphoproteome
    b. Quantifying dynamics of significantly regulated proteins in parkin wild-type and ligase-dead expressing HeLa cells
    c. Quantifying dynamics of significantly regulated ubiquitylation events in dependency of parkin during early and late stages of mitophagy
    d. Quantifying dynamics of significantly regulated phosphorylation events in the progression of parkin-dependent mitophagy with focus on proteins which are doubly modified by ubiquitylation and phosphorylation

2.) Parkin-dependent mitophagy occurs via proteasome-dependent steps sequentially targeting separate mitochondrial sub-compartments for autophagy
    a. Establishment of a quantitative proteomics approach to study proteasomal dependent steps during mitophagy
    b. Application of proteomic techniques to investigate mitochondrial subcompartment degradation on proteasomal activity.

3. Results

3.1. Manuscript I

Temporal Analysis of Protein Ubiquitylation and Phosphorylation During Parkin-Dependent Mitophagy (published)

Mol Cell Proteomics. 2022 Feb;21(2):100191. doi: 10.1016/j.mcpro.2021.100191.

Author contributions:

The study was designed by Anna Lechado-Terradas, Philipp Kahle, Boris Macek and me. After cell treatment and harvest by Anna Lechado-Terradas and Sven Geisler, subsequent sample preparation for LC-MS/MS analysis was performed at the Proteome Center Tuebingen, University of Tuebingen. All Western Blot and microscopy analysis were performed by Anna Lechado-Terradas. Subcellular fractionation, sample preparation for quantitative proteomics, phosphoproteomics and ubiquitylome as well as data analysis was performed by me with supervision from Nicolas Nalpas and Boris Macek. Input for the interpretation came from the MOMbrane consortium (Doron Rapaport) In summary, I am responsible for Figure 1 B/C, Figure 2 A-C, Figure 3 A-C, Figure 4 as well as Supplementary figure 1 B,C,D, Supplementary figure 2, A-C, Supplementary figure 3 A-E, Supplementary figure 4 A-D.

MCP RESEARCH

Temporal Analysis of Protein Ubiquitylation and Phosphorylation During Parkin-Dependent Mitophagy

Katharina I. Zittlau[1,‡], Anna Lechado-Terradas[2,3,‡], Nicolas Nalpas[1], Sven Geisler[2], Philipp J. Kahle[2,3,*], and Boris Macek[1,*]

Mitophagy, the selective degradation of mitochondria by autophagy, affects defective mitochondria following damage or stress. At the onset of mitophagy, parkin ubiquitylates proteins on the mitochondrial outer membrane. While the role of parkin at the onset of mitophagy is well understood, less is known about its activity during later stages in the process. Here, we used HeLa cells expressing catalytically active or inactive parkin to perform temporal analysis of the proteome, ubiquitylome, and phosphoproteome during 18 h after induction of mitophagy by mitochondrial uncoupler carbonyl cyanide *m*-chlorophenyl hydrazine. Abundance profiles of proteins downregulated in parkin-dependent manner revealed a stepwise and "outside–in" directed degradation of mitochondrial subcompartments. While ubiquitylation of mitochondrial outer membrane proteins was enriched among early parkin-dependent targets, numerous mitochondrial inner membrane, matrix, and cytosolic proteins were also found ubiquitylated at later stages of mitophagy. Phosphoproteome analysis revealed a possible crosstalk between phosphorylation and ubiquitylation during mitophagy on key parkin targets, such as voltage-dependent anion channel 2.

Mitochondria are involved in many cellular processes, such as apoptosis, lipid transfer, and cellular energy production. Under stress conditions that compromise their multifaceted functions (1, 2), selective autophagic elimination of mitochondria (mitophagy) is activated. One of the most studied mitophagy pathways is regulated by the serine/threonine-protein kinase phosphatase and tensin homolog–induced kinase 1 (PINK1) and the E3-ubiquitin ligase parkin. Mutations in these proteins have been directly linked with autosomal–recessive familial forms of Parkinson's disease (3, 4). Under basal conditions, PINK1 is constantly imported and degraded within mitochondria (5–7). Once the mitochondrial membrane potential is compromised, PINK1 accumulates at the mitochondrial outer membrane (MOM), where it becomes fully active upon autophosphorylation (8, 9). PINK1 phosphorylates parkin within its highly conserved ubiquitin-like domain at S65, inducing a conformational change on the E3-ligase enzyme that allows parkin to reach its complete active state (9, 10). Upon translocation to the MOM, parkin starts ubiquitylating several MOM proteins. The ubiquitin molecules added by parkin serve as a phosphorylation substrate to PINK1 and vice versa. This promotes a feed-forward signaling loop that amplifies the mitochondrial ubiquitylation signal (11).

Parkin is known to build different polyubiquitin chains but has different preferences for chain-linkage types, K63 and K48 being the most abundant chain types on MOM proteins (11). Other linkage chains, such as K27, K29, and K33, are known to be parkin dependent but are found to be less abundant on MOM proteins (11, 12). During the course of mitophagy, some MOM proteins are known to be eliminated at early stages (*i.e.*, mitofusins 1/2 [MFN1/2], mitochondrial GTPase miro1/2 [Ras homolog family member T1/2 [RHOT1/2], and translocase of outer mitochondrial membrane protein 70 [TOM70]), whereas some mitochondrial proteins remain ubiquitylated after intermediate depolarization times on damaged mitochondria (*i.e.*, voltage-dependent anion channel 1/2 [VDAC1/2], TOM20) (12–14). After extensive parkin-dependent ubiquitylation events, ubiquitin-binding autophagy receptor proteins are recruited, which trigger the engulfment of damaged mitochondria by the autophagosome. This eventually promotes mitochondrial degradation after the autophagosome fused

From the [1]Department of Biology, Quantitative Proteomics Group, Interfaculty Institute of Cell Biology, [2]Functional Neurogenetics, Laboratory of Neurodegeneration, Faculty of Medicine, Hertie Institute for Clinical Brain Research and German Center for Neurodegenerative Diseases, and [3]Department of Biochemistry, Faculty of Science, University of Tübingen, Tübingen, Germany

‡These authors contributed equally to this work.

*For correspondence: Philipp J. Kahle, philipp.kahle@uni-tuebingen.de; Boris Macek, boris.macek@uni-tuebingen.de.

Present address for Sven Geisler: Cell Analysis Core Facility, Institute for Systemic Inflammation Research, Universitätsklinikum Schleswig-Holstein, Campus Lübeck, Germany.

https://doi.org/10.1016/j.mcpro.2021.100191

with lysosomes (1, 15–18). Even though it is well accepted that damaged mitochondria are engulfed as a single whole entity (19, 20), an alternative hypothesis suggests a sequential subcompartment degradation. In this context, Yoshii *et al.* (21) demonstrated that autophagosomes engulf complete mitochondria after 6 h of depolarization, but MOM-ruptured and mitochondrial inner membrane (MIM)-ruptured mitochondria are engulfed after extensive depolarization times (12 h carbonyl cyanide *m*-chlorophenyl hydrazine [CCCP]). Recent advances in the field of quantitative proteomics and investigation of low-abundant ubiquitylation have allowed an in-depth analysis of parkin-dependent mitophagy (11). However, our understanding of molecular processes during later stages of mitophagy as well as the interplay between parkin-dependent ubiquitylation and phosphorylation is limited.

Here, we performed an in-depth temporal analysis of the proteome, ubiquitylome, and phosphoproteome during early and late stages of mitophagy. We identify novel parkin and downstream-acting substrates under mitophagy conditions; suggest that parkin-dependent mitochondrial degradation is tightly regulated in space and time; and indicate a potential crosstalk between ubiquitylation and phosphorylation able to influence specific protein degradation during PINK1/parkin-dependent mitophagy. Furthermore, we suggest an outside–in degradation of mitochondria, initiated by parkin activity during mitophagy.

EXPERIMENTAL PROCEDURES

Experimental Design and Statistical Rationale

In this study, we used HeLa cells in all experiments. This cell line was chosen because of the absence of endogenous parkin and the possibility to study late mitochondria-depleted stages of mitophagy (22) (supplemental Fig. S1*A*). To increase the level of mitophagy-related low-abundant proteins from different organelles, cells were first fractionated using a subcellular protein fractionation kit and pooled to remove highly abundant nuclear and cytoskeletal proteins. All Western blot analyses were performed at least twice for endogenous proteins and up to five times for transient overexpressed proteins (*i.e.*, VDAC2). All microscopy analyses were performed in duplicates. For in-depth proteome and phosphoproteome analysis, we chose a triple dimethyl labeling approach that covers all five treatment conditions in two sets sharing the untreated control. Both proteomic analyses were performed in two biological replicates. To study dynamics in the ubiquitylome, we adapted the recently presented Tandem Mass Tag 10-plex (TMT10-plex) approach by Udeshi *et al.* (23). In total, three replicates were performed to stabilize the quality of the quantified ubiquitylation sites. Only proteins identified in both replicates were further analyzed to investigate parkin-related dynamics on the proteome level. For phosphoproteome and ubiquitylome analysis, sites identified in at least one replicate were further processed. Mitochondrial proteins were annotated based on MitoCarta3.0 (24). Significantly regulated proteins (ANOVA $p < 0.1$ followed by post hoc test false discovery rate [FDR] <0.1) were subjected to hierarchical clustering. To identify parkin-dependent ubiquitylation sites, only strongly regulated ubiquitylation sites (z-scored fold change outside −2 and 2) were used for hierarchical clustering. This ratiometric approach was chosen based on the work from Hung *et al.* (25) because of varying identification rates of replicates that would have reduced the number of significant hits. To investigate dynamics on the phosphoproteome level, significantly regulated sites were determined (ANOVA $p < 0.1$ followed by post hoc test FDR < 0.1).

Cell Culture, Transfection, and Treatments

HeLa cells expressing stable 3xFlag-parkin WT or ligase-dead C431A parkin were generated as mentioned by Geisler *et al.* (13). Cells were cultured in Dulbecco's modified Eagle's medium supplemented with 10% (v/v) fetal bovine serum (FBS) at 37 °C with 5% CO_2. Cells were transfected with Fugene (Promega) with the indicated plasmids for at least 24 h. Mitochondrial depolarization was achieved by adding 10 μM of CCCP in the cell media. Upon harvest, cells were washed once with Dulbecco's PBS and stored until fractionation at −80 °C.

Expression Constructs

Full-length VDAC2 complementary DNA was amplified from HeLa 3xFlag-parkin stable cells. VDAC2 was cloned in pCMV-6xHIS vector using SalI and EcoRI fast digestion enzymes (Thermo Fisher Scientific), yielding an N-terminal tagged pCMV-6xHIS-VDAC2 construct. Phosphomimic and phosphodead point mutations were introduced in 6xHIS-VDAC2 using a two-step point-directed mutagenesis protocol. All complementary DNA sequences were verified by Sanger sequencing.

Western Blotting and Nickel–Nitrilotriacetic Acid Purification

Cells were washed with PBS and further pelleted at 972 g for 1 min at 4 °C. Cell pellets were resuspended in urea lysis buffer (10 mM Tris, pH 8.0, 100 mM NaH_2PO_4, and 8 M urea), passed five times through a 26-gauge needle, and pelleted at 3151 g for 15 min at 4 °C to obtain whole cell lysate fractions. Total protein measurement was performed using Bradford Protein Assay Kit (Bio-Rad). Samples were separated on 4 to 20% polyacrylamide gradient gels (TruPAGE precast gels; Merck) and run for 1 h at 100 V in Mops buffer. Proteins were transferred to poly(vinylidene fluoride) membranes (Immobilon-P; Merck) and blocked with 5% bovine serum albumin or nonfat dried milk in Tris-buffered saline with 0.1% Tween-20. Membranes were incubated overnight at 4 °C with the following primary antibodies: TOM70, 1:1000, ProteinTech (#14528-1-AP); TOM20, 1:6000, Santa Cruz (#sc-11415); VDAC1, 1:30000, Millipore (#AB10527); VDAC2, 1:50000, ProteinTech (#1663-1-AP); cytochrome c oxidase polypeptide IV (COX4), 1:1000, Cell Signaling (#4850); citrate synthase (CS), 1:6000, GeneTex (#GTX110624); SSBP1, 1:1000, R&D Systems (#AF6588); Vinculin, 1:6000, Sigma Aldrich (#V9131); Mfn1, 1:10000, Abnova (#H00055669-M04); 6HIS, 1:10000, Invitrogen (#HIS.H8); K27-ubiquitin, 1:50000, Abcam (#ab181537); Total Ubiquitin, 1:30000, Millipore (#MAB1510); pS65-ubiquitin, 1:1000, Millipore (#ABS1513); Parkin, 1:50000, Cell Signaling (#4211S); Flag, 1:10000, Sigma Aldrich (#F1804); pS757-ULK1, 1:1000, Cell signaling (#6888); PINK1, 1:1000, Cell Signaling (#6946S); and B-Actin, 1:5000, Sigma Aldrich (#A5441). Secondary antibody incubation were performed at room temperature (RT) for 1 h in 5% nonfat dried milk with the following antibodies: Goat anti-mouse HRP, Amersham Pharmacia (#115-035-003); Goat anti-rabbit HRP, Amersham Pharmacia (#111-035-003); and Goat anti-sheep HRP, Amersham Pharmacia (#718-035-147). Horseradish peroxidase chemiluminescent reaction was achieved using Western chemiluminescent-horseradish peroxidase substrate (Millipore) on Ultracruz autoradiography films (Santacruz). For nickel–nitrilotriacetic acid (Ni–NTA) pulldown, cell pellets were resuspended in urea lysis buffer at pH 8.0. At least 350 μg of total

protein supplemented with 10 mM imidazole was incubated with 30 µl of Ni–NTA beads for 21 h at 4 °C. Incubated lysates were shortly pelleted at 972 g for 1 min at 4 °C and washed three times with urea lysis buffer at pH 6.0 containing 20 mM of imidazole. Proteins were eluted with 50 µl of 2× Laemmli buffer for 15 min at 95 °C. One-fifth of the total eluate was subjected to Western blot analysis.

Immunostaining and Microscopy

Cells were seeded on precoated coverslips and treated with CCCP for the indicated time points. Cells were fixed with 4% paraformaldehyde in PBS for 20 min at RT and further permeabilized with 1% Triton X-100 for 5 min at RT. After three additional washing steps with PBS, cells were blocked with 10% of FBS in PBS for 1 h at RT. Cells were then incubated with the primary antibodies diluted in 5% FBS for 2 h at RT, and after three times washing with PBS, secondary antibodies diluted with 10% FBS were incubated for 1 h at RT in the dark. After two washing steps, cell nuclei were stained with 2 µg/ml Hoechst 33342 (Molecular Probes) in PBS for 5 min at RT. Cells were mounted onto coverslips using Fluorescent Mounting Medium (Dako). Imaging was performed using an AxioImager microscope equipped with an ApoTome imaging system using 63× objective (Carl Zeiss). The images were processed with AxioVision 4.9.1 software (Carl Zeiss). Primary and secondary antibodies used were the following: SSBP1, 1:1000, R&D Systems (#AF6588); K63-Ubiquitin, 1:1000, Millipore (#05-1308); Parkin, 1:1000, Cell Signaling (#4211S); TOM20, 1:1000, Santa Cruz (#sc-17764); Total Ubiquitin, 1:1000, Millipore (#MAB1510); COX4, 1:1000, Cell Signaling (#4850); p62/SQSTM, 1:1000, BD Biosciences (#610832); 6HIS, 1:1000, Invitrogen (#HIS.H8); CS, 1:1000, GeneTex (#GTX110624); Alexa Fluor 647 donkey anti-sheep, Invitrogen (A-21448); Alexa Fluor 488 donkey anti-mouse, Invitrogen (A-21202); Alexa Fluor 488 donkey anti-rabbit, Invitrogen (A-21206); Alexa Fluor donkey anti-mouse, Invitrogen (A-10037); and Alexa Fluor donkey anti-rabbit, Invitrogen (A-10042).

Subcellular Protein Fractionation

Mitochondrial proteins were enriched using subcellular protein fractionation kit for cultured cells (kit no.: 78840; Thermo Fisher Scientific) (supplemental Fig. S1*B* and supplemental Table S7). Cells were washed once with PBS, scraped in PBS, and further pelleted at 2188 g for 5 min at 4 °C. All steps were performed according to the vendor with around 1×10^7 cells per sample. Cytoplasmic extraction buffer, membrane extraction buffer, nuclear extraction buffer (NEB), and pellet extraction buffer were supplemented with Halt Protease Inhibitor Cocktail (1:100) immediately before use. Frozen cell pellets were resuspended in cytoplasmic extraction buffer and incubated for 10 min at 4 °C. After centrifugation at 500*g* for 10 min at 4 °C, the supernatants were stored as "cytoplasmic extract." The pellet was resuspended in membrane extraction buffer and incubated for 10 min at 4 °C. The supernatant was taken as "membrane extract" after centrifugation at 3000*g* for 10 min at 4 °C. "Soluble nuclear extract" was collected after incubation with NEB for 30 min at 4 °C and centrifugation at 5000*g* at 4 °C. "Chromatin-bound nuclear extract" was obtained after incubation with NEB supplemented with $CaCl_2$ and micrococcal nuclease for 15 min at RT and centrifugation at 16,000*g* for 5 min. For preparation of "cytoskeletal extract," pellets were incubated with phosphoenolpyruvate for 10 min at RT followed by centrifugation at 16,000*g* for 5 min. All namings are according to the vendor.

In a pilot experiment, the extracted cytoplasmic, membrane, soluble nuclear, chromatin-bound nuclear, and cytoskeletal fractions of the 3xFLAG-parkin clones and control cells were subjected to proteome analysis (supplemental Fig. S1, *C* and *D*). The principal component analysis revealed high similarity between fractions, independent of the expression of parkin WT or C431A and replicates (supplemental Fig. S1*C*). The first component explains 82% of the variance and allows discrimination of cytoplasmic, membrane, and soluble nuclear fractions (F1–F3) *versus* chromatin-bound and cytoskeletal fractions (F4–F5), whereas the second dimension (explaining 6% of the variance) differentiates fraction 4 from 5. Gene Ontology analysis of subcellular localization of detected proteins agreed with the vendor-defined naming of fractions, albeit with minor contamination in adjacent fractions (supplemental Fig. S1*D*). Therefore, all further analyses were performed on the pooled "cytoplasmic," "membrane," and "soluble nuclear" fractions that enabled the optimal recovery of mitochondrial and cytosolic proteins, while depleting the heavily post-translationally–modified cytoskeletal and chromatin-bound nuclear proteins.

Sample Preparation for Mass Spectrometry Analysis

Potentially present detergents in protein extracts were removed by acetone–methanol (acetone: eight volumes and methanol: one volume) precipitation overnight at −20 °C. Proteins were pelleted by centrifugation at 2500*g* for 20 min, and the remaining methanol was washed out with 80% of ice-cold acetone. Pellets were resuspended in denaturation buffer (6 M urea, 2 M thiourea, 10 mM Tris, pH 8), and the protein concentration was determined by Bradford assay. Within each experimental condition, the cytoplasmic, membrane, and nuclear extracts were mixed 1:1:1. Disulfide bonds were reduced with 10 mM DTT for 1 h, before alkylation for 1 h with either 55 mM iodoacetamide (phosphoproteome) or 55 mM chloracetamide (ubiquitylome). Predigestion was performed with Lys-C (Lysyl endopeptidase; Wako Chemicals) in a peptidase–protein ratio of 1:100 for 3 h at RT. For full overnight digestion, the fourfold volume of 50 mM ammonium bicarbonate was added before trypsin (Promega Corporation) in a peptidase–protein ratio of 1:100. Digestion was stopped by adding 1% TFA. Peptides were purified on Sep-Pak C18 Cartridges (Waters). For ubiquitylome analysis, peptides were eluted with 80% acetonitrile (ACN) and lyophilized for 24 h. Peptides were stored at −80 °C until GlyGly-peptide enrichment.

Sample Preparation for Quantitative Phosphorylation and Ubiquitylation Analysis

Peptides of the phosphoproteome samples were dimethyl-labeled on Sep-Pak C18 Cartridges. Except for 0 h CCCP-treated samples (2 mg), 1 mg of peptide per sample were labeled as previously described (26). Early and late triple dimethyl sets were mixed in a peptide ratio of 1:1:1 per labeling channel with 0 h light as a common time point. Successful label efficiency and label channel mixing were checked in pilot LC–MS/MS runs.

Each sample from GlyGly proteome (15 µg) was loaded on C18 StageTips and flushed once with Hepes buffer at pH 8. TMT10-plex labeling reagent was adjusted to RT and constituted in 40 µl ACN. Six microliters of TMT reagent was added to each sample and pushed through the C18 material to fully cover loaded peptides. After 1 h, labeled peptides were eluted with 80% ACN, and labeling reaction was quenched for 15 min with 5% hydroxylamine in 80% ACN. Peptides were concentrated prior to label efficiency check in pilot LC–MS/MS run.

High pH Reverse-Phase Chromatography

An off-line Ultimate 3000 HPLC System (Dionex, Thermo Fisher Scientific) equipped with xBridge BEH130 C_{18} 130 A, 3.5 µm, 4.6 × 250 mm column (Waters) was used to fractionate 3 mg per triple dimethyl (phosphoproteome set under basic conditions, as previously described (27)). In total, 66 fractions were collected every minute in an 80 min gradient at a flow rate of 1 ml/min by compositing buffer A

(5 mM NH_4OH) and B (5 mM NH_4OH in 90% ACN). From minute 0 to 45, buffer B composition was increased from 5 to 25%. For 10 min, the gradient was maintained at 40% B followed by 70% B for 5 min. For column re-equilibration, the gradient was reduced to 5% B over 5 min and held for further 10 min. Fractions were concentrated into 33 pools and dried by vacuum centrifugation overnight. After reconstitution in 80% ACN, 10 μg per fraction were concentrated and used for proteome analysis by LC–MS/MS measurement.

The Pierce High pH Reversed-Phase Peptide Fractionation Kit (kit no.: 84868; Thermo Fisher Scientific) was used to fractionate 50 μg of TMT10-plex–labeled and mixed proteome. Spin columns were conditioned twice with ACN and 0.1% TFA according to the vendor. Acidified peptides were loaded on columns and washed once with water. Peptides were eluted stepwise with 5%, 7.5%, 10%, 12.5%, 13.3%, 15%, 17.5%, 20%, and final 50% ACN/ammonia. Fractions were acidified to pH 2 to 3 and desalted on C18 StageTips prior to LC–MS/MS measurement.

Phosphopeptide Enrichment

Phosphopeptides were enriched using MagReSyn Ti-IMAC (titanium-immobilized metal affinity chromatography; ReSyn Bioscience) in two consecutive rounds of enrichment. About 15 μl of magnetic bead suspension per fraction and enrichment round was equilibrated first for 5 min with 70% ethanol, followed by washing twice for 10 min with 1% NH_4OH. Beads were washed further three times in 1-min intervals with loading buffer (1 M glycolic acid and 5% TFA in 80% ACN). Reconstituted peptides were mixed 1:1 with loading buffer and transferred to the equilibrated beads. The mixture was incubated for 20 min, and the flow-through was applied for a second round of enrichment. Nonspecifically bound peptides were removed by washing twice for 2 min with 1% TFA in 80% ACN and twice with 0.2% TFA in 10% ACN. Phosphopeptides were eluted three times with 1% NH_4OH for 20 min, and the pH was immediately adjusted with formic acid (FA) to 2 to 3. Both eluates of the same fraction were pooled and desalted on C18 StageTips prior to LC–MS/MS measurement.

GlyGly-Peptide Enrichment and On-Bead TMT Labeling

GlyGly-modified peptides were enriched using PTM-Scan ubiquitin remnant motif (K-ε-GG) kit (kit no.: 5562; Cell Signaling Technology) as described previously (23). Dimethyl pimelimidate crosslinked antibodies were washed twice with ice-cold immunoaffinity purification (IAP) buffer (50 mM Mops, pH 7.2, 10 mM sodium phosphate, and 50 mM NaCl). Lyophilized peptides were reconditioned in IAP buffer for 5 min, and insoluble material was removed by centrifugation at 5000*g* for 5 min at 4 °C. Supernatants (pH ~7) were transferred to the beads and incubated at 4 °C for 2 to 3 h with end-over-end rotation. Unbound peptides were removed by washing twice with ice-cold IAP buffer and once with PBS. For TMT labeling, beads were resuspended in Hepes buffer (pH 8.0–8.5) and incubated with 10 μl TMT for 15 min. The labeling reaction was quenched with 0.05% hydroxylamine for 5 min. Before elution, beads were washed twice with IAP and once with PBS. About 0.15% TFA was used for elution in two consecutive rounds for 5 min. TMT-labeled peptides were desalted on C18 StageTips prior to LC–MS/MS measurement.

LC–MS Analysis

All phosphoproteome and TMT-labeled samples were analyzed on an Q Exactive HF mass spectrometer (Thermo Fisher Scientific), and all proteome samples were analyzed on an Q Exactive HF-X mass spectrometer (Thermo Fisher Scientific). An online-coupled Easy-nLC 1200 UHPLC (Thermo Fisher Scientific) was used to separate peptides on a 20 cm analytical column (75 μm ID PicoTip fused silica emitter [New Objective]) in-house packed with ReproSil-Pur C18-AQ 1.9 μm resin (Dr Maisch GmbH Ltd). Gradient was generated by solvent A (0.1% FA) and solvent B (0.1% FA in 80% ACN), at 40 °C and a 200 nl/min flow rate. Phosphopeptides were eluted using 90 min, GlyGly peptides in a 130 min gradient. Dimethyl-labeled proteome samples were eluted in a 36 min gradient and TMT-labeled proteome fractions in a fraction-specific segmented linear 90 min gradient. Eluted peptides were ionized on an electrospray ionization source. Both mass spectrometers were operated in a positive ion and data-dependent acquisition mode. All full mass spectrometry (MS) were acquired in a scan range of 300 to 1750 *m/z* at a resolution of 60,000. For proteome samples, the 20 most intense multiple-charged ions were selected for higher-energy collisional dissociation fragmentation at a resolution of 15,000. For phosphoproteome and all TMT samples, top seven most intense peptides were picked with maximum injection time set to 220 ms for phospho and 110 ms set for TMT samples at MS2 resolution of 60,000. In addition, all TMT samples were measured with isolation window set to 0.7 *m/z* and normalized collision energy set to 35.

MS Data Analysis and Statistical Analysis

Raw data files were processed with the MaxQuant software suite (version 1.6.14.0) (28). MS/MS data were searched against UniProt *Homo sapiens* database (released December 11, 2019; 96,818 entries) containing PARK2 C431A mutant sequence and commonly observed contaminants. The mass tolerance for precursor ions was set to 4.5 ppm and for fragment ions to 20 pm. All search parameters were kept to default values except for the following. Dimethylation for light (28.03 Da), intermediate (32.06 Da), and heavy (36.08 Da) labels was allowed on lysine residues and peptide N termini for phosphoproteome data. Isobaric labeling and quantification on MS2 was enabled on lysine residues and peptide N termini with the TMT lot specific correction factors for ubiquitylome analysis. For all phospho raw files, phosphorylation on STY was defined as variable modification. GlyGly modification on K was configured to not create a new terminus and allowed for all GlyGly samples. Furthermore, oxidation of methionine and protein N-terminal acetylation were set as variable modifications. Carbamidomethylation of cysteine residues was allowed as fixed modification. All searches were performed in trypsin/P-specific digestion mode. Except for the analysis of GlyGly samples, maximum two missed cleavages were allowed. For GlyGly samples, the number of maximum missed cleavages was set to 4. Requantify and match-between runs and intensity-based absolute quantification options were enabled.

For the data analysis, only noncontaminant protein groups with at least two unique peptides were included. For subsequent proteome analysis, only protein groups were kept if quantified in two out of two replicates. For phosphoproteome and ubiquitylome analysis, identification in one replicate out of two or three was accepted after validation of high correlation between replicates. All data analyses were performed using Perseus software (version 1.6.7.0) (29). The density of data points with mitochondrial annotation or total between replicates was estimated by using default settings. For phosphoproteome and ubiquitylome analysis, the identified sites were normalized to the protein group prior to log2 transformation. Proteins were functionally annotated with GO cellular compartments as well as MitoCarta3.0. To investigate significantly changing protein abundances, two-way ANOVA test was performed to examine the influence of the cell line and treatment durations. Significantly regulated proteins ($-\log10\, p > 1$) were further analyzed by post hoc test (FDR: 0.1). Only proteins were kept that showed significant change between WT-parkin 0 h and longer treatment durations. The protein groups of WT-parkin samples were then hierarchically clustered (Euclidean distance followed by clustering on average). K-means was used to obtain 14 cluster groups

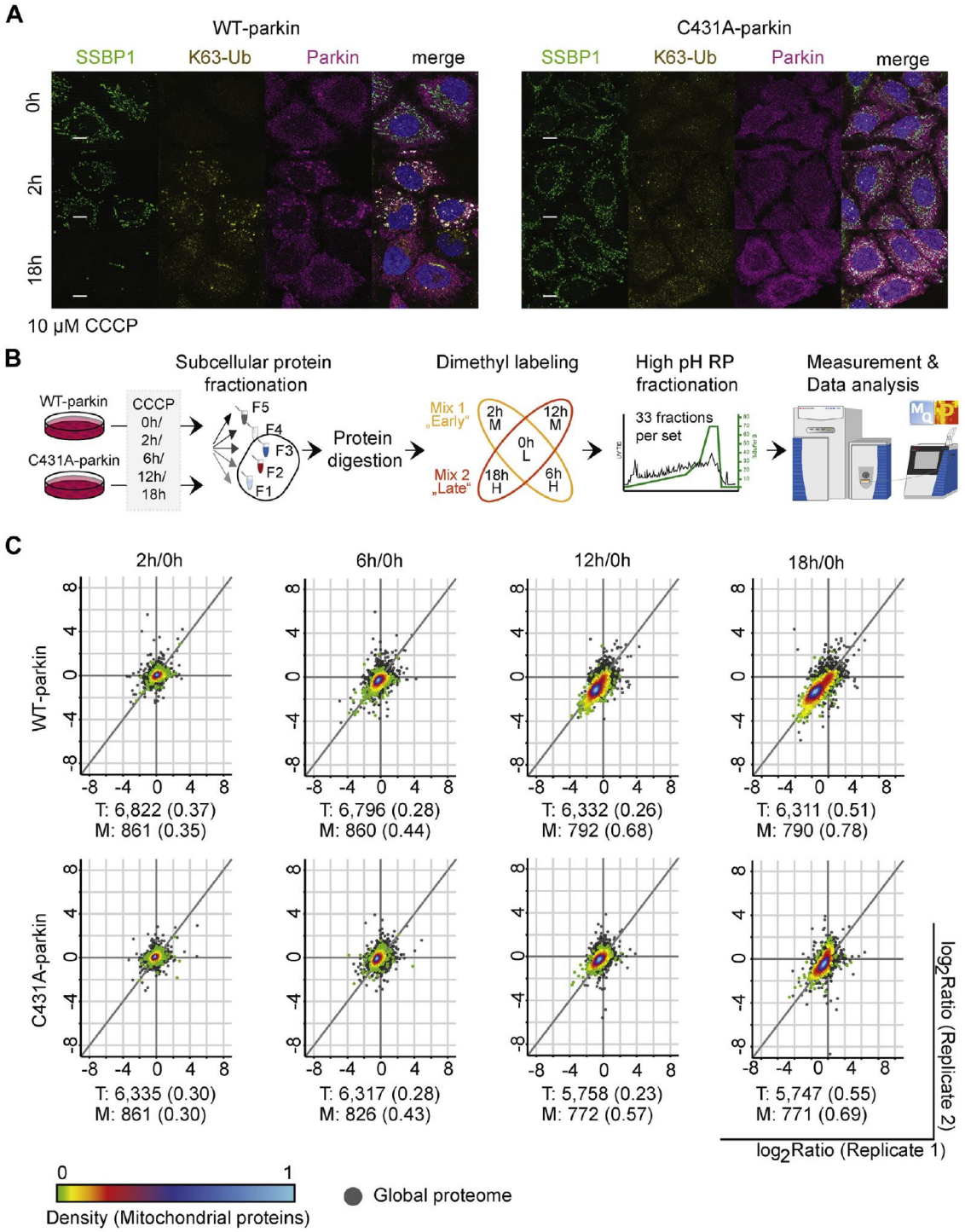

FIG. 1. **Parkin activity is essential for the removal of depolarized mitochondria.** *A*, immunofluorescence staining of WT-parkin and C431A-parkin cells after early (2 h) and late (18 h) depolarization times. Scale bars represent 5 µm. *B*, experimental setup combining subcellular protein fractionation with peptide dimethyl labeling and high pH reversed-phase fractionation during "early" and "late" mitophagy stages in WT-parkin and C431A-parkin cells. Basic workflow applied for proteome and phosphoproteome analysis. *C*, correlation plot

for proteome. Similar significant testing was performed for phosphoproteome analysis.

For ubiquitylome analysis, we used the average of all replicates and filtered for ubiquitylation events present in at least 50% in all conditions. Highly regulated ubiquitylation sites (z-score outside –2 and 2) of at least one condition of WT- or C431A-parkin samples across all treatment durations were used for hierarchical clustering. We identified 13 row clusters, based on k-means. For temporal treatment dynamics analysis, the profiles of each clusters were averaged. For overrepresentation analysis within clusters, Fisher exact test (Benjamini–Hochberg FDR ≤0.1) for relative enrichment to majority protein groups was applied. For graphical display, R environment was applied. For phosphoproteome analysis, only sites identified under all experimental conditions in at least one replicate were considered for subsequent analysis, whereas 75% identification in at least one replicate was required for ubiquitylome analysis. For generation of Venn diagrams, the online tool https://www.stefanjol.nl/venny was used.

Western-blot based statistical analysis for degradation of mitochondrial subcompartment proteins and the analysis of the site-directed mutagenesis of VDAC2 effect were performed using one-way ANOVA and Fisher's least significant difference analysis as a post hoc test. All data were from at least three independent experiments. Significance is indicated by asterisks: $^{*}p \leq 0.05$, $^{**}p \leq 0.01$, and $^{***}p < 0.001$.

RESULTS

We applied a quantitative proteomics approach to perform temporal analysis of protein abundance, ubiquitylation, and phosphorylation during early (0–6 h) and late stages (12–18 h) of parkin-dependent mitophagy. As a cellular system, we generated HeLa cell lines stably expressing WT- or ligase-dead (C431A) 3xFLAG-parkin at comparable levels. We chose HeLa cells as they are devoid of endogenous parkin activity (supplemental Fig. S1*A*). We treated these cells with the mitochondrial uncoupler CCCP to induce mitophagy and harvested them after 0, 2, 6, 12, and 18 h. After harvesting, we performed rough subcellular protein fractionation to reduce the levels of nuclear and cytoskeletal proteins (supplemental Fig. S1, *B–D*). The pooled "cytoplasmic," "membrane," and "soluble nuclear" extracts that enabled the optimal recovery of mitochondrial and cytosolic proteins were further investigated (see the Experimental Procedures section). We integrated the datasets on the temporal analysis of protein abundances, ubiquitylation, and phosphorylation during parkin-dependent mitophagy. In total, we identified 8359 proteins (supplemental Table S1), 1717 ubiquitylation sites (supplemental Table S2), and 20,464 phosphorylation sites (supplemental Table S3) with an FDR of 1% at the peptide and protein level.

Parkin-Dependent Proteome Dynamics During Mitophagy

Fluorescence microscopy confirmed FLAG-parkin recruitment to depolarized mitochondria within 2 h of CCCP treatment and the subsequent elimination of mitochondria in cells expressing WT- but not C431A-parkin (Fig. 1*A*). For temporal profiling of mitophagy-related changes in the proteome and phosphoproteome analyses, we used dimethyl labeling of tryptic peptides. To cover all five time points, we integrated two triple-dimethyl measurements using the 0 h CCCP treatment as the common time point of early (0, 2, and 6 h) and late (0, 12, and 18 h) stages of mitophagy for each cell line (Fig. 1*B*). In total, we identified 8359 proteins, of which 903 are annotated as mitochondrial. Furthermore, 83 of those are annotated as localized to the MOM, validating that our experimental design enriched for mitochondrial proteins. The reproducibility between biological replicates was high (supplemental Table S4). Next, we validated overall mitochondrial protein degradation by observing the density shift of data points related to mitochondrial proteins between cells expressing WT-parkin or C431A-parkin during prolonged CCCP treatment (Fig. 1*C*). In the presence of WT-parkin, we observed a downregulation of mitochondrial proteins after 6 h of mitophagy induction, and this trend continued until 18 h postdepolarization. In contrast, cells expressing C431A-parkin showed a mild shift of highly dense mitochondrial data points after 12 h of CCCP treatment. In addition, we validated mitochondrial protein degradation by Western blot analysis of established marker proteins (supplemental Fig. S1*E*). As expected, MOM proteins were degraded within 2 to 4 h of mitophagy induction only in cells expressing WT-parkin. To further validate that the observed mitochondrial degradation is a result of the activated PINK1/-parkin-dependent mitophagy pathway, we investigated additional hallmarks of mitophagy. First, we validated PINK1 accumulation after 2 h of CCCP treatment in WT-parkin–expressing cells. As PINK1 accumulated, the depolarized mitochondria were not eliminated in C431A-parkin cells (supplemental Fig. S1*E*). At later stages (8–18 h of mitochondrial depolarization), the dephosphorylation of S757 on ULK1 was observed in both WT-parkin and C431A-parkin cell lines, which revealed activation of general autophagy (supplemental Fig. S1*E*). Overall, we could validate successful execution of mitophagy in WT-parkin–expressing cells and also correct initiation in C431A-parkin–expressing cells. Late protein degradation in C431A-parkin cells may be associated with parkin-independent mitophagy and/or general autophagy induction.

between replicates after $\log_2$ transformation of protein ratios. Common light dimethyl labeling channel (0 h postdepolarization) allows comparison between "early" and "late" triple dimethyl-labeling sets per cell line. Parkin-dependent degradation of mitochondrial proteins reflected by shifting data points (density colored points) from "unregulated" toward "downregulated" in WT-parkin expressing cells in comparison to total proteome (*gray points*). Number of valid pairs per condition and Spearman rank correlation (*in brackets*) indicated for total (T) and mitochondrial annotated proteins (M).

"Outside–In" Degradation of Mitochondrial Subcompartments

During prolonged mitophagy induction, the temporal profiles of 5453 proteins identified in both replicates were obtained in both WT-parkin and C431A-parkin–expressing cells. Of these, 704 were mitochondrial, including 58 MOM annotated proteins (Fig. 2, *A* and *B*). Among proteins significantly downregulated upon CCCP treatment in WT-parkin–expressing cells (ANOVA FDR <0.1), more than 80% (269 proteins) were annotated as mitochondrial (Fig. 2*A*). For all mitochondrial subcompartments, we detected a clear downregulation of protein levels during prolonged CCCP treatment in WT-parkin cells (Fig. 2*B*). Only a minor decrease on the level of mitochondrial proteins was seen in C431A-parkin cells, which are likely because of parkin-independent mitophagy pathways or due to the impaired mitochondrial import machinery.

To assess the dynamics of parkin-dependent mitochondrial protein degradation of early and late substrates, we performed unsupervised hierarchical clustering of significantly downregulated proteins in WT-parkin–expressing cells after mitophagy induction (supplemental Fig. S2*A*). Of the 14 identified protein profile clusters, six did not contain mitochondrial proteins and were not considered for downstream analyses (supplemental Fig. S2*B*). To identify a time line of mitochondrial protein degradation, we averaged the protein profiles within each cluster. By overrepresentation analysis of mitochondrial subcompartments, we could connect cluster profiles of early (0–2 h), intermediate (2–6 h), and late (12–18 h) downregulated proteins to specific mitochondrial subcompartments (Fig. 2*C* and supplemental Fig. S2*C*). Interestingly, proteins annotated for MOM localization were downregulated already after 2 h upon depolarization. Downregulated proteins at intermediate time points (2–6 h) were predominantly annotated for MOM, inner mitochondrial space, and MIM localization. During late stages of CCCP treatment (6–12 h), downregulated proteins were annotated based on MIM or matrix localization. These findings were further supported by analyzing protein levels of representative proteins of each mitochondrial compartment *via* Western blot as well as the relative quantification of the corresponding Western blot (Fig. 2*D* and supplemental Fig. S2*D*). MOM proteins such as TOM70 or VDAC1 were degraded after 8 h of CCCP, whereas MIM and matrix proteins represented by COX4 and CS remained present even after prolonged mitochondrial depolarization times. In addition, we observed differential time-dependent degradation between early and late MOM substrates: TOM70 degradation was obvious after 2 h of CCCP induction, whereas VDAC1 or TOM20 was not completely degraded after 8 h of mitochondrial depolarization (Fig. 2*D*). These results point to an "outside–in" directed sequential degradation of mitochondria subcompartments during parkin-dependent mitophagy. MOM protein degradation took place mainly within 2 to 6 h of CCCP treatment, whereas MIM and matrix protein degradation was delayed until 12 to 18 h of mitophagy induction.

Protein Ubiquitylation Analysis Supports "Outside–In" Degradation Of Mitochondrial Subcompartments

To link the observed mitochondrial subcompartment protein degradation to parkin-dependent ubiquitylation, we further investigated the effect of parkin activity on site-specific ubiquitylome changes during early and late stages of mitophagy. Here, we applied the workflow of Udeshi *et al.* (23), which is based on the TMT labeling of GlyGly-modified peptides before elution from the ubiquitin remnant motif (K-ε-GG) antibody beads (supplemental Fig. S3*A*). In total, we identified 1717 ubiquitylation sites on 920 proteins. Of these, 245 sites were identified on 108 mitochondrial proteins (supplemental Fig. S3*B*). Although less ubiquitylated peptides were detected in two replicates, correlation of quantified GlyGly sites and proteins was high, and thus, all identified sites were considered in subsequent analyses (supplemental Table S5). Next, we compared levels of GlyGly-modified ubiquitin across time points and parkin cell lines (supplemental Fig. S3*C*). In both cell lines, we found high levels of GlyGly-modified ubiquitin on K48 during late stages of mitophagy (12–18 h). We also found a trend of increased levels of K6 and K63 GlyGly-modified ubiquitin after 2 h of depolarization in WT-parkin, whereas in C431A-parkin cells, these sites did not appear regulated.

Unsupervised hierarchical clustering identified 13 profile clusters containing regulated ubiquitylation sites (z-scored fold change outside −2 and 2) (Fig. 3*A* and supplemental Fig. S3*D*). We used overrepresentation analysis to connect specific ubiquitylation profile clusters with mitochondrial subcompartments (Fig. 3*B*). We further averaged four profile clusters with a parkin-dependent upregulation of ubiquitylation sites, either after 2, 6, 12, or 18 h of mitophagy induction (Fig. 3*C*). This revealed that MOM-annotated proteins showed an increase in ubiquitylation starting from 2 h of CCCP treatment and continued until 6 h. We found that MIM-annotated proteins predominantly ubiquitylated after 12 h of CCCP treatment, in addition to increased ubiquitylation after 6 and 18 h. In contrast, matrix-annotated proteins peaked after 18 h of mitochondrial depolarization. Interestingly, we identified ubiquitylation on parkin K48 among the late regulated ubiquitylation sites of cluster 13 (data not shown). This sequential pattern of ubiquitylation was almost exclusively found in WT-parkin but not C431A-parkin expressing cells.

We integrated the temporal dynamics of ubiquitylation events with significantly changing protein levels, based on their mitochondrial subcompartment localization (supplemental Fig. S3*E*). We identified 10 MOM annotated proteins with an early upregulated ubiquitylation site (2 h), which were degraded within 6 h of mitophagy induction. Among these, there were several validated parkin targets (*e.g.*,

Temporal Analysis of PTMs During Parkin-Dependent Mitophagy

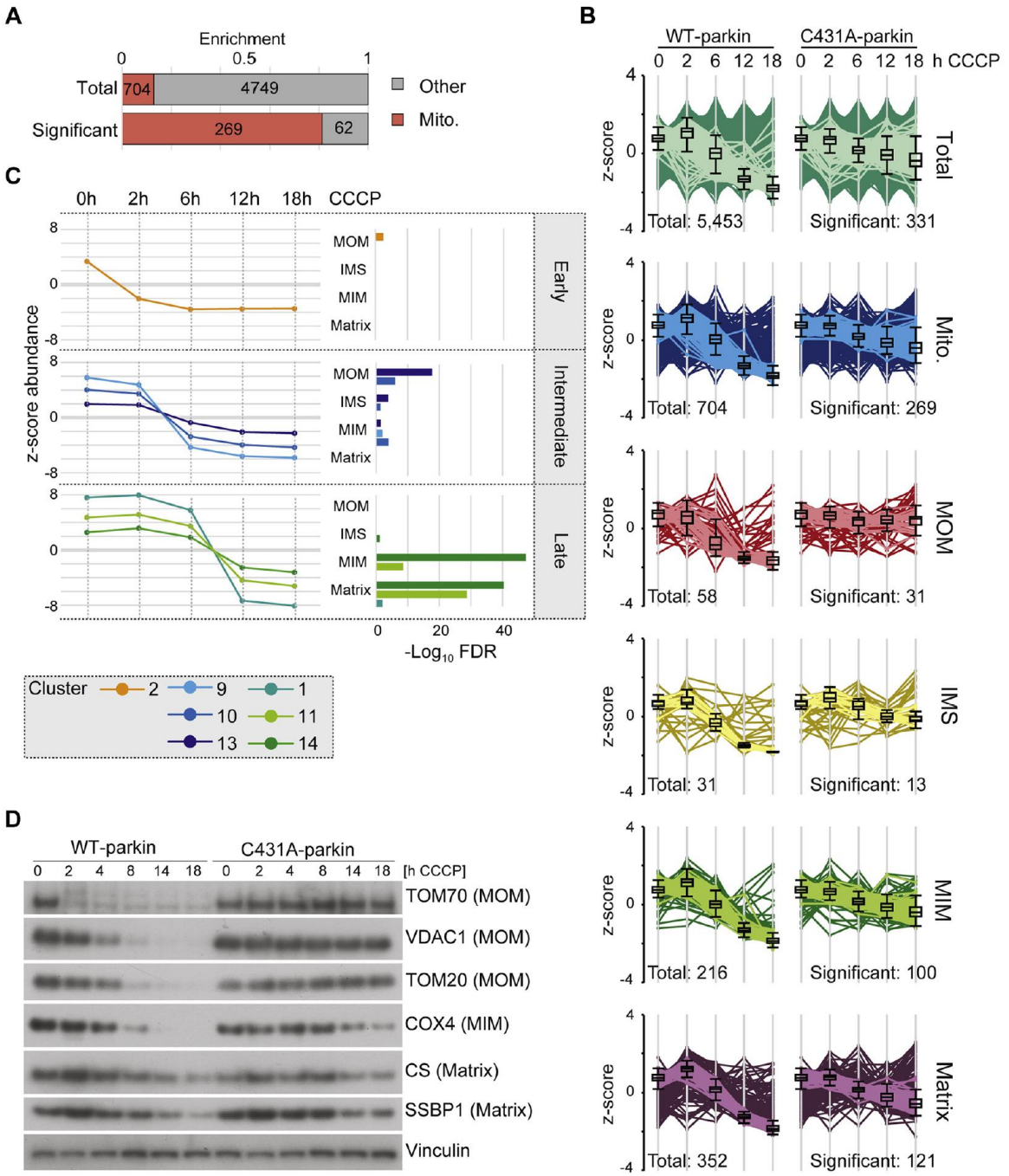

FIG. 2. **Outside–in degradation of mitochondrial proteins.** *A*, mitochondrial proteins were enriched among significantly regulated proteins. *B*, abundance profiles of significantly regulated proteins from various mitochondrial subcompartments show trends dependent on parkin activity. Indicated are size of total annotated proteins (*left*; *dark profiles*) and those after filtering (*right*; *bright profiles*); four mitochondrial proteins are of unknown or dual sublocalization (data not shown). *C*, average profile of each cluster sorted by half maximum in combination with over-representation analysis of mitochondrial subcompartments allows for the discrimination of "early" degraded MOM, "intermediate" degraded MOM/IMS/MIM, and "late" degraded MIM/matrix proteins. *D*, Western blot detection of mitochondrial subcompartment proteins during mitophagy validates stepwise degradation of mitochondrial subcompartments. IMS, inter membrane space; Mito, mitochondrion; MIM, mitochondrial inner membrane; MOM, mitochondrial outer membrane.

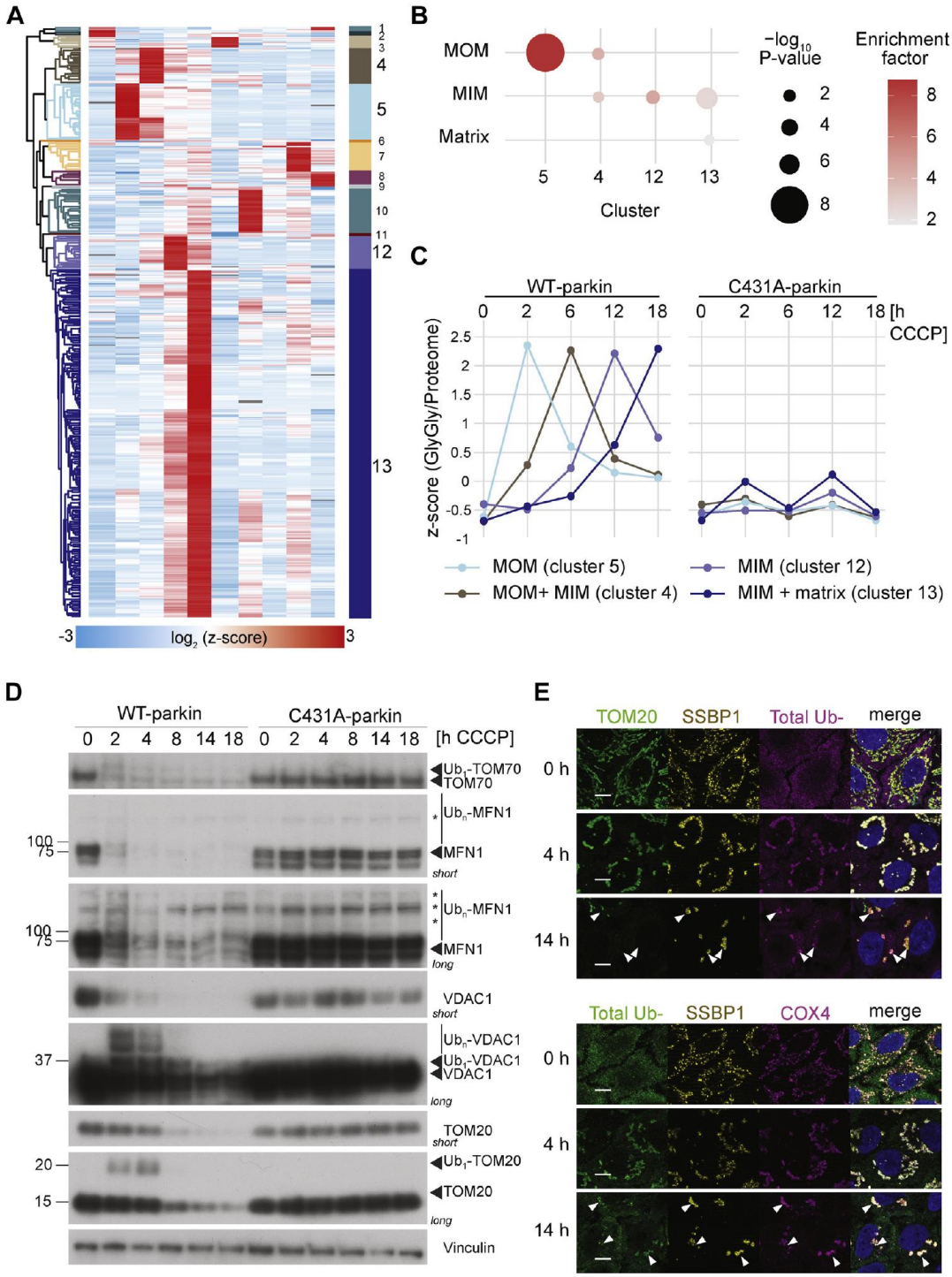

FIG. 3. **Ubiquitylation dynamics during mitophagy.** *A*, heat map after unsupervised hierarchical clustering into 13 clusters after filtering for significantly changing GlyGly sites (outside –2/2). *B*, average of profiles across CCCP treatment and parkin cell lines showing parkin-dependent and treatment-dependent response. *C*, overrepresentation of mitochondrial subcompartments across treatment duration changing clusters. *D*, Western blot detection of mitochondrial MOM parkin substrates over the course of mitophagy in WT-parkin and C431A-parkin cells. *Asterisks*

Temporal Analysis of PTMs During Parkin-Dependent Mitophagy

MFN1/2, RHOT2, or TOM70A). In contrast, 12 MIM (*e.g.*, PHB) and 3 matrix (*e.g.*, HSPD1) proteins showed protein degradation after 6 to 18 h with additional ubiquitylation during late stages (12–18 h). Ubiquitylation of MOM proteins was validated by Western blot analysis, which also revealed a time-dependent difference between early and late MOM parkin substrates (Fig. 3*D*). Proteins like MFN1 or TOM70 were rapidly ubiquitylated and degraded within 2 h of CCCP treatment. In contrast, other MOM proteins like TOM20 or VDAC2 became ubiquitylated shortly after incubation with CCCP and remained longer modified for up to 4 h. As expected, ubiquitylation changes were only detected in WT-parkin but not in C431A-parkin expressing cells (Fig. 3, *C* and *D*). However, immunofluorescence microscopy revealed that after 14 h of mitophagy induction—when MOM proteins (represented by TOM20) were mostly degraded—the inner mitochondrial proteins (represented by COX4 and SSBP1) appeared in clumpy profiles together with ubiquitin and the ubiquitin-binding p62/SQSTM autophagy receptor (Fig. 3*E* and supplemental Fig. S3*F*). When analyzing parkin localization during mitophagy, we observed that after intermediate (4–6 h) and late (>12 h) mitophagy induction time points, parkin is not detected on inner mitochondrial (or mitoplast) clumps but in the cytosol (Fig. 1*A* and supplemental Fig. S3*G*).

Taken together, the ubiquitylation data support the notion that parkin-dependent mitochondrial degradation takes place in a sequential "outside–in" manner, where extensive MOM ubiquitylation and further MOM elimination precede ubiquitylation and autophagy degradation of inner mitochondrial subcompartments (*i.e.*, MIM and matrix).

Protein Phosphorylation Dynamics During Mitophagy

Since ubiquitylation and phosphorylation play an important role during parkin-dependent mitophagy, we investigated a potential interplay of these two modifications during early and late stages of mitophagy. We extended our workflow to investigate proteome dynamics and integrated a phosphopeptide enrichment step after high pH reverse-phase fractionation. In total, we quantified 20,464 nonredundant phosphorylation events on 4930 proteins with high correlation between replicates (Fig. 4*A*, supplemental Fig. S4*A*, and supplemental Table S6). As shown earlier, we validated the accumulation of PINK1 on the MOM as a well-known initial step during PINK1/parkin-dependent mitophagy *via* Western blot analysis for both cell lines (supplemental Fig. S1*E*). Although we could not quantify PINK1 in our proteomics dataset, we validated the kinase activity by analyzing the phosphorylation dynamics of ubiquitin as it is established as a well characterized PINK1 target. After 2 h of postmitophagy induction, we detected strong upregulation of ubiquitin S65 phosphorylation, independent of parkin activity (supplemental Fig. S4*B*). This phosphorylation event showed a downward trend from 12 h of CCCP treatment in mitophagy-competent WT-parkin expressing cells. In contrast, pS65-ubiquitin continued to accumulate in mutant C431A-parkin expressing cells (supplemental Fig. S4*C*), consistent with the accumulation of PINK1 in the mitophagy-impaired C431A-parkin mutant cells (supplemental Fig. S1*E*). The higher molecular weight phospho-ubi adducts (supplemental Fig. S4*C*) must reflect ubiquitylations by ligases other than parkin, which evidently do not promote mitophagy as efficiently as those formed by parkin. Of all the identified phosphorylation events, 1449 were significantly regulated; however, no clear assignments to cellular compartments, signaling process, or specific regulatory differences between both cell lines or prolonged mitophagy induction were identified (supplemental Fig. S4*D*). We next addressed a potential interplay between phosphorylation and ubiquitylation events on identified significantly regulated proteins. Overall, we detected 284 doubly modified (phosphorylated and ubiquitylated) proteins indicating a modest crosstalk between these modifications during mitophagy (Fig. 4*B*). Six phosphorylation sites (on five proteins) showed significantly reduced protein abundance and highly regulated ubiquitylation and phosphorylation. Importantly, all these are either localized to the MOM (VDAC1, RMDN3, and TOM70) or to the MIM (AIFM1 and SLC25A11). All phosphorylation sites except for VDAC1 were found annotated in UniProt (30), but their functions remain unclear. Furthermore, we detected five phosphorylation sites on four MOM-annotated proteins, which showed a strongly regulated ubiquitylation site together with a nonsignificantly changing phosphorylation event (Fig. 4*C*). Both TOM70 phosphorylation events on T85 and S91 followed a similar trend of upregulation after 12 h in WT-parkin cells and downregulation in C431A-parkin cells. Similar regulation of phosphorylation dynamics between WT-parkin and C431A-parkin cells was found for RMDN3 S44 and S46 phosphorylation, following a downregulation trend after 6 h of CCCP treatment. Interestingly, we found VDAC1 and VDAC2 phosphorylation to be downregulated in WT-parkin expressing cells during intermediate and late stages of mitophagy but not in mutant C431A expressing cells. Taken together, these results point to a potential crosstalk between ubiquitylation and phosphorylation on MOM proteins degraded during parkin-dependent mitophagy.

Interplay of Phosphorylation and Ubiquitylation on VDAC2 During Mitophagy

In addition to parkin-dependent ubiquitylation events guiding the course of mitophagy, we hypothesized that prior phosphorylation or dephosphorylation events might influence

indicate unspecific bands. "Short" and "long" indicate corresponding developing exposure times. *E*, immunofluorescence staining of ubiquitylated mitochondria (4 h) and ubiquitylated mitochondria subcompartments (14 h). *Arrowheads* indicate inner mitochondrial clumps. The scale bar represents 5 μm. CCCP, carbonyl cyanide *m*-chlorophenyl hydrazine; MOM, mitochondrial outer membrane; Ub, ubiquitylated.

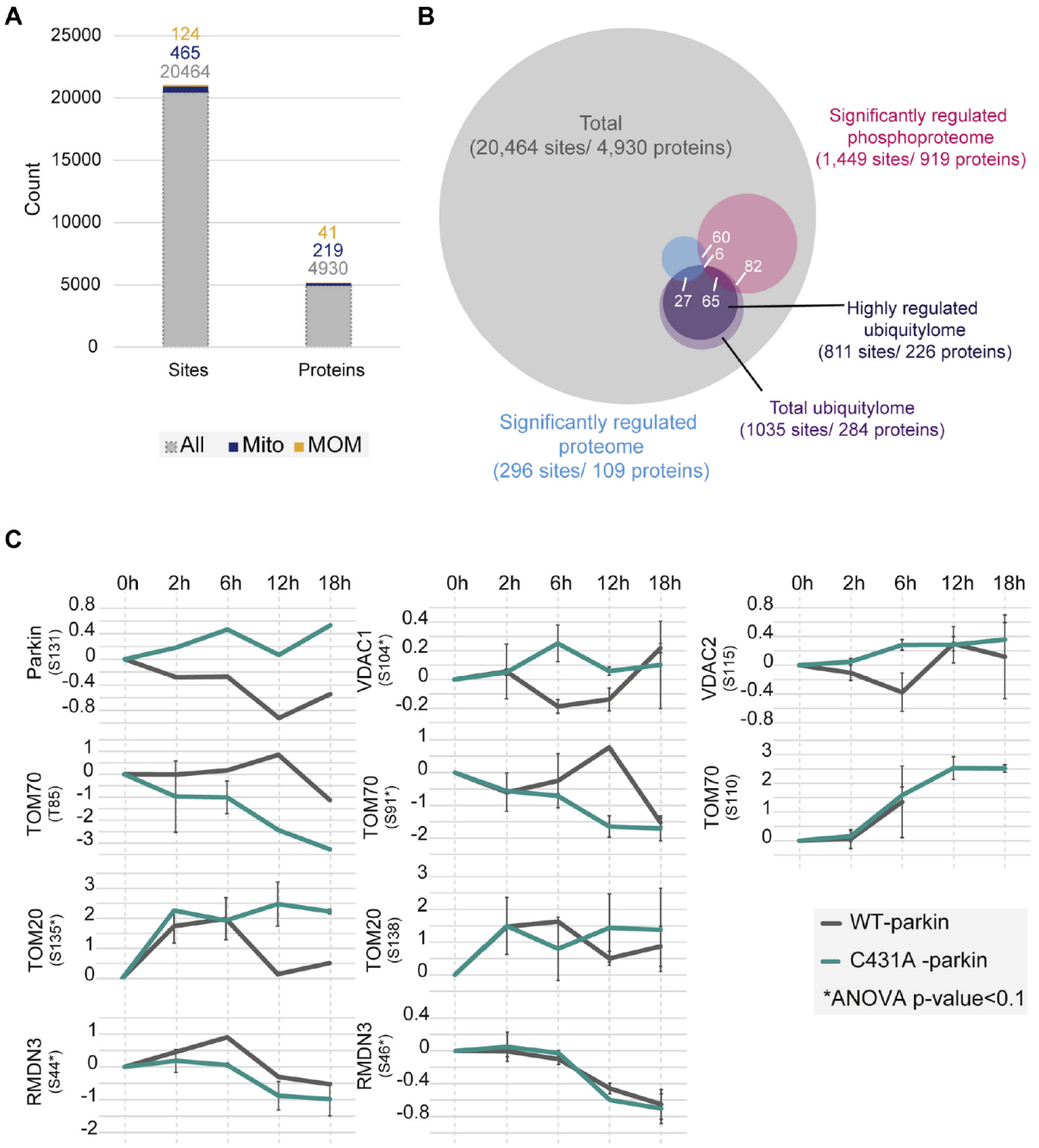

FIG. 4. **Phosphorylation dynamics during mitophagy.** *A*, identified phosphorylation sites of total, mitochondrial-annotated, and MOM-annotated proteins. *B*, overlap between proteome, ubiquitylome, and phosphoproteome datasets. Bulk-phosphorylation events are not simultaneously regulated on the protein and ubiquitylation levels. *C*, phosphorylation dynamics of MOM-annotated proteins with additional highly regulated ubiquitylation events. MOM, mitochondrial outer membrane.

subsequent ubiquitylation. For this purpose, we were interested in parkin substrates that also showed potential phosphorylation or dephosphorylation regulations.

VDAC proteins are parkin ubiquitylation targets that remain in the mitochondria after intermediate times of depolarization (Figs. 2*D* and 3*D*; supplemental Fig. S1*E*). In our screen, VDAC2

was modified by ubiquitin as well as phosphorylation moieties over the course of mitophagy (supplemental Tables S2 and S3). More specifically, MS data indicated that in WT-parkin expressing cells, VDAC2 was ubiquitylated at K120, whereas dephosphorylation of S115 was commencing after 2 h of CCCP treatment. In C431A-parkin cells, phosphorylation of S115 was increasing over time, whereas no ubiquitylation changes were found in K120 (supplemental Fig. S5*A*).

In order to decipher any possible crosstalk between dephosphorylation and ubiquitylation at this specific cytosolic loop of VDAC2, we generated 6xHIS-tagged VDAC2 constructs with phosphodead (S115A) and phosphomimic (S115D) serine substitutions. Total transfected levels of VDAC2 in whole cell lysate samples showed degradation of VDAC2 matching with mitophagy-dependent degradation of other MOM proteins (Fig. 5*A*). Moreover, there was an increase in VDAC2-S115D levels after 4 h, indicating a potential slower degradation of the phosphomimic mutant in comparison to the phosphodead form of VDAC2 (Fig. 5, *A*, *C*, and *D*). In order to understand if the slower degradation of the phosphomimic form of VDAC2 could be explained by the total ubiquitylation levels or specific ubiquitin-linkage chain levels, we performed Ni–NTA pull-down analysis. Total ubiquitin levels showed to be significantly increased in VDAC2-S115A in comparison to WT or VDAC2-S115D after mitochondrial depolarization (Fig. 5, *A* and *B*). In addition, there was a mild reduction of K27-ubiquitin–linked chain formation in VDAC2-S115D (Fig. 5, *A* and *B*).

We also analyzed the behavior of all VDAC2 transfected constructs over the course of mitophagy using immunofluorescence-based imaging techniques. Transfection of all 6xHIS-tagged VDAC2 constructs did not have an impact on overall mitophagy time course since we could observe mitochondrial fragmentation and complete elimination of mitochondria after 4 and 14 h of CCCP treatment, respectively (supplemental Fig. S5*B*). In addition, when performing single-cell quantification analysis of the number of cells with residual VDAC2 signal after 14 h CCCP, we observed a significant increase of positive cells, which were previously transfected with VDAC2-S115D (Fig. 5*E*), indicating that mimicking phosphorylation at S115D may delay VDAC2 degradation. We also assessed the impact of the phospho-VDAC2 mutations on the overall speed of mitophagy completion. For this purpose, we analyzed the mitochondria morphology of 6xHIS positive cells with the idea that, if delayed mitophagy was to be found, an increased number of cells would show mitochondrial clumps instead of mitochondria puncta after 14 h CCCP. Overall, around 80% of 6xHIS positive cells showed puncta mitochondrial morphology for all 6xHIS-VDAC2 transfected constructs, suggesting that bulk mitophagy completion was not affected when overexpressing VDAC2 point mutations (Fig. 5*F* and supplemental Fig. S5*B*).

Together, these data suggest that there is an interplay between ubiquitylation and phosphorylation at the fourth cytosolic loop (115–120 amino acids) of VDAC2, which seems to be dephosphorylated in order to be later ubiquitylated under parkin-dependent mitophagy conditions (supplemental Fig. S5*C*). Indeed, modifying phosphorylation status of S115 seems to have an impact on VDAC2 ubiquitylation and further protein degradation. When S115-phosphorylation is abolished, total ubiquitylation of VDAC2 is enhanced, and this leads to a faster VDAC2 degradation. Conversely, when S115-phosphorylation is mimicked, total VDAC2 ubiquitylations seem to mildly decrease, delaying VDAC2 degradation (Fig. 5, *A*, *B*, and *E*). In addition, it seems that mimicking S115-phosphorylation might have an impact on the topology of polyubiquitin chains that are assembled on this particular cytosolic loop of VDAC2, as K27-linked ubiquitin chains were slightly reduced when VDAC2-S115D was expressed (Fig. 5*D*).

DISCUSSION

Here, we provide a multilevel proteomic dataset comprising (phospho)proteome and ubiquitylome dynamics during early (2–6 h) and late (12–18 h) stages of parkin-dependent mitophagy. To link parkin activity with newly identified post-translational events, we compared conditions of successful and defective mitophagy in HeLa cells overexpressing similar levels of WT-parkin or C431A-parkin, respectively. As expected, we observed general mitochondrial elimination as well as ubiquitylation of known MOM proteins in WT-parkin cells only. GlyGly protein modification patterns of known MOM parkin substrates not only largely matched with the literature (11, 14, 31) but also yielded potential novel substrates, such as FIS1 or MARC1/2 (supplemental Table S2). Because of low protein levels, we could not validate PINK1 accumulation in all conditions *via* MS. Nevertheless, phosphorylation modification dynamics observed in our screen were in agreement with already published phosphoproteomic studies under parkin-dependent mitophagy conditions (32). For example, PINK1-dependent pS65-ubiquitin phosphorylation, together with autophagy adaptor phosphorylation, was observed in our dataset (supplemental Table S3). Taken together, our in-depth proteomic temporal analysis approach defined substrates at the protein, ubiquitylation, and phosphorylation levels, which are affected in early (0–2 h) intermediate (4–8 h), and late (12–18 h) stages of parkin-dependent mitophagy.

Outside–In Mitochondrial Subcompartment Degradation

Previous studies demonstrated that MOM ubiquitylation promotes recruitment of autophagy adaptors and engulfment of damaged mitochondria by the autophagosome complex (15, 16, 33, 34). However, our data support the sequential subcompartment mitochondrial degradation hypothesis. While we observed extensive MOM ubiquitylation and protein degradation from 2 to 6 h after mitochondrial depolarization, we could also identify an increasing ubiquitylation of inner

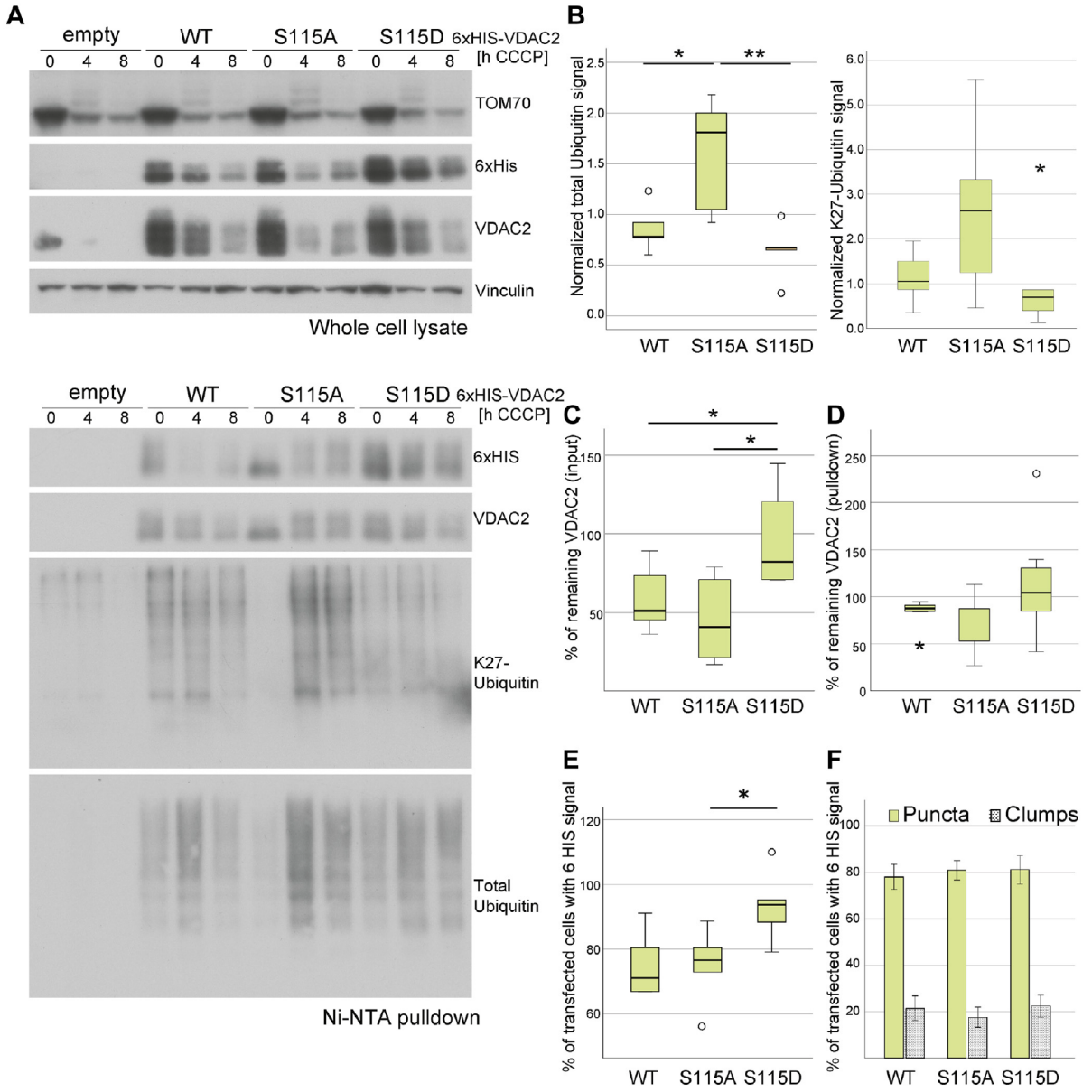

FIG. 5. **Effect of phosphomimic and phosphodead mutations on VDAC2 mitophagy-dependent degradation.** *A*, whole cell lysate and pulldown of transfected WT-parkin cells with 6xHis-WT and VDAC2 serine mutants. *B*, total ubiquitin and specific K27-linked ubiquitin chain levels of pulldown samples after 4 h of CCCP. *C* and *D*, remaining total VDAC2 levels after 4 h of CCCP in input and pulldown samples, respectively. *E*, percentage of transfected cells still showing VDAC2 signal after 14 h CCCP. *F*, mitochondria morphology of cells showing residual VDAC2 signal after 14 h of CCCP. Data of at least N = 3 independent experiments. Mean ± SEM. $^{*}p \leq 0.05$, $^{**}p \leq 0.01$. CCCP, carbonyl cyanide *m*-chlorophenyl hydrazine; VDAC2, voltage-dependent anion channel 2.

mitochondrial subcompartments at longer depolarization times (12 and 18 h CCCP) (Fig. 3, *B*, *C*, and *E*). Moreover, ubiquitylation of inner mitochondrial proteins matched with a delayed inner mitochondrial protein degradation (Fig. 2). Parkin is known to preferentially build K63-linked and K48-linked ubiquitin chains (12, 14, 19). Increase of K6 and K63 polyubiquitin chains after 2 h of depolarization in WT-parkin cells was in agreement with the reported increase of ubiquitin ligase activity between 2 and 6 h after mitochondrial depolarization (supplemental Fig. S3*C*). Conversely, K48-linked polyubiquitin

chains were increased at late time points of mitochondrial depolarization but not exclusively in WT-parkin expressing cells. These findings suggest that parkin targets the MOM proteins within the initial stages but not the inner mitochondrial proteins during later stages of mitophagy.

Inner mitochondrial protein ubiquitylation has already been reported under parkin-dependent mitophagy conditions but only after relatively early depolarization time points. Sarraf *et al.* identified inner mitochondrial ubiquitylation after 1 h of depolarization under endogenous parkin conditions (31). Similarly, Ordureau *et al.* found such ubiquitylations to be enriched under WT-parkin and inactive parkin (S65A) endogenous expressing conditions, after 6 h of depolarization (11). Remaining mitochondria clumps were found ubiquitylated as well as recognized by p62/SQSTM at later stages of the pathway (Fig. 3*E* and supplemental Fig. S3*E*); this might indicate that inner mitochondrial ubiquitylations may trigger a later autophagy elimination of mitochondria inner compartments. This is in accordance to what we observe after 4 h of mitochondrial depolarization where complete MOM ubiquitylation triggers p62/SQSTM recognition and further MOM elimination (Fig. 3*E* and supplemental Fig. S3*E*). In addition, we identified parkin K48 ubiquitylation that is localized within the ubiquitin-like domain. This site was upregulated especially during late stages of mitophagy (12–18 h) and was not regulated in C431A-parkin expressing cells. Polyubiquitylation in general and specifically K48-linked ubiquitin chains are well-known markers for protein degradation (19, 35). Because we did not find CCCP treatment–dependent changes in the protein level of parkin, we hypothesize that parkin K48 ubiquitylation may affect parkin activity rather than its degradation.

These data, together with the fact that inner mitochondrial ubiquitylations have also been reported in conditions of inactive (11) or nonendogenous parkin (36, 37), point out that inner mitochondrial protein ubiquitylation may happen in a parkin-independent manner. Further experiments are needed to decipher which E3-ubiquitin ligases are responsible for inner mitochondrial subcompartment protein ubiquitylation under WT-parkin expressing conditions. A potential candidate might be the E3-ligase HUEW1 on which K1107 ubiquitylation was upregulated after 2 h of depolarization. Based on the temporal profile of parkin-preferred polyubiquitin chain linkages, with the highest level after 2 h depolarization (supplemental Fig. S3*C*), we hypothesize that HUWE1 ubiquitylation might be regulated by parkin.

Crosstalk Between Ubiquitylation and Phosphorylation

The initiation of mitophagy relies on PINK1-dependent phosphorylation leading to parkin activation and translocation to the MOM (38–42). In addition, parkin-dependent ubiquitylation of mitochondrial proteins is known to promote mitochondrial degradation (19, 43). Here, we hypothesized that, in addition to parkin-dependent regulation of mitophagy by ubiquitylation, phosphorylation or dephosphorylation events could also play a role in specific MOM protein degradation or mitophagy progression. Ten phosphorylation sites on six significantly downregulated MOM proteins were detected in vicinity of regulated ubiquitylation sites. Among these were VDAC1 and VDAC2, which showed to be ubiquitylated and dephosphorylated at one of their cytosolic loops: 104 to 109 amino acids and 115 to 120 amino acids, respectively (supplemental Tables S2 and S3). Both are known parkin and non-PINK1 target sites. Site-directed mutagenesis of VDAC2 combined with mitochondrial depolarization assays indicated that mimicking dephosphorylation of S115 (S115A-VDAC2) promoted faster protein degradation because of an increased total ubiquitylation. On the other hand, mimicking phosphorylation of S115 (S115D-VDAC2) had the opposite effect; a delay in protein degradation because of a decreased total ubiquitylation.

Even though the role of K27-linked ubiquitin chains in cellular processes remains unknown, they have been suggested to be strongly increased in VDAC1 upon parkin-dependent ubiquitylation and have been linked with lysosomal targeting (12, 44). Considering that VDAC1 and VDAC2 show similarities in sequence and protein structure, we hypothesized that we might see changes in K27-linked ubiquitin chains when mutating S115. Indeed, even though data were statistically not significant, there seemed to be a decreased trend of K27-linked ubiquitin chain formation when dephosphorylation of S115 was abolished (Fig. 5*C*). This may indicate that K27-linked ubiquitin chains play a role in VDAC2 degradation as well but are not exclusive for the cytosolic loop of 115 to 120 amino acids. Taken together, our data provide evidence that protein degradation under parkin-dependent mitophagy conditions is likely to not only be regulated *via* parkin ubiquitylation but may implicate the role of phosphatases in the regulation of mitochondrial protein elimination.

In summary, our data indicate that degradation of complete mitochondrial or organelle subcompartment might happen in a sequential time-dependent manner and suggest that parkin may not be responsible for inner mitochondrial ubiquitylation events. In addition, we provide evidence that phosphorylation likely influences protein ubiquitylation and further degradation of some parkin substrates and thus, phosphatase and kinases are likely to play a role in the regulation of PINK1/parkin-dependent mitophagy.

DATA AVAILABILITY

The MS proteomics data have been deposited to the ProteomeXchange Consortium *via* the PRIDE (45) partner repository with the dataset identifier PXD027586. Visualization of MS/MS spectra is possible at https://msviewer.ucsf.edu/prospector/cgi-bin/msform.cgi?form=msviewer *via* the search keys: nrajlpjg0x (subcellular protein fractionation),

km5ojtsfoc (proteome), c0geshw3ie (phosphoproteome), and suxnuntnwt (ubiquitylome).

Supplemental data—This article contains supplemental data.

Acknowledgments—This research was funded by the German Research Foundation (DFG) through GRK2364. We thank Sandra Scheppers for contributing on the validation of ubiquitination of inner mitochondrial proteins.

Funding and additional information—B. M. and K. I. Z. acknowledge support by the High Performance and Cloud Computing Group at the Center for Data Processing of the University of Tübingen, the state of Baden-Wuerttemberg through bwHPC.

Author contributions—P. J. K. and B. M. methodology; P. J. K. and B. M. conceptualization; A. L.-T. formal analysis; A. L.-T. and S. G. investigation; K. I. Z. resources; A. L.-T. data curation; K. I. Z. and A. L.-T. writing–original draft; K. I. Z., A. L.-T. N. N., S. G., P. J. K., and B. M. writing–review and editing.

Conflict of interest—The authors declare no competing interests.

Abbreviations—The abbreviations used are: ACN, acetonitrile; CCCP, carbonyl cyanide *m*-chlorophenyl hydrazine; COX4, Cytochrome c oxidase polypeptide IV; CS, citrate synthase; FA, formic acid; FBS, fetal bovine serum; FDR, false discovery rate; IAP, immunoaffinity purification; MFN, mitofusin; MIM, mitochondrial inner membrane; MOM, mitochondrial outer membrane; MS, mass spectrometry; NEB, nuclear extraction buffer; Ni–NTA, nickel–nitrilotriacetic acid; PINK1, phosphatase and tensin homolog–induced kinase 1; RHOT1/2, Ras homolog family member T1/2; RT, room temperature; TMT, tandem mass tag; TOM70, translocase of outer mitochondrial membrane protein 70; VDAC1/2, voltage-dependent anion channel 1/2.

Received September 17, 2021, and in revised from, December 23, 2021 Published, MCPRO Papers in Press, December 30, 2021, https://doi.org/10.1016/j.mcpro.2021.100191

REFERENCES

1. Dikic, I., and Elazar, Z. (2018) Mechanism and medical implications of mammalian autophagy. *Nat. Rev. Mol. Cell Biol.* **19**, 349–364
2. Giacomello, M., Pyakurel, A., Glytsou, C., and Scorrano, L. (2020) The cell biology of mitochondrial membrane dynamics. *Nat. Rev. Mol. Cell Biol.* **21**, 204–224
3. Kitada, T., Asakawa, S., Hattori, N., Matsumine, H., Yamamura, Y., Minoshima, S., Yokochi, M., Mizuno, Y., and Shimizu, N. (1998) Mutations in the parkin gene cause autosomal recessive juvenile parkinsonism. *Nature* **392**, 605–608
4. Valente, E. M., Abou-Sleiman, P. M., Caputo, V., Muqit, M. M., Harvey, K., Gispert, S., Ali, Z., Del Turco, D., Bentivoglio, A. R., Healy, D. G., Albanese, A., Nussbaum, R., Gonzalez-Maldonado, R., Deller, T., Salvi, S., *et al*. (2004) Hereditary early-onset Parkinson's disease caused by mutations in PINK1. *Science* **304**, 1158–1160
5. Greene, A. W., Grenier, K., Aguileta, M. A., Muise, S., Farazifard, R., Haque, M. E., McBride, H. M., Park, D. S., and Fon, E. A. (2012) Mitochondrial processing peptidase regulates PINK1 processing, import and Parkin recruitment. *EMBO Rep.* **13**, 378–385
6. Jin, S. M., Lazarou, M., Wang, C., Kane, L. A., Narendra, D. P., and Youle, R. J. (2010) Mitochondrial membrane potential regulates PINK1 import and proteolytic destabilization by PARL. *J. Cell Biol.* **191**, 933–942
7. Meissner, C., Lorenz, H., Weihofen, A., Selkoe, D. J., and Lemberg, M. K. (2011) The mitochondrial intramembrane protease PARL cleaves human Pink1 to regulate Pink1 trafficking. *J. Neurochem.* **117**, 856–867
8. Aerts, L., Craessaerts, K., De Strooper, B., and Morais, V. A. (2015) PINK1 kinase catalytic activity is regulated by phosphorylation on serines 228 and 402. *J. Biol. Chem.* **290**, 2798–2811
9. Okatsu, K., Oka, T., Iguchi, M., Imamura, K., Kosako, H., Tani, N., Kimura, M., Go, E., Koyano, F., Funayama, M., Shiba-Fukushima, K., Sato, S., Shimizu, H., Fukunaga, Y., Taniguchi, H., *et al*. (2012) PINK1 autophosphorylation upon membrane potential dissipation is essential for Parkin recruitment to damaged mitochondria. *Nat. Commun.* **3**, 1016
10. Trempe, J. F., Sauve, V., Grenier, K., Seirafi, M., Tang, M. Y., Menade, M., Al-Abdul-Wahid, S., Krett, J., Wong, K., Kozlov, G., Nagar, B., Fon, E. A., and Gehring, K. (2013) Structure of parkin reveals mechanisms for ubiquitin ligase activation. *Science* **340**, 1451–1455
11. Ordureau, A., Paulo, J. A., Zhang, J., An, H., Swatek, K. N., Cannon, J. R., Wan, Q., Komander, D., and Harper, J. W. (2020) Global landscape and dynamics of parkin and USP30-dependent ubiquitylomes in iNeurons during mitophagic signaling. *Mol. Cell* **77**, 1124–1142.e10
12. Geisler, S., Holmstrom, K. M., Skujat, D., Fiesel, F. C., Rothfuss, O. C., Kahle, P. J., and Springer, W. (2010) PINK1/Parkin-mediated mitophagy is dependent on VDAC1 and p62/SQSTM1. *Nat. Cell Biol.* **12**, 119–131
13. Geisler, S., Jager, L., Golombek, S., Nakanishi, E., Hans, F., Casadei, N., Terradas, A. L., Linnemann, C., and Kahle, P. J. (2019) Ubiquitin-specific protease USP36 knockdown impairs Parkin-dependent mitophagy *via* downregulation of Beclin-1-associated autophagy-related ATG14L. *Exp. Cell Res.* **384**, 111641
14. Ordureau, A., Paulo, J. A., Zhang, W., Ahfeldt, T., Zhang, J., Cohn, E. F., Hou, Z., Heo, J. M., Rubin, L. L., Sidhu, S. S., Gygi, S. P., and Harper, J. W. (2018) Dynamics of PARKIN-dependent mitochondrial ubiquitylation in induced neurons and model systems revealed by digital Snapshot proteomics. *Mol. Cell* **70**, 211–227.e8
15. Heo, J. M., Ordureau, A., Paulo, J. A., Rinehart, J., and Harper, J. W. (2015) The PINK1-PARKIN mitochondrial ubiquitylation pathway drives a program of OPTN/NDP52 recruitment and TBK1 activation to promote mitophagy. *Mol. Cell* **60**, 7–20
16. Lazarou, M., Sliter, D. A., Kane, L. A., Sarraf, S. A., Wang, C., Burman, J. L., Sideris, D. P., Fogel, A. I., and Youle, R. J. (2015) The ubiquitin kinase PINK1 recruits autophagy receptors to induce mitophagy. *Nature* **524**, 309–314
17. Padman, B. S., Nguyen, T. N., Uoselis, L., Skulsuppaisarn, M., Nguyen, L. K., and Lazarou, M. (2019) LC3/GABARAPs drive ubiquitin-independent recruitment of Optineurin and NDP52 to amplify mitophagy. *Nat. Commun.* **10**, 408
18. Yamano, K., Matsuda, N., and Tanaka, K. (2016) The ubiquitin signal and autophagy: An orchestrated dance leading to mitochondrial degradation. *EMBO Rep.* **17**, 300–316
19. Harper, J. W., Ordureau, A., and Heo, J. M. (2018) Building and decoding ubiquitin chains for mitophagy. *Nat. Rev. Mol. Cell Biol.* **19**, 93–108
20. Pickrell, A. M., and Youle, R. J. (2015) The roles of PINK1, parkin, and mitochondrial fidelity in Parkinson's disease. *Neuron* **85**, 257–273
21. Yoshii, S. R., Kishi, C., Ishihara, N., and Mizushima, N. (2011) Parkin mediates proteasome-dependent protein degradation and rupture of the outer mitochondrial membrane. *J. Biol. Chem.* **286**, 19630–19640
22. Denison, S. R., Wang, F., Becker, N. A., Schule, B., Kock, N., Phillips, L. A., Klein, C., and Smith, D. I. (2003) Alterations in the common fragile site gene Parkin in ovarian and other cancers. *Oncogene* **22**, 8370–8378
23. Udeshi, N. D., Mani, D. C., Satpathy, S., Fereshetian, S., Gasser, J. A., Svinkina, T., Olive, M. E., Ebert, B. L., Mertins, P., and Carr, S. A. (2020) Rapid and deep-scale ubiquitylation profiling for biology and translational research. *Nat. Commun.* **11**, 359

24. Rath, S., Sharma, R., Gupta, R., Ast, T., Chan, C., Durham, T. J., Goodman, R. P., Grabarek, Z., Haas, M. E., Hung, W. H. W., Joshi, P. R., Jourdain, A. A., Kim, S. H., Kotrys, A. V., Lam, S. S., *et al*. (2021) MitoCarta3.0: an updated mitochondrial proteome now with sub-organelle localization and pathway annotations. *Nucl. Acids Res.* **49**, D1541–D1547
25. Hung, V., Zou, P., Rhee, H. W., Udeshi, N. D., Cracan, V., Svinkina, T., Carr, S. A., Mootha, V. K., and Ting, A. Y. (2014) Proteomic mapping of the human mitochondrial intermembrane space in live cells *via* ratiometric APEX tagging. *Mol. Cell* **55**, 332–341
26. Boersema, P. J., Raijmakers, R., Lemeer, S., Mohammed, S., and Heck, A. J. (2009) Multiplex peptide stable isotope dimethyl labeling for quantitative proteomics. *Nat. Protoc.* **4**, 484–494
27. Batth, T. S., and Olsen, J. V. (2016) Offline high pH reversed-phase peptide fractionation for deep phosphoproteome coverage. *Methods Mol. Biol.* **1355**, 179–192
28. Cox, J., and Mann, M. (2008) MaxQuant enables high peptide identification rates, individualized p.p.b.-range mass accuracies and proteome-wide protein quantification. *Nat. Biotechnol.* **26**, 1367–1372
29. Tyanova, S., Temu, T., Sinitcyn, P., Carlson, A., Hein, M. Y., Geiger, T., Mann, M., and Cox, J. (2016) The Perseus computational platform for comprehensive analysis of (prote)omics data. *Nat. Methods* **13**, 731–740
30. UniProt, C. (2021) UniProt: The universal protein knowledgebase in 2021. *Nucleic Acids Res.* **49**, D480–D489
31. Sarraf, S. A., Raman, M., Guarani-Pereira, V., Sowa, M. E., Huttlin, E. L., Gygi, S. P., and Harper, J. W. (2013) Landscape of the PARKIN-dependent ubiquitylome in response to mitochondrial depolarization. *Nature* **496**, 372–376
32. Lai, Y. C., Kondapalli, C., Lehneck, R., Procter, J. B., Dill, B. D., Woodroof, H. I., Gourlay, R., Peggie, M., Macartney, T. J., Corti, O., Corvol, J. C., Campbell, D. G., Itzen, A., Trost, M., and Muqit, M. M. (2015) Phosphoproteomic screening identifies Rab GTPases as novel downstream targets of PINK1. *EMBO J.* **34**, 2840–2861
33. Nguyen, T. N., Padman, B. S., and Lazarou, M. (2016) Deciphering the molecular signals of PINK1/parkin mitophagy. *Trends Cell Biol.* **26**, 733–744
34. Richter, B., Sliter, D. A., Herhaus, L., Stolz, A., Wang, C., Beli, P., Zaffagnini, G., Wild, P., Martens, S., Wagner, S. A., Youle, R. J., and Dikic, I. (2016) Phosphorylation of OPTN by TBK1 enhances its binding to Ub chains and promotes selective autophagy of damaged mitochondria. *Proc. Natl. Acad. Sci. U. S. A.* **113**, 4039–4044
35. Chan, N. C., Salazar, A. M., Pham, A. H., Sweredoski, M. J., Kolawa, N. J., Graham, R. L., Hess, S., and Chan, D. C. (2011) Broad activation of the ubiquitin-proteasome system by Parkin is critical for mitophagy. *Hum. Mol. Genet.* **20**, 1726–1737
36. Oshima, Y., Cartier, E., Boyman, L., Verhoeven, N., Polster, B. M., Huang, W., Kane, M., Lederer, W. J., and Karbowski, M. (2021) Parkin-independent mitophagy *via* Drp1-mediated outer membrane severing and inner membrane ubiquitination. *J. Cell Biol.* **220**, e202006043
37. Sulkshane, P., Duek, I., Ram, J., Thakur, A., Reis, N., Ziv, T., and Glickman, M. H. (2020) Inhibition of proteasome reveals basal mitochondrial ubiquitination. *J. Proteomics* **229**, 103949
38. Kazlauskaite, A., Kelly, V., Johnson, C., Baillie, C., Hastie, C. J., Peggie, M., Macartney, T., Woodroof, H. I., Alessi, D. R., Pedrioli, P. G., and Muqit, M. M. (2014) Phosphorylation of Parkin at Serine65 is essential for activation: Elaboration of a Miro1 substrate-based assay of parkin E3 ligase activity. *Open Biol.* **4**, 130213
39. Kazlauskaite, A., Kondapalli, C., Gourlay, R., Campbell, D. G., Ritorto, M. S., Hofmann, K., Alessi, D. R., Knebel, A., Trost, M., and Muqit, M. M. (2014) Parkin is activated by PINK1-dependent phosphorylation of ubiquitin at Ser65. *Biochem. J.* **460**, 127–139
40. Kondapalli, C., Kazlauskaite, A., Zhang, N., Woodroof, H. I., Campbell, D. G., Gourlay, R., Burchell, L., Walden, H., Macartney, T. J., Deak, M., Knebel, A., Alessi, D. R., and Muqit, M. M. (2012) PINK1 is activated by mitochondrial membrane potential depolarization and stimulates Parkin E3 ligase activity by phosphorylating Serine 65. *Open Biol.* **2**, 120080
41. McWilliams, T. G., Barini, E., Pohjolan-Pirhonen, R., Brooks, S. P., Singh, F., Burel, S., Balk, K., Kumar, A., Montava-Garriga, L., Prescott, A. R., Hassoun, S. M., Mouton-Liger, F., Ball, G., Hills, R., Knebel, A., *et al*. (2018) Phosphorylation of Parkin at serine 65 is essential for its activation *in vivo*. *Open Biol.* **8**, 180108
42. Zhuang, N., Li, L., Chen, S., and Wang, T. (2016) PINK1-dependent phosphorylation of PINK1 and Parkin is essential for mitochondrial quality control. *Cell Death Dis.* **7**, e2501
43. Nguyen, T. N., Padman, B. S., Usher, J., Oorschot, V., Ramm, G., and Lazarou, M. (2016) Atg8 family LC3/GABARAP proteins are crucial for autophagosome-lysosome fusion but not autophagosome formation during PINK1/Parkin mitophagy and starvation. *J. Cell Biol.* **215**, 857–874
44. Ikeda, H., and Kerppola, T. K. (2008) Lysosomal localization of ubiquitinated Jun requires multiple determinants in a lysine-27–linked polyubiquitin conjugate. *Mol. Biol. Cell* **19**, 4588–4601
45. Perez-Riverol, Y., Csordas, A., Bai, J., Bernal-Llinares, M., Hewapathirana, S., Kundu, D. J., Inuganti, A., Griss, J., Mayer, G., Eisenacher, M., Perez, E., Uszkoreit, J., Pfeuffer, J., Sachsenberg, T., Yilmaz, S., *et al*. (2019) The PRIDE database and related tools and resources in 2019: Improving support for quantification data. *Nucleic Acids Res.* **47**, D442–D450

3.2. Manuscript II

Parkin-dependent mitophagy occurs via proteasome-dependent steps sequentially targeting separate mitochondrial sub-compartments for autophagy (published)

Autophagy Reports, 1:1, 576-602, DOI: 10.1080/27694127.2022.2143214

Author contributions:

The experimental design of proteasomal inhibition in combination with mitophagy induction was designed by Anna Lechado-Terradas and Philipp Kahle. All proteomics experiments were designed by me and Boris Macek. Sandra Scheppers and Anna Lechado provided the sample material for downstream proteomics-based analysis. I performed the sample preparation for dimethyl label, the statistical analysis and interpretation of proteomics data. Therefore, my work contributed to figure 4 A-C and supplementary figure 4 A-E.

Parkin-dependent mitophagy occurs via proteasome-dependent steps sequentially targeting separate mitochondrial sub-compartments for autophagy

Anna Lechado-Terradas[1,2], Sandra Schepers[1], Katharina I. Zittlau[3], Karan Sharma[2,4], Orkun Ok[1,2], Julia C. Fitzgerald[4], Stefan Geimer[5], Benedikt Westermann[5], Boris Macek[3] and Philipp J. Kahle[1,2,6]

[1]Laboratory of Functional Neurogenetics, Department of Neurodegeneration, Hertie Institute for Clinical Brain Research, Faculty of Medicine, University of Tübingen, Tübingen, Germany; [2]Department of Biochemistry, Faculty of Science, University of Tübingen, Tübingen, Germany; [3]Quantitative Proteomics Group, Department of Biology, Interfaculty Institute of Cell Biology, University of Tübingen, Tübingen, Germany; [4]Mitochondrial Biology of Parkinson's Disease, Department of Neurodegeneration, Hertie Institute for Clinical Brain Research, Faculty of Medicine, University of Tübingen, Tübingen, Germany; [5]Laboratory of Cell Biology and Electron Microscopy, University of Bayreuth, Bayreuth, Germany, [6]German Center for Neurodegenerative Diseases, Tübingen, Germany

CONTACT

boris.macek@uni-tuebingen.de; philipp.kahle@uni-tuebingen.de

KEYWORDS

mitochondrial outer membrane; mitophagy; parkin; proteasome; ubiquitin

Abstract

PINK1/parkin-dependent mitophagy initially involves (phospho)ubiquitin-directed proteasome-dependent degradation of certain outer mitochondrial membrane (OMM) proteins (e.g. mitofusins) and the recruitment of autophagy effectors to a group of ubiquitinated OMM proteins, eventually leading to autophagic removal of damaged mitochondria in stressed cells. Here we provide evidence that mitochondrial degradation occurs via stepwise delivery of separate mitochondrial sub-compartments for autophagic degradation. OMM and inner mitochondrial material appears to become separately isolated for autophagolysosomal degradation, not only in parkin-overexpressing HeLa cells but also in cells that express endogenous parkin (human embryonic kidney cells and neural progenitor cells) with slower mitophagy kinetics. The remaining inner mitochondrial material becomes degraded only after much prolonged membrane depolarization, potentially involving another proteasome-sensitive step. The present combined microscopy and proteomics analyses support the idea that cell stress-induced parkin-dependent mitophagy is a complex multi-step process with distinct mitochondrial sub-compartments being separately targeted for autophagic degradation.

Abbreviations: BafA, Bafilomycin A; CCCP, carbonyl cyanide 3-chlorophenylhydrazone; COX IV, cytochrome c oxidase subunit IV; CS, citrate synthase; DMEM, Dulbecco's modified Eagle's medium; EGFP, enhanced green fluorescent protein; FBS, fetal bovine serum; IF, immunofluorescence; IMM, inner mitochondrial membrane; KO, knock-out; LC3, microtubule-associated protein 1 light chain 3; MDVs, mitochondria-derived vesicles; MFN, mitofusin; NPCs, neural progenitor cells; OMM, outer mitochondrial membrane; p62/SQSTM, 62kDa protein sequestosome-1; PBS, phosphate-buffered saline; PINK1, phosphatase and tensin homolog (PTEN)-induced putative kinase protein 1; RT, room temperature; SSBP1, single-stranded DNA binding protein 1; TAX1BP1, Tax1-binding protein 1; TEM, transmission electron microscopy, TOM20, translocase of outer mitochondrial membrane 20kDa subunit; TOM70, translocase of outer mitochondrial membrane 70kDa subunit; Ub, ubiquitin; UPS, ubiquitin proteasome system; VDAC, voltage-dependent anion-selective channel protein; WB, Western blot; WT, wild-type

Introduction

Acute mitochondrial stress conditions trigger the specific autophagic elimination of mitochondria in a process termed mitophagy. One of the most studied forms of mitophagy is the one orchestrated by the phosphatase and tensin homolog (PTEN)-induced putative kinase protein 1 (PINK1) and the E3 ubiquitin-protein ligase parkin [1]. Mutations in both proteins have been linked to the most common recessive hereditary forms of Parkinson's disease and are known to compromise successful mitophagy [2–5].

There are several ways to experimentally induce PINK1/parkin mitophagy [6]. One of the most widely used is treatment with the uncoupler carbonyl cyanide 3-chlorophenylhydrazone (CCCP), which promotes proton permeability of the inner mitochondrial membrane (IMM), harshly inducing mitochondrial depolarization [7]. When modeling mitophagy in neuron-like cell models that strongly rely on mitochondrial respiration, dissipation of the mitochondrial membrane potential might not be enough to promote mitophagy [6]. In neural cells mitophagy can be induced by respiratory complex III inhibition with Antimycin A [8,9].

Under depolarizing conditions, the mitochondrial protein import machinery cannot translocate PINK1 across the membranes and thus PINK1 accumulates at the outer mitochondrial membrane (OMM) [10]. There, PINK1 phosphorylates cytosolic ubiquitin (Ub) and the parkin Ub-like domain, both at Ser65 [11,12]. Such parkin phosphorylation stimulates its ubiquitin ligase activity and translocation to the OMM, where parkin strongly binds to phosphorylated ubiquitin (pS65-Ub) at its active center [13]. At this point, parkin assembles pS65-Ub chains on OMM substrates, which either trigger rapid degradation by the ubiquitin-proteasome system or promote the binding of autophagy adaptors [14–16].

Parkin-dependent mitochondria elimination involves the binding of ubiquitinated OMM proteins by autophagy adaptors, which specifically recognize ubiquitinated cargo through their ubiquitin binding domain and link ubiquitinated mitochondria to the autophagic membrane through their microtubule-associated protein 1 light chain 3 (LC3)-interacting region. Recognition of ubiquitinated mitochondria by autophagy adaptors promotes the engulfment of mitochondria in autophagosomes that eventually fuse with lysosomes for wholesale degradation [17,18]. However, there is recent evidence for selective sub-mitochondrial degradation pathways in yeast stationary-phase mitophagy [19].

Our most recent study on PINK1/parkin-dependent temporal ubiquitination and phosphorylation events indicated a stepwise mitochondrial degradation in wild-type parkin (WT-parkin) expressing HeLa cells [20]. Here, we examined the stepwise mitochondrial degradation mechanisms in greater detail and discuss the specific involvement of proteasome and autophagy mechanisms that influence PINK1/parkin mitophagy at early and late stages of the pathway. We provide evidence that OMM and IMM material is separately delivered to the lysosomal machinery, suggesting distinct degradation pathways for individual mitochondrial sub-compartments. This was not only observed in parkin-overexpressing HeLa cells, but also in cells with endogenous parkin expression levels (human embryonic kidney HEK293 cells and neural progenitor cells (NPCs)) that showed slower mitophagy kinetics. In addition to the OMM proteasome dependence for mitophagy initiation, we provide evidence for a potential second proteasome-sensitive IMM regulatory step for mitophagy elimination of matrix proteins. The

present integrative microscopy and proteomics analyses indicate that PINK1/parkin-dependent mitophagy is a multi-step process modulated at several levels by the proteasome, where distinct mitochondrial sub-compartments are separately targeted to autophagic degradation with distinct kinetics.

Results

Distinct subsets of OMM proteins are subject to immediate-early proteasomal and delayed autophagic degradation

When WT-parkin HeLa cells are exposed to the mitochondrial membrane uncoupler CCCP, mitochondria are subjected to PINK1/parkin-dependent degradation. Interestingly, the degradation of mitochondrial proteins does not take place at once, but rather follows a stepwise mitochondrial sub-compartment degradation dynamics [20]. OMM proteins are the first ones to be degraded, followed by IMM and matrix proteins. For example, mitofusin-1 (MFN)-1 was extremely rapidly degraded with a half-life time of <2 h (Figure 1A). The rapid removal of parkin-ubiquitinated MFN proteins occurs via direct proteasomal targeting [21]. Indeed, pretreatment with the proteasome inhibitor MG132 caused an accumulation of ubiquitinated MFN1 after 4 h CCCP treatment (Figure S1A).

Other OMM proteins such as voltage-dependent anion-selective channel (VDAC), translocase of outer mitochondrial membrane 70 kDa subunit (TOM70) and 20 kDa subunit (TOM20) had more delayed degradation rates with half-life times of 2-4 h (Figure 1A). At 4 h CCCP treatment, TOM20-immunopositive structures became devoid of the early proteasome targets MFN1 and TOM70 (Figure S1C and S1D), indicating engagement of delayed OMM substrates in mitophagy after the earlier proteasome substrates were removed. The IMM protein cytochrome c oxidase subunit IV (COX IV) had a slightly slower degradation rate, showing a half-life time of ≈4 h. However, the degradation of matrix proteins citrate synthase (CS) and single stranded DNA binding protein 1 (SSBP1) was hardly detectable at 4 h CCCP treatment, their half-life times being >8 h (Figure 1A). Indeed, when most of the OMM proteins were removed after 14 h (Figure 1A), remaining inner mitochondrial markers (SSBP1, COX IV) persisted while at this time point the TOM20 remnants were reduced to puncta (Figure 1B).

Pretreatment with proteasome inhibitors stabilized MFN1 and TOM70 also as higher molecular mass species (Figure S1A and S1B), indicating direct proteasome-targeting ubiquitinations for these rapidly degraded OMM proteins. In contrast, although the slower degradation of TOM20 and VDAC was likewise prevented by proteasome inhibitor pretreatment, this was not accompanied by an accumulation of ubiquitinated species (Figure S1A and S1B). The slower removal of such OMM proteins may therefore not occur through

direct ubiquitin-dependent proteasome degradation, but is mediated after an initial proteasome-dependent step (see below). Degradation of inner mitochondrial proteins (COX IV, CS) was also suppressed after pretreatment with proteasome inhibitors (Figure S1A and S1B). Thus, pretreatment with proteasome inhibitors blocks the removal of direct substrate proteins on the OMM and prevents an important early proteasome-dependent step for the initiation of mitophagy in CCCP-treated parkin-HeLa cells. Putative not proteasome-targeting ubiquitinations of VDAC and TOM20 that can be seen upon long exposure are in fact reduced after pretreatment with MG132 (Figure S1A). Such ubiquitinations can be visualized on TOM20-positive and SSBP1-positive structures in the course of mitophagy (Figure 1C), evidently recruiting ubiquitin-binding autophagy receptors such as the 62 kDa protein sequestosome-1 (p62/SQSTM) (Figure 1D) and Tax1-binding protein 1 (TAX1BP1) (Figure 1E).

The recruitment of ubiquitin-binding autophagy receptors should connect to the autophagy machinery via ATG8 proteins. Immunostaining of endogenous LC3B confirmed an association of TOM20 puncta after 8 h of mitochondrial depolarization (Figure S1E). Most TOM20 puncta (dissociated from SSBP1-positive mitochondrial structures) were in close apposition with LC3B puncta. At this time point, endogenous LC3B puncta also came in apposition to COX IV positive structures, while SSBP1-positive aggregates did not (yet) co-localize with endogenous LC3B (Figure S1E). Endogenous LC3B-positive autophagic puncta were dispersed throughout the cells with little enrichment on mitophagy cargo, perhaps indicating some limitation of the anti-LC3B immunostaining. Thus, transfection experiments with EGFP-LC3B were performed, which showed somewhat more prominent translocation to mitophagy cargo (Figure 1F). Consistent with the immunostaining results for endogenous LC3B, EGFP-LC3B was associated with most TOM20-only puncta (Figure 1F), either showing close apposition (arrows) or complete overlap (closed arrowheads). Rare EGFP-LC3B-negative TOM20-only puncta were observed (open arrowheads). Such features might represent mitochondria-derived vesicles (MDVs), which were described to be delivered to lysosomes independently from LC3 [22]. Alternatively, EGFP-LC3B-negative puncta could simply reflect TOM20 cargo that has not yet engaged LC3B phagophores at this time point. As for endogenous LC3B, the EGFP-tagged LC3B showed very little overlap with SSBP-1 positive aggregates devoid of OMM markers at this time point (Figure 1F, ROI 1), but some SSBP1-LC3B positive puncta started to become detectable (Figure 1F, ROI 2, arrows).

Autophagy completion depends on the formation of autophagosomes that are eventually fused with lysosomes, inside of which the targeted cargo is degraded by acidic hydrolases [17,23]. Indeed, as mitophagy progressed, the TOM20 puncta came to increasingly close apposition with the lysosomal-associated membrane protein 1 (LAMP1)

(Figure S1F), suggesting cargo delivery to lysosomes [24]. The active engagement in autophagolysosomes was confirmed with LysoTracker RED (Figure 1G), a fluorescent marker that can be used for monitoring lysosome acidification [24,25]. When lysosomal acidification as well as autophagosome-lysosome fusion was inhibited by pretreatment with Bafilomycin A (BafA), the number of TOM20-positive as well as SSBP1-positive puncta significantly increased after 8 h of CCCP treatment (Figure 1H and I), indicating that the mitochondrial material engaged in (autophagic) puncta was eventually delivered to lysosomes.

Additionally, in order to confirm that the degradation of mitochondrial sub-compartment proteins did rely on autophagy machinery targeting, HeLa cells lacking all autophagy adaptors (penta knock-out cell line, referred as pentaKO) [16] were examined. Upon parkin over-expression and mitochondrial depolarization with CCCP for 4 h, rapid degradation was observed only for the proteasome substrate MFN1 (Figure S1G). In contrast, degradation of OMM and inner- mitochondrial proteins was severely compromised in pentaKO cells compared to controls (Figure S1G-I), indicating that the degradation of the aforementioned OMM and IMM proteins in parkin-HeLa cells is mostly mediated by autophagy.

Inner mitochondrial material is targeted to separate, late degradation pathways

Although inner mitochondrial markers co-localized with TOM20 4 h after mitophagy induction (Figure 1B), the remaining TOM20 puncta that appeared after 14 h (likely representing OMM autophagolysosomes, see above) were clearly separate from inner mitochondrial material (Figure 1B). Moreover, most of the SSBP1 and CS-positive inner mitochondrial staining patterns at this late time point appeared as large mitochondrial aggregates of fragmented mitochondria rather than puncta (Figure 1B). Similar structures showing TOM20-positive mitochondrial condensates upon activation of PINK1/parkin-dependent mitophagy have been described previously as mitochondrial-aggresomes or mitochondrial aggregates [26,27]. While the presence of TOM20-negative mitochondrial condensates is surprising and has not been specifically described before, the morphology of these structures is similar to the ones described by Lee *et al.* [27]. Thus, mitochondrial condensates will be referred here as mitochondrial-aggresomes or mitochondrial aggregates.

To quantify the degradation dynamics of each mitochondrial sub-compartment, CellProfiler image-based analysis was performed at mid- and late stages of mitophagy (4 h vs. 14 h CCCP treatment) (Figure S2A-F). The mean number as well as the size of TOM20-positive (OMM) mitochondrial-aggresomes present after 4 h CCCP drastically decreased after 14 h of CCCP treatment (Figure S2A and B). Instead, TOM20 shapes were converted to (autophagolysosomal) puncta that were significantly degraded over the time course of

mitophagy (Figure 1B, F and Figure S1E-F) unless when blocked by BafA (Figure 1H and I). On the other hand, the mean number of COX IV-positive (IMM) mitochondrial material only decreased to half at late stages of mitophagy, similar to SSBP1-positive mitochondrial-aggresomes (Figure S2A and B). The size of IMM or matrix aggresomes remained similar or only decreased slightly, respectively (Figure S2C and D). The decrease observed on IMM clump number can be explained by an increased appearance of IMM puncta at later stages of mitophagy, while matrix puncta were barely detectable and did not seem to change up to the 14 h time point (Figure S2E). Interestingly, the mean number of observed IMM puncta at late stages of mitophagy (14 h) was similar to the ones of OMM after 4 h of mitochondria depolarization, suggesting a similar -but delayed- autophagic delivery of IMM proteins (Figure S2E).

In order to confirm if the remaining inner- mitochondrial-aggresomes were eventually targeted by the autophagy machinery, a delayed autophagy-inhibiting experiment was performed. Here, mitochondrial depolarization was extended to 24 h and BafA was administered 8 h after the initiation of mitophagy (Figure 2A and B), allowing the formation of TOM20-negative mitochondrial-aggresomes but subsequently blocking the delivery of autophagosomes to the lysosome network. Interestingly, a significant amount of TOM20- and SSBP1-positive puncta were observed after delayed autophagy inhibition, when comparing to extended depolarizing conditions alone (Figure 2A and B). These data suggest lysosome-dependent steps for the later processing of TOM20-negative mitochondrial aggresomes and additionally validate lysosomal-dependent degradation of TOM20 puncta. Thus, there could be at least two distinct pools of mitochondrial proteins targeted via autophagy; the targeting of OMM proteins would occur first followed by a later autophagy targeting of inner- mitochondrial proteins ($\geq$ 8 h CCCP).

As shown above, TOM20-negative mitochondrial aggresomes were positive for ubiquitin and targeted by the autophagy adaptors p62 and TAX1BP1 (Figure 1C-E). In addition, similar to TOM20-positive puncta, both endogenous as well as overexpressed forms of LC3B either overlapped or partially co-localized with COX IV puncta (Figure 2C and Figure S1E). Moreover, COX IV puncta merged with LAMP1-positive lysosomes at later time points (14 h CCCP) (Figure 2E) and co-localized with LysoTracker (Figure 2D). Similar to what was observed for the mitochondrial aggresome size, the relative cell area of OMM, IMM or matrix puncta was reduced when comparing early to late mitochondrial depolarization times (Figure S2F), even though the relative area of IMM puncta seemed to be larger than the ones of OMM or matrix puncta (Figure S2F). Remarkably, the matrix components remained without any LAMP1 co-localization up to 14 h CCCP treatment (Figure 2F). Taken together, these data indicate that inner mitochondrial material is targeted to the autophagy machinery and delivered

to the lysosome degrading network at a later stage of the pathway (8-14 h CCCP), suggesting that PINK1/parkin-dependent mitophagy can trigger mitochondrial turnover in a sub-compartment specific manner and not only by promoting the engulfment of entire mitochondria.

In order to confirm piecemeal mitophagy in cell lines with endogenous parkin levels, HEK293 cells were exposed to extended mitochondria depolarization and the presence of TOM20-positive puncta that were negative for COX IV, SSBP1 or CS was observed (Figure S2H). Importantly, these events could also be validated in human NPCs (Figure S2I). Although the kinetics of mitophagy were much slower than in parkin-overexpressing cell clones, these findings suggest that distinct stepwise mitochondrial sub-compartment degradation can also take place in cells with endogenous parkin expression levels.

To gain higher resolution insight into the process of mitophagy in these cells, transmission electron microscopy (TEM) imaging was performed. Consistently, elongated mitochondria were observed under basal conditions (Figure S3A). However, upon mitochondrial depolarization, mitochondrial-aggregates as well as mitochondria being engulfed by autophagosomes were observed (Figure S3B). In addition, examples of engulfed mitochondria with damaged OMM could be observed (Figure S3C). These findings confirm autophagy-dependent mitochondrial turnover in WT-parkin HeLa cells and indicate that OMM rupture might occur during mitophagy.

Mitophagy is regulated by several distinct proteasome-dependent steps

There is a number of immediate-early proteasome targets that are removed from the OMM, which play an important role in the initiation of mitophagy [21,28,29]. Indeed, pretreatment with the proteasome inhibitors MG132 (Figure S1A) or Bortezomib (Figure S1B) not only reduced the degradation of the known proteasomal-dependent targets MFN1 and TOM70, respectively, but also compromised the degradation of all mitochondrial sub-compartment markers after both intermediate and long depolarization times. Indeed, when the proteasome was inhibited throughout the time course of mitophagy, all mitochondrial sub-compartment markers remained colocalized for at least 18 h, both in parkin-overexpressing HeLa cells and in HEK293 cells expressing endogenous levels of parkin (Figure S2J and K).

Next, we wondered if analogous to the proteasome dependence for mitophagy initiation at the OMM (see above), progression of mitophagy through the IMM could also be influenced by proteasome activity. Thus, a delayed-proteasome inhibition experiment was designed where proteasome inhibition was achieved by MG132 treatment together with mitochondrial depolarization with CCCP at several time points (Figure 3A). As expected, when mitochondria depolarization was extended up to 24 h, inner mitochondrial proteins were almost completely

degraded (Figure 3B). Interestingly, when the proteasome was inhibited after TOM20 removal had taken place (24 h CCCP + 8 h MG132), the degradation of inner mitochondrial proteins was reduced (Figure 3B). Quantification of Western blot band densities revealed a trend of increased IMM protein COX IV and the matrix protein SSBP1 upon delayed inhibition of the proteasome, while a significant increase was found for CS under the same conditions in comparison to CCCP treatment only (Figure 3C).

To visualize proteasome influence on the late stages of mitophagy, morphology of mitochondrial remnant entities was analyzed in a quantitative manner, comparing extended CCCP treatment only (24 h CCCP) to extended CCCP treatment combined with late proteasome inhibition (24 h CCCP + 8 h MG132) (Figure 3D-F). Under normal depolarization conditions, the OMM was reduced to very few TOM20-postive puncta and SSBP1 appeared to be fully degraded. Surprisingly, once MG132 was added at an intermediate mitophagy stage (>8 h CCCP), the OMM seemed to still be reduced to TOM20-positive puncta but the matrix sub-compartment remained and appeared in SSBP1-matrix positive aggregates (Figure 3D). Single cell analysis of the average SSBP1-positive aggregate number and size showed a significant increase of both parameters when proteasome inhibitor was added after 8 h of CCCP treatment (Figure 3E and F). Thus, proteasome action may be involved in the degradation of inner- mitochondrial remnants, adding a possible novel step for the progression of mitophagy.

Global proteome measurements confirm proteasome-sensitive steps in mitophagy

To extend these findings to the proteomic level, we performed quantitative mass spectrometry measurements of the proteasome inhibition experiment using whole cell lysate samples in several experimental settings (Figure 4A). All three replicates of each experimental set-up showed high overlap in protein identification and high correlation in protein regulation (Figure S4A-E). Stepwise degradation of mitochondrial sub-compartments was in accordance with previous studies [20]. Indeed, while OMM and IMS proteins were mostly degraded within 8 h of CCCP treatment (Figure S4F), IMM and especially matrix protein degradation only took place at later stages of mitophagy (24 h CCCP) (Figure S4G).

Effects of proteasome inhibition prior to mitochondria depolarization (t -0.5 h) was analyzed on parkin-HeLa cells undergoing mitophagy. In agreement with previous results, CCCP failed to induce mitophagy after pretreatment with MG132. Compared to cells without MG132 treatment, OMM and IMS proteins primarily affected during the first 8 h of mitophagy were significantly less degraded after pretreatment with the proteasomal inhibitor MG132 (Figure 4B).

Next, the involvement of proteasome activity during late stages of mitophagy was assessed. In samples where proteasomal activity was inhibited after 8 h of CCCP treatment (24 h CCCP, t +8 h MG132), the degradation of OMM and IMS proteins was largely unaffected (Figure 4C). However, the degradation of IMM and matrix proteins was strongly reduced (Figure 4C, lower panel). In the presence of MG132 after 8 h of CCCP treatment most of the regulated proteins ($p \leq 0.05$; indicated by the 5% curves; $p \leq 0.1$; indicated by the 10% curves) are annotated for these sub-mitochondrial localizations (Figure 4C, upper panel) (Supplementary Table 1). For example, the cluster of mitochondrial ribosomal proteins of the large subunit (MRPL) was significantly ($p \leq 0.05$) less degraded after delayed addition of the proteasome (Figure 4C), underscoring that mitophagy of the matrix depends on a second, delayed proteasome-regulated step.

Discussion

PINK1/parkin-dependent mitophagy removes damaged mitochondria in stressed cells via autophagy [18]. Wholesale mitophagy might be the result of this pathway, but sequential mitochondrial sub-compartment turnover may also play a role [22,26,30,31]. Here we report parkin-dependent piecemeal mitophagy involving step-by-step sub-compartment degradation mechanisms where both the ubiquitin proteasome system (UPS) and autophagy pathways appear to be involved.

Distinct subsets of OMM proteins are subject to immediate-early proteasomal and delayed autophagic degradation

Proteasome degradation is known to be involved in early stages of PINK1/parkin-dependent mitophagy by contributing to mitochondrial fission in order to facilitate mitochondrial engulfment by autophagosomes [21,32]. This is likely due to the proteasome-dependent removal of the mitochondrial fusion factor MFN1. In addition, previous studies involving the inhibition of proteasome degradation by either MG132 or lactacystin have shown that PINK1/parkin mitophagy was prevented under proteasome inhibition conditions [21,28]. Our data support the notion that proteasome-degradation is essential for successful mitochondria elimination and indicate that early elimination of OMM substrates (i.e: MFN1) can be considered a first checkpoint for mitophagy initiation.

In addition to proteasomal turnover, the extended ubiquitination events on the OMM promote the recognition of autophagy adaptors [5,16,33] . Indeed, ubiquitination events of OMM proteins and TOM20-positive mitochondrial-aggresomes triggered the recognition of autophagy adaptors in our model (Figure 1C-E). Those events were followed by the formation

of autophagosomes, as evidenced by TOM20 puncta positive for LC3B (Figure 1F and Figure S1E). However, not all TOM20 puncta observed were co-localizing with L3CB structures. This could reflect (1) the involvement of additional mammalian ATG8 family members [34] in the removal of TOM20 or (2) LC3B-independent pathways on the removal of OMM substrates. Indeed, other forms of OMM turnover that do not require autophagosome formation for ultimate delivery to lysosomes have been previously described and are known as MDVs [22]. While the formation mechanisms of MDVs are not yet fully understood, it has been suggested that MDVs serve as a first line of defense against mild mitochondrial stress conditions [31,35]. Thus, OMM turnover could occur via direct lysosomal delivery of specific OMM substrates as well as proteasome/autophagy dependent pathways, the latter being more prominent under strong mitophagy inducing conditions, as studied here.

Inner mitochondrial material is targeted to separate, late degradation pathways

The turnover rate of inner- mitochondrial-aggresomes appeared much distinct from that of OMM proteins (Figure 1B). However, delayed autophagy inhibition experiments suggested an involvement of the autophagy machinery for the turnover of inner- mitochondrial-aggresomes (Figure 2A and B). Indeed, similarly to what was observed for TOM20 puncta turnover, the involvement of autophagic degradation in the turnover of inner- mitochondrial aggresomes could be confirmed by co-localization of COX IV puncta with LC3B as well as LysoTracker (Figure 2C and D).

Overall, these data point to a temporal selectivity of the autophagic machinery, leading to the involvement of two separate autophagic waves. However, while further studies are needed to confirm a possible autophagy adaptor selectivity between the recognition of ubiquitinated OMM or inner- mitochondrial substrates, prohibitin 2 has been proposed to act as an inner- mitochondrial adaptor protein that directly interacts with LC3B [36]. The presence of other specific IMM proteins capable of interacting with autophagosomes could offer future insights into the upstream events that trigger selective autophagic removal of different mitochondrial sub-compartments.

The exact nature of TOM20-negative inner mitochondrial-aggregates remains to be further characterized, particularly with regard to the OMM composition at advanced stages of mitophagy. TEM showed examples of OMM-damaged mitochondria engaged with autophagosomes after 4 h CCCP treatment (Figure S3C). These data are in agreement with other studies reporting OMM-damage upon PINK1/parkin mitophagy induction [28,36]. Further studies shall elucidate the specific temporal dynamics and mechanisms of the interactions of mitochondrial sub-compartments with their respective degradation machineries.

Moreover, while our model of parkin-dependent mitophagy globally differs from a wholesale mitophagy turnover model, the sporadic presence of OMM and matrix material engaged in LC3B structures (Figure 1F and Figure S1E) and the presence of TOM20 puncta negative for LC3B, suggests that parkin-dependent mitochondrial turnover might combine both wholesale and piecemeal mitophagy turnover pathways. Thus, while most of the evidence on endogenous parkin-dependent wholesale mitophagy has been reported on tissue-specific cells where mitochondrial survival is crucial for their metabolic or physiological demands (i.e: neurons and hepatocytes) [8,37,38], it is possible that when cell survival is not strictly dependent on mitochondrial functions, wholesale mitophagy partially switches to piecemeal mitophagy; possibly involving MDV formation as well selective autophagic removal of mitochondrial sub-compartment proteins (Figure 1 and 2).

In addition, the kinetics of the pathway might play an important role on sub-compartment availability since mitophagy progression has been shown to differ between cell lines, even under parkin-overexpression conditions [39–41]. Actually, while endogenous parkin-dependent mitophagy in HEK293 and NPC cells revealed TOM20 staining patterns clearly distinguishable from inner- mitochondrial material, the mitophagy process was more protracted in cell lines expressing lower levels of endogenous parkin (Figure S2H-J).

Mitophagy is regulated by several distinct proteasome-dependent steps

Mitophagy initiation involves parkin-dependent ubiquitination of specific OMM proteins that are directly targeted to the proteasome, especially affecting proteins that are involved in mitochondrial fusion or transport [1,21,28,42]. As expected, proteasome inhibition prevented the elimination of proteasomal-dependent substrates (Figure S1A and B) and compromised the overall mitochondrial turnover in different cell lines (Figure S2J and K), indicating that OMM-proteasome degradation is upstream of autophagy activation during parkin-dependent mitophagy. These data support the notion that a first proteasomal-dependent targeting of the OMM is needed for sub-sequent mitophagy progression [28].

On the other hand, advanced stages of parkin-dependent mitophagy were characterized by the presence of inner- mitochondrial aggresomes (Figure 1B, 14 h CCCP). Such structures showed to be ubiquitinated and recognized by the autophagy adaptors p62 and TAX1BP1 (Figure 1C-E), similarly to what we observed for TOM20-positive mitochondrial aggresomes (Figure 1B, 4 h CCCP).

Because OMM turnover involved both proteasome and autophagy-dependent pathways, we hypothesized that a similar contribution of the two pathways could influence the degradation of inner- mitochondrial aggresomes. Surprisingly, delayed proteasome inhibition promoted an increase in the amount of inner- mitochondrial aggresomes after extended

mitochondrial depolarization (Figure 3D), suggesting proteasome-dependent targeting of inner- mitochondrial aggresomes. Importantly, delayed proteasome inhibition did not only affect the turnover of matrix proteins alone but also had an influence on COX IV turnover (Figure 3A), indicating that the observed TOM20-negative mitochondrial aggresomes are indeed COX IV-positive. In addition, because COX IV turnover seems to be autophagy-dependent (Figure 2C) and the initial OMM-turnover seems to be bound to a prior proteasomal-dependent OMM-degradation, it is possible that the delayed proteasomal inhibition indirectly impairs the autophagic machinery to target IMM-positive mitochondrial aggresomes.

While the exact mechanisms explaining how the UPS may interact with inner-mitochondrial aggresomes remains to be elucidated, it is possible that late OMM-turnover promotes a partial exposure of the IMM to the cytosol, allowing the UPS to act upon IMM substrates. Indeed, Wei and colleagues reported a clear OMM-rupture that allowed phagophore accessibility to the IMM in a prohibitin-dependent manner [36], thus we suggest that OMM-ruptured patches could facilitate access of proteasomes to IMM exposed regions. Alternatively, proteasomes might remove newly synthesized nuclear-encoded inner mitochondrial proteins, adding to the natural turnover of such proteins.

Conclusions

Taken together, our findings demonstrate that PINK1/parkin mitophagy occurs in a sequential manner, where outer mitochondrial membrane autophagy cargo is firstly separated from inner mitochondrial material for sub-sequent autophagolysosomal targeting. Importantly, such piecemeal mitophagy might also be observed under endogenous parkin expressing conditions, even though following a considerably slower kinetics. Additionally, we provide evidence of a potential proteasome-sensitive step which may regulate the progression of mitophagy towards complete mitochondria degradation. In sum, our study reveals later additional mitophagy steps: involving the delivery of mitochondrial sub-compartments to the lysosomal machinery in two separate consecutive autophagy waves and additionally suggesting the involvement of proteasomal action at later stages of mitophagy, similarly as it is observed at early stages of PINK1/parkin mitophagy on OMM substrates (Figure 5).

Materials and Methods

Cell culture, treatments and transfection

HeLa cells stably expressing 3xFlag-parkin WT [43] as well as HEK293 cells were cultured in high-glucose Dulbecco's modified Eagle's medium (DMEM) supplemented with 10% (v/v) fetal bovine serum (FBS) at 37°C with 5% CO_2. PentaKO HeLa cells were a kind gift from Prof. Richard Youle (National Institute of Health, Bethesda, USA) and were used as described [16].

Depolarization of mitochondria was achieved by adding 10 μM CCCP (Sigma, C2759) to the media. For better visualization of LC3B puncta, transfection of pEGFP-C1-LC3B [46] in WT-parkin HeLa cells was done. Briefly, 24 h prior to CCCP treatment, cells were transfected with pEGFP-C1-LC3B using FuGene6® (Promega, E269A) according to manufacturer instructions.

For proteasomal inhibition studies, cells were pretreated with 20 μM MG132 (Sigma, C2211) for 30 min before addition of an equal volume of media containing 20 μM CCCP, bringing the final concentrations of both MG132 and CCCP to 10 μM for the indicated incubation times. In delayed proteasome inhibition experiments cells were treated with either 10 μM MG132 or 400 nM Bortezomib (Sellekchem, S1013) for the indicated time points before or after CCCP administration. For autophagy inhibition experiments, cells were treated with 400 nM BafA (Sigma, 1793) for the indicated time points before or after CCCP administration. All treatments were combined with 10 μM CCCP.

NPCs were derived from healthy, human induced pluripotent stem cells and have been previously characterized and labelled in this manuscript as wtNPC line 1 [44] or wtNPC line 2 [45]. NPCs were cultured on Matrigel (Corning, 354320) coated plates in NPC medium containing a 1:1 mixture of DMEM-Ham's F12 (Merck, F4815) with Neurobasal (Gibco, 21103049) containing L-glutamine (Gibco, 35050061) and Penicillin/Streptomycin (Merck, A2213). Media was supplemented with N2 (Gibco, 17502-048) and B27 (Gibco, 12587-010) plus 3 μM CHIR 99021 (Axon Medchem, 1386), 200 μM ascorbic acid (Sigma-Aldrich, 50-81-7) and 0.5 μM purmorphamine (Calbiochem, 540220). Mitochondria depolarization was achieved by adding 100 μM Antimycin A supplemented with 10 μM Y-27632 (Selleckchem, S1049) for the indicated time points.

Antibodies

Table 1: List of primary and secondary antibodies and concentration used in this study

Primary antibodies

TOM70	1:1000	ProteinTech, 14528-1-AP
TOM20	1:1000 (IF)	Santa Cruz, sc-11415
TOM20	1:6000 (WB)	Proteintech, 11802-1-AP
	1:1000 (IF)	
VDAC	1:30000	Millipore, AB10527
Total ubiquitin (FK2 clone)	1:1000	Enzo Life Sciences, BML-PW88100100
p62/SQSTM	1:1000	BD Biosciences, 610832
COX IV	1:6000 (WB)	Cell Signaling, 4850

	1:1000 (IF)	
CS	1:6000 (WB) 1:1000 (IF)	GeneTex, GTX110624
SSBP1	1:500 (WB)	R&D Systems, AF6588
	1:1000 (IF)	
Vinculin	1:6000	Sigma Aldrich, V9131
MFN1	1:10000 (WB)	Abnova, H00055669-M04
	1:1000 (IF)	
□-actin	1:5000	Sigma Aldrich, A5441
LAMP1	1:500	DSHB Hybridoma Bank, clone H4A3
LC3B	1:250	GeneTex, GT3612
TAX1BP1	1:500	Novus Biologicals, NBP1-86662
Parkin	1:10000 (WB)	Cell Signaling, 4211S
	1:1000 (IF)	
Secondary antibodies		
Goat anti-mouse HRP	1:10000	Amersham Pharmacia, 115-035-003
Goat anti-rabbit HRP	1:10000	Amersham Pharmacia, 111-035-003
Goat anti-sheep HRP	1:10000	Amersham Pharmacia, 718-035-147
Alexa Fluor 647 donkey anti-sheep	1:1000	Invitrogen, A-21448
Alexa Fluor 488 donkey anti-mouse	1:1000	Invitrogen, A-21202
Alexa Fluor 488 donkey anti-rabbit	1:1000	Invitrogen, A-21206
Alexa Fluor 568 donkey anti-mouse	1:1000	Invitrogen, A-10037
Alexa Fluor 568 donkey anti-rabbit	1:1000	Invitrogen, A-10042
Alexa Fluor 350 goat anti-rabbit	1:1000	Invitrogen, A-11046
Alexa Fluor 350 goat anti-mouse	1:1000	Invitrogen, A-10045

Western blotting

Cell harvest was performed directly after a single wash with phosphate-buffered saline (PBS). Cells were pelleted at 972 x *g* for 1 min at 4°C. Pellets were resuspended in urea lysis buffer (10 mM Tris, pH 8.0, 100 mM NaH_2PO_4, and 8 M urea) and passed through a 26-gauge needle for at least 5 times. Debris was pelleted at 3151 x *g* for 15 min at 4°C to obtain whole cell lysate supernatants. Total protein was measured using the standard Bradford Protein Assay Kit (Bio-Rad). Samples were separated on 10% or 15% polyacrylamide gels or 4-20% gradient gels (TruPAGE precast gels, Merck) and run for 2 h at 140 V or 1 h at 100 V, respectively. Proteins were transferred to polyvinylidene fluoride membranes (Immobilon-P, Merck) for 2 h at 100 V,

blocked with 5% bovine serum albumin or non-fat dry milk in Tris-buffered saline buffer containing 0.1% Tween-20 (TBS-T). Membranes were incubated overnight with the indicated primary antibodies, washed at least three times with TBS-T and further incubated with matching horseradish peroxidase conjugated secondary antibodies diluted in 5% milk. Chemiluminescent reaction was carried out with Western blot chemiluminescent-horseradish peroxidase substrate (Millipore). Three TBS-T washings of at least 5 min were performed between each incubation step. Ultracruz autoradiography films (Santa Cruz Biotechnology) were used for band visualizations.

Immunostaining and microscopy

Cells were seeded on pre-coated coverslips with poly-D-lysine (Sigma, P6407) and treated for the indicated time points. In addition, NPCs were cultured on Matrigel coated plates in NPC medium as previously described. Cells were fixed with 4% paraformaldehyde in PBS for 20 min at room temperature (RT). Cell permeabilization was achieved with 1% Triton X-100 for 5 min at RT and cells were washed three times with PBS. Blocking was performed with 10% FBS in PBS for 1 h at RT, followed by primary antibody incubation with 5% FBS for 2 h at RT. Cells were washed three times with PBS before incubating for 1 h at RT with the secondary antibody diluted in PBS with 10% FBS. Nuclei were stained with 2 µg/ml Hoechst (Molecular Probes, 3570) after washing the cells for at least three times with PBS. Cells were mounted onto coverslips using Fluorescent Mounting Medium (Dako). Imaging was performed using an AxioImager microscope equipped with an ApoTome imaging system using 63X or 100X objectives (Carl Zeiss). The images were processed with AxioVision 4.9.1 software (Carl Zeiss). For immunostaining of endogenous LC3B, normal goat serum instead of FBS was used.

For lysotracker staining of fixed cells, 500 nM LysoTracker RED (Invitrogen, LT528) was added to the cell culture 30 min before fixation. Then cells were washed with ice-cold DMEM for 10 min followed by two gentle washes of ice-cold PBS. Cells were fixed with 4% paraformaldehyde and the immunostaining was performed as previously described. LysoTracker red was imaged on 568 channel and mitochondrial markers were stained with Alexa fluor 350 and imaged on the Hoechst channel with an Apotome imaging system as described above.

CellProfiler analysis

Image analysis of mitochondrial morphology was performed using CellProfiler (4.2.1 version). The identification of mitochondrial-aggresomes and puncta was performed as follows: all

mitochondrial objects in between a range of 6-500 px range were identified and merged together as a new single object if the distance between the initial primary objects was ≤2 px apart. New merged single objects with a minimal area of 300-500 px were considered aggresomes and objects with an area <300 px were considered dots.

For delayed inhibition experiments, mitochondrial objects of at least 30 px were identified and merged as a single object if ≤15 px apart. New merged single objects with an area below 300 px were considered puncta, objects with an area of >300 were considered aggresomes.

Transmission electron microscopy

For TEM analysis, HeLa cells were cultured and treated with CCCP as described above for IFM, except cells were grown on 22 x 22 mm square glass coverslips. Cells were prefixed in culture medium with 2.5% glutaraldehyde and 4% paraformaldehyde, pH adjusted to 7.2, for 20 minutes at 37°C. Cells were then fixed in 0.1 M HEPES, 4 mM $CaCl_2$, 2.5% glutaraldehyde (Serva Electrophoresis,), 4% formaldehyde (Science Services), pH 7.2 for 1 h at RT plus 3 h at 4°C, the fixative being replaced a few times. Cells were postfixed with 1% OsO_4 (in distilled water) for 60 min at 4°C and then incubated in 1% uranyl acetate overnight at 4°C. Between each step the samples were washed 3-4 times for 5 min each with distilled water. Dehydration of the samples in ethanol, infiltration with Epon (Serva Electrophoresis) and flat embedding was done following standard procedures [50]. Ultrathin sections (~60-70 nm) were cut with a diamond knife (type ultra 35°; Diatome, Biel, Switzerland) with an EM UC6 ultramicrotome (Leica, Wetzlar, Germany) and mounted on single-slot Pioloform-coated copper grids (Plano, Wetzlar, Germany). Sections were stained with uranyl acetate and lead citrate [51] and viewed with a JEM-2100 transmission electron microscope (JEOL, Tokyo, Japan) operated at 80 kV. Micrographs were taken using a 4000 x 4000 charge-coupled device camera (UltraScan 4000; Gatan, Pleasanton, CA) and Gatan Digital Micrograph software (version 1.70.16.). Image brightness and contrast were adjusted and figures assembled using Adobe Photoshop 8.0.1 and Inkscape 1.0 beta.

Quantitative proteomics

For all proteomics studies, 10 µg of protein lysate per dimethyl labeling channel were used. First, disulfide bonds were reduced with 10 mM dithiothreitol for 1 h at RT, followed by alkylation with 55 mM iodoacetamide for 1 h at RT in the dark. Prior to overnight digestion with trypsin (Promega Corporation, V5280), pre-digestion with lysyl endopeptidase (Wako Chemicals, 121-05063) for 3 h was performed in a peptidase-protein ratio of 1:100 at RT.

Digestion was quenched by adding 1% trifluoroacetic acid. Peptides were dimethyl-labeled on C18 StageTips as described previously [47]. Label efficiency and peptide mixing ration of 1:1:1 was checked in pilot LC-MS/MS runs. For peptide fractionation the Pierce™ High pH Reversed-Phase Peptide Fractionation Kit (Thermo Fisher Scientific, 84868) was applied as described earlier [20]. Prior to LC-MS/MS measurement, peptides were desalted on C18 StageTips. All fractions were analyzed on an Q Exactive HF mass spectrometer (Thermo Fischer Scientific), online-coupled to Easy-nLC 1200 UHPLC (Thermo Fischer Scientific) as described earlier [20]. In short, peptides were separated on a 20 cm analytical column (75 µm ID PicoTip fused silica emitter, New Objective) in-house packed with ReproSil-Pur C18-AQ 1.9 µm resin (Dr Maisch GmbH), by a fraction-specific segmented 90 min gradient of solvent A (0.1% formic acid) and solvent B (0.1% formic acid in 80% acetonitrile) at 40°C and a 200 nl/min flow rate. Electrospray ionization was used to ionize eluted peptides. The mass spectrometer was operated in a positive ion mode. Full MS spectra were recorded in a scan range of 300-1650 m/z at resolution 60k. The top 12 most abundant multiple charged ions were selected for HCD fragmentation (AGC target: 3e6, Maximum IT: 25 ms). MS2 spectra were acquired at resolution 30k (AGC target: 1e5, Maximum IT: 45 ms).

LC-MS/MS raw data were searched against the Uniprot Homo sapiens database (released 11.12.2019, 96,818 entries) and commonly observed contaminants using the Andromeda search engine integrated into the MaxQuant software suite (version 2.0.3.0) [48]. All search parameters were kept to default except for the following. Carbamidomethylation of cysteine in addition to oxidation of methionine and protein N-terminal acetylation were set as fixed and variable modifications, respectively. Trypsin was selected as a protease and a maximum of two missed cleavages were allowed. Light (28.03 Da), intermediate (32.06 Da), and heavy (36.08 Da) dimethyl labels were specified for N termini and lysine residues. A minimum of two peptide ratio counts were required for protein quantification. Precursor ion mass tolerance was set to 4.5 ppm and fragment ions to 20 ppm, re-quantify and match-between runs between fractions of the same sample were enabled. The mass spectrometry proteomics data have been deposited to the ProteomeXchange Consortium via the PRIDE [49] partner repository with the dataset identifier PXD034136.

Statistics

CellProfiler analysis of mitochondrial sub-compartment degradation as well as late inhibition experiments was performed using one-way ANOVA and Tukey test as post-hoc analysis test, using Graph Pad prism 6 software. Graphs show mean ± SEM of cell populations from at least three independent experiments. Significance is indicated by asterisks as described in figure legends.

Statistical analysis of quantitative proteomics data was performed with Perseus software suite (version 1.6.15.0) [52]. First, all reverse and potentially contaminant hits were filtered out. For protein annotation MitoCarta 3.0 was used as a resource [53]. Only protein ratios present in two out of three replicates were considered for downstream analysis. To identify significantly regulated proteins between different treatments, a one-sample t-test was performed (p-value ≤ either 0.1 or 0.05).

Venn Diagrams, representing the overlap of protein identification between replicates were performed with the online tool http://www.interactivenn.net/ (accessed on 14th April 2022) [54].

Acknowledgements

This work was funded by the German Research Foundation (DFG) Research Training Group GRK2364 and the Hertie Foundation. We thank David Schüssele and Tassula Proikas-Cezanne for helpful suggestions and critically reading the manuscript. We also thank Richard Youle and Chunxin Wang for sharing the PentaKO HeLa cell line (also acknowledging Henrietta Lacks and her family).

References

1. Terradas AL, Zittlau KI, Macek B, Fraiberg M, Elazar Z, Kahle PJ. Regulation of mitochondrial cargo-selective autophagy by posttranslational modifications. J Biol Chem 2021 ; 297(5):101339. Pubmed: PMID 34688664

2. Kitada T, Aakawa S, Hattori N, Matsumine H, Yokochi M, Mizuno Y, Shimizu N. Mutations in the parkin gene causeautosomal recessive juvenile parkinsonism. Nat Lett 1998 ; 169(1993):166–9.

3. Valente EM, Abou-Sleiman PM, Caputo V, Muqit MMK, Harvey K, Gispert S, Ali Z, Del Turco D, Bentivoglio AR, Healy DG, et al. Hereditary early-onset Parkinson's disease caused by mutations in PINK1. Science (80-) 2004 ; 304(5674):1158–60. Pubmed: PMID 15087508

4. Springer W, Kahle PJ. Regulation of PINK1-Parkin-mediated mitophagy. Autophagy 2011 ; 7(3):266–78. Pubmed: PMID 21187721

5. Geisler S, Holmström KM, Skujat D, Fiesel FC, Rothfuss OC, Kahle PJ, Springer W. PINK1/Parkin-mediated mitophagy is dependent on VDAC1 and p62/SQSTM1. Nat Cell Biol 2010 ; 12(2):119–31. Pubmed: PMID 20098416

6. Georgakopoulos ND, Wells G, Campanella M. The pharmacological regulation of cellular mitophagy. Nat Chem Biol 2017 ; 13(2):136–46. Pubmed: PMID 28103219

7. Kasianowicz J, Benz R, McLaughlin S. The kinetic mechanism by which CCCP (carbonyl cyanide m-chlorophenylhydrazone) transports protons across membranes. J Membr Biol 1984 ; 82(2):179–90.

8. Ashrafi G, Schlehe JS, LaVoie MJ, Schwarz TL. Mitophagy of damaged mitochondria occurs locally in distal neuronal axons and requires PINK1 and Parkin. J Cell Biol 2014 ; 206(5):655–70. Pubmed: PMID 25154397

9. Chung-Han H, Atossa S, Ashley E. G, Alexandre B da C, Lena F. B, Lawrence ES, Birgitt S, Krainc D, D T, Palmer1, 2 and XW. Functional Impairment in Miro Degradation and Mitophagy Is a Shared Feature in Familial and Sporadic Parkinson's Disease. Physiol Behav 2017 ; 176(5):139–48.

10. Sekine S. PINK1 import regulation at a crossroad of mitochondrial fate: The molecular mechanisms of PINK1 import. J Biochem 2020 ; 167(3):217–24. Pubmed: PMID 31504668

11. Kondapalli C, Kazlauskaite A, Zhang N, Woodroof HI, Campbell DG, Gourlay R, Burchell L, Walden H, MacArtney TJ, Deak M, et al. PINK1 is activated by mitochondrial membrane potential depolarization and stimulates Parkin E3 ligase activity by phosphorylating Serine 65. Open Biol 2012 ; 2(MAY). Pubmed: PMID 22724072

12. Koyano F, Okatsu K, Kosako H, Tamura Y, Go E, Kimura M, Kimura Y, Tsuchiya H, Yoshihara H, Hirokawa T, et al. Ubiquitin is phosphorylated by PINK1 to activate parkin. Nature 2014 ; 510(7503):162–6. Pubmed: PMID 24784582

13. Matsuda N. Phospho-ubiquitin: Upending the PINK-Parkin-ubiquitin cascade. J Biochem 2016 ; 159(4):379–85. Pubmed: PMID 26839319

14. Ordureau A, Sarraf SA, Duda DM, Heo JM, Jedrychowski MP, Sviderskiy VO, Olszewski JL, Koerber JT, Xie T, Beausoleil SA, et al. Quantitative proteomics reveal a feedforward mechanism for mitochondrial PARKIN translocation and ubiquitin chain synthesis. Mol Cell 2014 ; 56(3):360–75. Pubmed: PMID 25284222

15. Heo JM, Ordureau A, Paulo JA, Rinehart J, Harper JW. The PINK1-PARKIN Mitochondrial Ubiquitylation Pathway Drives a Program of OPTN/NDP52 Recruitment and TBK1 Activation to Promote Mitophagy. Mol Cell 2015 ; 60(1):7–20. Pubmed: PMID 26365381

16. Lazarou M, Sliter DA, Kane LA, Sarraf SA, Wang C, Burman JL, Sideris DP, Fogel AI, Youle RJ. The ubiquitin kinase PINK1 recruits autophagy receptors to induce mitophagy. Nature 2015 ; 524(7565):309–14. Pubmed: PMID 26266977

17. Dikic I, Elazar Z. Mechanism and medical implications of mammalian autophagy. Nat Rev Mol Cell Biol 2018 ; 19(6):349–64. Pubmed: PMID 29618831

18. Wade Harper J, Ordureau A, Heo JM. Building and decoding ubiquitin hains for mitophagy. Nat Rev Mol Cell Biol 2018 ; 19(2):93–108. Pubmed: PMID 29358684

19. Kolitsida P, Zhou J, Rackiewicz M, Nolic V, Dengjel J, Abeliovich H. Phosphorylation of mitochondrial matrix proteins regulates their selective mitophagic degradation. Proc Natl Acad Sci U S A 2019 ; 116(41):20517–27. Pubmed: PMID 31548421

20. Zittlau KI, Lechado-Terradas A, Nalpas N, Geisler S, Kahle PJ, MacEk B. Temporal Analysis of Protein Ubiquitylation and Phosphorylation During Parkin-Dependent Mitophagy. Mol Cell Proteomics 2022 ; 21(2):100191. Pubmed: PMID 34974192

21. Tanaka A, Cleland MM, Xu S, Narendra DP, Suen DF, Karbowski M, Youle RJ. Proteasome and p97 mediate mitophagy and degradation of mitofusins induced by Parkin. J Cell Biol 2010 ; 191(7):1367–80. Pubmed: PMID 21173115

22. Soubannier V, McLelland GL, Zunino R, Braschi E, Rippstein P, Fon EA, McBride HM. A vesicular transport pathway shuttles cargo from mitochondria to lysosomes. Curr Biol 2012 ; 22(2):135–41. Pubmed: PMID 22226745

23. Mindell JA. Lysosomal acidification mechanisms. Annu Rev Physiol 2012 ; 74:69–86. Pubmed: PMID 22335796

24. Klionsky DJ, Abdelmohsen K, Abe A, Abedin MJ, Abeliovich H, Arozena AA, Adachi H, Adams CM, Adams PD, Adeli K, et al. Guidelines for the use and interpretation of assays for monitoring autophagy (3rd edition). Autophagy 2016 ; 12(1):1–222. Pubmed: PMID 26799652

25. Zhou J, Tan SH, Nicolas V, Bauvy C, Yang N Di, Zhang J, Xue Y, Codogno P, Shen HM. Activation of lysosomal function in the course of autophagy via mTORC1 suppression and autophagosome-lysosome fusion. Cell Res 2013 ; 23(4):508–23. Pubmed: PMID 23337583

26. Hsieh CW, Yang WY. Omegasome-proximal PtdIns(4,5)P 2 couples F-actin mediated mitoaggregate disassembly with autophagosome formation during mitophagy. Nat Commun 2019 ; 10(1):1–12. Pubmed: PMID 30814505

27. Lee JY, Nagano Y, Taylor JP, Lim KL, Yao TP. Disease-causing mutations in Parkin impair mitochondrial ubiquitination, aggregation, and HDAC6-dependent mitophagy. J Cell Biol 2010 ; 189(4):671–9. Pubmed: PMID 20457763

28. Yoshii SR, Kishi C, Ishihara N, Mizushima N. Parkin mediates proteasome-dependent protein degradation and rupture of the outer mitochondrial membrane. J Biol Chem 2011 ; 286(22):19630–40. Pubmed: PMID 21454557

29. Wang H, Song P, Du L, Tian W, Yue W, Liu M, Li D, Wang B, Zhu Y, Cao C, et al. Parkin ubiquitinates Drp1 for proteasome-dependent degradation: Implication of dysregulated mitochondrial dynamics in Parkinson disease. J Biol Chem 2011 ; 286(13):11649–58. Pubmed: PMID 21292769

30. Yang JY, Yang WY. Bit-by-bit autophagic removal of parkin-labelled mitochondria. Nat Commun 2013 ; 4. Pubmed: PMID 24013556

31. McLelland GL, Soubannier V, Chen CX, McBride HM, Fon EA. Parkin and PINK1 function in a vesicular trafficking pathway regulating mitochondrial quality control. EMBO J 2014 ; 33(4):282–95. Pubmed: PMID 24446486

32. Twig G, Elorza A, Molina AJA, Mohamed H, Wikstrom JD, Walzer G, Stiles L, Haigh SE, Katz S, Las G, et al. Fission and selective fusion govern mitochondrial segregation and elimination by autophagy. EMBO J 2008 ; 27(2):433–46. Pubmed: PMID 18200046

33. Shi J, Fung G, Deng H, Zhang J, Fiesel F, Springer W, Li X, Luo H. NBR1 is dispensable for PARK2-mediated mitophagy regardless of the presence or absence of SQSTM1. Cell Death Dis 2015 ; 6(10):1–9. Pubmed: PMID 26512954

34. Johansen T, Lamark T. Selective Autophagy: ATG8 Family Proteins, LIR Motifs and Cargo Receptors. J Mol Biol 2020 ; 432(1):80–103. Pubmed: PMID 31310766

35. Sugiura A, McLelland G, Fon EA, McBride HM. A new pathway for mitochondrial quality control: mitochondrial-derived vesicles. EMBO J 2014 ; 33(19):2142–56. Pubmed: PMID 25107473

36. Wei Y, Chiang W-C, Sumpter RJ, Mishra P, Levine B. Prohibitin 2 Is an Inner Mitochondrial Membrane Mitophagy Receptor. Cell 2018 ; 176(5):139–48.

37. Ylä-Anttila P, Vihinen H, Jokitalo E, Eskelinen EL. Chapter 10 Monitoring Autophagy by Electron Microscopy in Mammalian Cells. Methods Enzymol 2009 ; 451(C):143–64. Pubmed: PMID 19200881

38. Kim I, Lemasters JJ. Mitochondrial degradation by autophagy (mitophagy) in GFP-LC3 transgenic hepatocytes during nutrient deprivation. Am J Physiol - Cell Physiol 2011 ; 300(2):308–17. Pubmed: PMID 21106691

39. Kishi-Itakura C, Buss F. The use of correlative light-electron microscopy (CLEM) to study PINK1/Parkin-mediated mitophagy. Methods Mol Biol 2018 ; 1759(March 2017):29–39. Pubmed: PMID 28361485

40. Pickles S, Vigié P, Youle RJ. Mitophagy and Quality Control Mechanisms in Mitochondrial Maintenance. Curr Biol 2018 ; 28(4):R170–85. Pubmed: PMID 29462587

41. Grenier K, McLelland GL, Fon EA. Parkin- and PINK1-dependent mitophagy in neurons: Will the real pathway please stand up? Front Neurol 2013 ; 4 JUL(July):1–8.

42. Oshima Y, Cartier E, Boyman L, Verhoeven N, Polster BM, Huang W, Kane M, Jonathan Lederer W, Karbowski M. Parkin-independent mitophagy via drp1-mediated outer membrane severing and inner membrane ubiquitination. J Cell Biol 2021 ; 220(6). Pubmed: PMID 33851959

43. Geisler S, Jäger L, Golombek S, Nakanishi E, Hans F, Casadei N, Terradas AL, Linnemann C, Kahle PJ. Ubiquitin-specific protease USP36 knockdown impairs Parkin-dependent mitophagy via downregulation of Beclin-1-associated autophagy-related ATG14L. Exp Cell Res 2019 ; 384(2):111641. Pubmed: PMID 31550441

44. Bus C, Zizmare L, Feldkaemper M, Geisler S, Zarani M, Schaedler A, Klose F, Admard J, Mageean CJ, Arena G, et al. Human Dopaminergic Neurons Lacking PINK1 Exhibit Disrupted Dopamine Metabolism Related to Vitamin B6 Co-Factors. iScience 2020 ; 23(12). Pubmed: PMID 33299968

45. Schwarz L, Casadei N, Fitzgerald JC. Generation of R272Q, S156A and K572R

RHOT1/Miro1 point mutations in iPSCs from a healthy individual using FACS-assisted CRISPR/Cas9 genome editing. Stem Cell Res 2021 ; 55:102469. Pubmed: PMID 34359002

46. Krebiehl G, Ruckerbauer S, Burbulla LF, Kieper N, Maurer B, Waak J, Wolburg H, Gizatullina Z, Gellerich FN, Woitalla D, et al. Reduced basal autophagy and impaired mitochondrial dynamics due to loss of Parkinson's disease-associated protein DJ-1. PLoS One 2010 ; 5(2). Pubmed: PMID 20186336

47. Boersema PJ, Raijmakers R, Lemeer S, Mohammed S, Heck AJR. Multiplex peptide stable isotope dimethyl labeling for quantitative proteomics. Nat Protoc 2009 ; 4(4):484–94. Pubmed: PMID 19300442

48. Cox J, Mann M. MaxQuant enables high peptide identification rates, individualized p.p.b.-range mass accuracies and proteome-wide protein quantification. Nat Biotechnol 2008 ; 26(12):1367–72. Pubmed: PMID 19029910

49. Perez-Riverol Y, Bai J, Bandla C, García-Seisdedos D, Hewapathirana S, Kamatchinathan S, Kundu DJ, Prakash A, Frericks-Zipper A, Eisenacher M, et al. The PRIDE database resources in 2022: A hub for mass spectrometry-based proteomics evidences. Nucleic Acids Res 2022 ; 50(D1):D543–52. Pubmed: PMID 34723319

50. Rogowski M, Scholz D, Geimer S. Electron microscopy of flagella, primary cilia, and intraflagellar transport in flat-embedded cells. Methods Enzymol 2013 ; 524:243–63. Pubmed: PMID 23498744

51. Reynolds ES. The use of lead citrate at high pH as an electron-opaque stain in electron microscopy. J Cell Biol 1963 ; 17(1):208–12. Pubmed: PMID 13986422

52. Tyanova S, Temu T, Sinitcyn P, Carlson A, Hein MY, Geiger T, Mann M, Cox J. The Perseus computational platform for comprehensive analysis of (prote)omics data. Nat Methods 2016 ; 13(9):731–40. Pubmed: PMID 27348712

53. Rath S, Sharma R, Gupta R, Ast T, Chan C, Durham TJ, Goodman RP, Grabarek Z, Haas ME, Hung WHW, et al. MitoCarta3.0: An updated mitochondrial proteome now with sub-organelle localization and pathway annotations. Nucleic Acids Res 2021 ; 49(D1):D1541–7. Pubmed: PMID 33174596

54. Heberle H, Meirelles VG, da Silva FR, Telles GP, Minghim R. InteractiVenn: A web-based tool for the analysis of sets through Venn diagrams. BMC Bioinformatics 2015 ; 16(1):1–7. Pubmed: PMID 25994840

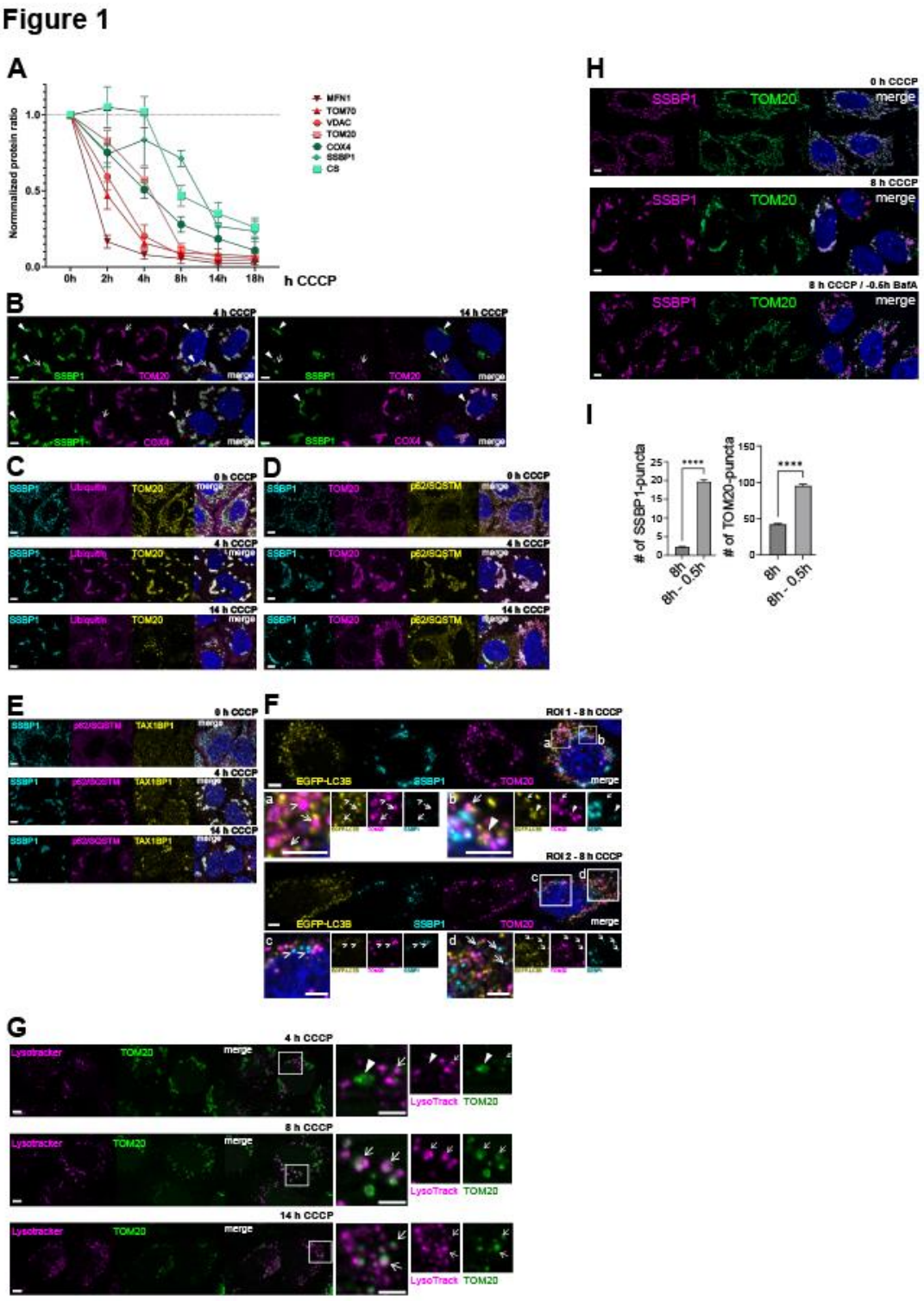

Figure 1: Differential degradation dynamics of mitochondrial sub-compartments correlate with delivery to the autophagolysosomal machinery. (**A**) Relative mitochondrial protein levels from Western blotting quantification. Data of at least three independent experiments. Data points: Mean ± SEM. (**B**) Representative immunofluorescence images of mitochondrial sub-compartments at the indicated CCCP treatment time points. Arrowheads indicate complete (4 h) or mitochondrial aggregates (14 h). Arrows indicate mitochondrial puncta. (**C**) TOM20-positive aggresomes (yellow) as well as SSBP1-aggregates (cyan) are positive for total

ubiquitin (magenta) at the indicated time points. (**D and E**) TOM20 (magenta) and SSSBP1-aggresomes (cyan) are positive for (**D**) p62/SQSTM (yellow) and (**E**) TAX1BP1 at the indicated time points of CCCP treatment. (**F**) Mitochondrial puncta (TOM20, magenta and SSBP, cyan) co-staining with EGFP-LC3B (yellow). Arrows indicate mitochondrial puncta partially engaged with EGFP-LC3B structures. Closed arrowheads indicate complete overlap of mitochondrial puncta and EGFP-LC3B. Open arrowheads indicate EGFP-LC3B-negative mitochondrial puncta. Two ROIs are chosen in order to show all observed features: ROI 1 indicates a representative mitophagy stage for the 8 h time point. ROI 2 represents <10% of cell population where SSBP1 puncta can be observed already. (**G**) Representative immunofluorescence images showing TOM20 puncta (green) co-localizing with LysoTracker (magenta) at the indicated time points. Arrows indicate mitochondrial puncta while arrowheads indicate TOM20-aggregates. (**H and I**) Influence of BafA inhibition on OMM mitochondrial degradation. (**H**) Representative immunofluorescence images showing TOM20 (green) and SSBP1 (magenta) structures at the indicated CCCP-treatment time points in combination with autophagy inhibition (BafA). (**I**) Single-cell analysis of mean number of mitochondrial SSBP1- and TOM20 puncta in (**H**). Bars: Mean ± SEM. ****: p≤0.0001. All scale bars = 5 µm.

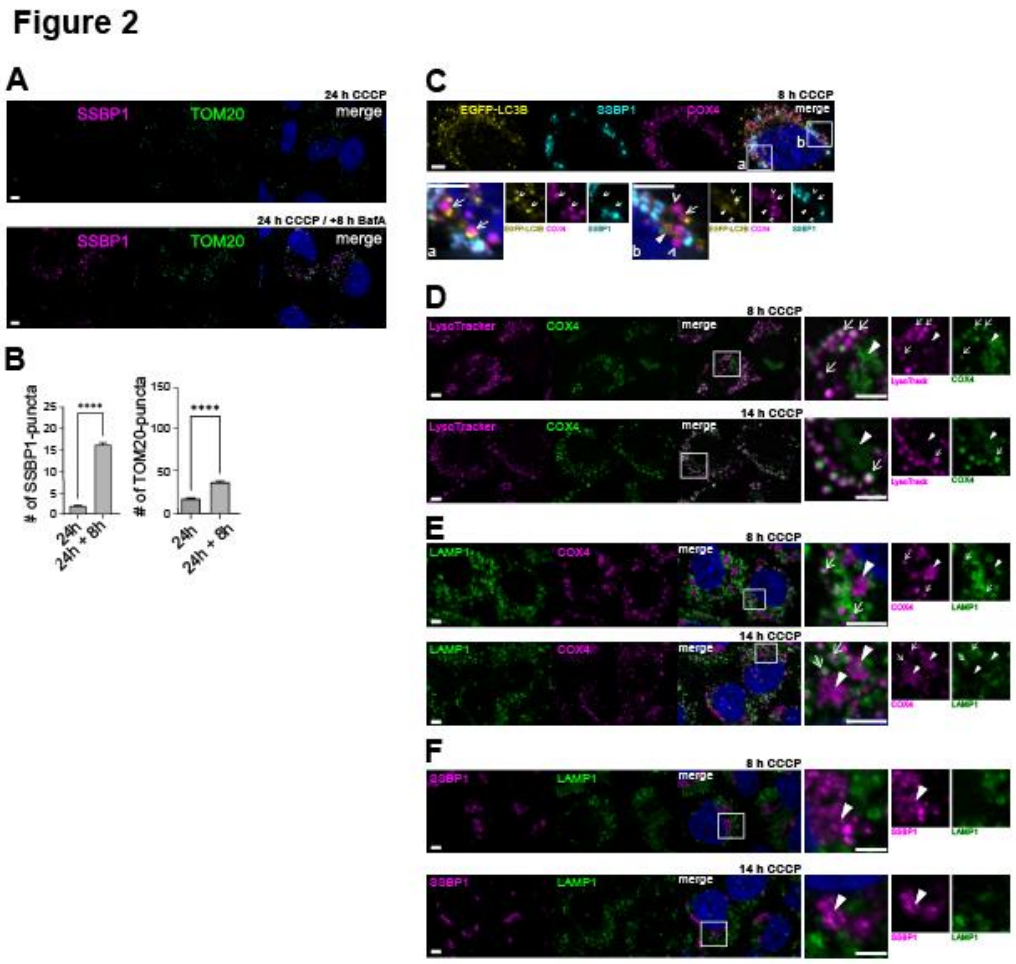

Figure 2: Autophagy activation and delivery to lysosomes of inner- mitochondrial material. (**A and B**) Influence of BafA inhibition on TOM20-negative mitochondrial-aggresomes. (**A**) Representative immunofluorescence images showing TOM20 (green) and SSBP1 (magenta)

structures at the indicated CCCP-treatment time points in combination with autophagy inhibition (BafA). (**B**) Single-cell analysis of mean number of mitochondrial SSBP1 and TOM20 puncta in (**A**). (**C**) COX IV-positive puncta (magenta) are positive for EGFP-LC3B (yellow). Arrows indicate COX IV puncta partially engaged with EGFP-LC3B structures. Closed arrowheads indicate complete overlap of COX IV puncta and EGFP-LC3B. Open arrowheads indicate COX IV puncta non co-localizing with EGFP-LC3B. (**D**) Representative immunofluorescence images showing COX IV-positive puncta (green) co-localizing with LysoTracker (magenta) at the indicated time points. Arrows indicate mitochondrial puncta while arrowheads indicate inner- mitochondrial remnants. (**E and F**) Representative immunofluorescence images showing (**E**) COX IV-positive (magenta) or (**F**) SSBP1-positive mitochondrial remnants (magenta) close to LAMP1 patches (green) at the indicated time points. Arrows indicate mitochondrial puncta while arrowheads indicate inner- mitochondrial remnants. ****: p ≤0.0001. All scale bars = 5 µm.

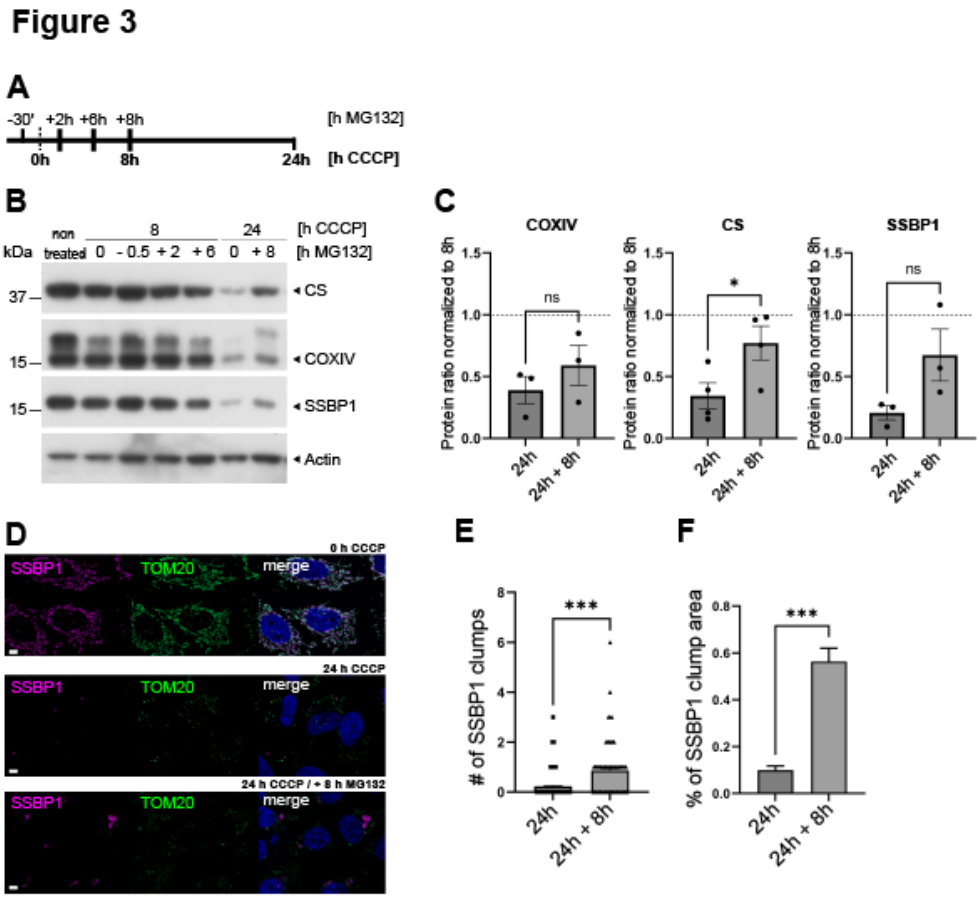

Figure 3: Proteasome action is required at late stages of mitophagy. (**A**) Scheme of treatment time points for proteasome inhibition experiments. Bold text indicates treatment with CCCP while normal text indicates treatment with proteasome inhibitor MG132. (**B and C**) Western blot analysis of proteasome-influence on the indicated inner- mitochondrial proteins. (**D**) Representative images of WT-parkin HeLa cells showing SSBP1 (magenta) and TOM20 (green) after 24 h of CCCP treatment or CCCP treatment combined with MG132 added after 8 h of mitochondria depolarization. Scale bar = 5 µm. (**E and F**) Single cell analysis of mean

SSBP1 clump number (**E**) and relative average SSBP1 clump area (**F**) per cell. Bars: Mean ± SEM. ns: non-significant; *: p≤0.05, ***: p≤0.001.

Figure 4

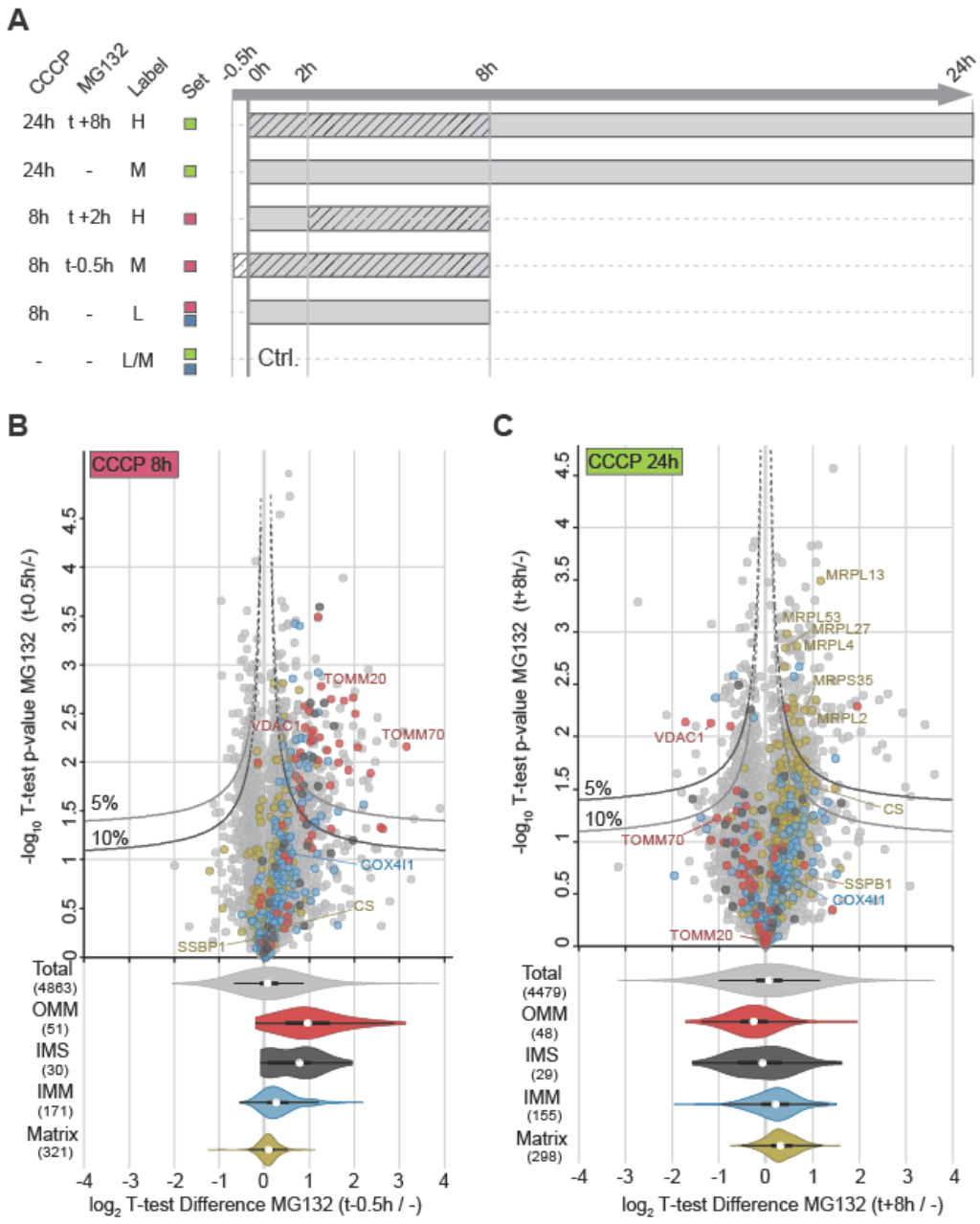

Figure 4: Proteomic validation of proteasome-sensitive steps during mitophagy. (**A**) Experimental design and dimethyl labelling scheme, where t defines the starting point of CCCP treatment. Color coding reflects dimethyl labelling sets. Solid: CCCP treatment, stripes: MG132 treatment. (**B**) Mitochondrial protein degradation after 8 h of mitophagy compared to cells pretreated with or without MG132 (t - 0.5 h) shows less degradation of OMM and IMS proteins. IMM and matrix proteins appeared less affected the 8 h time point as these sub-compartments were degraded during later stages of mitophagy. (**C**) Delayed MG132 (t + 8 h) treatment compared with not proteasome inhibited after 24 h of CCCP treatment highlights dependency of IMM and matrix protein degradation on proteasomal activity. The 5% and 10% curves in the

upper panels categorize p≤0.05 and p≤0.1 values, respectively, for proteins with log2 T-test Difference >1.3.

Figure 5

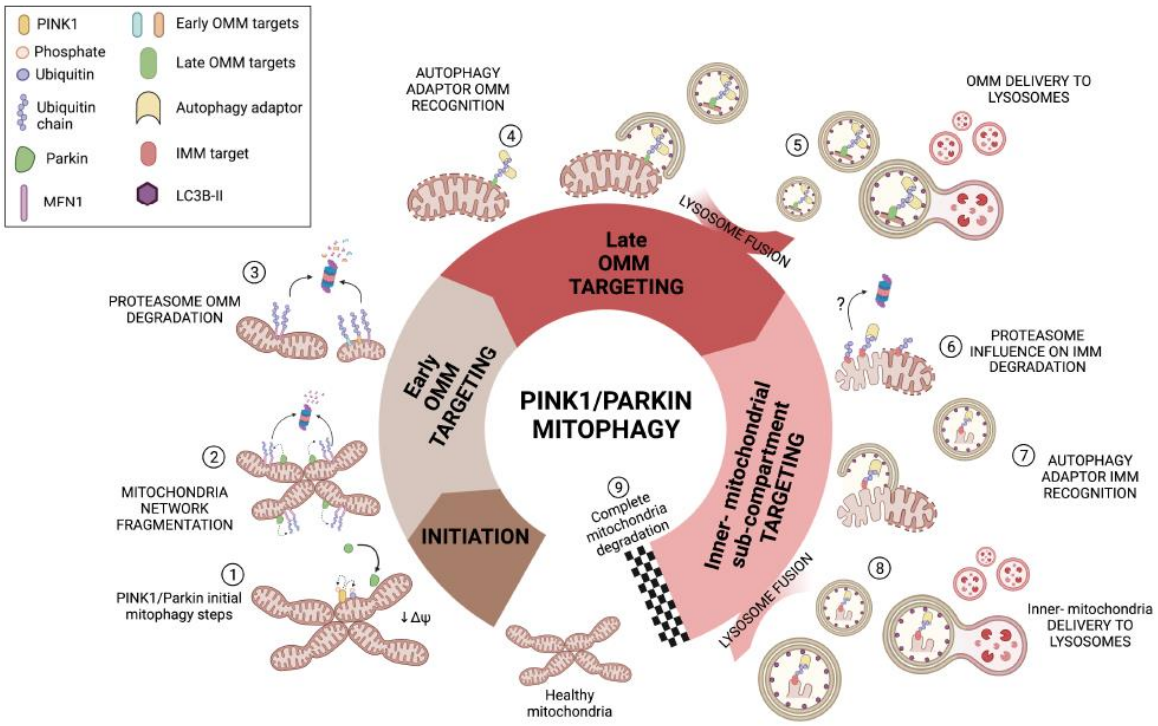

Figure 5: Schematic representation of PINK1/parkin mitophagy dynamics. After healthy mitochondria are compromised with depolarizing agents, PINK1/parkin initial steps take place (1) and further promote mitochondrial network fractionation where a first round of proteasomal degradation is involved (2-3). Ubiquitinations previously built by parkin on OMM substrates promote the docking of autophagy adaptors (4) which engage with building autophagosomes that will eventually fuse with lysosomes, promoting autophagic degradation of OMM substrates (5-6). After the OMM removal, inner- mitochondrial aggregates prevail. A potential late-proteasome degradation step is required for the final degradation of inner- mitochondrial proteins before they can be engulfed in autophagolysosomes (7). Similar as in step (5), ubiquitinations of inner- mitochondrial substrates lead to the docking of autophagy adaptors and autophagosome biogenesis is promoted on those particular spots leading to the delivery of inner- mitochondria remnants to lysosomes for complete final mitochondria degradation (8-10). Adapted from “Cell Cycle Checkpoints” by BioRender.com (2022). Retrieved from https://app.biorender.com/biorender-templates.

3.3. Manuscript III

Regulation of mitochondrial cargo-selective autophagy by posttranslational modifications (published)

J Biol Chem. 2021 Nov;297(5):101339. doi: 10.1016/j.jbc.2021.101339.

Author contributions:

For this review I contributed by the addition of the chapter “Large-scale analyses of mitophagy-related processes”, with the feedback from Boris Macek

JBC REVIEWS

Regulation of mitochondrial cargo-selective autophagy by posttranslational modifications

Received for publication, June 29, 2021, and in revised form, October 14, 2021 Published, Papers in Press, October 22, 2021,
https://doi.org/10.1016/j.jbc.2021.101339

Anna Lechado Terradas[1,2], Katharina I. Zittlau[3], Boris Macek[3], Milana Fraiberg[4], Zvulun Elazar[4], and Philipp J. Kahle[1,2,5,*]

From the [1]Laboratory of Functional Neurogenetics, Department of Neurodegeneration, Hertie Institute for Clinical Brain Research, [2]Interfaculty Institute of Biochemistry, and [3]Proteome Center Tübingen, University of Tübingen, Tübingen, Germany; [4]Department of Biomolecular Sciences, The Weizmann Institute of Science, Rehovot, Israel; [5]German Center for Neurodegenerative Diseases (DZNE), Tübingen, Germany

Edited by Paul Fraser

Mitochondria are important organelles in eukaryotes. Turnover and quality control of mitochondria are regulated at the transcriptional and posttranslational level by several cellular mechanisms. Removal of defective mitochondrial proteins is mediated by mitochondria resident proteases or by proteasomal degradation of individual proteins. Clearance of bulk mitochondria occurs *via* a selective form of autophagy termed mitophagy. In yeast and some developing metazoan cells (*e.g.*, oocytes and reticulocytes), mitochondria are largely removed by ubiquitin-independent mechanisms. In such cases, the regulation of mitophagy is mediated *via* phosphorylation of mitochondria-anchored autophagy receptors. On the other hand, ubiquitin-dependent recruitment of cytosolic autophagy receptors occurs in situations of cellular stress or disease, where dysfunctional mitochondria would cause oxidative damage. In mammalian cells, a well-studied ubiquitin-dependent mitophagy pathway induced by mitochondrial depolarization is regulated by the mitochondrial protein kinase PINK1, which upon activation recruits the ubiquitin ligase parkin. Here, we review mechanisms of mitophagy with an emphasis on posttranslational modifications that regulate various mitophagy pathways. We describe the autophagy components involved with particular emphasis on posttranslational modifications. We detail the phosphorylations mediated by PINK1 and parkin-mediated ubiquitylations of mitochondrial proteins that can be modulated by deubiquitylating enzymes. We also discuss the role of accessory factors regulating mitochondrial fission/fusion and the interplay with pro- and antiapoptotic Bcl-2 family members. Comprehensive knowledge of the processes of mitophagy is essential for the understanding of vital mitochondrial turnover in health and disease.

Mitochondria, development, aging, and Parkinson's disease (PD)

Mitochondria are specialized organelles present in most eukaryotic cells. In addition to energy production, mitochondria play important roles in nutrient and lipid metabolism as well as in apoptosis. Two specialized membranes compartmentalize mitochondria. This feature, together with remnants of an own genome (mitochondrial DNA; mtDNA), is likely due to their endosymbiont heritage. Although the vast majority of 1136 proteins in human mitochondria (www.broadinstitute.org/files/shared/metabolism/mitocarta/human.mitocarta3.0) are encoded in the nucleus, the mitochondrial genome codes for 13 proteins, all of which are components of the respiratory chain (1). During oxidative phosphorylation, electrons flow through the respiratory chain in the mitochondrial inner membrane (MIM). This process builds up the membrane potential (proton gradient) that drives ATP synthase. As a by-product, reactive oxygen species are produced (2). Oxidative stress and mtDNA damage are associated with age-related mitochondrial dysfunction in a complex manner (3). As their energy production is obligatorily dependent on oxidative phosphorylation, neurons are particularly vulnerable to mitochondrial dysfunctions. Oxidative damage is aggravated in age-dependent neurodegenerative diseases, such as PD (4, 5). Indeed, the two most common recessive PD gene products, phosphatase and tensin homolog (PTEN)-induced kinase 1 (PINK1) and the E3 ubiquitin ligase parkin, are enzymes that mediate the autophagic removal of mitochondria (mitophagy). This mitophagy pathway might offer therapeutic targets for the treatment of PD (6). Moreover, mitochondrial turnover is important for cellular homeostasis, and in a few cell types (reticulocytes, germ cells) mitochondria are eliminated during normal development.

Given the tremendous importance of mitophagy in development, aging, and neurodegeneration, it is imperative to understand the cellular mechanisms regulating cargo-selective autophagy of mitochondria. Enormous progress in understanding this process in diverse cells types has been made in the past two decades, unraveling key players including the aforementioned PINK1, parkin, and other mitochondrial outer membrane (MOM) ubiquitin ligases as well as ubiquitin-binding autophagy adaptors. Clearly, mitophagy is embedded in an intricate signaling network integrating mitochondrial elimination signals, complex posttranslational modifications (PTMs) of MOM proteins, and the coupling to autophagy

* For correspondence: Philipp J. Kahle, philipp.kahle@uni-tuebingen.de.

propagation toward autophagolysosomal degradation. These complex signaling events throughout the entire process of mitophagy are beginning to be understood, also thanks to recent proteomic studies. This review describes how the basic elements of the autophagy machinery and their coupling to cargo-selective mitochondrial removal are connected *via* PTMs mediated by mitophagy-regulating enzymes.

Brief introduction to autophagy

Macroautophagy (hereafter autophagy) is a major intracellular, tightly regulated catabolic process in eukaryotes that delivers cytosolic components including protein aggregates, damaged organelles, and invasive pathogens for lysosomal degradation (7). This process is activated in response to various stressful conditions such as nutrient starvation, growth factors deprivation, hypoxia and infections, and is essential for maintenance of cellular homeostasis (7, 8). For example, autophagy supplies nutrients and energy for vital anabolic cellular functions during fasting and other stresses (9). The core mechanism comprises the sequestration of "to-be-degraded" cargo into the cup-shaped isolation membrane termed phagophore, which expanses and seals into a double-membraned sphere-termed the autophagosome- which engulfs autophagic cargo. Upon maturation, the outer membrane of autophagosome fuses with the vacuole (in yeast and plants) or endosomes and lysosome (in metazoans), leading to the degradation of the autophagic body together with its cargo by lysosomal catabolic enzymes (7, 8, 10).

Autophagy is activated by cellular triggers such as amino acid deprivation, which inhibits the master cell growth regulator serine/threonine kinase "mammalian target of rapamycin" (mTOR), and reduced energy levels activating AMP-activated protein kinase (AMPK) (11). In high nutrient conditions, the mTOR complex 1 (mTORC1) binds and phosphorylates the uncoordinated protein 51-like kinase 1 (ULK1) at residue S757, which disrupts the interaction with inactive AMPK (12). Upon starvation, AMPK is activated, which blocks mTORC1 activity and initiates autophagy at the transcriptional level through dephosphorylation of the master transcription factor EB (TFEB) that is negatively regulated by mTORC1 (Fig. 1). Dephosphorylated TFEB is released from mTORC1 and translocates to the nucleus where it stimulates coordinated lysosomal expression and regulation (CLEAR) by binding to the CLEAR-box sequence (5′-GTCACGTGAC-3′) present in the regulatory region of many lysosomal and autophagy-associated genes (13). Moreover, inactive mTORC1 dissociates from the ULK1 complex, which reduces ULK1 S757 phosphorylation. Instead, starvation-activated AMPK binds to ULK1 and phosphorylates it on multiple distinct sites (12). The complex phosphorylation pattern of AMPK-activated ULK1 is not fully understood, but S555 is a prominently phosphorylated residue upon starvation and mitophagy induction (14).

Activated ULK1-bearing numerous PTMs forms an oligomeric megacomplex together with its cofactors, autophagy-related protein ATG13, focal adhesion kinase-interacting protein of 200 kDa (FIP200) and ATG101, which is translocated to ER-associated isolation membrane assembly sites (15, 16). The active ULK1 megacomplex is targeted to the isolation membrane *via* ATG14L (15). ATG14L together with beclin-1 associates with the lipid kinase vacuolar protein sorting-associated protein VPS34 and the pseudokinase VPS15 to form a PI3K-III (Fig. 1). The ULK1 complex component ATG13 targets ULK1 to its substrate ATG14L for S29 phosphorylation (17) and the ATG14L partner beclin-1 for S15 phosphorylation (18). In addition, a recent phosphoproteomic study identified VPS15 S861 as a major regulatory ULK1 target site that activates the VPS34 PI3K activity (19). Such regulation of PI3K promotes the local production of phosphatidylinositol 3-phosphate (PI3P) at an ER structure called "omegasome" (Fig. 1), recruiting the PI3P-binding double FYVE domain-containing protein DFCP1 (20). Subsequent binding of the WD40 repeat protein interacting with phosphoinositides WIPI2 (a mammalian otholog of yeast Atg18) mediates omegasome maturation into phagophores (21).

Phagophore elongation requires two conjugation systems, involving the E1 ubiquitin ligase ATG7 and the E2 ubiquitin-conjugating enzyme ATG10, which links the ubiquitin-like protein ATG12 to ATG5 (Fig. 1). ATG16L1 is recruited to the phagophore *via* binding to WIPI2 and conjugated to ATG5-ATG12, forming an ATG5-ATG12-ATG16L1 complex (7, 22). The other conjugation system targets the ATG8 proteins, which can be subgrouped into LC3 (microtubule-associated protein light chain 3) and GABARAP (γ-amino-butyric acid receptor-associated protein) family members. Nascent pro-ATG8 precursors are processed by ATG4 cysteine proteases. The proteolytically processed ATG8 proteins expose a C-terminal glycine, allowing conjugation to phosphatidylethanolamine by the ATG3 E2 conjugating enzyme after activation by ATG7 (Fig. 1). Such ATG8 lipidations promote phagophore expansion (7, 15). Lipidated ATG8 proteins play an important role in the recruitment of cargo destined to lysosomal degradation into autophagosome, a process mediated by autophagy receptors, which brings part of the machinery to the autophagosomal membrane. The ULK1 complex regulates the membrane supply for sealing and involves the ATG9 trafficking system. Additionally, ULK1 may also phosphorylate various autophagy receptors, thus playing a role in selective autophagy including mitophagy (23–25) (for more details, see below).

Following phagophore sealing, the autophagosome undergoes maturation that results in clearance of ATGs from the autophagosomal outer membrane and recruitment of two machineries: one responsible for lysosomal delivery, comprised of kinesin motor; and the other responsible for autophagosome fusion with the lysosome, comprised of a soluble N-ethylmaleimide-sensitive factor-attachment protein receptor (SNARE), including syntaxin17 and synaptosomal-associated protein 29 on the autophagosome and vesicle-associated membrane protein 8 on the lysosome (Fig. 1). The lysosomes are recruited and tethered to autophagosomes *via* the homotypic fusion and protein-sorting (HOPS) complex, which is composed of VPS11, VPS16, VPS18, VPS33A, VPS39, and

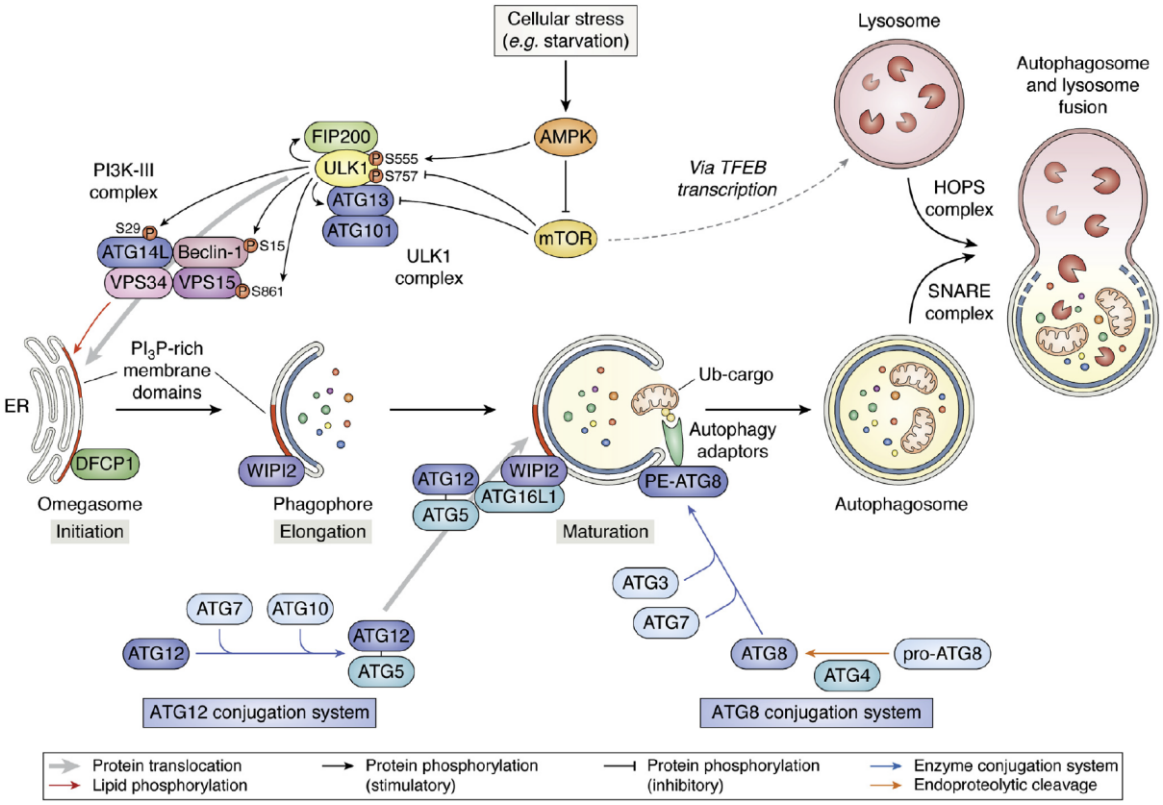

Figure 1. Key elements of the autophagy pathway. Cellular stress (*i.e.*, starvation) is sensed by AMPK, which directly activates the ULK1 complex by a complex phosphorylation pattern, including S555, and relieves it from the mTOR block by suppressing ULK1 S757 phosphorylation. The ULK1 kinase phosphorylates several components of the ULK1 megacomplex as well as the PI3K-III complex, promoting its translocation to the ER, where it generates membrane domains rich in PI3P that are eventually recognized by PI3P-binding proteins which promote phagophore formation. Two enzyme conjugation systems mediate phagophore maturation and insert lipidated ATG8 (or LC3-II) as anchors for autophagy receptors/adaptors that couple to ubiquitylated cargo. Finally, autophagosomes fuse with lysosomes (or the vacuole in yeast) *via* interaction of the SNARE and HOPS complexes, respectively. See text for details. *Thick gray arrows* indicate protein translocations, *thin black arrows* indicate protein phosphorylations (*arrowheads* stimulatory, *hammerheads* inhibitory), and the *thin red arrow* indicates lipid phosphorylation. *Blue arrows* indicate enzyme conjugation systems, and the *orange arrow* endoproteolytic cleavage. The *dashed line* indicates an indirect transcriptional (CLEAR) pathway for lysosome biogenesis.

VPS41 (26, 27). The HOPS complex interacts with the SNAREs and facilitates fusion of autophagosome with the lysosome (28).

Whereas bulk autophagy mediates a nonspecific engulfment and degradation of cytoplasmic material, selective autophagy is mediated by specific autophagy receptors. The main role of selective autophagy is to maintain the intracellular homeostasis by selectively degrading distinct cellular components such as damaged mitochondria (mitophagy), endoplasmic reticulum (ERphagy), lysosomes (lysophagy) invading pathogens (xenophagy), aggregated proteins (aggrephagy), and others (7, 29). The molecular machinery of selective autophagy must efficiently identify the cargo and sequester it within autophagosomes. Autophagic receptors/adaptors that contain ubiquitin-interacting motifs (*e.g.*, p62 sequestosome-1, optineurin, nuclear dot protein of 52 kDa (NDP52), next to breast cancer type 1 susceptibility gene 1 protein (NBR1) and autophagy-linked FYVE protein) connect their ubiquitylated cargo with the autophagosome *via* LC3-interacting region (LIR) motifs (29, 30). On the other hand, autophagy receptors such as the B cell lymphoma-2 (Bcl-2) 19 kDa protein-interacting proteins BNIP3 and BNIP3L/NIX or the FUN14 domain-containing protein 1 (FUNDC1) act independently of ubiquitin to deliver cargo to phagophores *via* their LIR motifs directly (30, 31).

General principles of cargo-selective mitochondrial autophagy

Mitophagy is the cellular catabolic process responsible for maintenance of mitochondrial homeostasis and quality control. Various developmental, environmental, physiological, and pathological stimuli activate mitophagosome formation resulting in mitochondrial clearance (32). Here we discuss cargo-associated PTMs that activate mitophagy.

Regulatory mechanisms of mitophagy in yeast

Activation of mitophagy in yeast may be achieved by their growing in nonfermentable medium or by nitrogen starvation (33). Atg32 was identified as an outer mitochondrial

membrane receptor essential for mitophagy (34). Atg32 directly interacts with Atg8 and the adaptor protein Atg11 (35). While the Atg11-Atg32 interaction is crucial for mitochondria recognition as a cargo and recruits the targeted mitochondria to the phagophore assembly site, the Atg8-Atg32 interaction through Atg32 LIR motif mediates phagophore expansion. The transcriptional levels of Atg32 may be upregulated due to oxidative stress or starvation conditions *via* suppression of TOR and release of transcriptional suppression of Atg32 by the Ume6-Sin3-Rpd3 complex (36). However, the main regulation of Atg32 is by posttranscriptional phosphorylation at S114 and S119 (37). Such phosphorylation facilitates Atg32 interaction with Atg11. Especially, phosphorylation at S114 is essential for successful mitophagy, since substitution of this serine residue to alanine prevents Atg11-Atg32 interaction and abolishes mitophagy (37). Regulation of mitophagy by phosphorylation and dephosphorylation of Atg32 is mediated by balanced activity of casein kinase 2 and protein phosphatase 2A complexed with factor arrest proteins (38).

Regulatory mechanisms of mitophagy in mammalian cells

Two pathways are responsible for mitophagy mediation in mammalian cells, the ubiquitin-mediated pathway and receptor-mediated pathway. The ubiquitin-mediated pathway is dependent on autophagy adaptors/receptors such as p62, optineurin, transient axonal glycoprotein 1 binding protein 1, NDP52, and NBR1 that contain ubiquitin-binding domains in addition to their LIR motif (30). These adaptors/receptors sequester the ubiquitylated mitochondrial proteins through their ubiquitin-binding domain and recruit the mitochondria into autophagosomes by interacting with lipidated ATG8s through their LIR motifs (39). The ubiquitylation pathway is mainly mediated by the E3 ubiquitin ligase, parkin (40). Upon mitochondrial depolarization, PINK1 accumulates on the outer membrane of damaged mitochondria and recruits parkin (41), which ubiquitylates MOM proteins and induces mitophagy. On the other hand, parkin ubiquitylation-independent mitophagy pathways are mediated by autophagy receptors such as NIX, BNIP3, FUNDC1, Bcl-2-like protein 13, and FK506-binding protein 8 (FKBP8) (30, 42). All of these receptors undergo MOM incorporation and recruit lipidated ATG8s *via* their LIR motif. Such recruitments label damaged mitochondria as a cargo and promote their engulfment into the growing phagophore.

In addition to protein receptors that mediate mitophagy, several lipids are also implicated in this process. Cardiolipin was reported to act as mitophagy receptor in neuronal cells. Upon mitochondrial stress, cardiolipin translocates from the MIM to the MOM and there, directly interacts with the N-terminus of LC3, mediating clearance of damaged mitochondria (43). Ceramide may also directly interact with lipidated LC3B on mitochondrial membrane, mediating mitophagy (44).

Removal of mitochondria *via* autophagy generally occurs under two conditions (45): (i) quality control removing dysfunctional mitochondria to maintain cellular homeostasis and viability (see below) and (ii) during organismal development, for example, when red blood cells lose all their organelles in the terminal step of erythropoiesis. Upregulation of the autophagy receptor NIX during terminal erythroid differentiation is the key trigger for cargo-selective autophagic removal of mitochondria from red blood cells (46, 47). A portion of mitochondria may lose membrane potential ($\Delta\Psi_m$) (46), which could stimulate stress-induced selective mitochondrial recruitment of membrane-conjugated ATG8 proteins *via* NIX (48). However, alternative macroautophagy independent of the ATG8 lipidation factors ATG5 and ATG7 is suggested as the major pathway for mitochondrial clearance during development (49). This alternative pathway involves the previously reported mitophagy effector ULK1 (50). The detailed mechanisms that govern mitochondrial autophagy in erythrocyte differentiation remain to be elucidated.

PINK1/parkin-dependent mitophagy

The discovery of mitophagy controlled by the two most common recessive PD genes encoding PINK1 and parkin (40, 51–53) offered tremendous insights into the cell biology of mitochondrial quality control. Under normal conditions, PINK1 is effectively transported into mitochondria, where it is immediately degraded. As the mitochondrial protein import machinery depends on $\Delta\Psi_m$, damaged mitochondria with collapsed $\Delta\Psi_m$ can no longer import PINK1. Instead, PINK1 massively accumulates on the MOM (41, 54). In this localization, PINK1 faces cytosolic kinase substrates, most notably ubiquitin and the parkin ubiquitin-like domain (Ubl) (55–57). The PINK1-catalyzed S65 phosphorylation of ubiquitin and parkin Ubl activate parkin E3 ubiquitin ligase activity (58, 59) toward mitochondrial substrates, targeting depolarized mitochondria for autophagic degradation (Fig. 2).

PINK1-dependent phosphorylations

Under healthy conditions, PINK1 is imported into mitochondria *via* an N-terminal mitochondrial targeting sequence (MTS). Once imported into the mitochondrial matrix, the MTS of pre-PINK1 is cleaved off by the mitochondrial processing protease (60). PINK1 then accesses the inner membrane active site of presenilin-associated rhomboid-like protease (PARL), which cleaves PINK1 within the membrane-anchoring segment (61, 62). In healthy cells, processed PINK1 is retrotranslocated into the cytosol for proteasomal degradation within 1 h (63, 64) (Fig. 2*A*). In most cell types, steady-state levels of PINK1 are practically undetectable in the absence of stress, but this does not rule out potential physiological functions of PINK1 (65, 66), which remain poorly understood to date.

When the kinase PINK1 cannot be imported for mitochondrial processing and clearance, it accumulates on depolarized mitochondria and thus acts as a molecular switch to trigger mitophagy. Following such accumulation at the MOM, PINK1 becomes autophosphorylated at S228 and S402, which

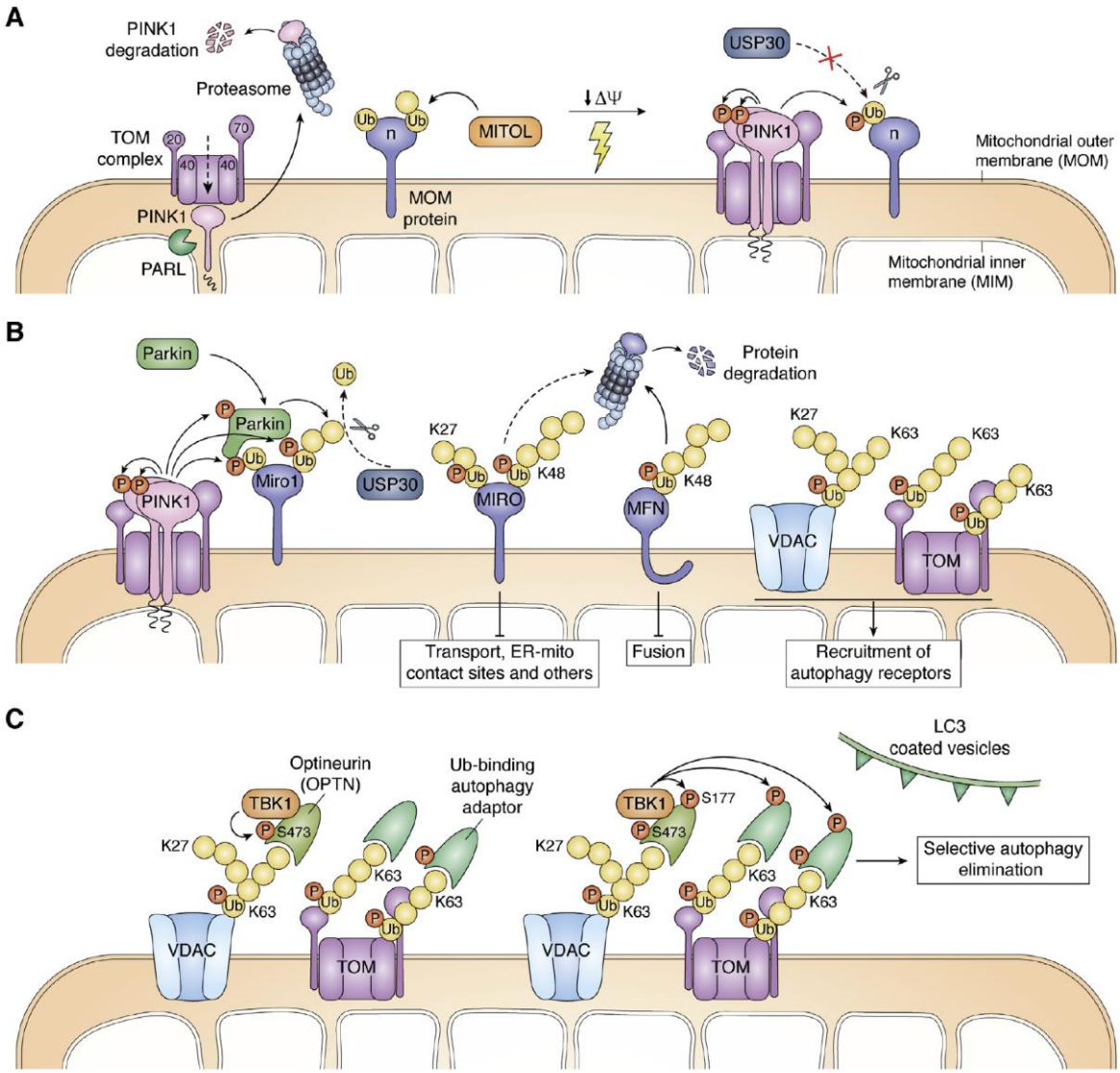

Figure 2. Schematic representation of parkin-dependent mitophagy time course. *A*, in normal conditions, PINK1 is imported and partially cleaved by the mitochondrial protease PARL, after which PINK1 gets eliminated by the UPS following the N-end rule, leading to very low endogenous PINK1 levels in healthy conditions. MITOL prepares a ubiquitin coat on MOM substrates. Upon mitochondrial membrane depolarization, the protein import machinery gets compromised and PINK1 is accumulated at the MOM. PINK1 gets auto-phosphorylated, and this triggers its activation: PINK1 starts phosphorylating ubiquitin molecules that were previously attached to MOM substrates, antogonizing USP30-mediated ubiquitin removal of those chains. *B*, phosphorylation of ubiquitin by PINK1 triggers parkin recruitment to the MOM. Direct PINK1 phosphorylation of the parkin Ubl and the binding to phosphorylated ubiquitin trigger a conformation change of parkin, which activates its E3-ubiquitin ligase potential. As a result, diversely linked ubiquitin chains are built on MOM substrates. Proteins involved in mitochondrial transport and fusion are mostly polyubiquitylated with K48-linked chains and are rapidly eliminated *via* the ubiquitin-proteasome system. MIRO1/2 is also ubiquitylated through K27-linked chains and is involved in multiple functions other than mitochondrial transport. Differential linkages might explain the remaining forms of ubiquitylated MIRO1/2 after mitochondria depolarization (*dashed arrow*). Other MOM proteins such as VDAC2 and TOM20 are mostly ubiquitylated with K63-linked and K27-linked chains, which triggers the recruitment of autophagy receptors. Ubiquitin chain building may be counteracted by USP30. *C*, S473 within the UBL domain of optineurin is phosphorylated by bound TBK1 when recruited to ubiquitylated MOM proteins, further enhancing optineurin recognition of ubiquitin chains. TBK1 also phosphorylates optineurin and additional autophagy receptors within the LIR motif (S177 in optineurin), which increases the affinity for lipidated ATG8/LC3 molecules and eventually triggers the recruitment of mitochondria to autophagosomes for their final elimination.

is important for PINK1 catalytic activity and the recruitment of parkin (67, 68). The individual contributions of phosphorylations at S228 and S402 for PINK1 functions are not entirely clear. Functional PINK1 autophosphorylation of S228 in mammals is conserved in insects, where the homologous residue S346 in *Drosophila melanogaster* is needed for PINK1 activity and parkin translocation to mitochondria (69). The corresponding residue S205 in *Tribolium castaneum* is likewise an autophosphorylation site *in vitro* and affects substrate binding (70).

Once PINK1 is activated, it phosphorylates ubiquitin as well as the parkin Ubl at S65 (55–57). Even though S65 is conserved among various ubiquitin-like modifiers and domains as well as ubiquitin itself (55), the affinity of PINK1 for the parkin Ubl is 10-fold higher in comparison to monomeric ubiquitin (70). Charging the really interesting new gene (RING)-type E3 enzyme parkin with ubiquitin requires the sequential action of the E1 ubiquitin-activating enzyme and a cognate E2 conjugating enzyme. In the resting state, parkin is folded in an auto-inhibited manner (71). Parkin activation occurs upon binding to PINK1-phosphorylated [pS65]ubiquitin, which together with S65 phosphorylation in the parkin Ubl domain causes a conformational change to the active state (59, 72, 73). When such structural reorganization of the Ubl domain and E2 binding site of parkin has taken place, the E3 ligase parkin promotes the attachment of ubiquitin to specific MOM substrates during mitophagy (Fig. 2*B*). These events are antagonized by PTEN-L, the first discovered ubiquitin phosphatase (74).

Priming steps for parkin translocation

At the onset of mitophagy, parkin is very efficiently translocated from the cytosol to the MOM of depolarized mitochondria, such that in model cells lines practically the entire immunofluorescence signal is found associated with mitochondria within an hour. Active PINK1 on the MOM is necessary and sufficient for this step (41). Abolishing PINK1 auto-phosphorylation at S228/S402 prevents parkin translocation after treatment of HeLa cells with the uncoupling agent carbonyl cyanide *m*-chlorophenyl hydrazone (CCCP) (67). Importantly, PD-linked PINK1 mutations also compromise this step and subsequent mitophagy (75, 76).

Pathogenic parkin mutations also impair mitophagy, either by preventing mitochondrial translocation to depolarized mitochondria or by failing to ubiquitylate its substrates (41, 52, 77). More specifically, targeting parkin catalytic activity by site-directed mutagenesis (C431S, C431F, and G430D) or rendering the PINK1 site unphosphorylatable (S65A) delay or compromise parkin translocation to the MOM after mitochondria depolarization (52, 57).

A straightforward model would posit that PINK1 accumulated on depolarized mitochondria would phosphorylate ubiquitin and parkin at the respective S65 residues, thereby activating the parkin ubiquitin ligase holoenzyme and enriching it on mitochondria by engagement with MOM substrates. Indeed, phosphorylation of parkin at S65 in the Ubl occurs without parkin reaching the MOM in cells expressing catalytically inactive parkin (C431S) (77). Thus, PINK1-mediated phosphorylation of the parkin Ubl S65 may trigger the induction of a fully active configuration of the parkin enzyme with [pS65]ubiquitin (78). Activation of parkin promotes its translocation from the cytosol to depolarized mitochondria. Accumulating on depolarized mitochondria, phospho-ubiquitin stimulated parkin strongly promotes the ubiquitylation of MOM proteins. Such ubiquitin molecules become substrates for further PINK1 phosphorylation, generating a feed-forward amplification loop at the MOM.

A specific subset of E2 ubiquitin-conjugating enzymes was identified that regulated parkin-dependent mitophagy (79, 80). Curiously, even the combined knockdown of these parkin coenzymes UBE2N, UBE2L3, and UBE2D2/3 only delays parkin recruitment and subsequent mitochondrial ubiquitylations and p62 localization to depolarized mitochondria, indicating additional regulatory steps for parkin recruitment and the process of mitophagy.

It seems hard to envision that cells rely for the intricate control of mitophagy on random vicinity of cytosolic ubiquitin and parkin with PINK1 accumulated on depolarized mitochondria. New insights into ubiquitin chain structures during mitophagy recently reveal similar relative amounts of mono-ubiquitylated and single-branched ubiquitin species in HeLa cells expressing catalytically active or inactive mutant (C431S) parkin, suggesting the presence of a mono-ubiquitin and single-branched ubiquitin coat in depolarized mitochondria (81). Likewise, recent global ubiquitylome analyses show similar amounts of mono-ubiquitylated and single-branched ubiquitylation species in induced neurons expressing both wild-type or nonphosphorylable parkin (S65 A) after 6 h of mitochondria depolarization (82). The mitochondrial E3 ligase MITOL mediates constitutive MOM protein ubiquitylation (83) that would become directly phosphorylated by PINK1 on the MOM of depolarized mitochondria, generating a phosphorylated MOM-ubiquitin coat available for parkin to ubiquitylate (Fig. 2*A*). In addition, the mitochondrial ubiquitin ligase MUL1 acts upstream of the PINK1/parkin pathway, restraining mitofusin-2 (MFN2) and hence maintaining mitochondrial morphology and ER-mitochondria contacts in stressed mature neurons (84).

Parkin-mediated ubiquitylations

Parkin can ubiquitylate at least 2000 substrate proteins (85) in an apparently peptide sequence nonspecific manner (83). While the determination of parkin substrate specificity is quite unclear, there is a cadence of consistent and functionally important ubiquitylations during the process of mitophagy (Fig. 2, *B* and *C*), some of which are highlighted in the following.

Mitochondrial Rho GTPase (MIRO) proteins are important factors for mitochondrial motility. In parkin-expressing HeLa and SH-SY5Y cells, they are rapidly poly-ubiquitylated. Interestingly, MIRO-2 is not completely eliminated for at least 90 min, and although the unmodified MIRO-1 band vanishes with a half-life time of ≈20 min (86, 87), poly-ubiquitylated MIRO-1 persists for several hours. Thus, parkin-mediated ubiquitylations do not directly target MIRO proteins to proteasomal degradation (88). Rather, MIRO-1 could initially stabilize parkin on the MOM of damaged mitochondria and thus contribute to parkin recruitment (89). PINK1 phosphorylation of parkin Ubl (S65) is necessary for the activity of parkin towards MIRO-1 (86). A priming role for PINK1-mediated phosphorylation of MIRO-1 S156 (88) could not be

confirmed (86, 87). Possibly the regulation of MIRO-1 turnover is more complex and involves additional phosphorylations at T298/299 (90). As the MIRO proteins drive mitochondrial trafficking, their subsequent degradation renders mitochondria more stationary for efficient autophagic removal (91). Moreover, by interaction with VPS13D, MIRO proteins regulate mitochondrial contacts with ER (92), possibly influencing the engagement with nascent phagophores.

Parkin recruited to depolarized mitochondria ubiquitylates MFN proteins and thereby marks them for rapid proteasomal degradation (93, 94). As a consequence of quick MFN degradation, the damaged mitochondrial network fragments, which is important for efficient mitophagy (95). Moreover, the PINK1/parkin-induced burst of MFN2 phospho-ubiquitylation triggers p97-mediated MFN2 complex disassembly and thus reduces the tethering of mitochondria with ER, facilitating mitophagy (96). On the other hand, parkin has also been reported to have an impact on mitochondrial fission by actively ubiquitylating the dynamin-related protein 1 (DRP1) and targeting it for rapid proteasomal degradation (97). In the context of mitophagy, where the mitochondrial network needs to be broken down (95), parkin-dependent degradation of the fission factor DRP1 would be counter-intuitive. Rather, PINK1 and parkin facilitate the recruitment of DRP1 and hence mitochondrial fission (98, 99). Indeed, proteomic studies identify strong parkin-dependent ubiquitylation sites of MFN1/2 after short times of mitochondrial depolarization, but hardly any consistent ubiquitylation events and no degradation of DRP1 seem to appear (82, 100). Thus, parkin-mediated poly-ubiquitylations directly downregulate fusion factors and more indirectly attract fission factors, which promote the mitochondrial fragmentation necessary for efficient autophagic removal.

Porins comprise a class of parkin substrates that was recognized early on in experiments knocking down VDAC1 (52). In mammals, these most abundant MOM proteins exist in three isoforms: voltage-dependent anion selective channel VDAC1-3. While the relative contribution of each individual VDAC for distinct steps of mitophagy was somewhat controversial (52, 101, 102), the cytosolic loops of all three VDACs were confirmed to contain lysine residues ubiquitylated by parkin (103). Ubiquitylation of VDAC1 as a paradigmatic parkin substrate was assessed after the gating step of MFN2 degradation and disruption of ER-mitochondria tethering upon induction of mitophagy (96). Furthermore, VDAC interacts with the mitochondria-associated isoform of hexokinase (HK2), which is implicated with parkin-mediated mitophagy as well (104, 105). Individual VDAC protein expression levels and ubiquitylation stoichiometry might differ with cell type and culture conditions, but VDACs are certainly targeted in parkin-mediated mitophagy, and it is possible that specific VDAC isoform PTMs affect selective aspects of mitochondrial quality control. For example, it was recently found that VDAC1 poly-ubiquitylations promoted mitophagy, whereas mono-ubiquitylation of VDAC1 at K274 rather conferred apoptosis (106).

In addition, parkin ubiquitylates and thus labels for degradation a number of additional MOM proteins, including subunits of the translocase of the outer membrane TOM20, TOM40, and TOM70 (107, 108). In fact, the TOM complex plays an important role in PINK1/parkin-mediated mitophagy (109), and the translocon is particularly targeted by one of the major deubiquitylating enzyme (DUB) modulators of parkin, the ubiquitin-specific protease USP30 (82, 110).

Mitophagy ubiquitin linkage code

Ubiquitin contains seven lysine residues (K6, K11, K27, K29, K33, K48, and K63). Depending on the lysine used as a linkage for attaching the next ubiquitin molecule, several distinct ubiquitin chains may form that will differ on their acquired structure. While some chains have clear physiological consequences such as K48 or K63-linkage chains, which trigger proteasomal degradation or autophagy activation, respectively, less is known about the other poly-ubiquitin chains (111).

Even though the detailed linkage types and structures of the ubiquitin chains built on parkin substrates are unknown to date, initial studies focused on ubiquitin chain types during mitophagy showed that parkin-dependent mitophagy triggers the elimination of mitochondrial substrates by building K48-linked, proteasome-targeting poly-ubiquitin chains (107) as well as the formation of K63-linked poly-ubiquitin chains targeting for autophagy (80, 101). Moreover, K27 linkages were detected (52, 86). Indeed, parkin is able to build other types of ubiquitin-linked chains (K6, K11, and K27) apart from K48 and K63, not only linear but also branched poly-ubiquitin chains (77, 82, 112). The timing of parkin target selection and the linkage specificity of ubiquitin chain elongation are likely regulated by PTMs and regulatory factors that need to be further elucidated. How parkin writes the ubiquitin code for the mitophagy process is a key question for future studies.

Role of DUBs

The MOM protein ubiquitylations formed during mitophagy are naturally subject to modulation by DUBs. The MOM residing DUB USP30 directly removes ubiquitin molecules attached by parkin on depolarized mitochondria, thus impeding parkin-dependent mitophagy progression (113, 114). Consequently, USP30 knockdown in a *Drosophila* model rescues defective mitophagy and fly behavior (113). Remarkably, USP30 acts poorly on K6-linked ubiquitins that are phosphorylated at the PINK1 site S65 (115, 116). Similarly, USP15 also has a direct impact on removing parkin-mediated mitochondrial ubiquitylations (117). Knockdown of USP15 in PD patient fibroblasts—which have reduced parkin levels—rescues mitophagy defects (117). Moreover, parkin itself is deubiquitylated on the MOM by USP33, notably at an apparently regulatory site (K435), leading to altered ubiquitin linkage activities and thus interfering with parkin recruitment and mitophagy (118). Conversely, USP8 actually promotes parkin-dependent mitophagy by preferentially removing autocatalytically formed K6-linked ubiquitin conjugates from parkin. In

the absence of USP8, persistent K6-linked poly-ubiqutin chains on parkin interfere with the translocation of parkin to depolarized mitochondria and the promotion of mitophagy, possibly by affecting the functional interactions with PINK1-phosphorylated ubiquitin and/or interactions with ubiquitin-binding autophagy receptors (119).

Additional DUBs regulate mitophagy in a more indirect manner. USP35, which associates with mitochondria under normal conditions, translocates to the cytosol when mitochondria are depolarized (114). Perhaps the dissociation of the DUB USP35 from depolarized mitochondria is sufficient to facilitate actions of the ubiquitin ligase parkin. It remains unknown whether USP35 additionally regulates components of the autophagy machinery as was shown, *e.g.*, for USP33 (120). In fact, USP36 is a powerful regulator of mitophagy although it remains nuclear and does not translocate to mitochondria even under conditions of mitophagy (121). Instead, USP36 regulates the expression of ATG14L/beclin-1, possibly *via* epigenetic mechanisms.

Taken together, the process of parkin-mediated mitophagy is modulated at multiple steps: the direct parkin DUBs affect parkin activity and recruitment to damaged mitochondria in a facilitating (USP8) or repressive manner (USP33), the parkin-mediated MOM protein ubiquitylations can be subsequently removed (USP15, USP30) or left untouched (USP35), and specific effectors of the autophagy/mitophagy machinery can be indirectly regulated (USP36).

Parkin-independent mitophagy

In addition to the PINK1/parkin-dependent mitophagy pathway described above, alternative parkin-independent pathways can recruit LC3 to mitochondria and promote their selective autophagic elimination (122, 123). Two different parkin-independent mechanisms can be distinguished: (1) receptor-mediated or (2) ubiquitin-mediated mitophagy (Fig. 3). In response to low oxygen (hypoxia) or mitochondrial uncoupling, receptor-mediated mitophagy will take place. Autophagy receptors residing at the MOM, which are regulated by phosphorylation or dephosphorylation, directly interact with LC3 molecules attached to the autophagosome, thereby promoting mitochondrial elimination through autophagy (124). BNIP3 and NIX are two MOM residing autophagy receptors that can be phosphorylated in their LIR domains (S17 or S34 and S45, respectively), promoting their interaction with LC3 (125, 126). Up to the present day, the kinases responsible for BNIP3 and NIX activation remain unknown. FUNDC1 is another MOM autophagy receptor that is auto-inhibited in basal conditions. FUNDC1 is intrinsically phosphorylated at Y18 and S13 by Src kinase and casein kinase 2, respectively. It becomes active under conditions of severe hypoxia, where the phosphoglycerate mutase family member 5—a mitochondrial serine/threonine-protein phosphatase dephosphorylates S13, allowing the interaction of the LIR domain with LC3 (127, 128). Additionally, ULK1 phosphorylation at S17 enhances LC3 interaction (25).

The activating molecule in beclin-1 regulated autophagy protein 1 (AMBRA1) was identified as a parkin-interacting protein mediating the propagation of mitophagy (129). Targeting of the autophagy receptor AMBRA1 to mitochondria directly couples to LC3 *via* a LIR motif and thus, launches mitophagy circumventing parkin and p62 (130). Like most autophagy receptors, AMBRA1 can be phosphorylated in the vicinity of the LIR motif (at S1014), which stimulates coupling to LC3B and promotes mitophagy. The inhibitor of nuclear factor κB (NF-κB) kinase-α was validated to phosphorylate its consensus sequence around S1014 -near the AMBRA1 LIR motif- upon mitophagy (131). How AMBRA1 and its associated factors accumulate on mitochondria for cargo-selective autophagic clearance remains to be further studied, as well

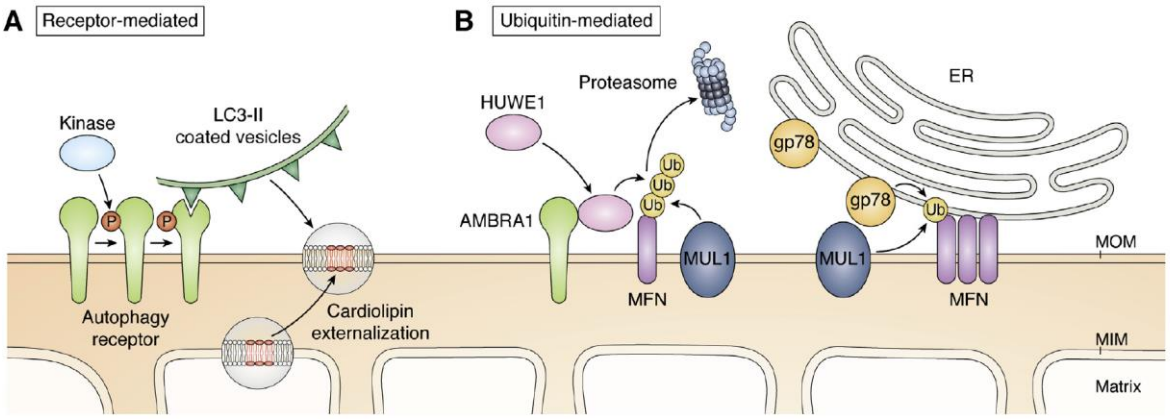

Figure 3. Parkin-independent driven mitochondria elimination. *A*, receptor-mediated mitophagy depends on phosphorylation of MOM-anchored autophagy receptors (*i.e.*, NIX, BNIP3, AMBRA1, FUNDC1). Additionally, phospholipids such as cardiolipin can also act as autophagy receptors once they are externalized to the MOM under mitochondrial stress conditions. *B*, ubiquitin-mediated mitophagy involves parkin-independent E3 ligase ubiquitylations that specifically decorate mitochondria for subsequent autophagic removal. Such ubiquitylations may be performed by MOM-residing E3 ligases (*i.e.*, MUL1), cytosolic E3 ligasses that translocate to mitochondria upon mitochondrial stress conditions (*i.e.*, HUWE1) or ER-residing E3 ligases (*i.e.*, gp78) that, together with MOM-residing ubiquitin ligases, act on ER–mitochondrial contact sites, enhancing mitochondria fragmentation and facilitating specific autophagic elimination of mitochondria.

as the potential regulatory role of Bcl-2 proteins interacting with AMBRA1 (132).

In addition to protein phosphorylations, other PTMs can also regulate autophagy. Protein lysine acetylation (133) is a straightforward part of the nutrient-sensing program, as all nutrients can be metabolized to acetyl-CoA under permissive cellular conditions. Specifically, general control of amino acid synthesis protein 5-like 1 (GCN5L1) is a positive regulator of protein acetylation in mitochondria (134). GCN5L1 deficiency leads to the association of LC3 and p62 with mitochondria and subsequent mitochondrial cargo-selective autophagy in an ATG-dependent but parkin-independent manner (135). In this experimental system using HepG2 cells, knockdown of the mitochondrial deacetylase sirtuin-3 (SIRT3) attenuated the mitochondrial recruitment of p62 and LC3-II promoted by GCN5L1 knockdown (135). In oxidatively stressed endothelial cells, induction of SIRT3 promotes mitophagy *via* deacetylation of the forkhead box protein O3, promoting the stimulation of gene batteries regulating mitochondrial biogenesis, fission/fusion, and the mitophagy effectors BNIP3, NIX, and LC3 (136). In oxidatively stressed endothelial cells, SIRT3 may directly impact on PINK1 and parkin (137). Moreover, SIRT3 can deacetylate optic atrophy protein 1 (OPA1), a mitochondrial fusion factor, which promotes mitochondrial integrity in stressed heart cells (138). Thus, the protein deacetylase SIRT3 could be a master regulator of mitochondrial turnover, quality control and mitophagy (139), both under normal conditions and in stressed cells with activated PINK1/parkin. However, the effects of SIRT3 are highly complex, and the molecular details for cargo-selective mitophagy in specific cell types remain to be resolved.

Mitochondria are rich in iron bound cytochromes and iron-sulfur clusters. Remarkably, the iron chelator deferiprone was a powerful inducer of PINK1/parkin-independent selective mitophagy even in PD patient fibroblasts (140). Deferiprone treatment causes the autophagy receptor FKBP8 on mitochondria to interact with LC3, thus initiating parkin-independent mitophagy (42, 141). Likewise, deferiprone induces mitochondrial clearance in myotubes by hypoxia-inducible factor 1-α mediated transcriptional induction of the LC3-binding autophagy receptors BNIP3 and NIX but, interestingly, instead of autophagic degradation in this case, mitochondria were secreted as extracellular vesicles (142). Taken together, iron homeostasis is important for PINK1/parkin-independent mitochondrial clearance.

Cardiolipin is a phospholipid normally residing at the MIM, which can be externalized under mitochondrial stress conditions by phospholipid scramblase-3. Such relocalization to the MOM allows cardiolipin to directly bind to LC3 (43), thus acting as a lipid kind of autophagy receptor in the regulation of parkin-independent mitophagy (122) (Fig. 3*A*).

Apart from parkin, other E3 ubiquitin ligases are also capable of decorating the MOM with the purpose of targeting them for specific autophagy elimination. The ubiquitin ligase homologous to the E6-AP carboxyl terminus, ubiquitin-associated and WWE domain-containing protein 1 (HUWE1) acts as an alternative to parkin, binding AMBRA1 upon mitophagy. Similar to parkin, HUWE1 can be recruited to depolarized mitochondria where it ubiquitylates MFN2 for proteasomal degradation (131). The ubiquitylation of MOM proteins may drive AMBRA1 activation and further mitophagy progression (131) (Fig. 3*B*).

Glycoprotein 78 (gp78), a ubiquitin ligase important for ER-associated degradation, has been shown to promote mitophagy in the absence of the ubiquitin ligase parkin (143). Like parkin, gp78 ubiquitylates MFN proteins to target them for proteasomal degradation, thereby promoting mitochondrial fragmentation. Interestingly, gp78 engages LC3 to ER-associated mitochondrial sites and promotes mitophagy in an ATG5-dependent manner. Gp78 levels are regulated by self-ubiquitylation as well as ubiquitylation by the ubiquitin ligase mahogunin RING finger protein 1 (MGRN1). Expression of a disease-causing prion protein disrupts the Ca^{2+}-dependent interaction of MGRN1 with gp78 (144), preventing the degradation of gp78 and thus initiating mitophagy. It is possible that calcium stress affects turnover of ER–mitochondria contact sites, involving the alternative ubiquitin ligase gp78, also in a PINK1-dependent manner (145).

The mitochondrial ubiquitin ligase MUL1 shares many substrates with parkin and is able to compensate for PINK1/parkin loss of function in the context of PD, in *Drosophila* and mouse neurons, ubiquitylating MFN2 and promoting its degradation through the proteasome system (146). MUL1 can act together with MFN2 to control mitochondria morphology and ER–mitochondria contracts, and thus, it is suggested that when MUL1-MFN2 pathway is disrupted, the PINK1/parkin mitophagy pathway will be activated (84).

In addition to completely PINK1/parkin-independent mitophagy pathways, the ariadne-1 homolog in humans (ARIH1) promotes mitophagy in cancer cells independently of parkin but in a PINK1-dependent manner (147). ARIH1 is structurally very similar to parkin (148), but the expression pattern of these two ubiquitin ligases is quite different. Whereas parkin is widely expressed in neuronal cells and absent in many cancer cell lines (149), ARIH1 is highly expressed in various cancer cells (147). Interestingly, ARIH1 expression in cancer cells allows for apoptosis avoidance against chemotoxicity, suggesting that ARIH1-mediated mitophagy contributes to a chemotherapy resistance mechanism (147).

PINK1 and parkin are not only expressed in the nervous tissue but also in the muscle (150, 151). Both neurons and myocytes strongly depend on mitochondria. Thus, the complete autophagic elimination of mitochondria *via* the PINK1/parkin pathway commonly studied in cultured cell lines that satisfy their energy demands largely by glycolysis may not be reflected on all accounts in the brain, muscle, and heart *in vivo*. While DRP1-mediated mitochondrial fission is important for mitophagy in neurons and cardiomyocytes, parkin acts merely as a facilitating factor but not as essential regulator of mitophagy in neurons and cardiomyocytes (152). In this case, labeling of mitochondria with ubiquitin and the recruitment of

p62 can occur even in the absence of the ubiquitin ligase parkin.

Roles of accessory factors

Mitochondrial fission/fusion factors

Mitochondrial fission was recognized early on to be important for mitophagy (95), likely to pinch off damaged fragments from the mitochondrial network for piecemeal mitophagy. Mitochondrial fission and autophagic removal are coupled by parkin *via* pathways associated with dephosphorylation of DRP1 at S637 in its GTPase domain (98). The mitochondrial dynamics protein of 51 kDa is an important cofactor for parkin/DRP1-mediated mitochondrial fragmentation and autophagic removal, with mitochondrial dynamics protein of 49 kDa and the mitochondrial fission factor (MFF) also contributing (98). The ULK1/*Atg1* kinase AMPK (14) also phosphorylates MFF at S172 (and S155) between the DRP1-interacting domain and the C-terminal mitochondrial targeting transmembrane domain (153) and may thus promote fission and mitophagy in cells suffering from energy crisis (Fig. 4*A*). Moreover, MFF expression is regulated by the RNA-binding translation repressor pumilio2 in an age-dependent manner (154). MFF/DRP1-fissioned mitochondria may then be delivered to the autophagolysosomal pathway by the ubiquitin-binding protein VPS13D (155). Moreover, MUL1 acts not only as a ubiquitin ligase but can also transfer the small ubiquitin-related modifier (SUMO) to DRP1. The mixed activities of MUL1 as a stabilizing DRP1-SUMO ligase and a destabilizing MFN2-ubiquitin ligase promote mitochondrial fission (156). Taken together, mitochondrial fragmentation and mitophagy are coordinated events ensuring optimal quality control for the mitochondrial network (Fig. 4).

Depletion of the mitochondrial fusion factors MFN and OPA1 causes hypofusion of the MOM and MIM, respectively (157). Downregulation of mitochondrial fusion factors would

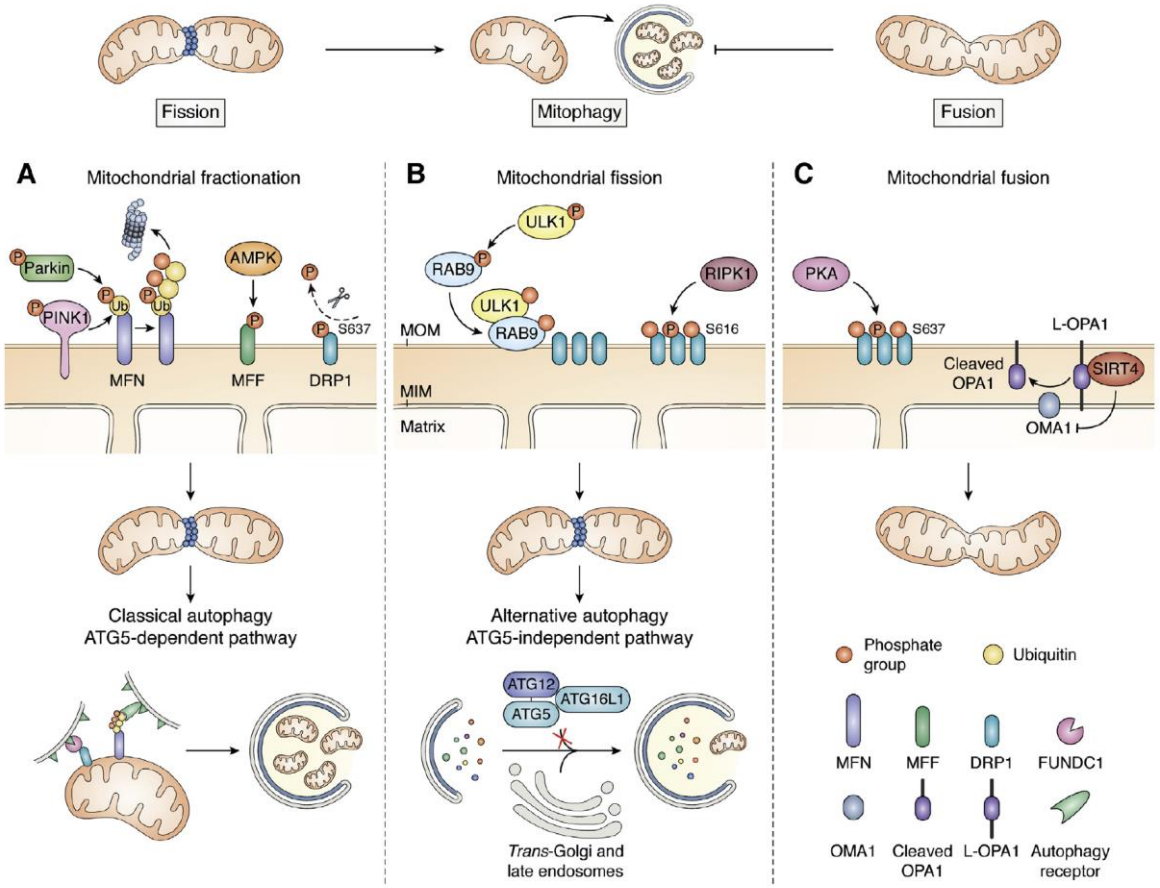

Figure 4. Fission and fusion factors driving mitophagy. Mitochondrial fragmentation triggers mitophagy while mitochondrial fusion has the opposite effect (*upper scheme*). *A*, mitochondrial fragmentation can occur through (1) parkin-dependent ubiquitylation of MFN, targeting MFN for proteasomal degradation, (2) phosphorylation of MFF by AMPK or (3) dephosphorylation of DRP1. Once mitochondria are fragmented, mitophagy is induced in an ATG5-dependent manner through recognition of ubiquitin chains *via* autophagy receptors or direct recognition of dephosphorylated DRP1 by FUNDC1. *B*, mitochondrial fission can be triggered by the RAB9/ULK1 complex, which indirectly influences the phosphorylation of DRP1. In this pathway, selective autophagy is activated in an ATG5-independent manner; the maturation of the phagosome is accomplished by the interaction of *trans*-golgi and late endosome membrane fusion. *C*, mitochondrial fusion can be driven through a change in DRP1 phosphorylation status by protein kinase A or by direct inhibition of L-OPA1 cleavage by SIRT4.

shift the mitochondrial morphology dynamics toward fragmentation. A major factor driving fragmentation of damaged mitochondria is the parkin-mediated ubiquitylation of MFN, targeting for proteasomal degradation of a key mitochondrial fusion factor (see above). Interestingly, depletion of MFN1 may also contribute to mitochondrial quality control in the female germline (158). Due to the relatively poor proofreading capacity of the mitochondrial DNA polymerase, mtDNA mutations accumulate that must be carefully removed from the maternal germline by purifying selection (159). As recently shown in *Drosophila*, mitochondrial fragmentation in early developing oocytes is necessary and sufficient for germline mtDNA selection (158). This process does not occur *via* the PINK1/parkin pathway. Rather the fragmented mutant mitochondria produced less ATP, which marked them for autophagic clearance involving *Atg1* and *BNIP3*, but not *Atg8a* (158). BNIP3-like targeting mitochondria to autophagy pathways independent of the ATG8 upstream activator ATG7 had been also suggested for the elimination of mitochondria from red blood cells (49, 160). An alternative macroautophagy pathway regulated by *Atg1*/ULK1 and beclin-1 was described in $Atg5^{-/-}/Atg7^{-/-}$ double-knockout mouse embryonic fibroblasts, where autophagosomes seem to be assembled in a RAB9-dependent manner by the fusion of isolation membranes with vesicles derived from the *trans*-Golgi and late endosomes (161) (Fig. 4*B*). Such a parkin- and ATG7-independent but ULK1- and RAB9-dependent alternative mitophagy pathway involving DRP1 protects cardiomyocytes against ischemic damage (162). ULK1 becomes phosphorylated prominently at the AMPK site S555 (14). In starved cardiomyocytes, (pS555)ULK1 phosphorylates RAB9 at S179, which leads to the formation of an (pS555)ULK1/(pS179) RAB9 complex on mitochondria, that recruits the receptor-interacting protein kinase 1, which in turn mediates the fission-promoting phosphorylation of DRP1 at S616 (162). This mitochondrial fission/mitophagy complex eventually associates also with the autophagolysosomal fusion SNARE syntaxin17. The regulation of mitochondrial cargo selectivity of alternative macroautophagy in developing and stressed cells remains to be studied in detail.

MFN1 is the major MOM fusion factor and OPA1 regulates MIM fusions (157). Similar to MFN depletion, OPA1 deficiency results in mitochondrial fragmentation due to hypofusion, which facilitates mitophagy in optic atrophy patient fibroblasts (163). Interestingly, the mitochondrial autophagy receptor FUNDC1 not only couples to LC3 during hypoxia-mediated mitophagy (164), but also promotes mitochondrial fragmentation by shifting the binding of FUNDC1 from OPA1 to the mitochondrial fission factor DRP1 (128). This shift is regulated by FUNDC1 dephosphorylation at S13 near the LIR motif. Thus, mitochondrial fission and autophagy engagement may be efficiently integrated cellular processes connected by multifunctional autophagy receptors, subject to regulation of PTMs.

Conversely, hyperfusion spares mitochondria from degradation upon starvation-induced autophagy (165, 166). In this case, phosphorylation of DRP1 prevents the mitophagy-facilitating fragmentation of mitochondria. In addition, mitochondrial fusion is achieved by preventing cleavage of the fusion-promoting long isoform L-OPA1 by the endopeptidase overlapping with the mitochondrial matrix ATPase associated with diverse cellular activities (m-AAA) protease 1 (OMA1) (Fig. 4*C*). Regulated expression of OMA1 may modulate mitophagy *via* OPA1-mediated morphology dynamics (167, 168). The mitochondrial sirtuin SIRT4 was reported to bind and elevate levels of L-OPA1, suppressing mitophagy by mitochondrial elongation (169). It remains to be further elucidated which protein deacetylations mediate sirtuin effects on mitochondrial metabolism and cargo-selective autophagy (see also above).

Bcl-2 family members

The MOM, which connects to the autophagy machinery during mitophagy, is strongly influenced by members of the Bcl-2 family. Bcl-2 proteins are key regulators of MOM permeability controlling the intrinsic, mitochondrial apoptosis pathway. It is becoming increasingly clear that Bcl-2 proteins have functions beyond their involvement in the regulation of apoptosis (170), including mitochondrial physiology and autophagy (Fig. 5). For example, interactions of anti-apoptotic Bcl-2 family members with beclin-1 repress autophagy (Fig. 5*A*). Specifically, beclin-1 contains a Bcl-2 homology 3 domain (BH3) and hence binds to antiapoptotic proteins such as Bcl-2, Bcl-W, Bcl-X_L, and the induced myeloid leukemia cell differentiation protein Mcl-1 (171, 172). Conversely, the BH3-only Bcl-2 associated agonist of cell death (BAD) disrupts the interaction of antiapoptotic Bcl-2 proteins with beclin-1, thereby antagonizing autophagy repression (171).

Bcl-2 family members are also affected in PINK1/parkin-dependent mitophagy. In CCCP-treated neurons, the upregulated PINK1 phosphorylates ubiquitin S65 and with a similar time course multiple serine residues of the Bcl-2 associated agonist of cell death, suppressing its proapoptotic translocation to mitochondria (173). Parkin can ubiquitylate the proapoptotic Bcl-2 associated protein X (174, 175) and Bcl-2 homologous antagonist/killer (BAK), the resulting proteasomal degradation of these proapoptotic Bcl-2 family members would prevent apoptosis to allow cells to cope with the mitophagic stress (176) (Fig. 5*B*). On the other hand, the ubiquitin ligase parkin can also target the prosurvival Mcl-1 for proteasomal degradation (177). Thus, parkin may promote mitochondrial quality control by triggering mitophagy while suppressing apoptosis by ubiquitylation-mediated proteasomal targeting of proapoptotic Bcl-2 family members but when the damage cannot be relieved, parkin-mediated degradation of Mcl-1 may switch cell fate to apoptosis (178) (Fig. 5*C*). Moreover, the prosurvival protein Bcl-X_L actually represses mitophagy by direct binding to parkin and hindering its translocation to mitochondria in various stressed cells (179–181). In addition, PINK1 can phosphorylate Bcl-X_L on the MOM of CCCP-treated SH-SY5Y cells, not regulating mitophagy but rather suppressing apoptosis by preventing the proapoptotic cleavage of Bcl-X_L (182). Taken together, the cytoprotective enzymes PINK1 and parkin are distinctively

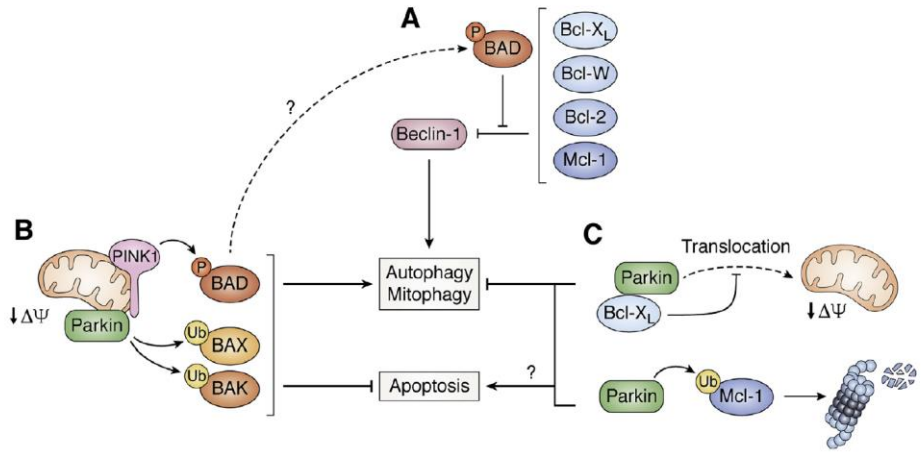

Figure 5. Bcl-2 like proteins influence on the activation of autophagy and apoptosis. *A*, Bcl-2 like proteins can interact with beclin-1, inhibiting its autophagy function. BAD is able to relieve this repression, interfering with these interactions. *B*, under mitochondrial stress conditions, PINK1 phosphorylates BAD and parkin ubiquitinates BAX and BAK, inhibiting their proapoptotic functions and promoting mitophagy. It is possible—though not yet proven—that phosphorylation of BAD inhibits its proapoptotic functions also in this case. *C*, mitophagy can be inhibited by parkin-dependent ubiquitylation of the antiapoptotic factor Mcl-1 or direct interaction of Bcl-X_L with parkin, which directly inhibits parkin translocation to mitochondria. It remains to be elucidated if both parkin-dependent ubiquitinations eventually trigger cell apoptosis and through which specific pathway. *Arrowheads* indicate activation, *hammerheads* indicate inhibition, *dashed arrows* indicate translocation.

interconnected with anti- and proapoptotic Bcl-2 family members and mitochondria at the crossroads of mitophagy and apoptosis (183), but the overall mechanism remains to be elucidated.

Large-scale analyses of mitophagy-related processes

Integrative (multiomics) studies address biological processes in which mitochondria play crucial roles, such as mitophagy and apoptosis, with a strong disease-related context (82, 103, 184). Development and improvement of biochemical and bioinformatic tools allow the analysis of PTMs of mitochondrial proteins, such as protein phosphorylations or ubiquitylations (185–187). In the analyses of disease-related changes in the ubiquitylome, further development of existing methods enables the investigation of the ubiquitin chain architecture. For example, the "Ub-clipping" technique revealed that parkin mainly generates ubiquitylations that are mono-ubiquitylated or only consist of a short chain with a preference for distal ubiquitin phosphorylation (81).

The integration of several layers of -omics studies is essential to gain a more complete view of mitochondrial biology. Recently such integrative studies were done in the field of systems biology, *e.g.*, for modeling biological processes involving mitochondria. For example, combination of transcriptomics, proteomics, and metabolomics data led to the identification of the activating transcription factor 4 as a key regulator of mitochondrial stress response in different mammalian cell lines (188). Integration of transcriptomics and proteomics data led to the identification of adaptive changes in the protein expression after blocking the TOM complex import machinery in yeast (189). Combination of multiomics datasets with information on multiple cellular pathways allows even broader analysis of functional relationships. An example is the switch between mitophagy and cell death, which represents a complex and so far only poorly understood process (190). Another example of the importance of -omic studies as a fundament for subsequent analysis is the VDAC1 ubiquitylome. Ordureau *et al.* (103) described parkin-dependent ubiquitylation events of multiple lysine residues on VDAC1 in a quantitative ubiquitylome analysis. VDAC1 serves as a poly-ubiquitin anchor during mitophagy but can become an essential part of the mitochondrial permeability transition pore in apoptosis. The choice of apoptosis or mitophagy may be driven by parkin-dependent mono- or poly-ubiquitylation on VDAC1 K274 (106). As mentioned above, the decision between mitophagy and apoptosis is also regulated by functional interactions of PINK1 and parkin with antiapoptotic and proapoptotic Bcl-2 family members. Large-scale mass spectrometric determinations of the phosphoproteome (173) and ubiquitylome (100) help to appreciate the contribution of PTMs in the complex interplay between mitophagy and apoptosis. More advanced technologies will allow for even better integration of multiomics data to ultimately enhance the diagnosis and therapy of mitochondrial dysfunction in human diseases (191, 192).

Mechanisms regulating mitochondrial cargo-selective autophagy

Autophagy receptors connecting to-be-degraded cargo to the autophagy machinery are logical regulatory effectors of selective autophagy. The tumor necrosis factor receptor–associated factor family member associated NF-κB activator-binding kinase 1 (TBK1) phosphorylates several autophagy receptor proteins on multiple, autophagy-relevant sites. When optineurin interacts with ubiquitin chains on

MOM proteins during mitophagy, the constitutively optineurin-bound TBK1 is recruited to mitochondria and becomes activated (193, 194). TBK1-mediated phosphorylation of optineurin at S473 (and S513) in the ubiquitin-binding region further enhances the affinity of optineurin for polyubiquitin chains (193)—including those phosphorylated by PINK1 (194), thus promoting PINK1/parkin-dependent mitophagy in a feed-forward manner (Fig. 2*C*). Moreover, TBK1-catalyzed phosphorylation of S177—near the optineurin LIR motif—stabilizes the binding of optineurin to ubiquitylated mitochondria (39, 194), in addition to an influence on LC3 recruitment (193). Curiously, the LIR motif of optineurin (and another mitophagy adaptor, NDP52) was recently found to be dispensable for PINK1/parkin-mediated LC3/GABARAP recruitment and selective mitophagy (195). Rather, the LIR motif mediates secondary, ubiquitin-independent recruitment of optineurin and NDP52 to nascent autophagosomes, amplifying ULK1-regulated mitophagy. NDP52 tethering to peroxysomes and mitochondria, respectively, is sufficient to promote the recruitment of the ULK1/FIP200 complex facilitated by TBK1 (196). The function of NDP52 is the local recruitment of ULK1 for cargo-selective pexophagy, mitophagy, and xenophagy (196, 197).

Conclusions and outlook

Selective removal of mitochondria—mitophagy—is essential for cellular quality control during stress and disease as well as in development. Thus, impaired mitophagy situations underlie the pathogenesis of a number of chronic diseases such as cancer, cardiovascular diseases, and neurodegenerative diseases, with a particular link to PD *via* the recessive gene products PINK1 and parkin. As outlined in this review, there are multiple pathways capable of promoting mitochondria elimination. While they all differ on their activation and action mode, all of them depend on accurate PTM regulations for their proper progression and functionality. Because it is essential to understand the molecular mechanisms that trigger mitophagy in all its possible ways, here we gathered the most important PTMs that influence mitochondria targeting mechanisms as well as autophagy-related processes, culminating with mitochondrial elimination.

Enormous research efforts in the past two decades identified the core elements of autophagy (Fig. 1), stress-related PINK1/parkin-dependent mitophagy (Fig. 2), receptor-mediated mitophagy during development (Fig. 3), and the involvement of fission/fusion factors (Fig. 4) and Bcl-2 family members (Fig. 5). Now is an exciting time to build on this knowledge to unravel the regulatory mechanisms that govern the different mitophagy pathways. Recent advances and future improvements in large-scale multiomic analyses will help in this endeavor.

The AMPK-ULK1 axis for starvation-induced autophagy is well established. However, much of the PINK1/parkin mitophagy knowledge is derived from cancer cell lines treated with bulk uncoupling agents. Due to the Warburg effect, though, cancer cells treated with uncoupling agents do not experience the same degree of energy crisis as cells subjected to nutrient starvation. The autophagy machinery is clearly activated during PINK1/parkin-mediated autophagy, but are the upstream mechanisms exactly the same as in nutrient starvation models? The recent discovery of a novel phosphorylation site in ULK1 regulating the alternative, ATG5-independent autophagy (198) is a precedent showing that even long-known players can exert novel modes for distinct autophagy pathways. Moreover, abrupt complete breakdown of $\Delta\Psi_m$ is obviously an idealized experimental condition with questionable relevance particularly to postmitotic neurons (199). The recent development of fluorescent reporter systems confirms the occurrence of mitophagy in neurons, but further research with more physiological systems and *in vivo* aging models is needed to clarify which mitophagy regulatory elements are global and which are more specific in distinct stressed organs.

A key question is how the various ubiquitin ligases establish the ubiquitin code on to-be-degraded mitochondria, and how the autophagy machinery deciphers this code. Some substrates appear straightforward, such as the proteasome-targeting K48-linked poly-ubiquitylation of MFNs. The differential dynamics of TOM ubiquitylations suggest a more regulatory impact of the mitochondrial protein import machinery for the insertion of PINK1 into the MOM and the execution of mitophagy. The complex ubiquitin linkages that occur throughout the time course of mitophagy (103) might indicate a meaningful pattern of ubiquitin chains that have a signaling capacity much beyond simple protein targeting. Methodological advances to detect ubiquitin linkages and topologies (200) are instrumental in this regard. Another issue is the experimental modeling of ubiquitylated proteins. While protein serine/threonine phosphorylations can be mimicked faithfully in many cases by site-directed mutageneis to aspartate/glutamate and substitution with glutamine resembles acetyl-lysine to a certain degree, protein ubiquitin modifications cannot be simply mimicked by site-directed mutagenesis. Nevertheless, expanding the genetic code with amber suppression at a desired residue combined with sortase-mediated transpeptidation may provide a first step toward introducing specific ubiquitylated protein species into cells and study their functions (201).

Another issue to be fully resolved is the sequential dynamics of PTMs on the MOM and accessory factors. While the initiation phase is reasonably well understood (*e.g.*, PINK1 phosphorylation of ubiquitin S65 and the activation of parkin, proteasome-targeting MFN ubiquitylations), it is less clear if there are later checkpoints. Are there more convergence points of PINK1/parkin labeled mitochondria with components of the autophagy machinery (for example, the ULK1 complex, ER–mitochondria contacts, phagophores, etc.), and how would those comprise checkpoints regulating mitophagy throughout the entire time course? Are priming phosphorylations and/or dephosphorylations required for subsequent ubiquitin modifications and substrate selection of the E3 ligase(s)? Would these be exclusively mediated by the currently known ubiquitin kinase PINK1 and phosphatases, respectively? Is the cascade of ubiquitin ligases MUL1-MITOL-

parkin established or would there be more E3 ligases involved, also in feedback with distinct autophagy regulators? Does this have an impact on the types of (phospho)ubiquitin chains built on MOM substrates and the writing of a putative mitophagy ubiquitin code? And finally, are the regulatory PTMs restricted to the interface of the MOM with autophagy membranes? The nuclear USP36 is a strong regulator of mitophagy controlling the expression of ATG14L (121). Could [pS65]ubiquitin act as a signal transducer from PINK1 accumulated on damaged mitochondria into the nucleus (202), affecting epigenetic and transcriptional regulators of stress-induced mitophagy?

Are protein phosphorylations, acetylations, and ubiquitin modifications the only PTMs regulating mitophagy? Recent evidence points to glycosylations. N-glycanase 1 (NGLY1) deficiency is a rare congenital disorder leading to global developmental delay and a multisystem syndrome including neuropathy. Interestingly, NGLY1 knockdown significantly impaired mitophagy in HeLa cells stably expressing parkin (203). While NGLY1 can regulate transcription of proteasomal genes *via* deglycosylation of the nuclear factor erythroid 2-like 1, a very recent study identified AMPKα as a novel NGLY1 target integrating energy sensing and mitochondrial homeostasis (204). It will be interesting to further study glycosylations in the regulation of autophagic turnover of mitochondria.

More questions arise when thinking of the cargo-selective specificity of (1) alternative macroautophagy in developing and stressed cells in general or (2) autophagy adaptors in particular, which may or not be driven by PTM modulations. More specifically, it still remains to be elucidated (1) which implications have sirtuin actions on mitochondrial metabolism and cargo-selective autophagy and (2) how do AMBRA1 and its associated factors accumulate on mitochondria for cargo-selective autophagy removal. Another interesting point to be addressed is how Bcl-2 like proteins may regulate autophagy adaptors (*i.e.*, AMBRA1) or other E3-ligases (*i.e.*, HUWE1, MITOL, MUL1). Increasingly sophisticated multiomic screens and future developments in biotechnological methodology combined with hypothesis-driven functional validations of PTM targets all along the mitophagy pathways will undoubtedly advance the comprehensive understanding of this vital process.

Acknowledgments—This work was supported by the German Research Foundation (DFG) Research Training Group GRK2364 "MOMbrane - multifaceted functions and dynamics of the mitochondrial outer membrane," the German Center for Neurodegenerative Diseases (DZNE) within the Helmholtz Association, and the Hertie Foundation. We are grateful for funding from the Israel Science Foundation (Grant #215/19), the Sagol Longevity Foundation, Joint NRF - ISF Research Fund (Grant #3221/19), and the Yeda-Sela Center for Basic Research.

Author contributions—P. K. conceptualization; B. M. and P. K. funding acquisition; A. L. T., K. I. Z., B. M., M. F., Z. E., and P. K. writing–original draft; A. L. T. and P. K. writing–review and editing.2

Funding and additional information—Z. E. is the incumbent of the Harold Korda Chair of Biology.

Conflict of interest—The authors declare that they have no conflict of interest with the contents of this article.

Abbreviations—The abbreviations used are: AMBRA1, activating molecule in beclin-1 regulated autophagy protein 1; AMPK, AMP-activated protein kinase; ARIH1, ariadne-1 homolog in humans; ATG, autophagy-related protein; BAD, Bcl-2 associated agonist of cell death; BAK, Bcl-2 homologous antagonist/killer; Bcl, B cell lymphoma; BH3, Bcl-2 homology 3 domain; BNIP, Bcl-2 19 kDa protein-interacting protein; CCCP, carbonyl cyanide *m*-chlorophenyl hydrazone; CLEAR, coordinated lysosomal expression and regulation; DFCP1, double FYVE domain-containing protein 1; $\Delta\Psi_m$, mitochondrial membrane potential; DRP1, dynamin-related protein 1; DUB, deubiquitylating enzyme; Far, factor arrest; FIP200, focal adhesion kinase-interacting protein of 200 kDa; FIS1, mitochondrial fission 1 protein; FKBP8, FK506-binding protein 8; FUNDC1, FUN14 domain-containing protein 1; GABARAP, γ-amino-butyric acid receptor-associated protein; GCN5L1, general control of amino acid synthesis protein 5-like 1; gp78, glycoprotein 78; HK2, hexokinase 2; HOPS, homotypic fusion and protein sorting; HUWE1, homologous to the E6-AP carboxyl terminus (HECT), ubiquitin-associated and WWE domain-containing protein 1; LC3, microtubule-associated protein light chain 3; LIR, LC3-interacting region; Mcl-1, induced myeloid leukemia cell differentiation protein; MFF, mitochondrial fission factor; MFN, mitofusin; MGRN1, mahogunin RING finger protein 1; MIM, mitochondrial inner membrane; MIRO, mitochondrial Rho GTPase; MITOL, mitochondrial ubiquitin ligase; MOM, mitochondrial outer membrane; mTOR, mammalian target of rapamycin; mTORC1, mTOR complex 1; MTS, mitochondrial targeting sequence; MUL1, mitochondrial ubiquitin ligase 1; NBR1, next to breast cancer type 1 susceptibility gene 1 protein; NDP52, nuclear dot protein of 52 kDa; NF-κB, nuclear factor-κB; NGLY1, N-glycanase 1; OMA1, overlapping with the mitochondrial matrix ATPase associated with diverse cellular activities (m-AAA) protease 1; OPA1, optic atrophy protein 1; PARL, presenilin-associated rhomboid-like protease; PD, Parkinson's disease; PI3P, phosphatidylinositol 3-phosphate; PINK1, phosphatase and tensin homolog (PTEN)-induced kinase 1; PTM, post-translational modification; RAB, Ras-associated binding protein; RING, really interesting new gene; SIRT, sirtuin; SNARE, soluble N-ethylmaleimide-sensitive factor-attachment protein receptor; SUMO, small ubiquitin-related modifier; TBK1, tumor necrosis factor receptor-associated factor family member associated NF-κB activator-binding kinase 1; TFEB, transcription factor EB; TOM, translocase of the outer membrane; Ubl, ubiquitin-like domain; ULK1, uncoordinated protein 51-like kinase 1; USP, ubiquitin-specific protease; VDAC, voltage-dependent anion selective channel; VPS, vacuolar sorting protein; WIPI, WD40 repeat protein interacting with phosphoinositides.

References

1. Calvo, S. E., and Mootha, V. K. (2010) The mitochondrial proteome and human disease. *Annu. Rev. Genomics Hum. Genet.* **11**, 25–44
2. Hernansanz-Agustín, P., and Enríquez, J. A. (2021) Generation of reactive oxygen species by mitochondria. *Antioxidants (Basel)* **10**, 415
3. Theurey, P., and Pizzo, P. (2018) The aging mitochondria. *Genes (Basel)* **9**, 22

4. Lin, M. T., and Beal, M. F. (2006) Mitochondrial dysfunction and oxidative stress in neurodegenerative diseases. *Nature* **443**, 787–795
5. Trist, B. G., Hare, D. J., and Double, K. L. (2019) Oxidative stress in the aging substantia nigra and the etiology of Parkinson's disease. *Aging Cell* **18**, e13031
6. Clark, E. H., Vázquez de la Torre, A., Hoshikawa, T., and Briston, T. (2021) Targeting mitophagy in Parkinson's disease. *J. Biol. Chem.* **296**, 100209
7. Dikic, I., and Elazar, Z. (2018) Mechanism and medical implications of mammalian autophagy. *Nat. Rev. Mol. Cell Biol.* **19**, 349–364
8. He, C., and Klionsky, D. J. (2009) Regulation mechanisms and signaling pathways of autophagy. *Annu. Rev. Genet.* **43**, 67–93
9. Mizushima, N., and Komatsu, M. (2011) Autophagy: Renovation of cells and tissues. *Cell* **147**, 728–741
10. Gatica, D., Lahiri, V., and Klionsky, D. J. (2018) Cargo recognition and degradation by selective autophagy. *Nat. Cell Biol.* **20**, 233–242
11. Grasso, D., Renna, F. J., and Vaccaro, M. I. (2018) Initial steps in mammalian autophagosome biogenesis. *Front. Cell Dev. Biol.* **6**, 146
12. Kim, J., Kundu, M., Viollet, B., and Guan, K.-L. (2011) AMPK and mTOR regulate autophagy through direct phosphorylation of Ulk1. *Nat. Cell Biol.* **13**, 132–141
13. Palmieri, M., Impey, S., Kang, H., di Ronza, A., Pelz, C., Sardiello, M., and Ballabio, A. (2011) Characterization of the CLEAR network reveals an integrated control of cellular clearance pathways. *Hum. Mol. Genet.* **20**, 3852–3866
14. Egan, D. F., Shackelford, D. B., Mihaylova, M. M., Gelino, S., Kohnz, R. A., Mair, W., Vasquez, D. S., Joshi, A., Gwinn, D. M., Taylor, R., Asara, J. M., Fitzpatrick, J., Dillin, A., Viollet, B., Kundu, M., *et al.* (2011) Phosphorylation of ULK1 (hATG1) by AMP-activated protein kinase connects energy sensing to mitophagy. *Science* **331**, 456–461
15. Gallagher, L. E., Williamson, L. E., and Chan, E. Y. (2016) Advances in autophagy regulatory mechanisms. *Cells* **5**, 24
16. Zachari, M., and Ganley, I. G. (2017) The mammalian ULK1 complex and autophagy initiation. *Essays Biochem.* **61**, 585–596
17. Park, J.-M., Jung, C. H., Seo, M., Otto, N. M., Grunwald, D., Kim, K. H., Moriarity, B., Kim, Y.-M., Starker, C., Nho, R. S., Voytas, D., and Kim, D.-H. (2016) The ULK1 complex mediates MTORC1 signaling to the autophagy initiation machinery via binding and phosphorylating ATG14. *Autophagy* **12**, 547–564
18. Russell, R. C., Tian, Y., Yuan, H., Park, H. W., Chang, Y.-Y., Kim, J., Kim, H., Neufeld, T. P., Dillin, A., and Guan, K.-L. (2013) ULK1 induces autophagy by phosphorylating Beclin-1 and activating VPS34 lipid kinase. *Nat. Cell Biol.* **15**, 741–750
19. Mercer, T. J., Ohashi, Y., Boeing, S., Jefferies, H. B. J., De Tito, S., Flynn, H., Tremel, S., Zhang, W., Wirth, M., Frith, D., Snijders, A. P., Williams, R. L., and Tooze, S. A. (2021) Phosphoproteomic identification of ULK substrates reveals VPS15-dependent ULK/VPS34 interplay in the regulation of autophagy. *EMBO J.* **40**, e105985
20. Axe, E. L., Walker, S. A., Manifava, M., Chandra, P., Roderick, H. L., Habermann, A., Griffiths, G., and Ktistakis, N. T. (2008) Autophagosome formation from membrane compartments enriched in phosphatidylinositol 3-phosphate and dynamically connected to the endoplasmic reticulum. *J. Cell Biol.* **182**, 685–701
21. Polson, H. E. J., de Lartigue, J., Rigden, D. J., Reedijk, M., Urbé, S., Clague, M. J., and Tooze, S. A. (2010) Mammalian Atg18 (WIPI2) localizes to omegasome-anchored phagophores and positively regulates LC3 lipidation. *Autophagy* **6**, 506–522
22. Dooley, H. C., Razi, M., Polson, H. E., Girardin, S. E., Wilson, M. I., and Tooze, S. A. (2014) WIPI2 links LC3 conjugation with PI3P, autophagosome formation, and pathogen clearance by recruiting Atg12-5-16L1. *Mol. Cell* **55**, 238–252
23. Turco, E., Fracchiolla, D., and Martens, S. (2020) Recruitment and activation of the ULK1/Atg1 kinase complex in selective autophagy. *J. Mol. Biol.* **432**, 123–134
24. Joo, J. H., Dorsey, F. C., Joshi, A., Hennessy-Walters, K. M., Rose, K. L., McCastlain, K., Zhang, J., Iyengar, R., Jung, C. H., Suen, D. F., Steeves, M. A., Yang, C. Y., Prater, S. M., Kim, D. H., Thompson, C. B., *et al.* (2011) Hsp90-Cdc37 chaperone complex regulates Ulk1- and Atg13-mediated mitophagy. *Mol. Cell* **43**, 572–585
25. Wu, W., Tian, W., Hu, Z., Chen, G., Huang, L., Li, W., Zhang, X., Xue, P., Zhou, C., Liu, L., Zhu, Y., Zhang, X., Li, L., Zhang, L., Sui, S., *et al.* (2014) ULK1 translocates to mitochondria and phosphorylates FUNDC1 to regulate mitophagy. *EMBO Rep.* **15**, 566–575
26. Jiang, P., Nishimura, T., Sakamaki, Y., Itakura, E., Hatta, T., Natsume, T., and Mizushima, N. (2014) The HOPS complex mediates autophagosome-lysosome fusion through interaction with syntaxin 17. *Mol. Biol. Cell* **25**, 1327–1337
27. Wartosch, L., Günesdogan, U., Graham, S. C., and Luzio, J. P. (2015) Recruitment of VPS33A to HOPS by VPS16 is required for lysosome fusion with endosomes and autophagosomes. *Traffic* **16**, 727–742
28. van der Beek, J., Jonker, C., van der Welle, R., Liv, N., and Klumperman, J. (2019) CORVET, CHEVI and HOPS - multisubunit tethers of the endo-lysosomal system in health and disease. *J. Cell Sci.* **132**, jcs189134
29. Zaffagnini, G., and Martens, S. (2016) Mechanisms of selective autophagy. *J. Mol. Biol.* **428**, 1714–1724
30. Khaminets, A., Behl, C., and Dikic, I. (2016) Ubiquitin-dependent and independent signals in selective autophagy. *Trends Cell Biol.* **26**, 6–16
31. Mancias, J. D., and Kimmelman, A. C. (2016) Mechanisms of selective autophagy in normal physiology and cancer. *J. Mol. Biol.* **428**, 1659–1680
32. Chu, C. T. (2019) Mechanisms of selective autophagy and mitophagy: Implications for neurodegenerative diseases. *Neurobiol. Dis.* **122**, 23–34
33. Kanki, T., and Klionsky, D. J. (2008) Mitophagy in yeast occurs through a selective mechanism. *J. Biol. Chem.* **283**, 32386–32393
34. Okamoto, K., Kondo-Okamoto, N., and Ohsumi, Y. (2009) Mitochondria-anchored receptor Atg32 mediates degradation of mitochondria via selective autophagy. *Dev. Cell* **17**, 87–97
35. Kondo-Okamoto, N., Noda, N. N., Suzuki, S. W., Nakatogawa, H., Takahashi, I., Matsunami, M., Hashimoto, A., Inagaki, F., Ohsumi, Y., and Okamoto, K. (2012) Autophagy-related protein 32 acts as autophagic degron and directly initiates mitophagy. *J. Biol. Chem.* **287**, 10631–10638
36. Aihara, M., Jin, X., Kurihara, Y., Yoshida, Y., Matsushima, Y., Oku, M., Hirota, Y., Saigusa, T., Aoki, Y., Uchiumi, T., Yamamoto, T., Sakai, Y., Kang, D., and Kanki, T. (2014) Tor and the Sin3-Rpd3 complex regulate expression of the mitophagy receptor protein Atg32 in yeast. *J. Cell Sci.* **127**, 3184–3196
37. Aoki, Y., Kanki, T., Hirota, Y., Kurihara, Y., Saigusa, T., Uchiumi, T., and Kang, D. (2011) Phosphorylation of serine 114 on Atg32 mediates mitophagy. *Mol. Biol. Cell* **22**, 3206–3217
38. Furukawa, K., Fukuda, T., Yamashita, S.-I., Saigusa, T., Kurihara, Y., Yoshida, Y., Kirisako, H., Nakatogawa, H., and Kanki, T. (2018) The PP2A-like protein phosphatase Ppg1 and the far complex cooperatively counteract CK2-mediated phosphorylation of Atg32 to inhibit mitophagy. *Cell Rep.* **23**, 3579–3590
39. Lazarou, M., Sliter, D. A., Kane, L. A., Sarraf, S. A., Wang, C., Burman, J. L., Sideris, D. P., Fogel, A. I., and Youle, R. J. (2015) The ubiquitin kinase PINK1 recruits autophagy receptors to induce mitophagy. *Nature* **524**, 309–314
40. Narendra, D., Tanaka, A., Suen, D.-F., and Youle, R. J. (2008) Parkin is recruited selectively to impaired mitochondria and promotes their autophagy. *J. Cell Biol.* **183**, 795–803
41. Narendra, D. P., Jin, S. M., Tanaka, A., Suen, D.-F., Gautier, C. A., Shen, J., Cookson, M. R., and Youle, R. J. (2010) PINK1 is selectively stabilized on impaired mitochondria to activate parkin. *PLoS Biol.* **8**, e1000298
42. Bhujabal, Z., Birgisdottir, A. B., Sjøttem, E., Brenne, H. B., Øvervatn, A., Habisov, S., Kirkin, V., Lamark, T., and Johansen, T. (2017) FKBP8 recruits LC3A to mediate parkin-independent mitophagy. *EMBO Rep.* **18**, 947–961
43. Chu, C. T., Ji, J., Dagda, R. K., Jiang, J. F., Tyurina, Y. Y., Kapralov, A. A., Tyurin, V. A., Yanamala, N., Shrivastava, I. H., Mohammadyani, D., Wang, K. Z. Q., Zhu, J., Klein-Seetharaman, J., Balasubramanian, K., Amoscato, A. A., *et al.* (2013) Cardiolipin externalization to the outer

mitochondrial membrane acts as an elimination signal for mitophagy in neuronal cells. *Nat. Cell Biol.* **15**, 1197–1205
44. Sentelle, R. D., Senkal, C. E., Jiang, W., Ponnusamy, S., Gencer, S., Selvam, S. P., Ramshesh, V. K., Peterson, Y. K., Lemasters, J. J., Szulc, Z. M., Bielawski, J., and Ogretmen, B. (2012) Ceramide targets autophagosomes to mitochondria and induces lethal mitophagy. *Nat. Chem. Biol.* **8**, 831–838
45. Dengjel, J., and Abeliovich, H. (2017) Roles of mitophagy in cellular physiology and development. *Cell Tissue Res.* **367**, 95–109
46. Sandoval, H., Thiagarajan, P., Dasgupta, S. K., Schumacher, A., Prchal, J. T., Chen, M., and Wang, J. (2008) Essential role for Nix in autophagic maturation of erythroid cells. *Nature* **454**, 232–235
47. Schweers, R. L., Zhang, J., Randall, M. S., Loyd, M. R., Li, W., Dorsey, F. C., Kundu, M., Opferman, J. T., Cleveland, J. L., Miller, J. L., and Ney, P. A. (2007) NIX is required for programmed mitochondrial clearance during reticulocyte maturation. *Proc. Natl. Acad. Sci. U. S. A.* **104**, 19500–19505
48. Novak, I., Kirkin, V., McEwan, D. G., Zhang, J., Wild, P., Rozenknop, A., Rogov, V., Löhr, F., Popovic, D., Occhipinti, A., Reichert, A. S., Terzic, J., Dötsch, V., Ney, P. A., and Dikic, I. (2010) Nix is a selective autophagy receptor for mitochondrial clearance. *EMBO Rep.* **11**, 45–51
49. Honda, S., Arakawa, S., Nishida, Y., Yamaguchi, H., Ishii, E., and Shimizu, S. (2014) Ulk1-mediated Atg5-independent macroautophagy mediates elimination of mitochondria from embryonic reticulocytes. *Nat. Commun.* **5**, 4004
50. Kundu, M., Lindsten, T., Yang, C.-Y., Wu, J., Zhao, F., Zhang, J., Selak, M. A., Ney, P. A., and Thompson, C. B. (2008) Ulk1 plays a critical role in the autophagic clearance of mitochondria and ribosomes during reticulocyte maturation. *Blood* **112**, 1493–1502
51. Dagda, R. K., Cherra, S. J., 3rd, Kulich, S. M., Tandon, A., Park, D., and Chu, C. T. (2009) Loss of PINK1 function promotes mitophagy through effects on oxidative stress and mitochondrial fission. *J. Biol. Chem.* **284**, 13843–13855
52. Geisler, S., Holmström, K. M., Skujat, D., Fiesel, F. C., Rothfuss, O. C., Kahle, P. J., and Springer, W. (2010) PINK1/parkin-mediated mitophagy is dependent on VDAC1 and p62/SQSTM1. *Nat. Cell Biol.* **12**, 119–131
53. Vives-Bauza, C., Zhou, C., Huang, Y., Cui, M., de Vries, R. L. A., Kim, J., May, J., Tocilescu, M. A., Liu, W., Ko, H. S., Magrané, J., Moore, D. J., Dawson, V. L., Grailhe, R., Dawson, T. M., *et al.* (2010) PINK1-dependent recruitment of parkin to mitochondria in mitophagy. *Proc. Natl. Acad. Sci. U. S. A.* **107**, 378–383
54. Matsuda, N., Sato, S., Shiba, K., Okatsu, K., Saisho, K., Gautier, C. A., Sou, Y., Saiki, S., Kawajiri, S., Sato, F., Kimura, M., Komatsu, M., Hattori, N., and Tanaka, K. (2010) PINK1 stabilized by mitochondrial depolarization recruits parkin to damaged mitochondria and activates latent parkin for mitophagy. *J. Cell Biol.* **189**, 211–221
55. Kazlauskaite, A., Kondapalli, C., Gourlay, R., Campbell, D. G., Ritorto, M. S., Hofmann, K., Alessi, D. R., Knebel, A., Trost, M., and Muqit, M. M. (2014) Parkin is activated by PINK1-dependent phosphorylation of ubiquitin at Ser65. *Biochem. J.* **460**, 127–139
56. Kondapalli, C., Kazlauskaite, A., Zhang, N., Woodroof, H. I., Campbell, D. G., Gourlay, R., Burchell, L., Walden, H., Macartney, T. J., Deak, M., Knebel, A., Alessi, D. R., and Muqit, M. M. (2012) PINK1 is activated by mitochondrial membrane potential depolarization and stimulates parkin E3 ligase activity by phosphorylating Serine 65. *Open Biol.* **2**, 120080
57. Shiba-Fukushima, K., Imai, Y., Yoshida, S., Ishihama, Y., Kanao, T., Sato, S., and Hattori, N. (2012) PINK1-mediated phosphorylation of the parkin ubiquitin-like domain primes mitochondrial translocation of parkin and regulates mitophagy. *Sci. Rep.* **2**, 1002
58. Wauer, T., Simicek, M., Schubert, A., and Komander, D. (2015) Mechanism of phospho-ubiquitin-induced PARKIN activation. *Nature* **524**, 370–374
59. Sauvé, V., Lilov, A., Seirafi, M., Vranas, M., Rasool, S., Kozlov, G., Sprules, T., Wang, J., Trempe, J.-F., and Gehring, K. (2015) A Ubl/ubiquitin switch in the activation of parkin. *EMBO J.* **34**, 2492–2505
60. Greene, A. W., Grenier, K., Aguileta, M. A., Muise, S., Farazifard, R., Haque, M. E., McBride, H. M., Park, D. S., and Fon, E. A. (2012) Mitochondrial processing peptidase regulates PINK1 processing, import and parkin recruitment. *EMBO Rep.* **13**, 378–385
61. Jin, S. M., Lazarou, M., Wang, C., Kane, L. A., Narendra, D. P., and Youle, R. J. (2010) Mitochondrial membrane potential regulates PINK1 import and proteolytic destabilization by PARL. *J. Cell Biol.* **191**, 933–942
62. Meissner, C., Lorenz, H., Weihofen, A., Selkoe, D. J., and Lemberg, M. K. (2011) The mitochondrial intramembrane protease PARL cleaves human Pink1 to regulate Pink1 trafficking. *J. Neurochem.* **117**, 856–867
63. Lin, W., and Kang, U. J. (2008) Characterization of PINK1 processing, stability, and subcellular localization. *J. Neurochem.* **106**, 464–474
64. Yamano, K., and Youle, R. J. (2013) PINK1 is degraded through the N-end rule pathway. *Autophagy* **9**, 1758–1769
65. Voigt, A., Berlemann, L. A., and Winklhofer, K. F. (2016) The mitochondrial kinase PINK1: Functions beyond mitophagy. *J. Neurochem.* **139 Suppl 1**, 232–239
66. Arena, G., and Valente, E. M. (2017) PINK1 in the limelight: Multiple functions of an eclectic protein in human health and disease. *J. Pathol.* **241**, 251–263
67. Okatsu, K., Oka, T., Iguchi, M., Imamura, K., Kosako, H., Tani, N., Kimura, M., Go, E., Koyano, F., Funayama, M., Shiba-Fukushima, K., Sato, S., Shimizu, H., Fukunaga, Y., Taniguchi, H., *et al.* (2012) PINK1 autophosphorylation upon membrane potential dissipation is essential for parkin recruitment to damaged mitochondria. *Nat. Commun.* **3**, 1016
68. Aerts, L., Craessaerts, K., De Strooper, B., and Morais, V. A. (2015) PINK1 kinase catalytic activity is regulated by phosphorylation on serines 228 and 402. *J. Biol. Chem.* **290**, 2798–2811
69. Zhuang, N., Li, L., Chen, S., and Wang, T. (2016) PINK1-dependent phosphorylation of PINK1 and parkin is essential for mitochondrial quality control. *Cell Death Dis.* **7**, e2501
70. Rasool, S., Soya, N., Truong, L., Croteau, N., Lukacs, G. L., and Trempe, J.-F. (2018) PINK1 autophosphorylation is required for ubiquitin recognition. *EMBO Rep.* **19**, e44981
71. Trempe, J.-F., Sauvé, V., Grenier, K., Seirafi, M., Tang, M. Y., Ménade, M., Al-Abdul-Wahid, S., Krett, J., Wong, K., Kozlov, G., Nagar, B., Fon, E. A., and Gehring, K. (2013) Structure of parkin reveals mechanisms for ubiquitin ligase activation. *Science* **340**, 1451–1455
72. Koyano, F., Okatsu, K., Kosako, H., Tamura, Y., Go, E., Kimura, M., Kimura, Y., Tsuchiya, H., Yoshihara, H., Hirokawa, T., Endo, T., Fon, E. A., Trempe, J.-F., Saeki, Y., Tanaka, K., *et al.* (2014) Ubiquitin is phosphorylated by PINK1 to activate parkin. *Nature* **510**, 162–166
73. Sauvé, V., Sung, G., Soya, N., Kozlov, G., Blaimschein, N., Miotto, L. S., Trempe, J.-F., Lukacs, G. L., and Gehring, K. (2018) Mechanism of parkin activation by phosphorylation. *Nat. Struct. Mol. Biol.* **25**, 623–630
74. Wang, L., Cho, Y.-L., Tang, Y., Wang, J., Park, J.-E., Wu, Y., Wang, C., Tong, Y., Chawla, R., Zhang, J., Shi, Y., Deng, S., Lu, G., Wu, Y., Tan, H. W.-S., *et al.* (2018) PTEN-L is a novel protein phosphatase for ubiquitin dephosphorylation to inhibit PINK1-parkin-mediated mitophagy. *Cell Res.* **28**, 787–802
75. Geisler, S., Holmström, K. M., Treis, A., Skujat, D., Weber, S. S., Fiesel, F. C., Kahle, P. J., and Springer, W. (2010) The PINK1/parkin-mediated mitophagy is compromised by PD-associated mutations. *Autophagy* **6**, 871–878
76. Rakovic, A., Grünewald, A., Seibler, P., Ramirez, A., Kock, N., Orolicki, S., Lohmann, K., and Klein, C. (2010) Effect of endogenous mutant and wild-type PINK1 on parkin in fibroblasts from Parkinson disease patients. *Hum. Mol. Genet.* **19**, 3124–3137
77. Ordureau, A., Sarraf, S. A., Duda, D. M., Heo, J.-M., Jedrychowski, M. P., Sviderskiy, V. O., Olszewski, J. L., Koerber, J. T., Xie, T., Beausoleil, S. A., Wells, J. A., Gygi, S. P., Schulman, B. A., and Harper, J. W. (2014) Quantitative proteomics reveal a feedforward mechanism for mitochondrial PARKIN translocation and ubiquitin chain synthesis. *Mol. Cell* **56**, 360–375
78. Gladkova, C., Maslen, S. L., Skehel, J. M., and Komander, D. (2018) Mechanism of parkin activation by PINK1. *Nature* **559**, 410–414

79. Fiesel, F. C., Moussaud-Lamodière, E. L., Ando, M., and Springer, W. (2014) A specific subset of E2 ubiquitin-conjugating enzymes regulate parkin activation and mitophagy differently. *J. Cell Sci.* **127**, 3488–3504
80. Geisler, S., Vollmer, S., Golombek, S., and Kahle, P. J. (2014) The ubiquitin-conjugating enzymes UBE2N, UBE2L3 and UBE2D2/3 are essential for parkin-dependent mitophagy. *J. Cell Sci.* **127**, 3280–3293
81. Swatek, K. N., Usher, J. L., Kueck, A. F., Gladkova, C., Mevissen, T. E. T., Pruneda, J. N., Skern, T., and Komander, D. (2019) Insights into ubiquitin chain architecture using Ub-clipping. *Nature* **572**, 533–537
82. Ordureau, A., Paulo, J. A., Zhang, J., An, H., Swatek, K. N., Cannon, J. R., Wan, Q., Komander, D., and Harper, J. W. (2020) Global landscape and dynamics of parkin and USP30-dependent ubiquitylomes in iNeurons during mitophagic signaling. *Mol. Cell* **77**, 1124–1142.e1110
83. Koyano, F., Yamano, K., Kosako, H., Tanaka, K., and Matsuda, N. (2019) Parkin recruitment to impaired mitochondria for nonselective ubiquitylation is facilitated by MITOL. *J. Biol. Chem.* **294**, 10300–10314
84. Puri, R., Cheng, X.-T., Lin, M.-Y., Huang, N., and Sheng, Z.-H. (2019) Mul1 restrains parkin-mediated mitophagy in mature neurons by maintaining ER-mitochondrial contacts. *Nat. Commun.* **10**, 3645
85. Rose, C. M., Isasa, M., Ordureau, A., Prado, M. A., Beausoleil, S. A., Jedrychowski, M. P., Finley, D. J., Harper, J. W., and Gygi, S. P. (2016) Highly multiplexed quantitative mass spectrometry analysis of ubiquitylomes. *Cell Syst.* **3**, 395–403.e394
86. Birsa, N., Norkett, R., Wauer, T., Mevissen, T. E. T., Wu, H.-C., Foltynie, T., Bhatia, K., Hirst, W. D., Komander, D., Plun-Favreau, H., and Kittler, J. T. (2014) Lysine 27 ubiquitination of the mitochondrial transport protein Miro is dependent on serine 65 of the parkin ubiquitin ligase. *J. Biol. Chem.* **289**, 14569–14582
87. Liu, S., Sawada, T., Lee, S., Yu, W., Silverio, G., Alapatt, P., Millan, I., Shen, A., Saxton, W., Kanao, T., Takahashi, R., Hattori, N., Imai, Y., and Lu, B. (2012) Parkinson's disease-associated kinase PINK1 regulates Miro protein level and axonal transport of mitochondria. *PLoS Genet.* **8**, e1002537
88. Wang, X., Winter, D., Ashrafi, G., Schlehe, J., Wong, Y. L., Selkoe, D., Rice, S., Steen, J., LaVoie, M. J., and Schwarz, T. L. (2011) PINK1 and parkin target Miro for phosphorylation and degradation to arrest mitochondrial motility. *Cell* **147**, 893–906
89. Safiulina, D., Kuum, M., Choubey, V., Gogichaishvili, N., Liiv, J., Hickey, M. A., Cagalinec, M., Mandel, M., Zeb, A., Liiv, M., and Kaasik, A. (2019) Miro proteins prime mitochondria for parkin translocation and mitophagy. *EMBO J.* **38**, e99384
90. Shlevkov, E., Kramer, T., Schapansky, J., LaVoie, M. J., and Schwarz, T. L. (2016) Miro phosphorylation sites regulate parkin recruitment and mitochondrial motility. *Proc. Natl. Acad. Sci. U. S. A.* **113**, E6097–E6106
91. López-Doménech, G., Covill-Cooke, C., Ivankovic, D., Halff, E. F., Sheehan, D. F., Norkett, R., Birsa, N., and Kittler, J. T. (2018) Miro proteins coordinate microtubule- and actin-dependent mitochondrial transport and distribution. *EMBO J.* **37**, 321–336
92. Guillén-Samander, A., Leonzino, M., Hanna, M. G., Tang, N., Shen, H., and De Camilli, P. (2021) VPS13D bridges the ER to mitochondria and peroxisomes via Miro. *J. Cell Biol.* **220**, e202010004
93. Tanaka, A., Cleland, M. M., Xu, S., Narendra, D. P., Suen, D.-F., Karbowski, M., and Youle, R. J. (2010) Proteasome and p97 mediate mitophagy and degradation of mitofusins induced by parkin. *J. Cell Biol.* **191**, 1367–1380
94. Gegg, M. E., Cooper, J. M., Chau, K.-Y., Rojo, M., Schapira, A. H. V., and Taanman, J.-W. (2010) Mitofusin 1 and mitofusin 2 are ubiquitinated in a PINK1/parkin-dependent manner upon induction of mitophagy. *Hum. Mol. Genet.* **19**, 4861–4870
95. Twig, G., Elorza, A., Molina, A. J., Mohamed, H., Wikstrom, J. D., Walzer, G., Stiles, L., Haigh, S. E., Katz, S., Las, G., Alroy, J., Wu, M., Py, B. F., Yuan, J., Deeney, J. T., *et al.* (2008) Fission and selective fusion govern mitochondrial segregation and elimination by autophagy. *EMBO J.* **27**, 433–446
96. McLelland, G.-L., Goiran, T., Yi, W., Dorval, G., Chen, C. X., Lauinger, N. D., Krahn, A. I., Valimehr, S., Rakovic, A., Rouiller, I., Durcan, T. M., Trempe, J.-F., and Fon, E. A. (2018) Mfn2 ubiquitination by PINK1/parkin gates the p97-dependent release of ER from mitochondria to drive mitophagy. *Elife* **7**, e32866
97. Wang, H., Song, P., Du, L., Tian, W., Yue, W., Liu, M., Li, D., Wang, B., Zhu, Y., Cao, C., Zhou, J., and Chen, Q. (2011) Parkin ubiquitinates Drp1 for proteasome-dependent degradation: Implication of dysregulated mitochondrial dynamics in Parkinson disease. *J. Biol. Chem.* **286**, 11649–11658
98. Buhlman, L., Damiano, M., Bertolin, G., Ferrando-Miguel, R., Lombès, A., Brice, A., and Corti, O. (2014) Functional interplay between parkin and Drp1 in mitochondrial fission and clearance. *Biochim. Biophys. Acta* **1843**, 2012–2026
99. Pryde, K. R., Smith, H. L., Chau, K.-Y., and Schapira, A. H. V. (2016) PINK1 disables the anti-fission machinery to segregate damaged mitochondria for mitophagy. *J. Cell Biol.* **213**, 163–171
100. Sarraf, S. A., Raman, M., Guarani-Pereira, V., Sowa, M. E., Huttlin, E. L., Gygi, S. P., and Harper, J. W. (2013) Landscape of the PARKIN-dependent ubiquitylome in response to mitochondrial depolarization. *Nature* **496**, 372–376
101. Narendra, D., Kane, L. A., Hauser, D. N., Fearnley, I. M., and Youle, R. J. (2010) p62/SQSTM1 is required for parkin-induced mitochondrial clustering but not mitophagy; VDAC1 is dispensable for both. *Autophagy* **6**, 1090–1106
102. Sun, Y., Vashisht, A. A., Tchieu, J., Wohlschlegel, J. A., and Dreier, L. (2012) Voltage-dependent anion channels (VDACs) recruit parkin to defective mitochondria to promote mitochondrial autophagy. *J. Biol. Chem.* **287**, 40652–40660
103. Ordureau, A., Paulo, J. A., Zhang, W., Ahfeldt, T., Zhang, J., Cohn, E. F., Hou, Z., Heo, J.-M., Rubin, L. L., Sidhu, S. S., Gygi, S. P., and Harper, J. W. (2018) Dynamics of PARKIN-dependent mitochondrial ubiquitylation in induced neurons and model systems revealed by digital snapshot proteomics. *Mol. Cell* **70**, 211–227.e218
104. McCoy, M. K., Kaganovich, A., Rudenko, I. N., Ding, J., and Cookson, M. R. (2014) Hexokinase activity is required for recruitment of parkin to depolarized mitochondria. *Hum. Mol. Genet.* **23**, 145–156
105. Heo, J.-M., Harper, N. J., Paulo, J. A., Li, M., Xu, Q., Coughlin, M., Elledge, S. J., and Harper, J. W. (2019) Integrated proteogenetic analysis reveals the landscape of a mitochondrial-autophagosome synapse during PARK2-dependent mitophagy. *Sci. Adv.* **5**, eaay4624
106. Ham, S. J., Lee, D., Yoo, H., Jun, K., Shin, H., and Chung, J. (2020) Decision between mitophagy and apoptosis by parkin via VDAC1 ubiquitination. *Proc. Natl. Acad. Sci. U. S. A.* **117**, 4281–4291
107. Chan, N. C., Salazar, A. M., Pham, A. H., Sweredoski, M. J., Kolawa, N. J., Graham, R. L. J., Hess, S., and Chan, D. C. (2011) Broad activation of the ubiquitin-proteasome system by parkin is critical for mitophagy. *Hum. Mol. Genet.* **20**, 1726–1737
108. Yoshii, S. R., Kishi, C., Ishihara, N., and Mizushima, N. (2011) Parkin mediates proteasome-dependent protein degradation and rupture of the outer mitochondrial membrane. *J. Biol. Chem.* **286**, 19630–19640
109. Bertolin, G., Ferrando-Miguel, R., Jacoupy, M., Traver, S., Grenier, K., Greene, A. W., Dauphin, A., Waharte, F., Bayot, A., Salamero, J., Lombès, A., Bulteau, A.-L., Fon, E. A., Brice, A., and Corti, O. (2013) The TOMM machinery is a molecular switch in PINK1 and PARK2/PARKIN-dependent mitochondrial clearance. *Autophagy* **9**, 1801–1817
110. Phu, L., Rose, C. M., Tea, J. S., Wall, C. E., Verschueren, E., Cheung, T. K., Kirkpatrick, D. S., and Bingol, B. (2020) Dynamic regulation of mitochondrial import by the ubiquitin system. *Mol. Cell* **77**, 1107–1123.e1110
111. Komander, D., and Rape, M. (2012) The ubiquitin code. *Annu. Rev. Biochem.* **81**, 203–229
112. Deol, K. K., Eyles, S. J., and Strieter, E. R. (2020) Quantitative middle-down MS analysis of parkin-mediated ubiquitin chain assembly. *J. Am. Soc. Mass Spectrom.* **31**, 1132–1139
113. Bingol, B., Tea, J. S., Phu, L., Reichelt, M., Bakalarski, C. E., Song, Q., Foreman, O., Kirkpatrick, D. S., and Sheng, M. (2014) The mitochondrial deubiquitinase USP30 opposes parkin-mediated mitophagy. *Nature* **510**, 370–375

114. Wang, Y., Serricchio, M., Jauregui, M., Shanbhag, R., Stoltz, T., Di Paolo, C. T., Kim, P. K., and McQuibban, G. A. (2015) Deubiquitinating enzymes regulate PARK2-mediated mitophagy. *Autophagy* **11**, 595–606
115. Gersch, M., Gladkova, C., Schubert, A. F., Michel, M. A., Maslen, S., and Komander, D. (2017) Mechanism and regulation of the Lys6-selective deubiquitinase USP30. *Nat. Struct. Mol. Biol.* **24**, 920–930
116. Sato, Y., Okatsu, K., Saeki, Y., Yamano, K., Matsuda, N., Kaiho, A., Yamagata, A., Goto-Ito, S., Ishikawa, M., Hashimoto, Y., Tanaka, K., and Fukai, S. (2017) Structural basis for specific cleavage of Lys6-linked polyubiquitin chains by USP30. *Nat. Struct. Mol. Biol.* **24**, 911–919
117. Cornelissen, T., Haddad, D., Wauters, F., Van Humbeeck, C., Mandemakers, W., Koentjoro, B., Sue, C., Gevaert, K., De Strooper, B., Verstreken, P., and Vandenberghe, W. (2014) The deubiquitinase USP15 antagonizes parkin-mediated mitochondrial ubiquitination and mitophagy. *Hum. Mol. Genet.* **23**, 5227–5242
118. Niu, K., Fang, H., Chen, Z., Zhu, Y., Tan, Q., Wei, D., Li, Y., Balajee, A. S., and Zhao, Y. (2020) USP33 deubiquitinates PRKN/parkin and antagonizes its role in mitophagy. *Autophagy* **16**, 724–734
119. Durcan, T. M., Tang, M. Y., Pérusse, J. R., Dashti, E. A., Aguileta, M. A., McLelland, G.-L., Gros, P., Shaler, T. A., Faubert, D., Coulombe, B., and Fon, E. A. (2014) USP8 regulates mitophagy by removing K6-linked ubiquitin conjugates from parkin. *EMBO J.* **33**, 2473–2491
120. Simicek, M., Lievens, S., Laga, M., Guzenko, D., Aushev, V. N., Kalev, P., Baietti, M. F., Strelkov, S. V., Gevaert, K., Tavernier, J., and Sablina, A. A. (2013) The deubiquitylase USP33 discriminates between RALB functions in autophagy and innate immune response. *Nat. Cell Biol.* **15**, 1220–1230
121. Geisler, S., Jäger, L., Golombek, S., Nakanishi, E., Hans, F., Casadei, N., Lechado Terradas, A., Linnemann, C., and Kahle, P. J. (2019) Ubiquitin-specific protease USP36 knockdown impairs parkin-dependent mitophagy via downregulation of Beclin-1-associated autophagy-related ATG14L. *Exp. Cell Res.* **384**, 111641
122. Teresak, P., Lapao, A., Subic, N., Boya, P., Elazar, Z., and Simonsen, A. (2021) Regulation of PRKN-independent mitophagy. *Autophagy*, 1–16
123. Villa, E., Marchetti, S., and Ricci, J.-E. (2018) No parkin zone: Mitophagy without parkin. *Trends Cell Biol.* **28**, 882–895
124. Liu, L., Sakakibara, K., Chen, Q., and Okamoto, K. (2014) Receptor-mediated mitophagy in yeast and mammalian systems. *Cell Res.* **24**, 787–795
125. Rogov, V. V., Suzuki, H., Marinkovic, M., Lang, V., Kato, R., Kawasaki, M., Buljubasic, M., Sprung, M., Rogova, N., Wakatsuki, S., Hamacher-Brady, A., Dotsch, V., Dikic, I., Brady, N. R., and Novak, I. (2017) Phosphorylation of the mitochondrial autophagy receptor Nix enhances its interaction with LC3 proteins. *Sci. Rep.* **7**, 1131
126. Zhu, Y., Massen, S., Terenzio, M., Lang, V., Chen-Lindner, S., Eils, R., Novak, I., Dikic, I., Hamacher-Brady, A., and Brady, N. R. (2013) Modulation of serines 17 and 24 in the LC3-interacting region of Bnip3 determines pro-survival mitophagy versus apoptosis. *J. Biol. Chem.* **288**, 1099–1113
127. Chen, G., Han, Z., Feng, D., Chen, Y., Chen, L., Wu, H., Huang, L., Zhou, C., Cai, X., Fu, C., Duan, L., Wang, X., Liu, L., Liu, X., Shen, Y., *et al.* (2014) A regulatory signaling loop comprising the PGAM5 phosphatase and CK2 controls receptor-mediated mitophagy. *Mol. Cell* **54**, 362–377
128. Chen, M., Chen, Z., Wang, Y., Tan, Z., Zhu, C., Li, Y., Han, Z., Chen, L., Gao, R., Liu, L., and Chen, Q. (2016) Mitophagy receptor FUNDC1 regulates mitochondrial dynamics and mitophagy. *Autophagy* **12**, 689–702
129. Van Humbeeck, C., Cornelissen, T., Hofkens, H., Mandemakers, W., Gevaert, K., De Strooper, B., and Vandenberghe, W. (2011) Parkin interacts with Ambra1 to induce mitophagy. *J. Neurosci.* **31**, 10249–10261
130. Strappazzon, F., Nazio, F., Corrado, M., Cianfanelli, V., Romagnoli, A., Fimia, G. M., Campello, S., Nardacci, R., Piacentini, M., Campanella, M., and Cecconi, F. (2015) AMBRA1 is able to induce mitophagy via LC3 binding, regardless of PARKIN and p62/SQSTM1. *Cell Death Differ.* **22**, 419–432
131. Di Rita, A., Peschiaroli, A., P, D. A., Strobbe, D., Hu, Z., Gruber, J., Nygaard, M., Lambrughi, M., Melino, G., Papaleo, E., Dengjel, J., El Alaoui, S., Campanella, M., Dötsch, V., Rogov, V. V., *et al.* (2018) HUWE1 E3 ligase promotes PINK1/PARKIN-independent mitophagy by regulating AMBRA1 activation via IKKα. *Nat. Commun.* **9**, 3755
132. Strappazzon, F., Vietri-Rudan, M., Campello, S., Nazio, F., Florenzano, F., Fimia, G. M., Piacentini, M., Levine, B., and Cecconi, F. (2011) Mitochondrial BCL-2 inhibits AMBRA1-induced autophagy. *EMBO J.* **30**, 1195–1208
133. Choudhary, C., Weinert, B. T., Nishida, Y., Verdin, E., and Mann, M. (2014) The growing landscape of lysine acetylation links metabolism and cell signalling. *Nat. Rev. Mol. Cell Biol.* **15**, 536–550
134. Wu, K., Scott, I., Wang, L., Thapa, D., and Sack, M. N. (2021) The emerging roles of GCN5L1 in mitochondrial and vacuolar organelle biology. *Biochim. Biophys. Acta Gene Regul. Mech.* **1864**, 194598
135. Webster, B. R., Scott, I., Han, K., Li, J. H., Lu, Z., Stevens, M. V., Malide, D., Chen, Y., Samsel, L., Connelly, P. S., Daniels, M. P., McCoy, J. P., Jr., Combs, C. A., Gucek, M., and Sack, M. N. (2013) Restricted mitochondrial protein acetylation initiates mitochondrial autophagy. *J. Cell Sci.* **126**, 4843–4849
136. Tseng, A. H. H., Shieh, S.-S., and Wang, D. L. (2013) SIRT3 deacetylates FOXO3 to protect mitochondria against oxidative damage. *Free Radic. Biol. Med.* **63**, 222–234
137. Wei, T., Huang, G., Gao, J., Huang, C., Sun, M., Wu, J., Bu, J., and Shen, W. (2017) Sirtuin 3 deficiency accelerates hypertensive cardiac remodeling by impairing angiogenesis. *J. Am. Heart Assoc.* **6**, e006114
138. Samant, S. A., Zhang, H. J., Hong, Z., Pillai, V. B., Sundaresan, N. R., Wolfgeher, D., Archer, S. L., Chan, D. C., and Gupta, M. P. (2014) SIRT3 deacetylates and activates OPA1 to regulate mitochondrial dynamics during stress. *Mol. Cell Biol.* **34**, 807–819
139. Meng, H., Yan, W.-Y., Lei, Y.-H., Wan, Z., Hou, Y.-Y., Sun, L.-K., and Zhou, J.-P. (2019) SIRT3 regulation of mitochondrial quality control in neurodegenerative diseases. *Front. Aging Neurosci.* **11**, 313
140. Allen, G. F. G., Toth, R., James, J., and Ganley, I. G. (2013) Loss of iron triggers PINK1/parkin-independent mitophagy. *EMBO Rep.* **14**, 1127–1135
141. Yoo, S.-M., Yamashita, S., Kim, H., Na, D., Lee, H., Kim, S. J., Cho, D.-H., Kanki, T., and Jung, Y.-K. (2020) FKBP8 LIRL-dependent mitochondrial fragmentation facilitates mitophagy under stress conditions. *FASEB J.* **34**, 2944–2957
142. Leermakers, P. A., Remels, A. H. V., Zonneveld, M. I., Rouschop, K. M. A., Schols, A. M. W. J., and Gosker, H. R. (2020) Iron deficiency-induced loss of skeletal muscle mitochondrial proteins and respiratory capacity; the role of mitophagy and secretion of mitochondria-containing vesicles. *FASEB J.* **34**, 6703–6717
143. Fu, M., St-Pierre, P., Shankar, J., Wang, P. T. C., Joshi, B., and Nabi, I. R. (2013) Regulation of mitophagy by the gp78 E3 ubiquitin ligase. *Mol. Biol. Cell* **24**, 1153–1162
144. Mukherjee, R., and Chakrabarti, O. (2016) Ubiquitin-mediated regulation of the E3 ligase gp78 by MGRN1 in trans affects mitochondrial homeostasis. *J. Cell Sci.* **129**, 757–773
145. Guardia-Laguarta, C., Liu, Y., Lauritzen, K. H., Erdjument-Bromage, H., Martin, B., Swayne, T. C., Jiang, X., and Przedborski, S. (2019) PINK1 content in mitochondria is regulated by ER-associated degradation. *J. Neurosci.* **39**, 7074–7085
146. Yun, J., Puri, R., Yang, H., Lizzio, M. A., Wu, C., Sheng, Z. H., and Guo, M. (2014) MUL1 acts in parallel to the PINK1/parkin pathway in regulating mitofusin and compensates for loss of PINK1/parkin. *Elife* **3**, e01958
147. Villa, E., Proics, E., Rubio-Patiño, C., Obba, S., Zunino, B., Bossowski, J. P., Rozier, R. M., Chiche, J., Mondragón, L., Riley, J. S., Marchetti, S., Verhoeyen, E., Tait, S. W. G., and Ricci, J.-E. (2017) Parkin-independent mitophagy controls chemotherapeutic response in cancer cells. *Cell Rep.* **20**, 2846–2859
148. Wenzel, D. M., Lissounov, A., Brzovic, P. S., and Klevit, R. E. (2011) UBCH7 reactivity profile reveals parkin and HHARI to be RING/HECT hybrids. *Nature* **474**, 105–108
149. Denison, S. R., Wang, F., Becker, N. A., Schüle, B., Kock, N., Phillips, L. A., Klein, C., and Smith, D. I. (2003) Alterations in the common fragile site gene parkin in ovarian and other cancers. *Oncogene* **22**, 8370–8378

150. Scheele, C., Nielsen, A. R., Walden, T. B., Sewell, D. A., Fischer, C. P., Brogan, R. J., Petrovic, N., Larsson, O., Tesch, P. A., Wennmalm, K., Hutchinson, D. S., Cannon, B., Wahlestedt, C., Pedersen, B. K., and Timmons, J. A. (2007) Altered regulation of the PINK1 locus: A link between type 2 diabetes and neurodegeneration? *FASEB J.* **21**, 3653–3665
151. Serdaroglu, P., Tasli, H., Hanagasi, H., and Emre, M. (2005) Parkin expression in human skeletal muscle. *J. Clin. Neurosci.* **12**, 927–929
152. Kageyama, Y., Hoshijima, M., Seo, K., Bedja, D., Sysa-Shah, P., Andrabi, S. A., Chen, W., Höke, A., Dawson, V. L., Dawson, T. M., Gabrielson, K., Kass, D. A., Iijima, M., and Sesaki, H. (2014) Parkin-independent mitophagy requires Drp1 and maintains the integrity of mammalian heart and brain. *EMBO J.* **33**, 2798–2813
153. Toyama, E. Q., Herzig, S., Courchet, J., Lewis, T. L., Jr., Losón, O. C., Hellberg, K., Young, N. P., Chen, H., Polleux, F., Chan, D. C., and Shaw, R. J. (2016) Metabolism. AMP-activated protein kinase mediates mitochondrial fission in response to energy stress. *Science* **351**, 275–281
154. D'Amico, D., Mottis, A., Potenza, F., Sorrentino, V., Li, H., Romani, M., Lemos, V., Schoonjans, K., Zamboni, N., Knott, G., Schneider, B. L., and Auwerx, J. (2019) The RNA-binding protein PUM2 impairs mitochondrial dynamics and mitophagy during aging. *Mol. Cell* **73**, 775–787.e710
155. Anding, A. L., Wang, C., Chang, T.-K., Sliter, D. A., Powers, C. M., Hofmann, K., Youle, R. J., and Baehrecke, E. H. (2018) Vps13D encodes a ubiquitin-binding protein that is required for the regulation of mitochondrial size and clearance. *Curr. Biol.* **28**, 287–295.e286
156. Peng, J., Ren, K.-D., Yang, J., and Luo, X.-J. (2016) Mitochondrial E3 ubiquitin ligase 1: A key enzyme in regulation of mitochondrial dynamics and functions. *Mitochondrion* **28**, 49–53
157. Song, Z., Ghochani, M., McCaffery, J. M., Frey, T. G., and Chan, D. C. (2009) Mitofusins and OPA1 mediate sequential steps in mitochondrial membrane fusion. *Mol. Biol. Cell* **20**, 3525–3532
158. Lieber, T., Jeedigunta, S. P., Palozzi, J. M., Lehmann, R., and Hurd, T. R. (2019) Mitochondrial fragmentation drives selective removal of deleterious mtDNA in the germline. *Nature* **570**, 380–384
159. Palozzi, J. M., Jeedigunta, S. P., and Hurd, T. R. (2018) Mitochondrial DNA purifying selection in mammals and invertebrates. *J. Mol. Biol.* **430**, 4834–4848
160. Zhang, J., Randall, M. S., Loyd, M. R., Dorsey, F. C., Kundu, M., Cleveland, J. L., and Ney, P. A. (2009) Mitochondrial clearance is regulated by Atg7-dependent and -independent mechanisms during reticulocyte maturation. *Blood* **114**, 157–164
161. Nishida, Y., Arakawa, S., Fujitani, K., Yamaguchi, H., Mizuta, T., Kanaseki, T., Komatsu, M., Otsu, K., Tsujimoto, Y., and Shimizu, S. (2009) Discovery of Atg5/Atg7-independent alternative macroautophagy. *Nature* **461**, 654–658
162. Saito, T., Nah, J., Oka, S., Mukai, R., Monden, Y., Maejima, Y., Ikeda, Y., Sciarretta, S., Liu, T., Li, H., Baljinnyam, E., Fraidenraich, D., Fritzky, L., Zhai, P., Ichinose, S., *et al.* (2019) An alternative mitophagy pathway mediated by Rab9 protects the heart against ischemia. *J. Clin. Invest.* **129**, 802–819
163. Liao, C., Ashley, N., Diot, A., Morten, K., Phadwal, K., Williams, A., Fearnley, I., Rosser, L., Lowndes, J., Fratter, C., Ferguson, D. J. P., Vay, L., Quaghebeur, G., Moroni, I., Bianchi, S., *et al.* (2017) Dysregulated mitophagy and mitochondrial organization in optic atrophy due to OPA1 mutations. *Neurology* **88**, 131–142
164. Liu, L., Feng, D., Chen, G., Chen, M., Zheng, Q., Song, P., Ma, Q., Zhu, C., Wang, R., Qi, W., Huang, L., Xue, P., Li, B., Wang, X., Jin, H., *et al.* (2012) Mitochondrial outer-membrane protein FUNDC1 mediates hypoxia-induced mitophagy in mammalian cells. *Nat. Cell Biol.* **14**, 177–185
165. Gomes, L. C., Di Benedetto, G., and Scorrano, L. (2011) During autophagy mitochondria elongate, are spared from degradation and sustain cell viability. *Nat. Cell Biol.* **13**, 589–598
166. Rambold, A. S., Kostelecky, B., Elia, N., and Lippincott-Schwartz, J. (2011) Tubular network formation protects mitochondria from autophagosomal degradation during nutrient starvation. *Proc. Natl. Acad. Sci. U. S. A.* **108**, 10190–10195
167. Baker, M. J., Lampe, P. A., Stojanovski, D., Korwitz, A., Anand, R., Tatsuta, T., and Langer, T. (2014) Stress-induced OMA1 activation and autocatalytic turnover regulate OPA1-dependent mitochondrial dynamics. *EMBO J.* **33**, 578–593
168. MacVicar, T. D. B., and Lane, J. D. (2014) Impaired OMA1-dependent cleavage of OPA1 and reduced DRP1 fission activity combine to prevent mitophagy in cells that are dependent on oxidative phosphorylation. *J. Cell Sci.* **127**, 2313–2325
169. Lang, A., Anand, R., Altinoluk-Hambüchen, S., Ezzahoini, H., Stefanski, A., Iram, A., Bergmann, L., Urbach, J., Böhler, P., Hänsel, J., Franke, M., Stühler, K., Krutmann, J., Scheller, J., Stork, B., *et al.* (2017) SIRT4 interacts with OPA1 and regulates mitochondrial quality control and mitophagy. *Aging (Albany, NY)* **9**, 2163–2189
170. Gross, A., and Katz, S. G. (2017) Non-apoptotic functions of BCL-2 family proteins. *Cell Death Differ.* **24**, 1348–1358
171. Maiuri, M. C., Le Toumelin, G., Criollo, A., Rain, J.-C., Gautier, F., Juin, P., Tasdemir, E., Pierron, G., Troulinaki, K., Tavernarakis, N., Hickman, J. A., Geneste, O., and Kroemer, G. (2007) Functional and physical interaction between Bcl-X(L) and a BH3-like domain in Beclin-1. *EMBO J.* **26**, 2527–2539
172. Pattingre, S., Tassa, A., Qu, X., Garuti, R., Liang, X. H., Mizushima, N., Packer, M., Schneider, M. D., and Levine, B. (2005) Bcl-2 antiapoptotic proteins inhibit Beclin 1-dependent autophagy. *Cell* **122**, 927–939
173. Wan, H., Tang, B., Liao, X., Zeng, Q., Zhang, Z., and Liao, L. (2018) Analysis of neuronal phosphoproteome reveals PINK1 regulation of BAD function and cell death. *Cell Death Differ.* **25**, 904–917
174. Cakir, Z., Funk, K., Lauterwasser, J., Todt, F., Zerbes, R. M., Oelgeklaus, A., Tanaka, A., van der Laan, M., and Edlich, F. (2017) Parkin promotes proteasomal degradation of misregulated BAX. *J. Cell Sci.* **130**, 2903–2913
175. Johnson, B. N., Berger, A. K., Cortese, G. P., and LaVoie, M. J. (2012) The ubiquitin E3 ligase parkin regulates the proapoptotic function of Bax. *Proc. Natl. Acad. Sci. U. S. A.* **109**, 6283–6288
176. Bernardini, J. P., Brouwer, J. M., Tan, I. K. L., Sandow, J. J., Huang, S., Stafford, C. A., Bankovacki, A., Riffkin, C. D., Wardak, A. Z., Czabotar, P. E., Lazarou, M., and Dewson, G. (2019) Parkin inhibits BAK and BAX apoptotic function by distinct mechanisms during mitophagy. *EMBO J.* **38**, e99916
177. Carroll, R. G., Hollville, E., and Martin, S. J. (2014) Parkin sensitizes toward apoptosis induced by mitochondrial depolarization through promoting degradation of Mcl-1. *Cell Rep.* **9**, 1538–1553
178. Zhang, C., Lee, S., Peng, Y., Bunker, E., Giaime, E., Shen, J., Zhou, Z., and Liu, X. (2014) PINK1 triggers autocatalytic activation of parkin to specify cell fate decisions. *Curr. Biol.* **24**, 1854–1865
179. Hollville, E., Carroll, R. G., Cullen, S. P., and Martin, S. J. (2014) Bcl-2 family proteins participate in mitochondrial quality control by regulating parkin/PINK1-dependent mitophagy. *Mol. Cell* **55**, 451–466
180. Yu, S., Du, M., Yin, A., Mai, Z., Wang, Y., Zhao, M., Wang, X., and Chen, T. (2020) Bcl-xL inhibits PINK1/parkin-dependent mitophagy by preventing mitochondrial parkin accumulation. *Int. J. Biochem. Cell Biol.* **122**, 105720
181. Zhang, Z., Chen, Z., Liu, R., Liang, Q., Peng, Z., Yin, S., Tang, J., Gong, T., and Liu, Y. (2020) Bcl-2 proteins regulate mitophagy in lipopolysaccharide-induced acute lung injury via PINK1/parkin signaling pathway. *Oxid. Med. Cell Longev.* **2020**, 6579696
182. Arena, G., Gelmetti, V., Torosantucci, L., Vignone, D., Lamorte, G., De Rosa, P., Cilia, E., Jonas, E. A., and Valente, E. M. (2013) PINK1 protects against cell death induced by mitochondrial depolarization, by phosphorylating Bcl-xL and impairing its pro-apoptotic cleavage. *Cell Death Differ* **20**, 920–930
183. Wanderoy, S., Hees, J. T., Klesse, R., Edlich, F., and Harbauer, A. B. (2020) Kill one or kill the many: Interplay between mitophagy and apoptosis. *Biol. Chem.* **402**, 73–88
184. Thiede, B., and Rudel, T. (2004) Proteome analysis of apoptotic cells. *Mass Spectrom. Rev.* **23**, 333–349
185. Zhao, X., Leon, I. R., Bak, S., Mogensen, M., Wrzesinski, K., Hojlund, K., and Jensen, O. N. (2011) Phosphoproteome analysis of functional

mitochondria isolated from resting human muscle reveals extensive phosphorylation of inner membrane protein complexes and enzymes. *Mol. Cell Proteomics* **10**. M110 000299
186. Bak, S., Leon, I. R., Jensen, O. N., and Hojlund, K. (2013) Tissue specific phosphorylation of mitochondrial proteins isolated from rat liver, heart muscle, and skeletal muscle. *J. Proteome Res.* **12**, 4327–4339
187. Lavie, J., De Belvalet, H., Sonon, S., Ion, A. M., Dumon, E., Melser, S., Lacombe, D., Dupuy, J. W., Lalou, C., and Benard, G. (2018) Ubiquitin-dependent degradation of mitochondrial proteins regulates energy metabolism. *Cell Rep.* **23**, 2852–2863
188. Quirós, P. M., Prado, M. A., Zamboni, N., D'Amico, D., Williams, R. W., Finley, D., Gygi, S. P., and Auwerx, J. (2017) Multi-omics analysis identifies ATF4 as a key regulator of the mitochondrial stress response in mammals. *J. Cell Biol.* **216**, 2027–2045
189. Boos, F., Kramer, L., Groh, C., Jung, F., Haberkant, P., Stein, F., Wollweber, F., Gackstatter, A., Zoller, E., van der Laan, M., Savitski, M. M., Benes, V., and Herrmann, J. M. (2019) Mitochondrial protein-induced stress triggers a global adaptive transcriptional programme. *Nat. Cell Biol.* **21**, 442–451
190. Kubli, D. A., and Gustafsson, A. B. (2012) Mitochondria and mitophagy: The yin and yang of cell death control. *Circ. Res.* **111**, 1208–1221
191. Rahman, J., and Rahman, S. (2018) Mitochondrial medicine in the omics era. *Lancet* **391**, 2560–2574
192. Wang, W., Karamanlidis, G., and Tian, R. (2016) Novel targets for mitochondrial medicine. *Sci. Transl. Med.* **8**, 326rv323
193. Heo, J. M., Ordureau, A., Paulo, J. A., Rinehart, J., and Harper, J. W. (2015) The PINK1-PARKIN mitochondrial ubiquitylation pathway drives a program of OPTN/NDP52 recruitment and TBK1 activation to promote mitophagy. *Mol. Cell* **60**, 7–20
194. Richter, B., Sliter, D. A., Herhaus, L., Stolz, A., Wang, C., Beli, P., Zaffagnini, G., Wild, P., Martens, S., Wagner, S. A., Youle, R. J., and Dikic, I. (2016) Phosphorylation of OPTN by TBK1 enhances its binding to Ub chains and promotes selective autophagy of damaged mitochondria. *Proc. Natl. Acad. Sci. U. S. A.* **113**, 4039–4044
195. Padman, B. S., Nguyen, T. N., Uoselis, L., Skulsuppaisarn, M., Nguyen, L. K., and Lazarou, M. (2019) LC3/GABARAPs drive ubiquitin-independent recruitment of Optineurin and NDP52 to amplify mitophagy. *Nat. Commun.* **10**, 408
196. Vargas, J. N. S., Wang, C., Bunker, E., Hao, L., Maric, D., Schiavo, G., Randow, F., and Youle, R. J. (2019) Spatiotemporal control of ULK1 activation by NDP52 and TBK1 during selective autophagy. *Mol. Cell* **74**, 347–362.e346
197. Ravenhill, B. J., Boyle, K. B., von Muhlinen, N., Ellison, C. J., Masson, G. R., Otten, E. G., Foeglein, A., Williams, R., and Randow, F. (2019) The cargo receptor NDP52 initiates selective autophagy by recruiting the ULK complex to cytosol-invading bacteria. *Mol. Cell* **74**, 320–329.e326
198. Torii, S., Yamaguchi, H., Nakanishi, A., Arakawa, S., Honda, S., Moriwaki, K., Nakano, H., and Shimizu, S. (2020) Identification of a phosphorylation site on Ulk1 required for genotoxic stress-induced alternative autophagy. *Nat. Commun.* **11**, 1754
199. Corti, O. (2019) Neuronal mitophagy: Lessons from a pathway linked to Parkinson's disease. *Neurotox Res.* **36**, 292–305
200. Mendes, M. L., Fougeras, M. R., and Dittmar, G. (2020) Analysis of ubiquitin signaling and chain topology cross-talk. *J. Proteomics* **215**, 103634
201. Fottner, M., Brunner, A.-D., Bittl, V., Horn-Ghetko, D., Jussupow, A., Kaila, V. R. I., Bremm, A., and Lang, K. (2019) Site-specific ubiquitylation and SUMOylation using genetic-code expansion and sortase. *Nat. Chem. Biol.* **15**, 276–284
202. Wall, C. E., Rose, C. M., Adrian, M., Zeng, Y. J., Kirkpatrick, D. S., and Bingol, B. (2019) PPEF2 opposes PINK1-mediated mitochondrial quality control by dephosphorylating ubiquitin. *Cell Rep.* **29**, 3280–3292.e3287
203. Yang, K., Huang, R., Fujihira, H., Suzuki, T., and Yan, N. (2018) N-glycanase NGLY1 regulates mitochondrial homeostasis and inflammation through NRF1. *J. Exp. Med.* **215**, 2600–2616
204. Han, S. Y., Pandey, A., Moore, T., Galeone, A., Duraine, L., Cowan, T. M., and Jafar-Nejad, H. (2020) A conserved role for AMP-activated protein kinase in NGLY1 deficiency. *PLoS Genet.* **16**, e1009258

4. Discussion

This chapter represents an extension of discussions from the manuscripts.

Understanding the underlying molecular mechanisms of PINK1/parkin-dependent mitophagy, helps to deepen our understanding of mitophagy and thereby to counteract severe diseases such as Parkinson´s disease[429]. The development of quantitative proteomics workflows in combination with techniques to study PTMs that are involved in mitophagy (phosphorylation and ubiquitylation) are therefore of great importance. In this thesis, a quantitative proteomics workflow was first established to assess parkin-dependent changes in the proteome, ubiquitylome and phosphoproteome. In addition to the previously described initiation mechanisms during PINK1/parkin-dependent mitophagy, the so far understudied late stages of mitophagy, which correspond to the final step of mitochondrial degradation, have been investigated. The mechanisms of mitochondrial degradation by lysosomal and proteasomal actions was investigated in more details in dedicated experiments.

4.1. The quantitative proteomics workflow

The application of subcellular protein fractionation in combination with high pH RP fractionation, proved to be highly efficient in increasing the number of mitochondrial proteins to around 62%, as annotated by MitoCarta3.0[333]. Out of the five generated subcellular protein fractions, three fractions that were enriched either for proteins related to mitochondria or mitophagy were pooled (fraction 1 to 3). Although alternative protocols were tested and evaluated for the efficiency of mitochondria enrichment, none of those met all the requirements to study dynamics on the proteome, phosphoproteome and ubiquitylome during early and late stages of mitophagy. An alternative procedure could have been the enrichment of pure or crude mitochondria[338,430]. This might have allowed an even deeper coverage of the mitochondrial proteome (e.g. stable identification of PINK1 across all samples). However, since most of mitochondria enrichment protocols depend on physical integrity of mitochondria (e.g. separation in a density gradient or by differential centrifugation) these protocols would not have allowed us to study the full mitochondrial proteome during late stages of mitophagy once mitochondria are disrupted or engulfed by the autophagosome and lysosome machinery[338,430]. An additional criterium was the ability to study all mitophagy relevant organelles. Since parkin is only recruited to the mitochondrion upon PINK1 accumulation and

phosphorylation of ubiquitin, the subcellular fraction enriched for cytoplasmic proteins that also had to be included in this analysis[230]. Although the subcellular protein fractionation kit allowed for the enrichment of proteins annotated for subcellular organelles in line with assignments by the vendor, contamination of mitochondrial proteins in other fractions was found. These minor contributions could derive from unavoidable imprecise transfer of fractions during sample preparation or by inter-organelle contact sites between mitochondria and the nucleus[431]. To preserve this information and to further increase the number of mitochondrial proteins, the fraction enriched for soluble nuclear proteins was included for subsequent analyses. Finally, since subsequent enrichment protocols for post-translational modifications, need high amounts of starting material (minimum 1 mg per condition), only the subcellular protein fractionation kit with pooling of fraction 1, 2 and 3 could be applied[432,433].

The quantitative approaches differ between (phospho-)proteome and ubiquitylome analysis. Undoubtably, the TMT-10plex labeling approach represents the more elegant labeling method in comparison to the complex dimethyl labeling scheme applied here. Instead of separating sets of three labeling channels that share a reference time point per cell line, the application of TMT allows to study all five treatment time points (0h, 2h, 6h, 12h, 18h) and the two cell lines (parkin wt, parkin C431A) at once. However, the high sample input material needed for the in-depth proteome and phosphoproteome coverage after RP high pH fractionation (3 mg per triple dimethyl set), prevented the costly TMT labeling approach for this application[434]. Application of the TMT labeling approach to study dynamics of ubiquitylation that usually requires high input material (up to 10 mg) was only feasible with the newly developed UbiSite approach that labeled only enriched GlyGly-remnant peptides[432]. Therefore, the applied quantitative workflow presented here reflects the adaptation for the actual sample requirements.

4.2. Studying parkin-dependent mitophagy in HeLa

The application of the HeLa cells to study late stages of mitophagy represents an important criterion. PINK1/parkin-dependent mitophagy can only be artificially introduced to HeLa cells that normally do not express parkin[435]. Therefore, other groups studied mitophagy on more clinically relevant cell lines like human embryonic stem cell (hNESC) iNeurons[236]. Several reasons prompted us to use the HeLa cell line instead. First, the lack of endogenous parkin, allowed us to study effects of parkin-

ligase dead in a parkin-free background. Second, the parkin C431A cell line had already been validated as highly efficient to study parkin-dependent mitophagy[436]. HeLa cells tolerate the complete loss of mitochondria better than neuronal cells[435]. Due to the so-called Warburg effect present in cancer cells, HeLa predominantly obtain ATP from glycolysis rather than the ETC[437]. Therefore, HeLa cells exclusively allow for studying parkin-dependent mitophagy not only during early, but also late stages.

Several key events during parkin-dependent mitophagy were validated by my proteomics approach. First, the activity of PINK1 was validated by an upregulation of S65 phosphorylation on ubiquitin. This is one of the most upstream events during mitophagy (2h post-mitophagy induction), and is therefore not impacted by ligase-dead parkin[219]. Next, parkin activity was validated by the relative abundance of the parkin-preferred K6 and K63- polyubiquitin linkage chains[236]. Because information on all polyubiquitin linkages are lost during tryptic digestion, the GlyGly-modifications on ubiquitin were used as a readout. With this approach, the window of parkin activity was narrowed down predominantly to early stages of mitophagy (2-6 h post mitophagy induction). Finally, the decrease of mitochondrial annotated proteins only in the presence of functional parkin was evaluated as a correct initiation and progression of mitophagy. Further indications would have been the accumulation on PINK1 and the S65 phosphorylation on parkin[227,438]. Due to the very low protein abundance even under conditions of depolarized mitochondria, I could only detect PINK1 in the most extreme case during late stages of mitophagy and in the presence of the parkin mutant. Phosphorylated parkin on serine 65 had mostly been identified by western blot analysis and only after pull-down assays of parkin by MS[439]. In a separate experiment to study the parkin interactome, flag-tagged parkin was pulled down (unpublished data). Here phosphorylation on serine 65 after 2h of CCCP treatment had been detected.

4.3. Mechanisms of mitochondrial degradation

To understand the role of parkin during late stages of mitophagy and the degradation process, I next defined the mitochondrial proteome sensitive to mitophagy. These are significantly regulated proteins with a high portion of mitochondrial annotated proteins (more than 80%). Most of the non-mitochondrial significantly regulated proteins are annotated as mitochondrial by other databases (like UniProt) or belong to organelles that are in contact with mitochondria (e.g. PLD3, HAX1)[440]. In accordance with the known chronology of mitophagy events, mitochondrial protein degradation already

starts after 2h upon mitophagy induction[441]. However, the observed sequential degradation of mitochondrial subcompartments was surprising. The same outside-in pattern was observed for the ubiquitylation of proteins annotated for mitochondrial subcompartments (discussed in detail in Manuscript I).

Although parkin lacks a stringent recognition motif, its activity window of 2-6h suggests that it targets especially proteins of the OMM. However, protein ubiquitylation of IMM and matrix proteins are more likely down-stream effects of parkin-activity. Most likely other E3-protein ubiquitin ligases become activated and targeted to mitochondria only after the OMM had been removed. In total eight candidate ligases were identified, which show an upregulation of putative activating ubiquitylation events and 17 with a significantly regulated ubiquitylation site. Ubiquitylation sites like HUWE1 K1107 that match the parkin-activity window are of special importance for the regulation of down-stream ubiquitylation of IMM and matrix proteins. E3-ligases can even be connected to lysosomes. For example, the E3 ligase DTX3L was annotated for lysosomal localization[442]. Interestingly, DTX3L serine 539 phosphorylation was identified as a significantly up-regulated site after 12h of CCCP treatment. However, only in parkin wild-type expressing cells. Located in close proximity to the zinc finger region (RING domain), this phosphorylation site might have a regulatory role in mediating late stages ubiquitylation events.

Although phosphorylation usually plays a fundamental role in cellular signaling, mitophagy is primarily controlled by protein ubiquitylation. Only ~7% of quantified phosphorylation sites were found to be significantly regulated, in contrast to 28% of significantly regulated protein ubiquitylation sites. However, these sites could not be connected to a distinct subcellular localization or biological process. One reason for this high background could be the cell line used. As a cancer cell line, HeLa in general shows a high activation of phosphorylation-mediated signaling[443]. Of the dually significantly regulated sites by phosphorylation and ubiquitylation on significantly regulated proteins most are annotated for OMM (VDAC1, RMDN3, TOMM70) or IMM (SLC25A11, AIFM1) localization. Interestingly, RMDN3 carries two significantly regulated phosphorylation sites (serine 44 and 46), that peak after 6h post-mitophagy induction and are further down-regulated during late stages of mitophagy. Both sites are localized close to the N-terminal transmembrane domain of RMDN3, which was shown to be important for the integration into the OMM and induction of apoptosis[444].

Therefore, it can be hypothesized, that the severe mitochondrial dysfunction induced by very long treatment with CCCP (12-18h), start to reprogram the cell for apoptosis[445]. However, dedicated experiments need to be performed, that pinpoint the switch from mitophagy to apoptosis[445]. Although the experimental design described in this thesis does not allow for clear distinction of mitophagy to other processes of the MQC, I found evidences for prohibition of mitochondrial fusion during early stages and the induction of apoptosis during late stages. Among the very early ubiquitylation targets during parkin-dependent mitophagy (2h post mitophagy induction) are MFN1/2 which are involved in mitochondrial fusion[446]. Steric hindrance by ubiquitylation and/ or subsequent protein degradation prohibit mitochondrial fusion and lead to small fragmented mitochondria that are therefore prepared for selective degradation[447].

The detailed mechanisms of mitochondrial degradation were further analyzed in subsequent efforts. After it was discovered, that proteasomal inhibition completely inhibits mitophagy, a proteomics approach in addition to Western Blot, fluorescence and electron microscopy was applied. While after 8h post-mitophagy induction OMM annotated proteins and to a minor extend IMS and IMM are degraded, the degradation of OMM proteins almost completely failed under conditions of proteasome inhibition. Among these were proteins involved in mitochondrial fission (FIS1) and mitochondrial fusion (MFN1). MFN1/2 dependent degradation by proteasome- and a AAA+ ATPase p97 already suggested that proteins involved in mitochondrial dynamics are among early targets, since the degradation of these prevent the fusion and subsequently contamination of healthy mitochondria[232]. However, this experimental design does not reveal whether the accumulation of OMM proteins is indeed an effect of dysfunctional proteasome activity (reduced degradation), or secondary effects due to prolonged MG132 treatment that causes oxidative stress and leads to reduced mitochondrial import and sorting and accumulation of non-degraded mitochondrial proteins in the cytoplasm[448–450]. However, inhibition of proteasomal activity after 2h of in total 8h of CCCP treatment validated the dependency on proteasomal activity for the degradation of OMM proteins. In contrast the degradation of mitochondrial matrix proteins was found to be less impacted by proteasomal inhibition. Of these, subunits of the mitochondrial ribosome machinery are especially prone to proteasomal inhibition. This high dependency on proteasomal degradation can be linked to the excess synthesis of these and the resulting fast degradation of non-assembled subunits[451]. However, the chronology of mitochondrial subcompartment degradation assigned in this work

only reflects a rough time course. To investigate the mitochondrial subcompartment degradation (e.g. IMM) in dependency of the proteasome, a more detailed degradation profile is required.

Taken together, in this work application of quantitative proteomics tools validated the findings from the Kahle group that mitochondrial subcompartments are degraded not only by the lysosome (mitochondrial matrix), but also by the proteasome (OMM).

5. Conclusion and future perspectives

Quantitative proteomics showed to be a powerful tool to study not only the cross-talk between protein ubiquitylation, phosphorylation and protein degradation during the early, but also late stages of parkin-dependent mitophagy. By combining subcellular protein fractionation techniques with quantitative strategies (dimethyl or TMT labeling) and PTM enrichment (phosphorylated- and GlyGly-remnant peptides), the understudied mechanisms of mitochondrial degradation process during late stages of mitophagy had been examined. Furthermore, quantitative proteomics was applied to investigate the impact of proteasomal activity on the degradation of submitochodrial compartments. Taken together, this study led to the following conclusions:

1.) Temporal analysis of protein ubiquitylation and phosphorylation during parkin-dependent mitophagy
    a. Pooling mitophagy relevant fractions of the subcellular protein fractionation kit (Thermo Fisher) enabled the best combination with down-stream PTM enrichment and reduced background signal of proteins unrelated to mitophagy (e.g. histones).
    b. Parkin-dependent mitochondrial degradation takes place in an outside-in procession in which degradation of OMM precedes degradation of IMS, IMM and finally mitochondrial matrix proteins.
    c. Protein ubiquitylation follows the observed outside-in pattern during parkin-dependent mitophagy. In several cases protein ubiquitylation preceded protein degradation.
    d. Protein phosphorylation plays only a minor role during parkin-dependent mitophagy. Mostly OMM proteins showed a dual regulation by phosphorylation and ubiquitylation (e.g. VDAC2).

2.) Parkin-dependent mitophagy occurs via proteasome-dependent steps sequentially targeting separate mitochondrial sub-compartments for autophagy
    a. A dimethyl labeling strategy in combination with high pH RP peptide fractionation was established to compare proteasomal-dependent degradation steps during “early” and “late” stages of mitophagy.

b. Progression of mitophagy depends on proteasomal activity. Inhibition of the proteasome inhibits the degradation of OMM, but only to a minor extent degradation of matrix proteins.

Instead of the general hypothesis that mitochondrial are engulfed as a whole by the autophagosome machinery and subsequently digested within lysosomes, this thesis shows evidences for a “piecemeal” destruction of mitochondria. Therefore, these results encourage to clarify resulting open questions.

Among the late parkin-dependent upregulated ubiquitylation sites I found an ubiquitylation site on parkin itself. Lysine 48 is localized within parkin’s UBL domain and could therefore serve as protein turnover signal. Pulsed SILAC follow-up studies on CRISPR/Cas-mediated mutation on this site (K48R) hint for a delayed turnover in dependency of this ubiquitylation site during parkin-dependent mitophagy. Therefore, lysine 48 might transpire as important stop-signal for parkin activity during mitophagy. So far, we only investigated the role of parkin lysine 48 ubiquitylation on parkin turnover in HeLa cell lines. However, further characterization of this putative regulatory site in a more clinically relevant cell line (e.g. in iNeurons) might help to investigate effects on protein turnover and activity in a more sensitive way.

Our experimental design lead to the complete loss of mitochondria, which is an extreme situation for cells. In addition, it would be interesting to study the recovery of mitochondrial stress. With the deeper knowledge on the time course on mitochondrial degradation during parkin-dependent mitophagy in HeLa cell, questions on mitochondrial dynamics and the “point of no return” for mitophagy could be distinguished.

The generated data sets on protein ubiquitylation and phosphorylation allow further analysis of potential down-stream activities of PINK1/parkin mediated mitophagy. Several E3 ubiquitin ligases were identified that are modified by significantly regulated ubiquitylation or/and phosphorylation sites. To deepen our understanding on how late stages of mitophagy are connected to parkin activity and which E3-ligases are responsible for the ubiquitylation of IMM and matrix proteins, site directed mutagenesis (e.g. by CRISPR/Cas) of these putative sites can be performed.

Clarification of these points will help to better understand the underlying mechanisms of mitochondrial degradation and to better counteract malfunctions of parkin-dependent mitophagy.

6. References

1. Javadov, S., Kozlov, A. v. & Camara, A. K. S. Mitochondria in Health and Diseases. *Cells* vol. 9 (2020).
2. Pfanner, N., Warscheid, B. & Wiedemann, N. Mitochondrial proteins: from biogenesis to functional networks. *Nature Reviews Molecular Cell Biology* vol. 20 267–284 (2019).
3. Kurland, C. G. & Andersson, S. G. E. Origin and Evolution of the Mitochondrial Proteome. *Microbiology and Molecular Biology Reviews* **64**, 786–820 (2000).
4. Archibald, J. M. Endosymbiosis and eukaryotic cell evolution. *Current Biology* vol. 25 R911–R921 (2015).
5. Friedman, J. R. & Nunnari, J. Mitochondrial form and function. *Nature* vol. 505 335–343 (2014).
6. Gorman, G. S. *et al.* Mitochondrial diseases. *Nat Rev Dis Primers* **2**, 1–22 (2016).
7. Parfrey, L. W., Lahr, D. J. G., Knoll, A. H. & Katz, L. A. Estimating the timing of early eukaryotic diversification with multigene molecular clocks. *Proc Natl Acad Sci U S A* **108**, 13624–13629 (2011).
8. Gray, M. W. Mitochondrial evolution. *Cold Spring Harb Perspect Biol* **4**, (2012).
9. Knoll, A. H., Javaux, E. J., Hewitt, D. & Cohen, P. Eukaryotic organisms in Proterozoic oceans. *Philosophical Transactions of the Royal Society B: Biological Sciences* vol. 361 1023–1038 (2006).
10. Margulis, L. Origin of eukaryotic cells: Evidence and research implications for a theory of the origin and evolution of microbial, plant and animal cells on the. (1970).
11. Martin, W. F., Garg, S. & Zimorski, V. Endosymbiotic theories for eukaryote origin. *Philosophical Transactions of the Royal Society B: Biological Sciences* vol. 370 (2015).
12. Booth, A. & Doolittle, W. F. Eukaryogenesis, how special really? *Proceedings of the National Academy of Sciences* **112**, 10278–10285 (2015).
13. Hampl, V., Čepička, I. & Eliáš, M. Was the Mitochondrion Necessary to Start Eukaryogenesis? *Trends in Microbiology* vol. 27 96–104 (2019).
14. Gabaldón, T. Relative timing of mitochondrial endosymbiosis and the “pre-mitochondrial symbioses” hypothesis. *IUBMB Life* vol. 70 1188–1196 (2018).
15. Williams, T. A., Foster, P. G., Cox, C. J. & Embley, T. M. An archaeal origin of eukaryotes supports only two primary domains of life. *Nature* vol. 504 231–236 (2013).
16. Spang, A. *et al.* Asgard archaea are the closest prokaryotic relatives of eukaryotes. *PLoS Genetics* vol. 14 (2018).
17. Imachi, H. *et al.* Isolation of an archaeon at the prokaryote–eukaryote interface. *Nature* **577**, 519–525 (2020).
18. Zaremba-Niedzwiedzka, K. *et al.* Asgard archaea illuminate the origin of eukaryotic cellular complexity. *Nature* **541**, 353–358 (2017).
19. Fan, L. *et al.* Phylogenetic analyses with systematic taxon sampling show that mitochondria branch within Alphaproteobacteria. *Nat Ecol Evol* **4**, 1213–1219 (2020).
20. Gray, M. W., Burger, G. & Lang, B. F. Mitochondrial evolution. *Science* vol. 283 1476–1481 (1999).
21. Duy, D., Soll, J. & Philippar, K. Solute channels of the outer membrane: From bacteria to chloroplasts. *Biological Chemistry* vol. 388 879–889 (2007).
22. Schleiff, E. & Soll, J. Membrane protein insertion: mixing eukaryotic and prokaryotic concepts. *EMBO Rep* **6**, 1023–1027 (2005).
23. Basu, U., Bostwick, A. M., Das, K., Dittenhafer-Reed, K. E. & Patel, S. S. Structure, mechanism, and regulation of mitochondrial DNA transcription initiation. *Journal of Biological Chemistry* **295**, 18406–18425 (2020).
24. Mechta, M., Ingerslev, L. R., Fabre, O., Picard, M. & Barrès, R. Evidence suggesting absence of mitochondrial DNA methylation. *Front Genet* **8**, (2017).
25. Wang, Z. & Wu, M. An integrated phylogenomic approach toward pinpointing the origin of mitochondria. *Sci Rep* **5**, 1–12 (2015).

26. Carvalho, D. S. *et al.* What are the Evolutionary Origins of Mitochondria? A Complex Network Approach. *PLoS One* **10**, e0134988 (2015).
27. Martijn, J., Vosseberg, J., Guy, L., Offre, P. & Ettema, T. J. G. Deep mitochondrial origin outside the sampled alphaproteobacteria. *Nature* **557**, 101–105 (2018).
28. Mills, D. B. The origin of phagocytosis in Earth history. *Interface Focus* **10**, (2020).
29. Martin, W. F., Tielens, A. G. M., Mentel, M., Garg, S. G. & Gould, S. B. The Physiology of Phagocytosis in the Context of Mitochondrial Origin. *Microbiology and Molecular Biology Reviews* **81**, (2017).
30. Bremer, N., Tria, F. D. K., Skejo, J., Garg, S. G. & Martin, W. F. Ancestral State Reconstructions Trace Mitochondria But Not Phagocytosis to the Last Eukaryotic Common Ancestor. *Genome Biol Evol* **14**, (2022).
31. Davidov, Y. & Jurkevitch, E. Predation between prokaryotes and the origin of eukaryotes. *BioEssays* **31**, 748–757 (2009).
32. Davidov, Y., Huchon, D., Koval, S. F. & Jurkevitch, E. A new α-proteobacterial clade of Bdellovibrio-like predators: Implications for the mitochondrial endosymbiotic theory. *Environ Microbiol* **8**, 2179–2188 (2006).
33. Searcy, D. G. Metabolic integration during the evolutionary origin of mitochondria. *Cell Res* **13**, 229–238 (2003).
34. Zachar, I. & Boza, G. Endosymbiosis before eukaryotes: mitochondrial establishment in protoeukaryotes. *Cellular and Molecular Life Sciences* vol. 77 3503–3523 (2020).
35. Baum, D. A. & Baum, B. An inside-out origin for the eukaryotic cell. *BMC Biol* **12**, (2014).
36. Andersson, S. G. & Kurland, C. G. Origins of mitochondria and hydrogenosomes. *Current Opinion in Microbiology* vol. 2 535–541 (1999).
37. Sagan, L. On the origin of mitosing cells. *J Theor Biol* **14**, (1967).
38. Mills, D. B. *et al.* Eukaryogenesis and oxygen in Earth history. *Nature Ecology and Evolution* vol. 6 520–532 (2022).
39. Spang, A. *et al.* Proposal of the reverse flow model for the origin of the eukaryotic cell based on comparative analyses of Asgard archaeal metabolism. *Nat Microbiol* **4**, 1138–1148 (2019).
40. Schirrmacher, V. Mitochondria at work: New insights into regulation and dysregulation of cellular energy supply and metabolism. *Biomedicines* vol. 8 1–38 (2020).
41. Iovine, J. C., Claypool, S. M. & Alder, N. N. Mitochondrial compartmentalization: emerging themes in structure and function. *Trends in Biochemical Sciences* vol. 46 902–917 (2021).
42. Logan, D. C. The mitochondrial compartment. *J Exp Bot* **57**, 1225–1243 (2006).
43. Lane, N. & Martin, W. The energetics of genome complexity. *Nature* **467**, 929–934 (2010).
44. Lane, N. Bioenergetic constraints on the evolution of complex life. *Cold Spring Harb Perspect Biol* **6**, (2014).
45. Fritz-Laylin, L. K. *et al.* The Genome of Naegleria gruberi Illuminates Early Eukaryotic Versatility. *Cell* **140**, 631–642 (2010).
46. Kelly, S. The economics of organellar gene loss and endosymbiotic gene transfer. *Genome Biol* **22**, (2021).
47. Roger, A. J., Muñoz-Gómez, S. A. & Kamikawa, R. The Origin and Diversification of Mitochondria. *Current Biology* vol. 27 R1177–R1192 (2017).
48. Formaggioni, A., Luchetti, A. & Plazzi, F. Mitochondrial genomic landscape: A portrait of the mitochondrial genome 40 years after the first complete sequence. *Life* **11**, (2021).
49. Rehkopf, D. H., Gillespie, D. E., Harrell, M. I. & Feagin, J. E. Transcriptional mapping and RNA processing of the Plasmodium falciparum mitochondrial mRNAs. *Mol Biochem Parasitol* **105**, 91–103 (2000).
50. Burger, G., Gray, M. W., Forget, L. & Lang, B. F. Strikingly bacteria-like and gene-richmitochondrial genomes throughout jakobid protists. *Genome Biol Evol* **5**, 418–438 (2013).

51. Anderson, S. *et al.* Sequence and organization of the human mitochondrial genome. *Nature* **290**, 457–465 (1981).
52. Chinnery, P. F. & Hudson, G. Mitochondrial genetics. *British Medical Bulletin* vol. 106 135–159 (2013).
53. Boengler, K., Heusch, G. & Schulz, R. Nuclear-encoded mitochondrial proteins and their role in cardioprotection. *Biochimica et Biophysica Acta - Molecular Cell Research* vol. 1813 1286–1294 (2011).
54. Wiedemann, N. & Pfanner, N. Mitochondrial Machineries for Protein Import and Assembly. *Annu Rev Biochem* **86**, 685–714 (2017).
55. Vögtle, F. N. *et al.* Global Analysis of the Mitochondrial N-Proteome Identifies a Processing Peptidase Critical for Protein Stability. *Cell* **139**, 428–439 (2009).
56. Genge, M. G. & Mokranjac, D. Coordinated Translocation of Presequence-Containing Precursor Proteins Across Two Mitochondrial Membranes: Knowns and Unknowns of How TOM and TIM23 Complexes Cooperate With Each Other. *Front Physiol* **12**, 2375 (2022).
57. Neupert, W. & Herrmann, J. M. Translocation of Proteins into Mitochondria. *Annu Rev Biochem* **76**, 723–749 (2007).
58. Calvo, S. E. *et al.* Comparative analysis of mitochondrial N-termini from mouse, human, and yeast. *Molecular and Cellular Proteomics* **16**, 512–523 (2017).
59. Araiso, Y., Imai, K. & Endo, T. Structural snapshot of the mitochondrial protein import gate. *FEBS Journal* **288**, 5300–5310 (2021).
60. Bausewein, T. *et al.* Cryo-EM Structure of the TOM Core Complex from Neurospora crassa. *Cell* **170**, 693-700.e7 (2017).
61. Bausewein, T., Naveed, H., Liang, J. & Nussberger, S. The structure of the TOM core complex in the mitochondrial outer membrane. *Biological Chemistry* vol. 401 687–697 (2020).
62. van Wilpe, S. *et al.* Tom22 is a multifunctional organizer of the mitochondrial preprotein translocase. *Nature* **401**, 485–489 (1999).
63. Yamamoto, H. *et al.* Roles of Tom70 in import of presequence-containing mitochondrial proteins. *Journal of Biological Chemistry* **284**, 31635–31646 (2009).
64. Yamano, K. *et al.* Tom20 and Tom22 share the common signal recognition pathway in mitochondrial protein import. *Journal of Biological Chemistry* **283**, 3799–3807 (2008).
65. Abe, Y. *et al.* Structural basis of presequence recognition by the mitochondrial protein import receptor Tom20. *Cell* **100**, 551–560 (2000).
66. Esaki, M. *et al.* Tom40 protein import channel binds to non-native proteins and prevents their aggregation. *Nat Struct Biol* **10**, 988–994 (2003).
67. Araiso, Y. *et al.* Structure of the mitochondrial import gate reveals distinct preprotein paths. *Nature* **575**, 395–401 (2019).
68. Demishtein-Zohary, K. & Azem, A. The TIM23 mitochondrial protein import complex: function and dysfunction. *Cell and Tissue Research* vol. 367 33–41 (2017).
69. Schulz, C. *et al.* Tim50's presequence receptor domain is essential for signal driven transport across the TIM23 complex. *Journal of Cell Biology* **195**, 643–656 (2011).
70. Truscott, K. N. *et al.* A presequence- and voltage-sensitive channel of the mitochondrial preprotein translocase formed by Tim23. *Nat Struct Biol* **8**, 1074–1082 (2001).
71. Kang, P. J. *et al.* Requirement for hsp70 in the mitochondrial matrix for translocation and folding of precursor proteins. *Nature* **348**, 137–143 (1990).
72. Gakh, O., Cavadini, P. & Isaya, G. Mitochondrial processing peptidases. *Biochimica et Biophysica Acta - Molecular Cell Research* vol. 1592 63–77 (2002).
73. Ieva, R. *et al.* Mgr2 functions as lateral gatekeeper for preprotein sorting in the mitochondrial inner membrane. *Mol Cell* **56**, 641–652 (2014).
74. Pagliarini, D. J. *et al.* A Mitochondrial Protein Compendium Elucidates Complex I Disease Biology. *Cell* **134**, 112–123 (2008).
75. Stiller, S. B. *et al.* Mitochondrial OXA Translocase Plays a Major Role in Biogenesis of Inner-Membrane Proteins. *Cell Metab* **23**, 901–908 (2016).

76. Habich, M., Salscheider, S. L. & Riemer, J. Cysteine residues in mitochondrial intermembrane space proteins: more than just import. *British Journal of Pharmacology* vol. 176 514–531 (2019).
77. Chacinska, A. *et al.* Essential role of Mia40 in import and assembly of mitochondrial intermembrane space proteins. *EMBO Journal* **23**, 3735–3746 (2004).
78. Edwards, R., Eaglesfield, R. & Tokatlidis, K. The mitochondrial intermembrane space: The most constricted mitochondrial sub-compartment with the largest variety of protein import pathways. *Open Biology* vol. 11 (2021).
79. Jores, T. *et al.* Characterization of the targeting signal in mitochondrial β-barrel proteins. *Nat Commun* **7**, (2016).
80. Höhr, A. I. C., Straub, S. P., Warscheid, B., Becker, T. & Wiedemann, N. Assembly of β-barrel proteins in the mitochondrial outer membrane. *Biochimica et Biophysica Acta - Molecular Cell Research* vol. 1853 74–88 (2015).
81. Becker, T. *et al.* Biogenesis of the mitochondrial TOM complex: Mim1 promotes insertion and assembly of signal-anchored receptors. *Journal of Biological Chemistry* **283**, 120–127 (2008).
82. Kemper, C. *et al.* Integration of tail-anchored proteins into the mitochondrial outer membrane does not require any known import components. *J Cell Sci* **121**, 1990–1998 (2008).
83. Chen, Z. *et al.* Genetic mosaic analysis of a deleterious mitochondrial DNA mutation in *Drosophila* reveals novel aspects of mitochondrial regulation and function. *Mol Biol Cell* **26**, 674–684 (2015).
84. Hewitt, V., Alcock, F. & Lithgow, T. Minor modifications and major adaptations: The evolution of molecular machines driving mitochondrial protein import. *Biochimica et Biophysica Acta - Biomembranes* vol. 1808 947–954 (2011).
85. Koumandou, V. L. *et al.* Molecular paleontology and complexity in the last eukaryotic common ancestor. *Crit Rev Biochem Mol Biol* **48**, 373–396 (2013).
86. Becker, T. & Wagner, R. Mitochondrial Outer Membrane Channels: Emerging Diversity in Transport Processes. *BioEssays* **40**, 1800013 (2018).
87. Sharma, J., Kumari, R., Bhargava, A., Tiwari, R. & Mishra, P. K. Mitochondrial-induced Epigenetic Modifications: From Biology to Clinical Translation. *Curr Pharm Des* **27**, 159–176 (2020).
88. Fernandez-Marcos, P. J. & Auwerx, J. Regulation of PGC-1α, a nodal regulator of mitochondrial biogenesis. *Am J Clin Nutr* **93**, 884S-890S (2011).
89. Liang, H. & Ward, W. F. PGC-1α: A key regulator of energy metabolism. *American Journal of Physiology - Advances in Physiology Education* vol. 30 145–151 (2006).
90. Rius-Pérez, S. *et al.* PGC-1 α, Inflammation, and Oxidative Stress: An Integrative View in Metabolism. *Oxid Med Cell Longev* **2020**, (2020).
91. Wu, Z. *et al.* Mechanisms controlling mitochondrial biogenesis and respiration through the thermogenic coactivator PGC-1. *Cell* **98**, 115–124 (1999).
92. Fontecha-barriuso, M. *et al.* The role of PGC-1α and mitochondrial biogenesis in kidney diseases. *Biomolecules* vol. 10 (2020).
93. Knutti, D., Kressler, D. & Kralli, A. Regulation of the transcriptional coactivator PGC-1 via MAPK-sensitive interaction with a repressor. *Proc Natl Acad Sci U S A* **98**, 9713–9718 (2001).
94. Herzig, S. & Shaw, R. J. AMPK: Guardian of metabolism and mitochondrial homeostasis. *Nature Reviews Molecular Cell Biology* vol. 19 121–135 (2018).
95. Cantó, C. & Auwerx, J. PGC-1α, SIRT1 and AMPK, an energy sensing network that controls energy expenditure. *Current Opinion in Lipidology* vol. 20 98–105 (2009).
96. Martínez-Reyes, I. & Chandel, N. S. Mitochondrial TCA cycle metabolites control physiology and disease. *Nature Communications* vol. 11 1–11 (2020).
97. Gonzalez, S. The Role of Mitonuclear Incompatibility in Bipolar Disorder Susceptibility and Resilience Against Environmental Stressors. *Frontiers in Genetics* vol. 12 347 (2021).

98. Vizioli, M. G. *et al.* Mitochondria-to-nucleus retrograde signaling drives formation of cytoplasmic chromatin and inflammation in senescence. *Genes Dev* **34**, 428–445 (2020).
99. Chandel, N. S. Evolution of Mitochondria as Signaling Organelles. *Cell Metabolism* vol. 22 204–206 (2015).
100. Mitra, K. Mitochondrial fission-fusion as an emerging key regulator of cell proliferation and differentiation. *BioEssays* **35**, 955–964 (2013).
101. Chandel, N. S. *et al.* Mitochondrial reactive oxygen species trigger hypoxia-induced transcription. *Proc Natl Acad Sci U S A* **95**, 11715–11720 (1998).
102. Horvath, S. E. & Daum, G. Lipids of mitochondria. *Progress in Lipid Research* vol. 52 590–614 (2013).
103. Dimmer, K. S. & Rapaport, D. Mitochondrial contact sites as platforms for phospholipid exchange. *Biochimica et Biophysica Acta - Molecular and Cell Biology of Lipids* vol. 1862 69–80 (2017).
104. Kornmann, B. *et al.* An ER-mitochondria tethering complex revealed by a synthetic biology screen. *Science (1979)* **325**, 477–481 (2009).
105. Mejia, E. M. & Hatch, G. M. Mitochondrial phospholipids: role in mitochondrial function. *Journal of Bioenergetics and Biomembranes* vol. 48 99–112 (2016).
106. Elbaz, Y. & Schuldiner, M. Staying in touch: The molecular era of organelle contact sites. *Trends in Biochemical Sciences* vol. 36 616–623 (2011).
107. Brisac, C. *et al.* Calcium Flux between the Endoplasmic Reticulum and Mitochondrion Contributes to Poliovirus-Induced Apoptosis. *J Virol* **84**, 12226–12235 (2010).
108. Illescas, M., Peñas, A., Arenas, J., Martín, M. A. & Ugalde, C. Regulation of Mitochondrial Function by the Actin Cytoskeleton. *Frontiers in Cell and Developmental Biology* vol. 9 3656 (2021).
109. Schwarz, T. L. Mitochondrial trafficking in neurons. *Cold Spring Harb Perspect Biol* **5**, (2013).
110. Kruppa, A. J. & Buss, F. Motor proteins at the mitochondria–cytoskeleton interface. *Journal of Cell Science* vol. 134 (2021).
111. Pietrocola, F., Galluzzi, L., Bravo-San Pedro, J. M., Madeo, F. & Kroemer, G. Acetyl coenzyme A: A central metabolite and second messenger. *Cell Metabolism* vol. 21 805–821 (2015).
112. Wellen, K. E. *et al.* ATP-citrate lyase links cellular metabolism to histone acetylation. *Science (1979)* **324**, 1076–1080 (2009).
113. Lozoya, O. A. *et al.* Mitochondrial acetyl-CoA reversibly regulates locusspecific histone acetylation and gene expression. *Life Sci Alliance* **2**, (2019).
114. Toyama, E. Q. *et al.* Metabolism: AMP-activated protein kinase mediates mitochondrial fission in response to energy stress. *Science (1979)* **351**, 275–281 (2016).
115. Hu, Y. *et al.* The AMPK-MFN2 axis regulates MAM dynamics and autophagy induced by energy stresses. *Autophagy* **17**, 1142–1156 (2021).
116. Yang, S. & Lian, G. ROS and diseases: role in metabolism and energy supply. *Molecular and Cellular Biochemistry* vol. 467 1–12 (2020).
117. Stöcker, S., van Laer, K., Mijuskovic, A. & Dick, T. P. The Conundrum of Hydrogen Peroxide Signaling and the Emerging Role of Peroxiredoxins as Redox Relay Hubs. *Antioxidants and Redox Signaling* vol. 28 558–573 (2018).
118. Vandenbroucke, K. *et al.* Hydrogen peroxide-induced gene expression across kingdoms: A comparative analysis. *Mol Biol Evol* **25**, 507–516 (2008).
119. Santucci, R., Sinibaldi, F., Cozza, P., Polticelli, F. & Fiorucci, L. Cytochrome c: An extreme multifunctional protein with a key role in cell fate. *International Journal of Biological Macromolecules* vol. 136 1237–1246 (2019).
120. Dadsena, S., Jenner, A. & García-Sáez, A. J. Mitochondrial outer membrane permeabilization at the single molecule level. *Cellular and Molecular Life Sciences* vol. 78 3777–3790 (2021).

121. Riley, J. S. & Tait, S. W. Mitochondrial DNA in inflammation and immunity . *EMBO Rep* **21**, (2020).
122. Fang, Y. *et al.* Cytosolic mtdna released from pneumolysin-damaged mitochondria triggers ifn- β production in epithelial cells. *Can J Microbiol* **66**, 435–445 (2020).
123. Gabaldón, T. A metabolic scenario for the evolutionary origin of peroxisomes from the endomembranous system. *Cellular and Molecular Life Sciences* **71**, 2373–2376 (2014).
124. Mohanty, A. & McBride, H. M. Emerging roles of mitochondria in the evolution, biogenesis, and function of peroxisomes. *Frontiers in Physiology* vol. 4 SEP 268 (2013).
125. Giacomello, M., Pyakurel, A., Glytsou, C. & Scorrano, L. The cell biology of mitochondrial membrane dynamics. *Nature Reviews Molecular Cell Biology* vol. 21 204–224 (2020).
126. Krüger, V. *et al.* Identification of new channels by systematic analysis of the mitochondrial outer membrane. *Journal of Cell Biology* **216**, 3485–3495 (2017).
127. Gupta, A. & Becker, T. Mechanisms and pathways of mitochondrial outer membrane protein biogenesis. *Biochimica et Biophysica Acta - Bioenergetics* vol. 1862 148323 (2021).
128. Cogliati, S. *et al.* Mitochondrial cristae shape determines respiratory chain supercomplexes assembly and respiratory efficiency. *Cell* **155**, 160–171 (2013).
129. Tamura, Y. *et al.* Phosphatidylethanolamine biosynthesis in mitochondria: Phosphatidylserine (PS) trafficking is independent of a PS decarboxylase and intermembrane space proteins Ups1p and Ups2p. *Journal of Biological Chemistry* **287**, 43961–43971 (2012).
130. Li, X. X., Tsoi, B., Li, Y. F., Kurihara, H. & He, R. R. Cardiolipin and Its Different Properties in Mitophagy and Apoptosis. *Journal of Histochemistry and Cytochemistry* vol. 63 301–311 (2015).
131. Tirrell, P. S., Nguyen, K. N., Luby-Phelps, K. & Friedman, J. R. MICOS subcomplexes assemble independently on the mitochondrial inner membrane in proximity to ER contact sites. *Journal of Cell Biology* **219**, (2020).
132. Harner, M. *et al.* The mitochondrial contact site complex, a determinant of mitochondrial architecture. *EMBO J* **30**, 4356–4370 (2011).
133. Bohnert, M. *et al.* Role of mitochondrial inner membrane organizing system in protein biogenesis of the mitochondrial outer membrane. *Mol Biol Cell* **23**, 3948–3956 (2012).
134. Khosravi, S. & Harner, M. E. The MICOS complex, a structural element of mitochondria with versatile functions. *Biological Chemistry* vol. 401 765–778 (2020).
135. Edwards, R., Gerlich, S., Gerlich, S. & Tokatlidis, K. The biogenesis of mitochondrial intermembrane space proteins. *Biological Chemistry* vol. 401 737–747 (2020).
136. Schreiner, B. *et al.* Role of the AAA protease Yme1 in folding of proteins in the intermembrane space of mitochondria. *Mol Biol Cell* **23**, 4335–4346 (2012).
137. Bragoszewski, P., Gornicka, A., Sztolsztener, M. E. & Chacinska, A. The Ubiquitin-Proteasome System Regulates Mitochondrial Intermembrane Space Proteins. *Mol Cell Biol* **33**, 2136–2148 (2013).
138. Stewart, J. B. & Chinnery, P. F. Extreme heterogeneity of human mitochondrial DNA from organelles to populations. *Nature Reviews Genetics* vol. 22 106–118 (2021).
139. Mazunin, I. O., Levitskii, S. A., Patrushev, M. v. & Kamenski, P. A. Mitochondrial matrix processes. *Biochemistry (Moscow)* vol. 80 1418–1428 (2015).
140. al Ojaimi, M., Salah, A. & El-Hattab, A. W. Mitochondrial Fission and Fusion: Molecular Mechanisms, Biological Functions, and Related Disorders. *Membranes* vol. 12 (2022).
141. Westermann, B. Mitochondrial fusion and fission in cell life and death. *Nature Reviews Molecular Cell Biology* vol. 11 872–884 (2010).
142. Pangou, E. & Sumara, I. The Multifaceted Regulation of Mitochondrial Dynamics During Mitosis. *Frontiers in Cell and Developmental Biology* vol. 9 3120 (2021).

143. Gandre-Babbe, S. & van der Bliek, A. M. The novel tail-anchored membrane protein Mff controls mitochondrial and peroxisomal fission in mammalian cells. *Mol Biol Cell* **19**, 2402–2412 (2008).
144. Prudent, J. & McBride, H. M. Mitochondrial Dynamics: ER Actin Tightens the Drp1 Noose. *Current Biology* vol. 26 R207–R209 (2016).
145. Lee, J. E., Westrate, L. M., Wu, H., Page, C. & Voeltz, G. K. Multiple dynamin family members collaborate to drive mitochondrial division. *Nature* **540**, 139–143 (2016).
146. Gottlieb, R. A. *et al.* At the heart of mitochondrial quality control: many roads to the top. *Cellular and Molecular Life Sciences* vol. 78 3791–3801 (2021).
147. Legros, F., Lombès, A., Frachon, P. & Rojo, M. Mitochondrial fusion in human cells is efficient, requires the inner membrane potential, and is mediated by mitofusins. *Mol Biol Cell* **13**, 4343–4354 (2002).
148. Ban, T. *et al.* Molecular basis of selective mitochondrial fusion by heterotypic action between OPA1 and cardiolipin. *Nat Cell Biol* **19**, 856–863 (2017).
149. Abrisch, R. G., Gumbin, S. C., Wisniewski, B. T., Lackner, L. L. & Voeltz, G. K. Fission and fusion machineries converge at ER contact sites to regulate mitochondrial morphology. *Journal of Cell Biology* **219**, (2020).
150. Shen, K. *et al.* Mitochondria as Cellular and Organismal Signaling Hubs. *Annu Rev Cell Dev Biol* **38**, (2022).
151. Bratic, I. & Trifunovic, A. Mitochondrial energy metabolism and ageing. *Biochimica et Biophysica Acta - Bioenergetics* vol. 1797 961–967 (2010).
152. Kunji, E. R. S. *et al.* The transport mechanism of the mitochondrial ADP/ATP carrier. *Biochim Biophys Acta Mol Cell Res* **1863**, 2379–2393 (2016).
153. Bartlett, K. & Eaton, S. Mitochondrial beta-oxidation. *Eur J Biochem* **271**, 462–469 (2004).
154. Xia, C., Fu, Z., Battaile, K. P. & Kim, J. J. P. Crystal structure of human mitochondrial trifunctional protein, a fatty acid β-oxidation metabolon. *Proc Natl Acad Sci U S A* **116**, 6069–6074 (2019).
155. des Rosiers, C., Labarthe, F., Lloyd, S. G. & Chatham, J. C. Cardiac anaplerosis in health and disease: Food for thought. *Cardiovasc Res* **90**, 210–219 (2011).
156. Nolfi-Donegan, D., Braganza, A. & Shiva, S. Mitochondrial electron transport chain: Oxidative phosphorylation, oxidant production, and methods of measurement. *Redox Biology* vol. 37 101674 (2020).
157. Allen, J. F. *et al.* The function of genomes in bioenergetic organelles. in *Philosophical Transactions of the Royal Society B: Biological Sciences* vol. 358 19–38 (Royal Society, 2003).
158. Zhao, R. Z., Jiang, S., Zhang, L. & Yu, Z. bin. Mitochondrial electron transport chain, ROS generation and uncoupling (Review). *International Journal of Molecular Medicine* vol. 44 3–15 (2019).
159. Zorova, L. D. *et al.* Functional Significance of the Mitochondrial Membrane Potential. *Biochemistry (Moscow) Supplement Series A: Membrane and Cell Biology* vol. 12 20–26 (2018).
160. Davies, K. M. *et al.* Macromolecular organization of ATP synthase and complex I in whole mitochondria. *Proc Natl Acad Sci U S A* **108**, 14121–14126 (2011).
161. Wolf, D. M. *et al.* Individual cristae within the same mitochondrion display different membrane potentials and are functionally independent. *EMBO J* **38**, (2019).
162. de Cubas, L., Pak, V. v., Belousov, V. v., Ayté, J. & Hidalgo, E. The Mitochondria-to-Cytosol H2O2 Gradient Is Caused by Peroxiredoxin-Dependent Cytosolic Scavenging. *Antioxidants* **10**, 731 (2021).
163. Lee, S. *et al.* Mitochondrial H2 O2 generated from electron transport chain complex i stimulates muscle differentiation. *Cell Res* **21**, 817–834 (2011).
164. Mazat, J. P., Devin, A. & Ransac, S. Modelling mitochondrial ROS production by the respiratory chain. *Cellular and Molecular Life Sciences* vol. 77 455–465 (2020).
165. Murphy, M. P. How mitochondria produce reactive oxygen species. *Biochemical Journal* vol. 417 1–13 (2009).

166. Mansouri, A., Gattolliat, C. H. & Asselah, T. Mitochondrial Dysfunction and Signaling in Chronic Liver Diseases. *Gastroenterology* vol. 155 629–647 (2018).
167. Sharma, P. & Sampath, H. Mitochondrial DNA integrity: Role in health and disease. *Cells* vol. 8 (2019).
168. Spinelli, J. B. & Haigis, M. C. The multifaceted contributions of mitochondria to cellular metabolism. *Nature Cell Biology* vol. 20 745–754 (2018).
169. Mills, C. A., Trub, A. G. & Hirschey, M. D. Sensing Mitochondrial Acetyl-CoA to Tune Respiration. *Trends in Endocrinology and Metabolism* vol. 30 1–3 (2019).
170. van Vranken, J. G. *et al.* ACP Acylation Is an Acetyl-CoA-Dependent Modification Required for Electron Transport Chain Assembly. *Mol Cell* **71**, 567-580.e4 (2018).
171. Read, A. D., Bentley, R. E., Archer, S. L. & Dunham-Snary, K. J. Mitochondrial iron–sulfur clusters: Structure, function, and an emerging role in vascular biology: Mitochondrial Fe-S Clusters – a review. *Redox Biology* vol. 47 (2021).
172. Shi, R., Hou, W., Wang, Z. Q. & Xu, X. Biogenesis of Iron–Sulfur Clusters and Their Role in DNA Metabolism. *Frontiers in Cell and Developmental Biology* vol. 9 (2021).
173. Baranovskiy, A. G., Siebler, H. M., Pavlov, Y. I. & Tahirov, T. H. Iron–Sulfur Clusters in DNA Polymerases and Primases of Eukaryotes. in *Methods in Enzymology* vol. 599 1–20 (Academic Press Inc., 2018).
174. Raffaello, A., Mammucari, C., Gherardi, G. & Rizzuto, R. Calcium at the Center of Cell Signaling: Interplay between Endoplasmic Reticulum, Mitochondria, and Lysosomes. *Trends in Biochemical Sciences* vol. 41 1035–1049 (2016).
175. Romero-Garcia, S. & Prado-Garcia, H. Mitochondrial calcium: Transport and modulation of cellular processes in homeostasis and cancer (Review). *International Journal of Oncology* vol. 54 1155–1167 (2019).
176. Patra, S. *et al.* Intricate role of mitochondrial calcium signalling in mitochondrial quality control for regulation of cancer cell fate. *Mitochondrion* vol. 57 230–240 (2021).
177. Song, J., Herrmann, J. M. & Becker, T. Quality control of the mitochondrial proteome. *Nature Reviews Molecular Cell Biology* vol. 22 54–70 (2021).
178. Eldeeb, M. A., Esmaili, M., Hassan, M. & Ragheb, M. A. The Role of PTEN-L in Modulating PINK1-Parkin-Mediated Mitophagy. *Neurotoxicity Research* vol. 40 1103–1114 (2022).
179. Schon, E. A. & Gilkerson, R. W. Functional complementation of mitochondrial DNAs: Mobilizing mitochondrial genetics against dysfunction. *Biochimica et Biophysica Acta - General Subjects* vol. 1800 245–249 (2010).
180. Mercer, T. R. *et al.* The human mitochondrial transcriptome. *Cell* **146**, 645–658 (2011).
181. Russell, O. & Turnbull, D. Mitochondrial DNA disease-molecular insights and potential routes to a cure. *Experimental Cell Research* vol. 325 38–43 (2014).
182. Rong, Z. *et al.* The Mitochondrial Response to DNA Damage. *Frontiers in Cell and Developmental Biology* vol. 9 1212 (2021).
183. Kennedy, S. R., Salk, J. J., Schmitt, M. W. & Loeb, L. A. Ultra-Sensitive Sequencing Reveals an Age-Related Increase in Somatic Mitochondrial Mutations That Are Inconsistent with Oxidative Damage. *PLoS Genet* **9**, (2013).
184. DiMauro, S. & Schon, E. A. Mitochondrial Respiratory-Chain Diseases. *New England Journal of Medicine* **348**, 2656–2668 (2003).
185. Yang, Q. *et al.* LONP-1 and ATFS-1 sustain deleterious heteroplasmy by promoting mtDNA replication in dysfunctional mitochondria. *Nat Cell Biol* **24**, 181–193 (2022).
186. Lieber, T., Jeedigunta, S. P., Palozzi, J. M., Lehmann, R. & Hurd, T. R. Mitochondrial fragmentation drives selective removal of deleterious mtDNA in the germline. *Nature* **570**, 380–384 (2019).
187. Fan, W. *et al.* A mouse model of mitochondrial disease reveals germline selection against severe mtDNA mutations. *Science (1979)* **319**, 958–962 (2008).
188. Sato, M. & Sato, K. Maternal inheritance of mitochondrial DNA by diverse mechanisms to eliminate paternal mitochondrial DNA. *Biochimica et Biophysica Acta - Molecular Cell Research* vol. 1833 1979–1984 (2013).

189. Tworzydlo, W., Sekula, M. & Bilinski, S. M. Transmission of functional, wild-type mitochondria and the fittest mtDNA to the next generation: Bottleneck phenomenon, Balbiani body, and Mitophagy. *Genes* vol. 11 (2020).
190. Ikeda, Y. *et al.* Endogenous Drp1 mediates mitochondrial autophagy and protects the heart against energy stress. *Circ Res* **116**, 264–278 (2015).
191. Davies, V. J. *et al.* Opa1 deficiency in a mouse model of autosomal dominant optic atrophy impairs mitochondrial morphology, optic nerve structure and visual function. *Hum Mol Genet* **16**, 1307–1318 (2007).
192. Chen, H. *et al.* Mitofusins Mfn1 and Mfn2 coordinately regulate mitochondrial fusion and are essential for embryonic development. *Journal of Cell Biology* **160**, 189–200 (2003).
193. Ono, T., Isobe, K., Nakada, K. & Hayashi, J. I. Human cells are protected from mitochondrial dysfunction by complementation of DNA products in fused mitochondria. *Nat Genet* **28**, 272–275 (2001).
194. Tondera, D. *et al.* SlP-2 is required for stress-induced mitochondrial hyperfusion. *EMBO Journal* **28**, 1589–1600 (2009).
195. Mandal, A. *et al.* Retrograde mitochondrial transport is essential for organelle distribution and health in Zebrafish Neurons. *Journal of Neuroscience* **41**, 1371–1392 (2021).
196. Youle, R. J. & van der Bliek, A. M. Mitochondrial fission, fusion, and stress. *Science* vol. 337 1062–1065 (2012).
197. Kleele, T. *et al.* Distinct fission signatures predict mitochondrial degradation or biogenesis. *Nature* **593**, 435–439 (2021).
198. Agrawal, A. & Koslover, E. F. Optimizing mitochondrial maintenance in extended neuronal projections. *PLoS Comput Biol* **17**, e1009073 (2021).
199. Opalińska, M. & Jańska, H. AAA proteases: Guardians of mitochondrial function and homeostasis. *Cells* **7**, (2018).
200. Bahr, T., Katuri, J., Liang, T. & Bai, Y. Mitochondrial chaperones in human health and disease. *Free Radical Biology and Medicine* vol. 179 363–374 (2022).
201. Iorio, R., Celenza, G. & Petricca, S. Mitophagy: Molecular mechanisms, new concepts on parkin activation and the emerging role of ampk/ulk1 axis. *Cells* vol. 11 (2022).
202. Sulkshane, P. *et al.* Ubiquitination and receptor-mediated mitophagy converge to eliminate oxidation-damaged mitochondria during hypoxia. *Redox Biol* **45**, 102047 (2021).
203. Palikaras, K., Daskalaki, I., Markaki, M. & Tavernarakis, N. Mitophagy and age-related pathologies: Development of new therapeutics by targeting mitochondrial turnover. *Pharmacology and Therapeutics* vol. 178 157–174 (2017).
204. Gan, Z. Y. *et al.* Activation mechanism of PINK1. *Nature* **602**, 328–335 (2022).
205. Vives-Bauza, C. & Przedborski, S. Mitophagy: The latest problem for Parkinson's disease. *Trends in Molecular Medicine* vol. 17 158–165 (2011).
206. Xu, Y. *et al.* PINK1 deficiency in gastric cancer compromises mitophagy, promotes the Warburg effect, and facilitates M2 polarization of macrophages. *Cancer Lett* **529**, 19–36 (2022).
207. Li, J. *et al.* PINK1-parkin-mediated neuronal mitophagy deficiency in prion disease. *Cell Death Dis* **13**, 1–12 (2022).
208. Wu, Y. *et al.* PINK1/Parkin-mediated mitophagy in cardiovascular disease: From pathogenesis to novel therapy. *International Journal of Cardiology* vol. 361 61–69 (2022).
209. Pickrell, A. M. & Youle, R. J. The roles of PINK1, Parkin, and mitochondrial fidelity in parkinson's disease. *Neuron* vol. 85 257–273 (2015).
210. Truban, D., Hou, X., Caulfield, T. R., Fiesel, F. C. & Springer, W. PINK1, Parkin, and Mitochondrial Quality Control: What can we Learn about Parkinson's Disease Pathobiology? *Journal of Parkinson's Disease* vol. 7 13–29 (2017).

211. Ge, P., Dawson, V. L. & Dawson, T. M. PINK1 and Parkin mitochondrial quality control: A source of regional vulnerability in Parkinson's disease. *Molecular Neurodegeneration* vol. 15 1–18 (2020).
212. Maruszczak, K. K., Jung, M., Rasool, S., Trempe, J. F. & Rapaport, D. The role of the individual TOM subunits in the association of PINK1 with depolarized mitochondria. *J Mol Med* **100**, 747–762 (2022).
213. Greene, A. W. *et al.* Mitochondrial processing peptidase regulates PINK1 processing, import and Parkin recruitment. *EMBO Rep* **13**, 378–385 (2012).
214. Spinazzi, M. & de Strooper, B. PARL: The mitochondrial rhomboid protease. *Seminars in Cell and Developmental Biology* vol. 60 19–28 (2016).
215. Yamano, K. & Youle, R. J. PINK1 is degraded through the N-end rule pathway. *Autophagy* **9**, 1758–1769 (2013).
216. Burman, J. L. *et al.* Mitochondrial fission facilitates the selective mitophagy of protein aggregates. *Journal of Cell Biology* **216**, 3231–3247 (2017).
217. Sekine, S. *et al.* Reciprocal Roles of Tom7 and OMA1 during Mitochondrial Import and Activation of PINK1. *Mol Cell* **73**, 1028-1043.e5 (2019).
218. Okatsu, K. *et al.* PINK1 autophosphorylation upon membrane potential dissipation is essential for Parkin recruitment to damaged mitochondria. *Nat Commun* **3**, 1–10 (2012).
219. Kane, L. A. *et al.* PINK1 phosphorylates ubiquitin to activate parkin E3 ubiquitin ligase activity. *Journal of Cell Biology* **205**, 143–153 (2014).
220. Shiba-Fukushima, K. *et al.* PINK1-mediated phosphorylation of the Parkin ubiquitin-like domain primes mitochondrial translocation of Parkin and regulates mitophagy. *Sci Rep* **2**, (2012).
221. Wauer, T. *et al.* Ubiquitin Ser65 phosphorylation affects ubiquitin structure, chain assembly and hydrolysis. *EMBO J* **34**, 307–325 (2015).
222. Ye, S. X. *et al.* Ubiquitin is double-phosphorylated by PINK1 for enhanced pH-sensitivity of conformational switch. *Protein and Cell* vol. 10 908–913 (2019).
223. Kazlauskaite, A. *et al.* Accelerated publication: Parkin is activated by PINK1-dependent phosphorylation of ubiquitin at Ser65. *Biochemical Journal* **460**, 127–139 (2014).
224. Kazlauskaite, A. *et al.* Binding to serine 65-phosphorylated ubiquitin primes Parkin for optimal PINK 1-dependent phosphorylation and activation . *EMBO Rep* **16**, 939–954 (2015).
225. Zhang, Y. *et al.* Parkin functions as an E2-dependent ubiquitin-protein ligase and promotes the degradation of the synaptic vesicle-associated protein, CDCrel-1. *Proc Natl Acad Sci U S A* **97**, 13354–13359 (2000).
226. Chaugule, V. K. *et al.* Autoregulation of Parkin activity through its ubiquitin-like domain. *EMBO Journal* **30**, 2853–2867 (2011).
227. McWilliams, T. G. *et al.* Phosphorylation of Parkin at serine 65 is essential for its activation in vivo. *Open Biol* **8**, (2018).
228. Callegari, S. *et al.* Phospho-ubiquitin-PARK2 complex as a marker for mitophagy defects. *Autophagy* **13**, 201–211 (2017).
229. Wauer, T., Simicek, M., Schubert, A. & Komander, D. Mechanism of phospho-ubiquitin-induced PARKIN activation. *Nature* **524**, 370–374 (2015).
230. Koyano, F., Yamano, K., Kosako, H., Tanaka, K. & Matsuda, N. Parkin recruitment to impaired mitochondria for nonselective ubiquitylation is facilitated by MITOL. *Journal of Biological Chemistry* **294**, 10300–10314 (2019).
231. Geisler, S. *et al.* PINK1/Parkin-mediated mitophagy is dependent on VDAC1 and p62/SQSTM1. *Nat Cell Biol* **12**, 119–131 (2010).
232. Tanaka, A. *et al.* Proteasome and p97 mediate mitophagy and degradation of mitofusins induced by Parkin. *Journal of Cell Biology* **191**, 1367–1380 (2010).
233. Meyer, H. & Weihl, C. C. The VCP/p97 system at a glance: Connecting cellular function to disease pathogenesis. *J Cell Sci* **127**, 3877–3883 (2014).

234. Ordureau, A. *et al.* Quantitative proteomics reveal a feedforward mechanism for mitochondrial PARKIN translocation and ubiquitin chain synthesis. *Mol Cell* **56**, 360–375 (2014).
235. Swatek, K. N. *et al.* Insights into ubiquitin chain architecture using Ub-clipping. *Nature* **572**, 533–537 (2019).
236. Ordureau, A. *et al.* Global Landscape and Dynamics of Parkin and USP30-Dependent Ubiquitylomes in iNeurons during Mitophagic Signaling. *Mol Cell* **77**, 1124-1142.e10 (2020).
237. Seibenhener, M. L. *et al.* Sequestosome 1/p62 Is a Polyubiquitin Chain Binding Protein Involved in Ubiquitin Proteasome Degradation. *Mol Cell Biol* **24**, 8055–8068 (2004).
238. Runwal, G. *et al.* LC3-positive structures are prominent in autophagy-deficient cells. *Sci Rep* **9**, 1–14 (2019).
239. Li, Y. *et al.* BNIP3L/NIX-mediated mitophagy: molecular mechanisms and implications for human disease. *Cell Death and Disease* vol. 13 1–11 (2022).
240. Rüb, C., Wilkening, A. & Voos, W. Mitochondrial quality control by the Pink1/Parkin system. *Cell and Tissue Research* vol. 367 111–123 (2017).
241. Morgenstern, M. *et al.* Quantitative high-confidence human mitochondrial proteome and its dynamics in cellular context. *Cell Metab* **33**, 2464-2483.e18 (2021).
242. Murphy, M. P. & Hartley, R. C. Mitochondria as a therapeutic target for common pathologies. *Nature Reviews Drug Discovery* vol. 17 865–886 (2018).
243. Meyers, D. E., Basha, H. I. & Koenig, M. K. Mitochondrial cardiomyopathy: Pathophysiology, diagnosis, and management. *Texas Heart Institute Journal* vol. 40 385–394 (2013).
244. Vafai, S. B. & Mootha, V. K. Mitochondrial disorders as windows into an ancient organelle. *Nature* vol. 491 374–383 (2012).
245. Weissig, V. Drug Development for the Therapy of Mitochondrial Diseases. *Trends in Molecular Medicine* vol. 26 40–57 (2020).
246. Goto, Y. I., Nonaka, I. & Horai, S. A mutation in the tRNALeu(UUR) gene associated with the MELAS subgroup of mitochondrial encephalomyopathies. *Nature* **348**, 651–653 (1990).
247. de Laat, P. *et al.* Three families with ‘de novo’ m.3243A > G mutation. *BBA Clin* **6**, 19–24 (2016).
248. Shoffner, J. M. *et al.* Myoclonic epilepsy and ragged-red fiber disease (MERRF) is associated with a mitochondrial DNA tRNALys mutation. *Cell* **61**, 931–937 (1990).
249. Karaa, A. & Goldstein, A. The spectrum of clinical presentation, diagnosis, and management of mitochondrial forms of diabetes. *Pediatric Diabetes* vol. 16 1–9 (2015).
250. Houshmand, M., Panahi, M. S., Hosseini, B., Dorraj, G. & Tabassi, A. Investigation on mtDNA deletions and twinkle gene mutation (G1423C) in Iranian patients with chronic progressive external opthalmoplagia. *Neurol India* **54**, 182–185 (2006).
251. Sundaram, C. *et al.* Contribution of muscle biopsy and genetics to the diagnosis of chronic progressive external opthalmoplegia of mitochondrial origin. *Journal of Clinical Neuroscience* **18**, 535–538 (2011).
252. Fassati, A. *et al.* Chronic progressive external ophthalmoplegia: A correlative study of quantitative molecular data and histochemical and biochemical profile. *J Neurol Sci* **123**, 140–146 (1994).
253. Viscomi, C. & Zeviani, M. MtDNA-maintenance defects: syndromes and genes. *J Inherit Metab Dis* **40**, 587–599 (2017).
254. Singh, K. K., Ayyasamy, V., Owens, K. M., Koul, M. S. & Vujcic, M. Mutations in mitochondrial DNA polymerase-γ promote breast tumorigenesis. *J Hum Genet* **54**, 516–524 (2009).
255. Lionaki, E. *et al.* Mitochondrial protein import determines lifespan through metabolic reprogramming and de novo serine biosynthesis. *Nat Commun* **13**, 1–16 (2022).

256. Lebleu, V. S. *et al.* PGC-1α mediates mitochondrial biogenesis and oxidative phosphorylation in cancer cells to promote metastasis. *Nat Cell Biol* **16**, 992–1003 (2014).
257. Trevisan, T. *et al.* Manipulation of Mitochondria Dynamics Reveals Separate Roles for Form and Function in Mitochondria Distribution. *Cell Rep* **23**, 1742–1753 (2018).
258. Bernhardt, D., Müller, M., Reichert, A. S. & Osiewacz, H. D. Simultaneous impairment of mitochondrial fission and fusion reduces mitophagy and shortens replicative lifespan. *Sci Rep* **5**, (2015).
259. Collier, T. J., Kanaan, N. M. & Kordower, J. H. Ageing as a primary risk factor for Parkinson's disease: Evidence from studies of non-human primates. *Nature Reviews Neuroscience* vol. 12 359–366 (2011).
260. Kasten, M. *et al.* Genotype-Phenotype Relations for the Parkinson's Disease Genes Parkin, PINK1, DJ1: MDSGene Systematic Review. *Movement Disorders* vol. 33 730–741 (2018).
261. Tyers, M. & Mann, M. From genomics to proteomics. *Nature* vol. 422 193–197 (2003).
262. Salzberg, S. L. Open questions: How many genes do we have? *BMC Biology* vol. 16 (2018).
263. Aebersold, R. *et al.* How many human proteoforms are there? *Nature Chemical Biology* vol. 14 206–214 (2018).
264. Ayoubi, T. A. & van de Ven, W. J. Regulation of gene expression by alternative promoters. *FASEB J* **10**, 453–60 (1996).
265. Ponomarenko, E. A. *et al.* The Size of the Human Proteome: The Width and Depth. *International Journal of Analytical Chemistry* vol. 2016 (2016).
266. Schaffer, L. v. *et al.* Identification and Quantification of Proteoforms by Mass Spectrometry. *Proteomics* vol. 19 e1800361 (2019).
267. Corthals, C. L., Wasinger, V. C., Hochstrasser, D. F. & Sanchez, J. C. The dynamic range of protein expression: A challenge for proteomic research. *Electrophoresis* vol. 21 1104–1115 (2000).
268. Angel, T. E. *et al.* Mass spectrometry-based proteomics: Existing capabilities and future directions. *Chem Soc Rev* **41**, 3912–3928 (2012).
269. Mendes, M. L. & Dittmar, G. Targeted proteomics on its way to discovery. *Proteomics* **22**, 2100330 (2022).
270. Moradian, A., Kalli, A., Sweredoski, M. J. & Hess, S. The top-down, middle-down, and bottom-up mass spectrometry approaches for characterization of histone variants and their post-translational modifications. *Proteomics* **14**, 489–497 (2014).
271. Vimer, S., Ben-Nissan, G. & Sharon, M. Mass Spectrometry Analysis of Intact Proteins from Crude Samples. *Analytical Chemistry* vol. 92 12741–12749 (2020).
272. Duong, V. A., Park, J. M. & Lee, H. Review of three-dimensional liquid chromatography platforms for bottom-up proteomics. *International Journal of Molecular Sciences* vol. 21 1524 (2020).
273. Yates, J. R. The revolution and evolution of shotgun proteomics for large-scale proteome analysis. *Journal of the American Chemical Society* vol. 135 1629–1640 (2013).
274. Steen, H. & Mann, M. The ABC's (and XYZ's) of peptide sequencing. *Nature Reviews Molecular Cell Biology* vol. 5 699–711 (2004).
275. Giansanti, P., Tsiatsiani, L., Low, T. Y. & Heck, A. J. R. Six alternative proteases for mass spectrometry-based proteomics beyond trypsin. *Nat Protoc* **11**, 993–1006 (2016).
276. Dau, T., Bartolomucci, G. & Rappsilber, J. Proteomics Using Protease Alternatives to Trypsin Benefits from Sequential Digestion with Trypsin. *Anal Chem* **92**, 9523–9527 (2020).
277. Cupp-Sutton, K. A. & Wu, S. High-throughput quantitative top-down proteomics. *Molecular Omics* vol. 16 91–99 (2020).
278. Henneman, A. & Palmblad, M. Retention time prediction and protein identification. in *Methods in Molecular Biology* vol. 2051 115–132 (Humana Press Inc., 2020).

279. Zhang, Y., Fonslow, B. R., Shan, B., Baek, M. C. & Yates, J. R. Protein analysis by shotgun/bottom-up proteomics. *Chemical Reviews* vol. 113 2343–2394 (2013).
280. Ramazi, S. & Zahiri, J. Post-translational modifications in proteins: resources, tools and prediction methods. *Database* **2021**, (2021).
281. Zecha, J. *et al.* Linking post-translational modifications and protein turnover by site-resolved protein turnover profiling. *Nat Commun* **13**, 1–14 (2022).
282. Loroch, S., Dickhut, C., Zahedi, R. P. & Sickmann, A. Phosphoproteomics-More than meets the eye. *Electrophoresis* **34**, 1483–1492 (2013).
283. Raju, T. S. Phosphorylation of Proteins. in *Co and Post-Translational Modifications of Therapeutic Antibodies and Proteins* 163–175 (John Wiley & Sons, Inc., 2019). doi:10.1002/9781119053354.ch13.
284. Spoel, S. H. Orchestrating the proteome with post-translational modifications. *J Exp Bot* **69**, 4499–4503 (2018).
285. Vasiljević, J., Torkko, J. M., Knoch, K. P. & Solimena, M. The making of insulin in health and disease. *Diabetologia* vol. 63 1981–1989 (2020).
286. Olzscha, H. Posttranslational modifications and proteinopathies: How guardians of the proteome are defeated. *Biological Chemistry* vol. 400 895–915 (2019).
287. Azevedo, C. & Saiardi, A. Why always lysine? The ongoing tale of one of the most modified amino acids. *Advances in Biological Regulation* vol. 60 144–150 (2016).
288. Bludau, I. *et al.* The structural context of posttranslational modifications at a proteome-wide scale. *PLoS Biol* **20**, e3001636 (2022).
289. Leutert, M., Entwisle, S. W. & Villén, J. Decoding post-translational modification crosstalk with proteomics. *Molecular and Cellular Proteomics* vol. 20 (2021).
290. Ohtake, F. *et al.* Ubiquitin acetylation inhibits polyubiquitin chain elongation. *EMBO Rep* **16**, 192–201 (2015).
291. Casado, P. *et al.* Kinase-substrate enrichment analysis provides insights into the heterogeneity of signaling pathway activation in leukemia cells. *Science Signaling* vol. 6 (2013).
292. Ardito, F., Giuliani, M., Perrone, D., Troiano, G. & Muzio, L. lo. The crucial role of protein phosphorylation in cell signalingand its use as targeted therapy (Review). *International Journal of Molecular Medicine* vol. 40 271–280 (2017).
293. Lapek, J. D., Tombline, G., Kellersberger, K. A., Friedman, M. R. & Friedman, A. E. Evidence of histidine and aspartic acid phosphorylation in human prostate cancer cells. *Naunyn Schmiedebergs Arch Pharmacol* **388**, 161–173 (2015).
294. Buchowiecka, A. K. Puzzling over protein cysteine phosphorylation-assessment of proteomic tools for s-phosphorylation profiling. *Analyst* **139**, 4118–4123 (2014).
295. Olsen, J. v. *et al.* Global, In Vivo, and Site-Specific Phosphorylation Dynamics in Signaling Networks. *Cell* **127**, 635–648 (2006).
296. Xu, X. *et al.* Phosphorylation-Mediated IFN-γR2 Membrane Translocation Is Required to Activate Macrophage Innate Response. *Cell* **175**, 1336-1351.e17 (2018).
297. Swaffer, M. P., Jones, A. W., Flynn, H. R., Snijders, A. P. & Nurse, P. CDK Substrate Phosphorylation and Ordering the Cell Cycle. *Cell* **167**, 1750-1761.e16 (2016).
298. Niemi, N. M. & Mackeigan, J. P. Mitochondrial phosphorylation in apoptosis: Flipping the death switch. *Antioxidants and Redox Signaling* vol. 19 572–582 4982 (2013).
299. Humphrey, S. J., James, D. E. & Mann, M. Protein Phosphorylation: A Major Switch Mechanism for Metabolic Regulation. *Trends in Endocrinology and Metabolism* vol. 26 676–687 (2015).
300. Vlastaridis, P. *et al.* The pivotal role of protein phosphorylation in the control of yeast central metabolism. *G3: Genes, Genomes, Genetics* **7**, 1239–1249 (2017).
301. Hardwick, L. J. A., Azzarelli, R. & Philpott, A. Cell cycle-dependent phosphorylation and regulation of cellular differentiation. *Biochem Soc Trans* **46**, 1083–1091 (2018).
302. Lim Kam Sian, T. C. C., Chüeh, A. C. & Daly, R. J. Proteomics-based interrogation of the kinome and its implications for precision oncology. *Proteomics* **21**, 2000161 (2021).

303. Attwood, M. M., Fabbro, D., Sokolov, A. v., Knapp, S. & Schiöth, H. B. Trends in kinase drug discovery: targets, indications and inhibitor design. *Nature Reviews Drug Discovery* vol. 20 839–861 (2021).
304. Mok, J. *et al.* Deciphering protein kinase specificity through large-scale analysis of yeast phosphorylation site motifs. *Sci Signal* **3**, ra12 (2010).
305. Cole, S. & Prabakaran, S. PhosphoEffect: Prioritizing Variants On or Adjacent to Phosphorylation Sites through Their Effect on Kinase Recognition Motifs. *iScience* **23**, 101321 (2020).
306. Hoermann, B. *et al.* Dissecting the sequence determinants for dephosphorylation by the catalytic subunits of phosphatases PP1 and PP2A. *Nat Commun* **11**, 1–20 (2020).
307. Sugiyama, N., Imamura, H. & Ishihama, Y. Large-scale Discovery of Substrates of the Human Kinome. *Sci Rep* **9**, 1–12 (2019).
308. Pickart, C. M. & Eddins, M. J. Ubiquitin: Structures, functions, mechanisms. *Biochimica et Biophysica Acta - Molecular Cell Research* vol. 1695 55–72 (2004).
309. Ohtake, F. & Tsuchiya, H. The emerging complexity of ubiquitin architecture. *J Biochem* **161**, mvw088 (2016).
310. Mevissen, T. E. T. & Komander, D. Mechanisms of deubiquitinase specificity and regulation. *Annual Review of Biochemistry* vol. 86 159–192 (2017).
311. Schulman, B. A. & Wade Harper, J. Ubiquitin-like protein activation by E1 enzymes: The apex for downstream signalling pathways. *Nature Reviews Molecular Cell Biology* vol. 10 319–331 (2009).
312. Yang, Q., Zhao, J., Chen, D. & Wang, Y. E3 ubiquitin ligases: styles, structures and functions. *Molecular Biomedicine* vol. 2 (2021).
313. Ebner, P., Versteeg, G. A. & Ikeda, F. Ubiquitin enzymes in the regulation of immune responses. *Crit Rev Biochem Mol Biol* **52**, 425–460 (2017).
314. Wijk, S. J. L. & Timmers, H. T. M. The family of ubiquitin-conjugating enzymes (E2s): deciding between life and death of proteins. *The FASEB Journal* **24**, 981–993 (2010).
315. Akimov, V. *et al.* Ubisite approach for comprehensive mapping of lysine and n-terminal ubiquitination sites. *Nat Struct Mol Biol* **25**, 631–640 (2018).
316. Deol, K. K., Lorenz, S. & Strieter, E. R. Enzymatic Logic of Ubiquitin Chain Assembly. *Frontiers in Physiology* vol. 10 (2019).
317. Wang, Y. & Wang, F. Post-Translational Modifications of Deubiquitinating Enzymes: Expanding the Ubiquitin Code. *Frontiers in Pharmacology* vol. 12 (2021).
318. Komander, D. & Rape, M. The ubiquitin code. *Annu Rev Biochem* **81**, 203–229 (2012).
319. Akutsu, M., Dikic, I. & Bremm, A. Ubiquitin chain diversity at a glance. *J Cell Sci* **129**, 875–880 (2016).
320. Teixeira, L. K. & Reed, S. I. Ubiquitin ligases and cell cycle control. *Annu Rev Biochem* **82**, 387–414 (2013).
321. Cockram, P. E. *et al.* Ubiquitination in the regulation of inflammatory cell death and cancer. *Cell Death and Differentiation* vol. 28 591–605 (2021).
322. Hu, H. & Sun, S. C. Ubiquitin signaling in immune responses. *Cell Research* vol. 26 457–483 (2016).
323. Zhou, S. *et al.* Role of H2B mono-ubiquitination in the initiation and progression of cancer. *Bulletin du Cancer* vol. 108 385–398 (2021).
324. Jacobson, A. D. *et al.* The lysine 48 and lysine 63 ubiquitin conjugates are processed differently by the 26 S proteasome. *Journal of Biological Chemistry* **284**, 35485–35494 (2009).
325. Liu, P. *et al.* K63-linked polyubiquitin chains bind to DNA to facilitate DNA damage repair. *Sci Signal* **11**, (2018).
326. Y, W., S, H., P, X. & Y, L. [Progress in atypical ubiquitination via K6-linkages]. *Sheng Wu Gong Cheng Xue Bao* **38**, (2022).
327. Fulda, S., Rajalingam, K. & Dikic, I. Ubiquitylation in immune disorders and cancer: From molecular mechanisms to therapeutic implications. *EMBO Molecular Medicine* vol. 4 545–556 (2012).

328. Gray, M. W. Mosaic nature of the mitochondrial proteome: Implications for the origin and evolution of mitochondria. *Proc Natl Acad Sci U S A* **112**, 10133–10138 (2015).
329. Gabaldón, T. & Huynen, M. A. From Endosymbiont to Host-Controlled Organelle: The Hijacking of Mitochondrial Protein Synthesis and Metabolism. *PLoS Comput Biol* **3**, e219 (2007).
330. Rabilloud, T. *et al.* Two-dimensional electrophoresis of human placenta mitochondria and protein identification by mass spectrometry: Toward a human mitochondrial proteome. *Electrophoresis* **19**, 1006–1014 (1998).
331. Calvo, S. E., Clauser, K. R. & Mootha, V. K. MitoCarta2.0: An updated inventory of mammalian mitochondrial proteins. *Nucleic Acids Res* **44**, D1251–D1257 (2016).
332. Mootha, V. K. *et al.* Integrated Analysis of Protein Composition, Tissue Diversity, and Gene Regulation in Mouse Mitochondria. *Cell* **115**, 629–640 (2003).
333. Rath, S. *et al.* MitoCarta3.0: An updated mitochondrial proteome now with sub-organelle localization and pathway annotations. *Nucleic Acids Res* **49**, D1541–D1547 (2021).
334. Habel, J. E. Biotin Proximity Labeling for Protein–Protein Interaction Discovery: The BioID Method. in *Methods in Molecular Biology* vol. 2261 357–379 (Humana Press Inc., 2021).
335. Antonicka, H. *et al.* A High-Density Human Mitochondrial Proximity Interaction Network. *Cell Metab* **32**, 479-497.e9 (2020).
336. Rensvold, J. W. *et al.* Defining mitochondrial protein functions through deep multiomic profiling. *Nature* **606**, 382–388 (2022).
337. Schäfer, J. A., Bozkurt, S., Michaelis, J. B., Klann, K. & Münch, C. Global mitochondrial protein import proteomics reveal distinct regulation by translation and translocation machinery. *Mol Cell* **82**, 435-446.e7 (2022).
338. Morgenstern, M. *et al.* Definition of a High-Confidence Mitochondrial Proteome at Quantitative Scale. *Cell Rep* **19**, 2836–2852 (2017).
339. Fukasawa, Y. *et al.* MitoFates: Improved prediction of mitochondrial targeting sequences and their cleavage sites. *Molecular and Cellular Proteomics* **14**, 1113–1126 (2015).
340. Savojardo, C., Martelli, P. L. uigi, Fariselli, P. & Casadio, R. TPpred2: improving the prediction of mitochondrial targeting peptide cleavage sites by exploiting sequence motifs. *Bioinformatics* **30**, 2973–2974 (2014).
341. Savojardo, C., Bruciaferri, N., Tartari, G., Martelli, P. L. & Casadio, R. DeepMito: Accurate prediction of protein sub-mitochondrial localization using convolutional neural networks. *Bioinformatics* **36**, 56–64 (2020).
342. Kumar, R., Kumari, B. & Kumar, M. Proteome-wide prediction and annotation of mitochondrial and sub-mitochondrial proteins by incorporating domain information. *Mitochondrion* **42**, 11–22 (2018).
343. Neagu, A. N. *et al.* Applications of Tandem Mass Spectrometry (MS/MS) in Protein Analysis for Biomedical Research. *Molecules* vol. 27 (2022).
344. Pitt, J. J. Principles and applications of liquid chromatography-mass spectrometry in clinical biochemistry. *Clin Biochem Rev* **30**, 19–34 (2009).
345. Kim, M. S. *et al.* A draft map of the human proteome. *Nature* **509**, 575–581 (2014).
346. Thakur, S. S. *et al.* Deep and highly sensitive proteome coverage by LC-MS/MS without prefractionation. *Molecular and Cellular Proteomics* **10**, (2011).
347. Ganesh, V., Poorna Basuri, P., Sahini, K. & Nalini, C. N. Retention behaviour of analytes in reversed-phase high-performance liquid chromatography—A review. *Biomedical Chromatography* e5482 (2022) doi:10.1002/bmc.5482.
348. Baczek, T. & Kaliszan, R. Predictions of peptides' retention times in reversed-phase liquid chromatography as a new supportive tool to improve protein identification in proteomics. *Proteomics* vol. 9 835–847 (2009).
349. Aguilar, M. I. HPLC of peptides and proteins: basic theory and methodology. *Methods Mol Biol* **251**, 3–8 (2004).

350. Wang, N. H., Lee, W. L. & Her, G. R. Signal enhancement for peptide analysis in liquid chromatography- electrospray ionization mass spectrometry with trifluoroacetic acid containing mobile phase by postcolumn electrophoretic mobility control. *Anal Chem* **83**, 6163–6168 (2011).
351. Wilson, S. R., Vehus, T., Berg, H. S. & Lundanes, E. Nano-LC in proteomics: Recent advances and approaches. *Bioanalysis* vol. 7 1799–1815 (2015).
352. Kuster, B. *et al.* Robust microflow LC-MS/MS for proteome analysis: 38 000 runs and counting. *Anal Chem* **93**, 3686–3690 (2021).
353. Bouwmeester, R., Gabriels, R., Hulstaert, N., Martens, L. & Degroeve, S. DeepLC can predict retention times for peptides that carry as-yet unseen modifications. *Nat Methods* **18**, 1363–1369 (2021).
354. Moruz, L. *et al.* Chromatographic retention time prediction for posttranslationally modified peptides. *Proteomics* **12**, 1151–1159 (2012).
355. Noor, Z., Ahn, S. B., Baker, M. S., Ranganathan, S. & Mohamedali, A. Mass spectrometry–based protein identification in proteomics—a review. *Brief Bioinform* **22**, 1620–1638 (2021).
356. Zhang, X. *et al.* Multi-dimensional liquid chromatography in proteomics-A review. *Analytica Chimica Acta* vol. 664 101–113 (2010).
357. Yates, J. R., Ruse, C. I. & Nakorchevsky, A. Proteomics by mass spectrometry: Approaches, advances, and applications. *Annual Review of Biomedical Engineering* vol. 11 49–79 (2009).
358. Batth, T. S., Francavilla, C. & Olsen, J. v. Off-line high-pH reversed-phase fractionation for in-depth phosphoproteomics. *J Proteome Res* **13**, 6176–6186 (2014).
359. Arevalo, R., Ni, Z. & Danell, R. M. Mass spectrometry and planetary exploration: A brief review and future projection. *Journal of Mass Spectrometry* **55**, e4454 (2020).
360. Kelstrup, C. D. *et al.* Performance Evaluation of the Q Exactive HF-X for Shotgun Proteomics. *J Proteome Res* **17**, 727–738 (2018).
361. El-Aneed, A., Cohen, A. & Banoub, J. Mass spectrometry, review of the basics: Electrospray, MALDI, and commonly used mass analyzers. *Applied Spectroscopy Reviews* vol. 44 210–230 (2009).
362. Wilm, M. Principles of electrospray ionization. *Molecular and Cellular Proteomics* vol. 10 (2011).
363. Ho, C. S. *et al.* Electrospray ionisation mass spectrometry: principles and clinical applications. *Clin Biochem Rev* **24**, 3–12 (2003).
364. Yamashita, M. & Fenn, J. B. Electrospray ion source. Another variation on the free-jet theme. *Journal of Physical Chemistry* **88**, 4451–4459 (1984).
365. Konermann, L., Metwally, H., Duez, Q. & Peters, I. Charging and supercharging of proteins for mass spectrometry: Recent insights into the mechanisms of electrospray ionization. *Analyst* vol. 144 6157–6171 (2019).
366. Nguyen, J. M., Smith, J., Rzewuski, S., Legido-Quigley, C. & Lauber, M. A. High sensitivity LC-MS profiling of antibody-drug conjugates with difluoroacetic acid ion pairing. *MAbs* **11**, 1358–1366 (2019).
367. Banerjee, S. & Mazumdar, S. Electrospray Ionization Mass Spectrometry: A Technique to Access the Information beyond the Molecular Weight of the Analyte. *Int J Anal Chem* **2012**, 1–40 (2012).
368. Sun, W., Wu, S., Wang, X., Zheng, D. & Gao, Y. A systematical analysis of tryptic peptide identification with reverse phase liquid chromatography and electrospray ion trap mass spectrometry. *Genomics, proteomics & bioinformatics / Beijing Genomics Institute* **2**, 174–183 (2004).
369. Keller, C. *et al.* Comparison of Vacuum MALDI and AP-MALDI Platforms for the Mass Spectrometry Imaging of Metabolites Involved in Salt Stress in Medicago truncatula. *Front Plant Sci* **9**, 1238 (2018).
370. Glish, G. L. & Vachet, R. W. The basics of mass spectrometry in the twenty-first century. *Nature Reviews Drug Discovery* vol. 2 140–150 (2003).

371. Pelander, A., Decker, P., Baessmann, C. & Ojanperä, I. Evaluation of a high resolving power time-of-flight mass spectrometer for drug analysis in terms of resolving power and acquisition rate. *J Am Soc Mass Spectrom* **22**, 379–385 (2011).
372. Li, C. *et al.* Towards Higher Sensitivity of Mass Spectrometry: A Perspective From the Mass Analyzers. *Frontiers in Chemistry* vol. 9 1148 (2021).
373. Cunsolo, V., Muccilli, V., Saletti, R. & Foti, S. Mass spectrometry in food proteomics: a tutorial. *Journal of Mass Spectrometry* **49**, 768–784 (2014).
374. Zubarev, R. A. & Makarov, A. Orbitrap mass spectrometry. *Anal Chem* **85**, 5288–5296 (2013).
375. Perry, R. H., Cooks, R. G. & Noll, R. J. Orbitrap mass spectrometry: Instrumentation, ion motion and applications. *Mass Spectrom Rev* **27**, 661–699 (2008).
376. Singhal, N., Kumar, M., Kanaujia, P. K. & Virdi, J. S. MALDI-TOF mass spectrometry: An emerging technology for microbial identification and diagnosis. *Frontiers in Microbiology* vol. 6 (2015).
377. Niessen, W. M. A. & Falck, D. Introduction to Mass Spectrometry, a Tutorial. in *Analyzing Biomolecular Interactions by Mass Spectrometry* 1–54 (Wiley-VCH Verlag GmbH & Co. KGaA, 2015). doi:10.1002/9783527673391.ch1.
378. Glish, G. L. & Burinsky, D. J. Hybrid Mass Spectrometers for Tandem Mass Spectrometry. *J Am Soc Mass Spectrom* **19**, 161–172 (2008).
379. Neilson, K. A. *et al.* Less label, more free: Approaches in label-free quantitative mass spectrometry. *Proteomics* **11**, 535–553 (2011).
380. Goldfarb, D., Wang, W. & Major, M. B. MSAcquisitionSimulator: Data-dependent acquisition simulator for LC-MS shotgun proteomics. *Bioinformatics* **32**, 1269–1271 (2016).
381. Bateman, N. W. *et al.* Maximizing peptide identification events in proteomic workflows using data-dependent acquisition (DDA). *Molecular and Cellular Proteomics* **13**, 329–338 (2014).
382. Matafora, V. & Bachi, A. Missing Value Monitoring to Address Missing Values in Quantitative Proteomics. in *Methods in Molecular Biology* vol. 2228 401–408 (Humana Press Inc., 2021).
383. Li, K. W., Gonzalez-Lozano, M. A., Koopmans, F. & Smit, A. B. Recent Developments in Data Independent Acquisition (DIA) Mass Spectrometry: Application of Quantitative Analysis of the Brain Proteome. *Front Mol Neurosci* **13**, 248 (2020).
384. Gupta, S., Ahadi, S., Zhou, W. & Röst, H. DIAlignR provides precise retention time alignment across distant runs in DIA and targeted proteomics. *Molecular and Cellular Proteomics* **18**, 806–817 (2019).
385. Pino, L. K. *et al.* The Skyline ecosystem: Informatics for quantitative mass spectrometry proteomics. *Mass Spectrometry Reviews* vol. 39 229–244 (2020).
386. Bruderer, R. *et al.* Optimization of experimental parameters in data-independent mass spectrometry significantly increases depth and reproducibility of results. *Molecular and Cellular Proteomics* **16**, 2296–2309 (2017).
387. Röst, H. L., Aebersold, R. & Schubert, O. T. Automated swath data analysis using targeted extraction of ion chromatograms. in *Methods in Molecular Biology* vol. 1550 289–307 (Humana Press Inc., 2017).
388. Chen, C., Hou, J., Tanner, J. J. & Cheng, J. Bioinformatics methods for mass spectrometry-based proteomics data analysis. *International Journal of Molecular Sciences* vol. 21 (2020).
389. Prieto, G. & Vázquez, J. Protein Probability Model for High-Throughput Protein Identification by Mass Spectrometry-Based Proteomics. *J Proteome Res* **19**, 1285–1297 (2020).
390. Tyanova, S., Temu, T. & Cox, J. The MaxQuant computational platform for mass spectrometry-based shotgun proteomics. *Nat Protoc* **11**, 2301–2319 (2016).
391. Perkins, D. N., Pappin, D. J. C., Creasy, D. M. & Cottrell, J. S. Probability-based protein identification by searching sequence databases using mass spectrometry data. in *Electrophoresis* vol. 20 3551–3567 (Wiley-VCH Verlag, 1999).

392. Brodbelt, J. S. & Russell, D. H. Focus on the 20-Year Anniversary of SEQUEST. *Journal of the American Society for Mass Spectrometry* vol. 26 1797–1798 (2015).
393. Parker, C. E., Mocanu, V., Mocanu, M., Dicheva, N. & Warren, M. R. Mass spectrometry for post-translational modifications. in *Neuroproteomics* 93–113 (CRC Press, 2009). doi:10.1201/9781420076264.ch6.
394. Virág, D. *et al.* Current Trends in the Analysis of Post-translational Modifications. *Chromatographia* vol. 83 1–10 (2020).
395. Marmelstein, A. M., Moreno, J. & Fiedler, D. Chemical Approaches to Studying Labile Amino Acid Phosphorylation. *Topics in Current Chemistry* vol. 375 (2017).
396. Tsai, C. F. *et al.* Mass Spectrometry-Based Proteomics for Analysis of Hydrophilic Phosphopeptides. in *Methods in Molecular Biology* vol. 2259 247–257 (Humana Press Inc., 2021).
397. Thingholm, T. E. & Larsen, M. R. Phosphopeptide Enrichment by Immobilized Metal Affinity Chromatography. in 123–133 (Springer, New York, NY, 2016). doi:10.1007/978-1-4939-3049-4_8.
398. Fulzele, A. & Bennett, E. J. Ubiquitin diGLY proteomics as an approach to identify and quantify the ubiquitin-modified proteome. in *Methods in Molecular Biology* vol. 1844 363–384 (Humana Press Inc., 2018).
399. Nielsen, M. L. *et al.* Iodoacetamide-induced artifact mimics ubiquitination in mass spectrometry. *Nature Methods* vol. 5 459–460 (2008).
400. Lehmann, W. D. *et al.* Neutral loss-based phosphopeptide recognition: A collection of caveats. *J Proteome Res* **6**, 2866–2873 (2007).
401. Ulintz, P. J. *et al.* Comparison of MS 2-Only, MSA, and MS 2/MS 3 methodologies for phosphopeptide identification. *J Proteome Res* **8**, 887–899 (2009).
402. Potel, C. M., Lemeer, S. & Heck, A. J. R. Phosphopeptide Fragmentation and Site Localization by Mass Spectrometry: An Update. *Analytical Chemistry* vol. 91 126–141 (2019).
403. Parker, C. E., Warren, M. R. E., Mocanu, V., Greer, S. F. & Borchers, C. H. Mass Spectrometric Determination of Protein Ubiquitination. in *Post-translational Modifi cations of Proteins* 109–130 (Humana Press, 2008). doi:10.1007/978-1-60327-084-7_8.
404. Schubert, O. T., Röst, H. L., Collins, B. C., Rosenberger, G. & Aebersold, R. Quantitative proteomics: Challenges and opportunities in basic and applied research. *Nature Protocols* vol. 12 1289–1294 (2017).
405. Bantscheff, M., Schirle, M., Sweetman, G., Rick, J. & Kuster, B. Quantitative mass spectrometry in proteomics: A critical review. *Anal Bioanal Chem* **389**, 1017–1031 (2007).
406. Gerber, S. A., Rush, J., Stemman, O., Kirschner, M. W. & Gygi, S. P. Absolute quantification of proteins and phosphoproteins from cell lysates by tandem MS. *Proc Natl Acad Sci U S A* **100**, 6940–6945 (2003).
407. Schmidt, C., Lenz, C., Grote, M., Lührmann, R. & Urlaub, H. Determination of protein stoichiometry within protein complexes using absolute quantification and multiple reaction monitoring. *Anal Chem* **82**, 2784–2796 (2010).
408. Becker, E. *et al.* AQUA Mutant Protein Quantification of Endomyocardial Biopsy-Sized Samples From a Patient With Hypertrophic Cardiomyopathy. *Front Cardiovasc Med* **9**, (2022).
409. Vasilogianni, A. M. *et al.* Proteomic quantification of perturbation to pharmacokinetic target proteins in liver disease. *J Proteomics* **263**, 104601 (2022).
410. Schwanhäusser, B. *et al.* Global quantification of mammalian gene expression control. *Nature* **473**, 337–342 (2011).
411. Zhao, L. *et al.* Comparative evaluation of label-free quantification strategies. *J Proteomics* **215**, 103669 (2020).
412. Mann, M. Functional and quantitative proteomics using SILAC. *Nature Reviews Molecular Cell Biology* vol. 7 952–958 (2006).

413. Ong, S.-E. & Mann, M. Stable Isotope Labeling by Amino Acids in Cell Culture for Quantitative Proteomics. in 37–52 (Humana Press, 2007). doi:10.1007/978-1-59745-255-7_3.
414. Tzouros, M. *et al.* Development of a 5-plex SILAC Method tuned for the quantitation of tyrosine phosphorylation dynamics. *Molecular and Cellular Proteomics* **12**, 3339–3349 (2013).
415. Han, J. *et al.* Improved SILAC method for double labeling of bacterial proteome. *J Proteomics* **194**, 89–98 (2019).
416. Schütz, W., Hausmann, N., Krug, K., Hampp, R. & Macek, B. Extending SILAC to proteomics of plant cell lines. *Plant Cell* **23**, 1701–1705 (2011).
417. Krüger, M. *et al.* SILAC Mouse for Quantitative Proteomics Uncovers Kindlin-3 as an Essential Factor for Red Blood Cell Function. *Cell* **134**, 353–364 (2008).
418. Sury, M. D., Chen, J. X. & Selbach, M. The SILAC fly allows for accurate protein quantification in vivo. *Molecular and Cellular Proteomics* **9**, 2173–2183 (2010).
419. Ross, A. B., Langer, J. D. & Jovanovic, M. Proteome turnover in the spotlight: Approaches, applications, and perspectives. *Molecular and Cellular Proteomics* vol. 20 (2021).
420. Gevaert, K. *et al.* Stable isotopic labeling in proteomics. *Proteomics* vol. 8 4873–4885 (2008).
421. Castillo, M. J., Reynolds, K. J., Gomes, A., Fenselau, C. & Yao, X. Quantitative protein analysis using enzymatic [18O]water labeling. *Curr Protoc Protein Sci* **76**, (2014).
422. Boersema, P. J., Raijmakers, R., Lemeer, S., Mohammed, S. & Heck, A. J. R. Multiplex peptide stable isotope dimethyl labeling for quantitative proteomics. *Nat Protoc* **4**, 484–494 (2009).
423. Hsu, J. L. & Chen, S. H. Stable isotope dimethyl labelling for quantitative proteomics and beyond. *Philosophical Transactions of the Royal Society A: Mathematical, Physical and Engineering Sciences* vol. 374 (2016).
424. Rauniyar, N. & Yates, J. R. Isobaric labeling-based relative quantification in shotgun proteomics. *Journal of Proteome Research* vol. 13 5293–5309 (2014).
425. Hutchinson-Bunch, C. *et al.* Assessment of TMT Labeling Efficiency in Large-Scale Quantitative Proteomics: The Critical Effect of Sample pH. *ACS Omega* **6**, 12660–12666 (2021).
426. McAlister, G. C. *et al.* Increasing the multiplexing capacity of TMTs using reporter ion isotopologues with isobaric masses. *Anal Chem* **84**, 7469–7478 (2012).
427. Li, J. *et al.* TMTpro-18plex: The Expanded and Complete Set of TMTpro Reagents for Sample Multiplexing. *J Proteome Res* **20**, 2964–2972 (2021).
428. Bachor, R., Waliczek, M., Stefanowicz, P. & Szewczuk, Z. Trends in the design of new isobaric labeling reagents for quantitative proteomics. *Molecules* **24**, (2019).
429. Miller, S. & Muqit, M. M. K. Therapeutic approaches to enhance PINK1/Parkin mediated mitophagy for the treatment of Parkinson's disease. *Neuroscience Letters* vol. 705 7–13 (2019).
430. Liao, P. C., Bergamini, C., Fato, R., Pon, L. A. & Pallotti, F. Isolation of mitochondria from cells and tissues. in *Methods in Cell Biology* vol. 155 3–31 (Academic Press Inc., 2020).
431. Desai, R. *et al.* Mitochondria form contact sites with the nucleus to couple prosurvival retrograde response. *Sci Adv* **6**, (2020).
432. Udeshi, N. D. *et al.* Rapid and deep-scale ubiquitylation profiling for biology and translational research. *Nat Commun* **11**, 1–11 (2020).
433. Schmitt, M. *et al.* Quantitative proteomics links the intermediate filament nestin to resistance to targeted BRAF inhibition in melanoma cells. *Molecular and Cellular Proteomics* **18**, 1096–1109 (2019).
434. Zecha, J. *et al.* TMT labeling for the masses: A robust and cost-efficient, in-solution labeling approach. *Molecular and Cellular Proteomics* **18**, 1468–1478 (2019).

435. Narendra, D., Tanaka, A., Suen, D. F. & Youle, R. J. Parkin is recruited selectively to impaired mitochondria and promotes their autophagy. *Journal of Cell Biology* **183**, 795–803 (2008).
436. Geisler, S. *et al.* Ubiquitin-specific protease USP36 knockdown impairs Parkin-dependent mitophagy via downregulation of Beclin-1-associated autophagy-related ATG14L. *Exp Cell Res* **384**, 111641 (2019).
437. Liberti, M. v. & Locasale, J. W. The Warburg Effect: How Does it Benefit Cancer Cells? *Trends in Biochemical Sciences* vol. 41 211–218 (2016).
438. Jin, S. M. *et al.* Mitochondrial membrane potential regulates PINK1 import and proteolytic destabilization by PARL. *Journal of Cell Biology* **191**, 933–942 (2010).
439. Iguchi, M. *et al.* Parkin-catalyzed ubiquitin-ester transfer is triggered by PINK1-dependent phosphorylation. *Journal of Biological Chemistry* **288**, 22019–22032 (2013).
440. Bateman, A. *et al.* UniProt: the universal protein knowledgebase in 2021. *Nucleic Acids Res* **49**, D480–D489 (2021).
441. McWilliams, T. G. & Muqit, M. M. PINK1 and Parkin: emerging themes in mitochondrial homeostasis. *Current Opinion in Cell Biology* vol. 45 83–91 (2017).
442. Mosen, P., Sanner, A., Singh, J. & Winter, D. Targeted quantification of the lysosomal proteome in complex samples. *Proteomes* **9**, 1–17 (2021).
443. Sharma, K. *et al.* Ultradeep Human Phosphoproteome Reveals a Distinct Regulatory Nature of Tyr and Ser/Thr-Based Signaling. *Cell Rep* **8**, 1583–1594 (2014).
444. Lv, B. F. *et al.* Protein tyrosine phosphatase interacting protein 51 (PTPIP51) is a novel mitochondria protein with an N-terminal mitochondrial targeting sequence and induces apoptosis. *Apoptosis* **11**, 1489–1501 (2006).
445. Wanderoy, S., Tabitha Hees, J., Klesse, R., Edlich, F. & Harbauer, A. B. Kill one or kill the many: Interplay between mitophagy and apoptosis. *Biological Chemistry* vol. 402 73–88 (2020).
446. Gegg, M. E. & Schapira, A. H. V. PINK1-parkin-dependent mitophagy involves ubiquitination of mitofusins 1 and 2: Implications for Parkinson disease pathogenesis. *Autophagy* vol. 7 243–245 (2011).
447. Gegg, M. E. *et al.* Mitofusin 1 and mitofusin 2 are ubiquitinated in a PINK1/parkin-dependent manner upon induction of mitophagy. *Hum Mol Genet* **19**, 4861–4870 (2010).
448. Krämer, L., Groh, C. & Herrmann, J. M. The proteasome: friend and foe of mitochondrial biogenesis. *FEBS Lett* **595**, 1223–1238 (2021).
449. Wright, G., Terada, K., Yan, M., Sergeev, I. & Mori, M. Oxidative stress inhibits the mitochondrial import of preproteins and leads to their degradation. *Exp Cell Res* **263**, 107–117 (2001).
450. Sulkshane, P. *et al.* Inhibition of proteasome reveals basal mitochondrial ubiquitination. *J Proteomics* **229**, 103949 (2020).
451. Bogenhagen, D. F., Ostermeyer-Fay, A. G., Haley, J. D. & Garcia-Diaz, M. Kinetics and Mechanism of Mammalian Mitochondrial Ribosome Assembly. *Cell Rep* **22**, 1935–1944 (2018).

7. Abbreviations

abbrevation	explanation
aac1/2/3/4	arylamine N-acetyltransferase 1/2/3/4
ACAD	acyl-CoA dehydrogenase
ACP	acyl-carrier protein
ADP	adenosin diphosphate
AMKPK	5' adenosine monophosphate-activated protein kinase
AMP	adenosin monophosphate
APAF1	apoptotic protease activating factor 1
API	atmospheric pressure ionization
AQUA	absolute quantification
ARPD	autosomal recessive Parkinsons Disease
ATP	adenosin triphosphat
AYR1	acyl-dihydroxyacetone phosphate reductase
BCL2	b-cell lymphoma 2
BioID	biotin identification
BNIP3	BCL2/adenovirus E1B 19 kDa protein-interacting protein 3
CAA	chloracetamide
CCCP	2-[2-(3-Chlorophenyl)hydrazinylyidene]propanedinitrile
cGAS-STING	cyclic GMP-AMP Synthase - Stimulator of Interferon Genes
CID	collision-induced dissociation
CL	cardiolipin
CMT2A	Charcot-Marie-Tooth type 2a
COX	cytochrome c oxidase
CPEO	chronic progressive external ophthalmoplegia
CRISPR	clustered regularly interspaced short palindromic repeats
DDA	data dependent acquisition
DIA	data indpendent acquisition
DNA	desoxribonucleic acid
DRP1	dynamin-1-like protein
DUB	deubiquitinating enzyme
DYN2	dynamin2
ECH	2-enoyl-CoA hydratase
EGT	endosymbiotic gene transfer
ER	endoplasmatic reticulum
ERMES	ER-mitochondria encounter structure
ESI	electrospray ionization
ESRRA	estrogen related receptor alpha
ETC	electron transport chain
ETD	electron transfer dissociation
$FAD/FADH_2$	oxidized/reduced flavin adenine dinucleotide
FDR	false discovery rate
Fe-S	iron-sulfur cluster
Fis1	fission protein 1, mitochondrial
FTICR	fourier-transform ion cyclotron resonance mass spectrometry

FUNDC1	FUN14 domain containing 1
GSH	glutathion
h2o2	hydrogen peroxide
HAD	3-hydroxy-CoA dehydrogenase
HECT	homologous to the E6-AP carboxyl terminus
HPLC	high performance liquid chromatography
HSP	heat-shock protein
IAA	iodoacetamide
iBAQ	intensity based absolute qunatification
IBM	inner boundary membrane
IFN β	interferon beta
IMAC	Immobilized metal affinity chromatography
IMM	inner mitochondrial membrane
IMS	inner membrane space
ISA	iron-sulfur assembly protein 1
ISC	iron-sulfur cluster protein
iTRAQ	isobaric tags for relative and absolute quantification
KSS	Kearns–Sayre syndrome
KT	3-ketothiolase
LC	liquid chromatography
LC3	protein light chain 3
LECA	last eucaryotic common anchestor
LFQ	label-free quantification
LPS	lipopolysaccharide
LTQ	linear ion trap
m/z	mass to charge ratio
MALDI	matrix assisted laser desorption/ionization
MCS	membrane contact sites
MCU	mitochondrial calcium uniporter
MDM	mitochondrial distribution and morphology protein
MELAS	mitochondrial encephalopathy, lactic acidosis, and stroke-like episodes
MERRF	myoclonic epilepsy with ragged red fibers
MFF	mitochondrial fission factor
MFN1/2	mitofusion 1/2
MIA	mitochondrial intermembrane space assembly
MICOS	mitochondrial contact site and christea organizing system
MIDD	maternally inherited diabetes and deafness
MIM complex	mitochondrial import complex
MIRO	mitochondrial Rho GTPase
MOAC	metal oxide affinity chromatography
MOMP	mitochondrial outer membrane permeabilization
MPP	mitochondrial -processing peptidase
MQC	mitochondrial quality control
mRNA	messenger RNA
ms	mass spectrometry
MS/MS	tandem mass spectrometry
MSA	multi stage activation

mtDNA	mitochondrial DNA
mTOR	mammalian target of rapamycin
MT-TL1	mitochondrially encoded tRNA leucine 1
NAD+/NADH	oxidized/ reduced nicotinamidadenin dinucleotid
nDNA	nuclear DNA
NEDD8	neural precursor cell expressed developmentally down-regulated protein 8
NFS1	cysteine desulfurase, mitochondrial
NHS	N-Hydroxysuccinimide
NRF1/2	nuclear respiratory factor 1/2
OMM	outer mitochondrial membrane
OPA1	optic atrophy protein 1
OXA	oxidase assembly
OXPHOS	oxidative phosphorylation
PAM	presequence translocase-associated motor
PARL	Presenilins-associated rhomboid-like protein, mitochondrial
PC	Phosphatidylcholine
PE	phosphatidylethanolamine
PGC-1 α	peroxisome proliferator-activated rreceptor gamma coactivator 1 alpha
PHB2	prohibitin-2
PINK1	PTEN-induced putative kinase protein 1
PP	phosphatase
PPI	Protein-protein interaction
ppm	parts per million
PS	phosphatdudylserine
PTM	post translational modifications
QMF	quadrupole mass fiter
RF	radio frequency
RING	really interesting new gene
RNA	ribonucleic acid
ROS	reactive oxygen species
RP	reversed phase
SAM	sorting and assembly machinery
SILAC	stable isotope labeling by amino acids
SLP2	stomatin-like protein 2
SOXR	transcription factor SOX-3
sqstm1	sequestosome-1
SUMO	small ubiquitin-like modifier
TCA	tricarbon acid cycle
TFAM	transcription factor A, mitochondrial
TFP	trifunctional protein
TIM	translocase of the inner membrane
TMT	tandem mass tag
TOF	time-of-flight
TOM	translocase of the outer membrane
TRAK	trafficking kinesin-binding protein
tRNA	transfer RNA
UBL domain	ubiquitin-like domain

UPS	Ubiquitin–proteasome system
USP	Ubiquitin proteasome system
VDAC	voltage dependent anion channel
VLCAD	very long chain acyl CoA dehydrogenase
YME1	ATP-dependent zinc metalloprotease YME1L1
Δψ	membrane potential

8. Acknowledgments

I would like to take the opportunity to thank all those, that helped me to make this work successful.

First, I would like to acknowledge Prof. Dr. Boris Macek for his supervision throughout the last 4 years. I would like to thank especially for the trust in me to work on those many interesting projects, the lively discussions and the support I received.

I would also like to thank the members of my thesis advisory committee Prof. Dr. Michal Sharon and Prof. Dr. Ana Garcia-Seaz for the encouraging and lively discussion during our meetings and my internships in your groups. My thanks especially to Prof. Dr. Michal Sharon for the supervision of my dissertation.

Furthermore, I would like to thank the MOMbrane RTG, especially Prof. Dr. Doron Rappaport and Dr. Julia Fitzgerald for the supportive atmosphere and vivid discussions during our biweekly seminars and collaboration projects. I would like to especially thank Prof. Philipp Kahle and Anna Lechado-Terradas for the inspiring and great collaboration we had throughout the last years.

I would like to thank all current and alumni members of the Proteome Center Tübingen for a great supportive atmosphere in the group, motivating words and lively social activities. My thanks goes especially to Nicolas, Marisa, Philipp, Payal and Claudia for their motivation, kindness and help at all time in the lab and outside. Thanks to all members of the group that helped me with work and left me with great memories on PCT: Irina, Mirita, Silke, Siggi, Anke, Uli, Lena, Ana, and Johannes. Also, I would like to thank all the students I had the pleasure to work with and who helped me with the projects (Johanna, Nisha, Naomi, Laura-Marie, and Bianca).

Mein ganz besonderer Dank geht an meine Eltern, Erhard und Reinhild, die mich immer mit viel Liebe in meinen Entscheidungen und meinem Studium unterstütz haben, immer Verständnis für meine Sorgen hatten und sich immer über meine Erfolge am meisten gefreut haben. Ebenso würde ich gerne meinem Freund Benedikt danken, der mich motivert und unterstützt und mir viele Lasten abgenommen hat.